Beyond-mean-field corrections and effective interactions in the nuclear many-body problem

Kassem Moghrabi

UNIVERSITÉ PARIS-SUD XI
INSTITUT DE PHYSIQUE NUCLÉAIRE D'ORSAY

THÈSE

Présentée en vue d'obtenir le grade de Docteur
Spécialité: Physique Nucléaire

par
Kassem Moghrabi

Beyond-mean-field corrections and effective interactions in the nuclear many-body problem.

Thèse soutenue le 12 Septembre 2013 devant le jury composé de:

M. Gianluca Colò	
M^{me} Marcella Grasso	Directeur
M. Elias Khan	
M. Ubirajara van Kolck	
M. Takashi Nakatsukasa	Rapporteur
M. Luis Robledo	Rapporteur

Abstract

Mean-field approaches successfully reproduce nuclear bulk properties like masses and radii within the Energy Density Functional (EDF) framework. However, complex correlations are missing in mean-field theories and several observables related to single-particle and collective nuclear properties cannot be predicted accurately. The necessity to provide a precise description of the available data as well as reliable predictions in the exotic regions of the nuclear chart motivates the use of more sophisticated beyond-mean-field models. Correlations and higher-order corrections (beyond the leading mean-field order) are introduced. A crucial aspect in these calculations is the choice of the effective interaction to be used when one goes beyond the leading order (available effective interactions are commonly adjusted at the mean-field level).

In the first part, we deal with the equation of state of nuclear matter evaluated up to the second order with the phenomenological Skyrme force. We analyze the ultraviolet divergence that is related to the zero range of the interaction and we introduce Skyrme-type regularized interactions that can be used at second order for matter. Cutoff regularization and dimensional regularization techniques are explored and applied. In the latter case, connections are naturally established between the EDF framework and some techniques employed in Effective Field Theories.

In the second part, we check whether the regularized interactions introduced for nuclear matter can be employed also for finite nuclei. As an illustration, this analysis is performed within the particle- vibration model that represents an example of beyond mean-field models where an ultraviolet divergence appears if zero-range forces are used. These first applications suggest several directions to be explored to finally provide regularized interactions that are specially tailored for beyond- mean-field calculations for finite nuclei. Conclusions and perspectives are finally illustrated.

"The kind of science that is separated from religion and does not consider itself engaged to the religion will have no other results than the prevailing currents in todays world; science has turned into a tool for bullying, exploiting others and a means to destroy generations and products. On one hand, atomic bombs are the products of science; on the other hand, another product of science are these pernicious drugs. The product of science are some politicians who have come to power in so many countries and who are away from all human emotions. Science should be associated with religion. Science should be acquired for sake of God and should be used in the Gods path. This should become part of our basic teachings everywhere."

"The Leader of Islamic republic of Iran Imam Sayyed Ali Khamenei."

Contents

List of Tables

List of Figures

Chapter 1

Introduction. The nuclear many-body problem

The essential goal of quantum many-body physics is to study the nature and the effects of the interaction between particles as well as the behavior of systems formed by a large number of particles. It aims at describing and predicting the observable properties of many-particle systems.
Among the first applications of the many-body physics, we mention those made by Brueckner and Gell-Mann [1, 2] who have studied the many-body problem for strongly interacting electronic systems and have calculated the interaction energy in a sequence of linked cluster terms. Many authors have studied the perturbation series for the energy of an electron gas [2, 3, 4] and of nuclear systems [5, 6, 7, 8].
In the domain of nuclear physics, the nuclear many-body problem is of special relevance because of its long history, full of developments and discoveries and its rich perspectives for the coming years and decades. Several domains of research in nuclear physics at the limits of stability, including the study of the r and rp-process nuclei, the shell closure evolution as well as the investigation of very heavy elements, will be further investigated by the future new-generation facilities where more exotic nuclei will be produced and studied experimentally. We mention for example, the SPIRAL2 project in France, the EURISOL project that is a long-term project and a continuation of SPIRAL2, FAIR in Germany, RIBF (already working) in Japan. The future new measurements will provide new data. Theoreticians will have the important role of predicting the nuclear properties in the exotic regions of the nuclear chart (and thus also suggesting new experiments) and interpreting the trends and the values of the measured observables.

There are certain rules that one should follow to construct the nuclear many-body problem:

1. In the first place, one chooses the suitable degrees of freedom that should be taken into account in the analysis of the properties of the many-body systems. For example, in low-energy nuclear physics, since the energy scales are of the order of $\sim 10 \div 100$ MeV, the associated degrees of freedom are the nucleons, i.e., the neutrons and the protons

and their internal degrees of freedom are typically not considered.

2. Secondly, the interaction among these constituent degrees of freedom has to be introduced. The force acting on the nucleons, hadrons and baryons is the strong force. Since the nucleon-nucleon (NN) interaction is not completely known, in contrast to what happens for electronic systems where the Coulomb interaction is perfectly known, several directions are followed (they will be briefly described in Chapter 2). We can identify three main ways to introduce the nuclear interaction:

   - Realistic interactions.
   - Phenomenological interactions.
   - Interactions derived by employing the Effective Field Theory (EFT).

3. Once the constituents and their interactions are chosen, one should in principle solve the Schrödinger equation. Since the velocities inside the nucleus are small enough $\left(\left(\frac{v}{c}\right)^2 \sim 0.1\right)$, one can treat the nuclear many-body problem in a non-relativistic manner by neglecting all the relativistic effects.
   In principle, the Schrödinger equation that describes the dynamics of a many-body system composed by A nucleons is given by:

   $$H\Psi = E\Psi,$$

   where the Hamiltonian is the sum of a kinetic term T and an interaction term V, that represents in principle a 2-body, 3-body, $\cdots$, up to a $A-$body force,

   $$H = T + V.$$

   In other words, the Schrödinger equation may be written as:

   $$H\Psi = \left\{ \sum_{i=1}^{A} -\frac{\hbar^2}{2m}\nabla_i^2 + \text{2-body} + \text{3-body} + \cdots + \sum_{i_1<i_2<\cdots<i_A} v(i_1, i_2 \cdots, i_A) \right\} = E\Psi,$$

   where i represents all coordinates of the i^{th} nucleon.
   From the phenomenological point of view, it turns out that, in most cases, the interaction is well enough described by the 2-body (and possibly the 3-body) terms, and therefore the Schrödinger equation reduces to:

   $$H \sim \sum_{i=1}^{A} -\frac{\hbar^2}{2m}\nabla_i^2 + \frac{1}{2}\sum_{i\neq j=1} V(i,j).$$

4. Finally, once the theoretical framework is settled, one devotes his attention to study the properties of the many-body system. However, it is known that it is not so easy to obtain a solution of the Schrödinger equation even with the above simplification on the many-body interaction without adopting some approximations. We will see, for example, in Chapter 3 that a first approximation can be adopted by treating the wave-function Ψ as a Slater determinant in the framework of the so-called mean-field models.

Motivation and summary

The techniques of the many-body physics provide a useful language for discussing the methods for calculating correlations, as well as an intuitive graphical representation.
The work of my thesis is centered on the inclusion of correlations at a beyond mean-field level in nuclear matter, with the objective of making finally applications to finite systems. Several technical and formal problems, that are encountered when one goes beyond the mean-field framework, are considered and analyzed in details. For nuclear matter, we have studied several aspects:

1. The ultraviolet (UV) divergence which appears due to the zero-range character of the nuclear Skyrme interaction when second-order corrections beyond the mean-field level are introduced. Two regularization techniques were being adopted to treat this divergence:

   (a) Momentum cutoff procedure (cutoff dependence). Drawbacks of this adopted procedure are that the divergence is absorbed (and not suppressed) and that the procedure breaks some symmetry laws (e.g., translational invariance).

   (b) Dimensional regularization (DR) with a minimal subtraction (MS) scheme which preserves symmetry laws (no cutoff dependence). This technique is widely employed in the framework of effective field theories.

2. The adjustment of the parameters of the Skyrme interaction in order to design a Skyrme force that is well adapted for calculations at this beyond mean-field level. The long-term objective is to use this type of interactions, for example, in particle-vibration coupling (PVC) models.

3. The energy per particle is derived analytically at the second-order beyond the mean-field approximation in infinite nuclear matter.

   (a) The linear UV divergence is analyzed in symmetric nuclear matter with a simplified Skyrme interaction (the so-called $t_0 - t_3$ model). A momentum cutoff procedure is adopted and followed by an adjustment of the parameters of the Skyrme interaction to have a reasonable equation of state (EoS). It is shown that for any value of the momentum cutoff Λ, it is possible to determine a new interaction that is well adapted for calculations at the second-order beyond the mean-field level [9].

   (b) After that, we have extended the same strategy in nuclear matter to the case of the full nuclear Skyrme interaction. Due to the velocity-dependent terms (i.e., non-local terms of the nuclear Skyrme interaction), the divergence becomes of order $\sim \Lambda^5$. In this case, the adjustment of parameters is performed for both symmetric and nuclear matter with different neutron-to-proton ratios [10].

   (c) DR/MS is adopted to treat the UV divergence. In this case, the divergence is suppressed and the resulting EoS at the second-order is independent of the used

regulator. Thus, a unique set of parameters is obtained for the adjusted effective interaction [11].

In finite systems, we couple two currently used methods in nuclear physics, the Hartree-Fock (HF) approach and the random-phase approximation (RPA). This can take into account the coupling between the individual and the collective degrees of freedom of the nucleus (particle-vibration coupling). Second-order corrections (already encountered in nuclear matter) have to be subtracted to avoid double counting. The interactions designed and regularized for nuclear matter are employed to verify whether the performed regularization is enough to regularize the results also for finite nuclei. We employ again the Skyrme interaction.

The present manuscript is organized as follows:

- In Chapter 2, we give a short review of the theory of nuclear forces starting from the early developments of the realistic interactions, for example, the Yukawa potential. Then, we introduce the phenomenological effective interactions with both zero range (Skyrme interaction) and finite range (Gogny force). Finally, we introduce the concept of EFT interactions.

- In Chapter 3, we present the self-consistent mean-field models for describing nuclear structure. We present these models as effective energy-density functionals (EDF), for example, the Skyrme EDF. We also say some words about nuclear matter and its fundamental properties: EoS, pressure, incompressibility and symmetry energy.

- In Chapter 4, we mention the reasons to go beyond the mean-field level and give some examples of beyond-mean-field models. We list the conceptual and technical problems that may occur when using such models: problems of double counting, of irregularities and of UV divergences. For the latter problem, we introduce some subtraction schemes to cure the UV divergences: the momentum cutoff and the DR schemes.

- In Chapter 5, we take the second-order energy correction as an example to go beyond the mean-field level in nuclear matter. We use as a first try the simplified $t_0 - t_3$ model for symmetric matter. Then we include the velocity-dependent terms of the nuclear Skyrme interaction and consider also asymmetric nuclear matter.

- In Chapter 6, we use the techniques of DR to treat the UV divergences. We consider again the second-energy corrections in nuclear matter. We list some limits of the phenomenological approaches.

- In Chapter 7, we introduce the PVC approach as an example of beyond-mean-field theories. In this chapter, we test the interactions that we introduce in Chapters 5 and 6 for nuclear matter. We try to answer whether the regularization done for matter (at second order) has some effect on the results that we obtain for nuclei.

Chapter 2

Nuclear forces

2.1 Introduction

One of the most fundamental goals of theoretical nuclear physics is to explain the static and dynamic properties of atomic nuclei by employing a nucleon-nucleon force. However, the knowledge of nuclear forces is limited because of their complexity. In practice, in low-energy nuclear physics, one can neglect some degrees of freedom of the strong interaction. Three possible directions may be followed:

1. One direction that is actually followed to obtain quantitative information is the theory of nucleons interacting via the exchange of mesons. These nuclear forces are called realistic interactions.

2. A second way is to treat the nucleus as a nuclear many-body system composed of A nucleons interacting among themselves by $2-$, $3-$,$\cdots$, $A-$body forces. It turns out that the two-nucleon interaction is the most basic and important interaction. Three-body forces were included in the original works by Skyrme [12, 13] and were replaced later by Vautherin and Brink [14] by a density-dependent two-body term. Without the latter term, saturation of nuclear matter is not achieved. This is the so-called "phenomenological" theory of nuclear forces.

3. The third direction has attempted to derive the nuclear force from field theory and to include the other degrees of freedom that are usually neglected. This is the so-called EFT. The point of using EFT is to describe low-energy physics with minimal assumptions about higher-energy behavior. In most problems of physics, separation of scales is essential to identify the physical phenomena and the relevant degrees of freedom for each system.

2.2 Realistic interactions

An important date in the development of all nuclear realistic interactions is the year 1949 when Hideki Yukawa received the Noble Prize in physics for having predicted the existence

of the π mesons.

2.2.1 Yukawa's interaction

In 1934, Yukawa developed the first quantum field theory of the strong force [15] with the introduction of a particle that he called $'U'$. He argued that U has a non-zero mass that is about 200 times larger than that of the electron ($m_U \approx 200\ m_e$). Moreover, he suggested that this meson is the mediator of the strong interaction similarly to the photon which is the mediator of the electromagnetic interaction. Shortly after Yukawa's prediction, a particle with almost precisely this mass was discovered in cosmic ray phenomena. Moreover, Yukawa has demonstrated, by using simple arguments, that the exchange of mesons of mass m can be described by an attractive potential that has the following form:

$$V(r) = -g^2 \frac{e^{-mr}}{r},$$

where g is a coupling constant and m is the mass of the pion. Some comments could be addressed at this level:

1. If the mass of the pion was zero, then the potential would be equivalent to a Coulomb potential of the form $1/r$.

2. It is important to emphasize that the pion determines only the long-range part of the nuclear potential.

2.2.2 Developments of the realistic interactions

In general, realistic interactions, as shown in Figure 2.1, are thought to be characterized by three distinct regions [16, 17]:

I. The long-range part that corresponds to $r \geq 2$ fm is well understood and describes the static one-pion-exchange processes.

II. The medium-range part is attributed to nonstatic part of the pion exchange, multi-pion exchanges and heavy meson exchanges. This part corresponds to 1 fm $\leq r \leq 2$ fm.

III. The short-range part $r \leq 1$ fm describes a strong repulsive core [18].

It has to be noted that the long-range part and the medium-range part are attractive, whereas the short-range part is repulsive. The balance between the attraction in regions (I) and (II) and the repulsion in (III) is crucial for nuclear binding.
The origin of the short-range character of the nuclear force is thought to be closely related to the quark-gluon structure of the nucleon. However, this issue has long been debated and it remains an open question in QCD [19].
The implementation of the short-range part is essential for describing the NN scattering

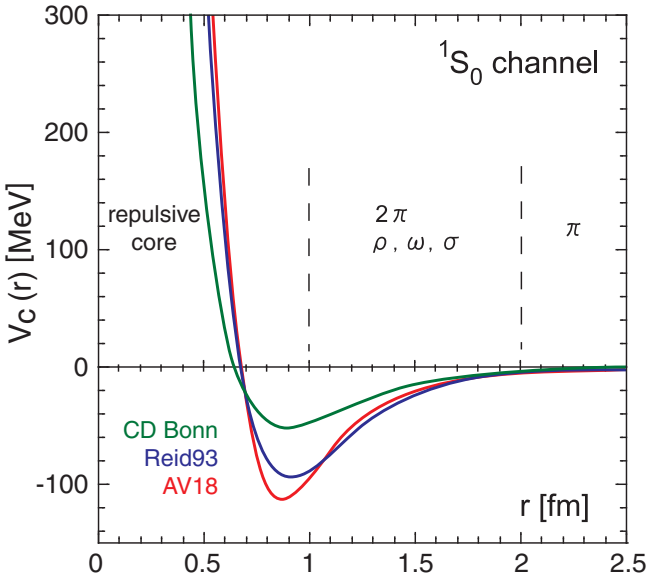

Figure 2.1: Three examples of the modern NN potential in the $^1S_0$ (spin singlet and s-wave) channel: CD-Bonn [20], Reid93 [21] and AV18 [22].

data at high energy. Moreover, it has been shown that the repulsive core is also essential for the stability and saturation of atomic nuclei, for determining the maximum mass of neutron stars, and for igniting the Type II supernova explosions [23].

The theory of nuclear forces has a long history [24] (see Table 2.1). In 1935, Yukawa introduced the pion-exchange to account for the strong interaction between the nucleons [15]. It turned out that this one pion-exchange is very useful in explaining the NN scattering data and in particular the properties of the deuteron [25]. However, the "pion theories" of the 1950s failed to achieve more progress. The multi-pion exchange introduced by Taketani [26] could not be resolved in a satisfactory way because at that time the chiral symmetry was unknown.

In the 1960s, an experimental discovery of heavy mesons ($\omega,\ \rho \equiv 800$) MeV saved the situation. The one-boson exchange potentials (OBEP) were introduced to describe the NN interaction [27]. The empirical evidence of the scalar-isoscalar "σ" or "ϵ" boson remains controversial [24].

In the last decades, well-known realistic interactions have been constructed. The real development in the study of the medium-range part (II) was achieved in the 1970s when two popular models of nuclear forces were introduced: the Paris potential [28] and the Bonn potenial [29].

The Paris potential was introduced by M. Lacombe et al. The Paris group followed a semi-phenomenological approach to derive the two-pion exchange contribution. They also applied the dispersion technique to the πN scattering amplitudes and treated the short-range part

as a purely phenomenological potential.
The Bonn potenial was proposed by R. Machleidt et al.. They derived the one-boson exchange and its non-static part by considering not only the pion, but also the σ, ρ, ω, η and δ. In their approach, the short-range part was described by the ω exchange.
In the 1990s, high-precision realistic potentials are introduced like CD-Bonn [20], Reid93 [21], Argonne V_{18} [22] and Nijmegen I and II [30, 31].
The main source of information of such models is the NN scattering data as well as spectroscopic properties of the deuteron and other few-body nuclear systems like ^{3}H and ^{3}He. The parameters (around 50) of these realistic potentials are adjusted to reproduce the above observables.
So far, it appears that the nuclear force problem is solved despite the little knowledge of the short-range character of the nuclear force. With the development of the theory of quantum chromo-dynamics (QCD), the NN short-range repulsion was explained in terms of the quark substructure of the nucleon by Neudatchin, Smirnov and Tamagaki [32] in 1977. In their paper, they argued that the origin of the repulsion may be explained by the Fermi-Dirac statistics of the spin 1/2 of the quarks (Pauli principle) alone or combined with the hyperfine interaction of quarks.
Moreover, it was discovered that the underlying theory of QCD behaves non-perturbatively in the low-energy regime of nuclear physics. This has led to the invention of the so-called QCD-inspired quark models. Besides their success of explaining the structure of hadrons and hadron-hadron interaction on an equal footing, these approaches are considered as models and not "theories" and thus they do not represent a fundamental progress.

2.2.3 Limits of realistic interactions

The main difficulty in using bare realistic interactions for nucleons in a medium (nucleons in nuclei or nuclear matter) is related to the existence of the infinite repulsive hard core (Region III) at short distances. The existence of an infinite repulsion makes some of the usual concepts of the many-body problem complicated. Therefore, realistic interactions cannot be treated straightforwardly. There are two directions that may be followed: a perturbative approach and a V_{low-k} interaction.

2.2.4 Perturbative approach: The $G-$matrix.

It can be argued that the nucleons in a nucleus do not feel the bare nucleon-nucleon interaction (with the infinite hard core) because the scattering of pairs of nucleons from an initial to a final state in a nucleus is well defined [33]. Taking into account the above observation and the fact that nucleons interact with each other in the presence of many other nucleons, permits one to introduce an effective nucleon-nucleon interaction which is rather well behaved and allows one applications of the usual many-body methods, such as the Hartree-Fock theory.
In 1955, Brueckner [33] replaced the bare interaction by an effective interaction which is itself a reaction matrix that represents an infinite sum of scattering processes of two nucleons

in the nuclear medium. This $G-$matrix or Brueckner matrix, that describes the scattering of nucleons in a medium, is an extension of the $T-$matrix that represents the scattering of nucleons in vacuum. Later in 1957, Bethe and Goldstone [34] derived the equation for the $G-$matrix which is known under the name of Bethe-Goldstone equation:

$$G^E_{ab,cd} = \bar{v}_{ab,cd} + \frac{1}{2}\sum_{\epsilon_m,\epsilon_n>\epsilon_F} \bar{v}_{ab,mn}\frac{1}{E-\epsilon_m-\epsilon_n+i\eta}G^E_{mn,cd},$$

where $\bar{v}$ is the interaction, ab, mn and cd are single-particle indices and ϵ_F is the Fermi energy.
One of the advantages of the $G-$matrix approach is the elimination of the hard-core divergence even if the interaction diverges.
The main fields of application [35] are: (i) the ground-state properties of nuclei, where the scattering of two nucleons within the nuclear medium has to be considered; (ii) the equation of state of matter.

2.2.5 V_{low-k} interactions.

The traditional microscopic approaches are "model dependent" owing to the fact that there is no a unique V_{NN} to start from. For example, even if the Brueckner G matrix eliminates the divergence at short distances, it remains model-space dependent as well as energy dependent. The goal of introducing low-momentum NN potentials, the so-called V_{low-k} potentials, is to integrate out the high-momentum components of different models of V_{NN} in the sense of the Renormalization Group (RG) [36]. This is done to remove the model dependence that arises at short distances in the various V_{NN} models, so to allow one to use the same interaction in different nuclear regions [37, 38]. It can be shown that the use of V_{low-k} interactions preserves the deuteron binding energy.
The V_{low-k} approach was motivated from the recent applications of EFT and RG to low-energy nuclear systems [36, 39, 40]. This new philosophy inspired from EFT and RG is based on the fact that an infinite number of potentials are capable of accurately describing low-energy physics [36].
The advantages of V_{low-k} interactions are:

1. V_{low-k} is far easier to be used than the G matrix. It is a smooth NN potential which can be used directly in nuclear structure calculations.

2. It does not depend either on the starting energy or on the model space, as is instead the case of the G matrix, which is defined in the nuclear medium.

3. It preserves the deuteron binding energy as well as low-energy scattering phase-shifts of V_{NN}.

Below is a table which describes the developments of the theory of nuclear forces in eight decades.

1935	Yukawa: Meson Theory
1950′s	The Pion Theories. One-pion exchange: good; Multi-pion exchange: Strong difficulties.
1960′s	Many pions: multi-pion resonances: σ, ρ, ω, $\cdots$. The One-Boson-Exchange Model: success.
1970′s	Refinement of meson theory: Sophisticated 2π exchange models; Partovi-Lomon, Stony Brook, Paris, Bonn.
1980′s	Nuclear physicists discover QCD: Quark Models
1990′s and beyond	Nuclear physicists employ EFT; Weinberg, van Kolck, . . . Back to Yukawa's Meson (Pion) Theory! But, constrained by Chiral Symmetry.

Table 2.1: The theory of Nuclear Forces: Eight Decades of Developments.

2.3 Phenomenological effective interactions

Many efforts have been devoted not only to derive the microscopic effective interactions from the bare nucleon-nucleon interaction but also to study the properties, the structure and the range of validity of these effective interactions. Another possible direction is to introduce phenomenological interactions that are simpler to use and that are currently employed in the nuclear many-body problem. Such interactions depend on phenomenological parameters that are adjusted to fit experimental data.

2.3.1 Phenomenological interactions: Examples

Phenomenological interactions have been applied to problems in nuclear physics to explore the properties of nuclear structure and reactions. These interactions contain around ten parameters that are adjusted to reproduce some experimental data. It turns out that the use of phenomenological interactions is extremely successful because it allows one to perform more easily sophisticated numerical calculations for medium-mass and heavy nuclei with only a few parameters chosen once and for all. There exists a large number of phenomenological interactions, each of them has been constructed for a special purpose. Phenomenological interactions, like the Gogny and Skyrme forces, are actually very currently employed in the framework of mean-field theories to calculate bulk properties of nuclei such as binding energies and radii. Gogny and Skyrme forces differ by their range; the first has a finite range and the second a zero range.
The analysis of nucleon-nucleon scattering [41, 42] in terms of a potential indicate the presence of strong non-central forces and of a "*repulsive core*" at small distances. In low-energy nuclear physics, data are generally insensitive to the details of interactions at short distance (high-energy processes) because the complete knowledge of physics at very short distances is not required for an accurate understanding of usual low-energy experiments [43]. Nuclear physicists have exploited this fact and they have replaced the effects of the non-local interactions at short distances in terms of local operators in a derivative expansion, the effective

Hamiltonian. In this context, locality means that only a finite number of operators are needed up to a given truncated error. Thus, the higher an operator's dimension, the smaller the effect it has on low-energy physics. Hence, one can obtain a useful phenomenological theory by retaining operators only up to some dimension, fitting their coefficients to data [36].
The use of effective interactions in nuclear physics dates back to the 70s, to the pioneering works due to Gogny [44, 45] and Vautherin, Brink [14]. Vautherin and Brink were inspired by the interaction introduced by Skyrme in the 50s [12, 13]. Skyrme had written the interaction as a zero-range interaction using the Born approximation where high-momentum components are neglected. Vautherin and Brink replaced the three-body part by a density-dependent two-body part and made the first applications in the mean-field framework.
Introducing the concept of effective interactions has led to some advantages. The complexity of the many-body problem is greatly simplified and this paves the way for introducing higher-order energy corrections and include more correlations. However, when going beyond the mean-field level, physical observables may be plagued by infinities due to the high-energy processes or the short-range character of the interaction.
While field theory approaches to many-body physics are already well-established (*e.g.*, [46] and [47]), the treatment of divergences and renormalization issues in nuclear physics is presently evolving [48, 49, 50, 51].
The old-style approach to renormalization theory treats renormalization as a technical device to get rid of divergences in perturbation theory. Whereas, the modern viewpoint in particle physics defines "renormalization as an expression of the variation of the structure of physical interactions with changes in the scale of the phenomena being probed" [52].
This modern point of view of renormalization has led to powerful and elegant renormalization group methods [40], and to the development of the EFT approach. The EFT approach is based on the idea that at low energies, the effective parameters matter and not the details of the potential. This means that the low-energy observables can be reproduced by using any complete set of regularized local interactions. A corollary is that, unlike the goal of phenomenological description of nuclear force, the EFT perspective says that there is no "best" potential [52].

2.3.2 Zero-range interactions

It is known that the nuclear force is regarded as a short-range force when the momentum transfer is not very large [35, 53]. In this case, one does not explore the internal structure of the composite system and thus the nucleons are regarded as point particles (or elementary particles) with a good approximation [53]. One of the simplest short-range nuclear forces is the one where its radial dependence is described by a $\delta-$function. Such forces are called zero-range interactions. These interactions are simple to handle and they describe quite well many nuclear properties. An example of zero-range forces is the Skyrme force which will be introduced in the next Chapter.

2.3.3 Finite-range interactions

It has been argued that finite-range forces, and not zero-range forces, are able to simulate the long-range and even the intermediate-range parts of the realistic effective interaction [35]. Moreover, Dechargé and Gogny [45] have argued that the long-range forces and consequently finite-range forces smooth the fluctuations of the HF field as compared to short-range interaction. This takes into account the local variation in the HF density, an effect which is emphasized by the self-consistency. Furthermore, by using finite-range forces, UV divergences are avoided at the beyond mean-field level.
Finite-range interactions have been introduced in 1967 by Brink and Boeker as the sum of two Gaussians that contain spin-, and isospin-exchange terms [54]. However, using such form does not permit one to reproduce correctly the binding energies at the HF level. After that, in 1975, Gogny kept the same form of Gaussians because of their computational advantages. He also added a density-dependent and a spin-orbit term chosen of short range to reduce the computation time [44]. Later, in 1980, Gogny and Dechargé [45], proposed a phenomenological effective force of finite range whose parametrization is simple enough to render feasible many applications in the framework of the self-consistent HF approach. This force is called the Gogny force:

$$\begin{aligned} V_{Gogny}(r_1,r_2) &= \sum_{j=1}^{2} e^{-\frac{|r_1-r_2|^2}{\mu_j}} \left(W_j + B_j\hat{P}_\sigma - H_j\hat{P}_\tau - M_j\hat{P}_\sigma\hat{P}_\tau\right) \\ &\quad + t_3\left(1+x_0\hat{P}_\sigma\right)\delta(r_1-r_2)\rho^\alpha\left(\frac{r_1+r_2}{2}\right) + iW_{ls}\left(\hat{\sigma}_1+\hat{\sigma}_2\right)\cdot\hat{k}^\dagger\times\delta(r_1-r_2)\hat{k}, \end{aligned}$$

where $\hat{P}_\sigma = \frac{1}{2}\left(1+\hat{\sigma}_1\cdot\hat{\sigma}_2\right)$ and $\hat{P}_\tau = \frac{1}{2}\left(1+\hat{\tau}_1\cdot\hat{\tau}_2\right)$ are the spin- and isospin-exchange operators, respectively. The first term is the central Gaussian term, the second is the zero-range density-dependent term (that generates saturation) and the third term is the spin-orbit term. The quantities B_j, H_j, M_j, W_j, μ_j, t_3, x_0, α and W_{ls} are parameters of the interaction. These parameters were adjusted to reproduce the properties of finite nuclei and of nuclear matter. There exists only a few parametrizations due to the complex numerical calculation of Hartree-Fock-Bogolibouv (HFB) with finite-range interaction. We mention the D1 [45], D1S [55] and D1N [56, 57] parametrizations. The original parametrization D1 has been reconsidered to correct for a too-large surface coefficient leading to an overestimate of the fission barrier of ^{240}Pu. The new adjustment was called the D1S parametrization. However, in the D1S parametrization, there is some deficiencies in the neutron matter EoS and a drift of binding energies along isotopic chains. A new adjustment was done, to fit the EoS of neutron matter, and called the D1N parametrization.
The density-dependent zero-range force has been chosen with a spin-exchange mixture $x_0 = 1$ such that it does not contribute to the $T = 1$ pairing channel. In this way, the usual problem of UV divergence of a zero-range interaction in the pairing channel is avoided, which enables one to use the Gogny interaction simultaneously in both mean-field and pairing channels. The spin-orbit interaction introduces a very weak divergence and is rarely taken into account in the pairing channel.

2.4 EFT

A major breakthrough occurred when nuclear physicists like Weinberg, van Kolck, and others applied the concept of EFT [58] to the nuclear case, by establishing a firm link with QCD. Weinberg's arguments were based on the '*folk theorem*' [58] by having the EFT to satisfy all relevant symmetries of the underlying theory:
If one writes down the most general possible Lagrangian, including all terms consistent with assumed symmetry principles, and then calculates matrix elements with this Lagrangian to any given order of perturbation theory, the result will simply be the most general possible S-matrix consistent with analyticity, perturbative unitarity, cluster decomposition, and the assumed symmetry principles.
In summary, the EFT procedure consists of the following steps:

1. Identify all the scales and the degrees of freedom appropriate for (low-energy) nuclear physics. In this case, we integrate out the heavy mesons and nucleon resonances and we deal with pions and nucleons as effective degrees of freedom rather than quarks and gluons.

2. Identify the relevant symmetries of low-energy QCD and investigate if and how they are broken, for example, the (broken) chiral symmetry.

3. Construct the most general Lagrangian consistent with those symmetries and symmetry breakings.

4. Design an organizational scheme (power counting) that can distinguish between more and less important contributions: a low-momentum expansion.

5. Design a power-counting scheme that allows us the computation, up to the desired accuracy, of low-energy observables in terms of the parameters that summarize the effect of short-range interactions.

One of the conclusions that can be drawn is that EFT adds to the usual Yukawa's meson theory the (broken) chiral symmetry which is crucial to generate and control the dynamics and to establish a clear connection with the underlying theory QCD.

2.4.1 Chiral EFT

The chiral EFT (χEFT) relies on the spontaneously broken chiral symmetry of QCD that strongly constrains the interactions of pions that are identified with the corresponding pseudo-Goldstone bosons [59, 60, 61]. The χEFT allows to calculate pion and pion-nucleon low-energy observables within the frame of chiral perturbation theory. In other words, it exhibits a power counting in the ratio Q/Λ_χ with Q being the low-momentum scale being probed and Λ_χ the cutoff, which is of the order of 1 GeV.
In the χEFT framework, nucleons interact by exchanging a single or multiple pions. For example, the one-pion exchange (OPE) determines the long-range part of nuclear forces, which

leads to a static Yukawa force of the range of the Compton wave length of the pion. It also induces a strong tensor force that causes a significant $D-$wave component in the deuteron wave function. The intermediate-range part shows a strong attraction, which comes mainly from two-pion exchange (TPE) and vector-meson exchanges. This is the attraction that binds nucleons into nuclei [61]. The short-range part of the nuclear force is described by the exchange of heavy mesons like ω [61] and it shows a very strong repulsive contribution. It can be naturally parameterized by contact interactions with an increasing number of derivatives due to the following two reasons:

1. The short-range part ($r \leq \Lambda_\chi^{-1}$) of the nucleon-nucleon (NN) potential is obtained by the Fourier transform of the propagator of heavy mesons:

$$\int d^3q \frac{e^{i\vec{q}\cdot\vec{r}}}{m_\omega^2+q^2} \approx \int d^3q\, e^{i\vec{q}\cdot\vec{r}} \frac{1}{m_\omega^2} \sum_{n=0}^{\infty} \frac{(-1)^n}{n!} \left(\frac{q^2}{m_\omega^2}\right)^n = \sum_{n=0}^{\infty} C_n \nabla^{2n}.$$

2. A second reason of using contact terms is that they play an important role in the renormalization procedure because they pick up infinities and remove the scale dependence. This is why they are also known as counter terms. These counter terms are parametrized in terms of low-energy constants (LECs) that are determined by a fit to experimental data [36].

In terms of "Weinberg counting", the NN interaction in leading order (LO) corresponds to the OPE potential $V_{1\pi}^{(0)}$ plus a Dirac-delta $V_{ct}^{(0)}$, when considering an EFT of nuclear forces based on a chiral expansion of the effective Lagrangian:

$$V_{LO} = V_{ct}^{(0)} + V_{1\pi}^{(0)}.$$

The chiral forces have been applied for instance to nuclear few-body systems with a good deal of success [64]. However, there are still some pretty basic open issues that need our full attention, like the proper renormalization of the two-nucleon potential [62, 63]. In field theories, divergent integrals are common and methods have been designed to deal with them. One regulates the integrals and then removes the dependence on the regularization parameters (scales, cutoffs) by renormalization. Therefore, the theory and its predictions do not depend on cutoffs or renormalization scales. It has to be noted that the EFTs are renormalized by counter terms (contact terms) that are introduced order by order in increasing numbers.

Chapter 3

Self-consistent mean-field (SCMF) models with the Skyrme force

3.1 Introduction

A very good starting point for studying the properties of nuclei is to assume that nucleons move independently of one another. According to this simple picture, nucleons are subject to a common average potential created by all the nucleons in the nucleus. This approximation is valid in those systems when the mean free path of the particles is comparable with or larger than the size of the system. Indeed, the mean free path in the nucleus of a nucleon having 10 MeV-kinetic energy is around 15 fm, that is, larger than the size of the nucleus [65]. The Pauli principle is responsible for the fact that the nucleons do not collide very frequently one with the others in a nucleus [65]. A model that describes the dynamics of the nucleons only with such an average (mean-field) potential is called the independent-particle model.

The shell model is based on the independent-particle model. It describes the dynamics of valence nucleons, i.e., nucleons outside the closed shell, with a mean-field potential and a residual force. This model in its simplest non-interacting version was introduced in 1949 by Goeppert-Mayer [66], Haxel et al. [67]. They found a similarity between the quantum numbers assigned to nuclear ground states and those of a harmonic oscillator in its ground state for a potential which includes a centrifugal term and a spin-density dependent force in the form of a strong spin-orbit component. The model has a great success in providing a description for most of the low-energy properties of nuclei. For example, the shell model reproduces the correct magic numbers [68] and successfully describes properties like the magnetic and quadrupole moments, beta-decay rates and reaction cross-sections [35]. Later, much work has been done to refine the shell model to yield a more quantitative agreement with experiment. This refinement has at first taken the form of adding to the independent-particle Hamiltonian a direct two-body interaction (residual interaction) among the nucleons outside the closed shells [35].

3.2 SCMF models

The mean-field theory is widely used for the description of interacting many-body systems in physics. This method is based on the independent-particle approximation so that the many-body system is treated by describing the interaction between the nucleons with an average self-consistent mean field. For fermionic systems, this may lead to the Density Functional Theory (DFT) or to the so-called Hartree-Fock mean-field approximation, that are not strictly the same models.
For a nucleus with A nucleons, the mean-field approximation implies that:

1. The complex wave function is replaced by a Slater determinant, that is an anti-symmetrized product of single-particle wave functions ϕ of the nucleons:

$$\Psi_{HF}(x_1, \cdots, x_A) \;=\; \frac{1}{\sqrt{A!}} \det\{\phi_{\alpha_1}\phi_{\alpha_2}\cdots\phi_{\alpha_A}\}.$$

2. When the state of the system is described by the Slater determinant Ψ, then all the information on it is contained in the one-body density matrix ρ. This is true because there is a one-to-one correspondence between the Slater determinant Ψ and its single-particle density ρ [35].

3. The one-body density matrix ρ is defined as: $\rho_{ij} = \langle\Psi|a_j^\dagger a_i|\Psi\rangle$ with $\mathrm{tr}\rho = A$ and $\rho^2 = \rho$ (it has the properties of a projector).

4. Static and dynamical properties of the systems are obtained by solving N coupled equations for single-particle states.

5. Slater determinants correspond to a specific example of trial states that are particularly well adapted to describe one-body observables.

6. Within this approximation, the HF energy becomes a functional of the density:

$$E = \frac{\langle\Psi|E|\Psi\rangle}{\langle\Psi|\Psi\rangle} = E[\Psi] = E[\rho].$$

7. The ground-state energy is determined by a minimization procedure of the energy (variational procedure), i.e., $\delta E[\Psi] = 0$.

Mean-field methods predict ground-state properties of nuclei with increasing accuracy as $1/A \to 0$. Thus, they are particularly useful for describing masses, radii, shapes and deformations of relatively heavy nuclei. In this sense, the mean-field model (medium-mass and heavy nuclei) and the shell model (light and medium-mass nuclei) are complementary one with respect to the other. Mean-field theory is very efficient for the description of many-body systems like finite nuclei or infinite nuclear matter, as well as the neutron-rich nuclear matter which exists in neutron stars.

3.3 Standard formulation of the Skyrme force

As was pointed out in Chapter 2, a way of treating the many-body systems may be to use phenomenological effective NN and NNN interactions instead of realistic ones. In this scenario, some microscopic details of the nuclear force such as meson-exchange, are not explicitly considered and all the physically relevant information is carried by the parameters of the phenomenological force.
The basic idea is to parametrize these interactions either by zero-range forces like the force of Skyrme or by short finite-range forces like the Gogny interaction in order to describe the ground-state properties of finite nuclei and nuclear matter.
In 1956, Skyrme [12, 13] introduced a low-momentum version of the nuclear force in momentum space within the spirit of many-body physics. Besides the two-body force, he added a three-body force in order to better take into account the many-body effects. This effective force has the following ansatz for the form of the effective interaction:

$$V = \sum_{i<j} V_{12}(\vec{r}_i, \vec{r}_j) + \sum_{i<j<k} V_{123}(\vec{r}_i, \vec{r}_j, \vec{r}_k).$$

Skyrme argued that: *"It is generally believed that the most important part of the two-body interaction can be represented by a contact potential"*. This means that the two-body and three-body terms can be written as:

$$V_{12}(\vec{r}_i, \vec{r}_j) = V_{12}(k, k^{'})\delta(\vec{r}_i - \vec{r}_j) \quad V_{123}(\vec{r}_i, \vec{r}_j, \vec{r}_k) = t_3\delta(\vec{r}_i - \vec{r}_j)\delta(\vec{r}_j - \vec{r}_k),$$

where t_3 is an undetermined constant.
The zero-range character of the Skyrme interaction is an idealization which is consistent with the smoothly varying dependence of the mean-field state on spatial coordinates.
Moreover, because of Galilean invariance, the interaction depends only on relative momenta k and $k^{'}$ of the incoming and outgoing nucleons. Since the system is probed at low resolution, a polynomial expansion of the two-body term in powers of k and $k^{'}$ is possible:

$$V_{12}(k, k^{'}) = C_0 + \frac{1}{2}C_1[\vec{k}^{'2} + \vec{k}^2] + C_2\vec{k}^{'} \cdot \vec{k} + \cdots . \tag{3.1}$$

Some points should be remarked:

1. The structure of the Skyrme force allows one to derive analytical expression of all variables characterizing infinite nuclear matter within the mean-field framework.

2. Although the Skyrme force is formulated as a zero-range force in the space of coordinates, it has spatial non-local terms (or velocity-dependent terms) that exhibit some finite-range features [69]. This means that some correlation effects are included through in the parameters of the force.

3. This form is valid for low energy-processes at the mean-field level. However, large momentum transfers will lead to the presence of UV divergences. This means that

the parameters C_i must encode the short-range dynamics of these processes. Therefore, the effective force becomes able to describe the low-energy physics with minimal assumptions about higher-energy behavior. This is known as regularization and renormalization.

4. It is also important to note that Eq. (3.1) is not simply the term-by-term momentum-space expansion of an underlying potential because the coefficients also contain short-distance contributions from loop graphs.

Later, due to the work of Vautherin and Brink [14] in the 1970s, the zero-range three-body part has been replaced by a two-body density-dependent term when used in calculations of ground-state properties. Consequently, Skyrme-like effective interactions have been built according to the following analytical form which we will refer to as the standard form:

$$\begin{aligned} V(\vec{r}_1,\vec{r}_2) &= t_0(1+x_0\hat{P}_\sigma)\delta(\vec{r}_1-\vec{r}_2) \\ &\quad +\frac{1}{2}t_1(1+x_1\hat{P}_\sigma)[\vec{k}'^2\delta(\vec{r}_1-\vec{r}_2)+\delta(\vec{r}_1-\vec{r}_2)\vec{k}^2] \\ &\quad +t_2(1+x_2\hat{P}_\sigma)\vec{k}'\cdot\delta(\vec{r}_1-\vec{r}_2)\vec{k} \\ &\quad +\frac{t_3}{6}(1+x_3\hat{P}_\sigma)\delta(\vec{r}_1-\vec{r}_2)\rho^\alpha \\ &\quad +iW_0(\vec{\sigma}_1+\vec{\sigma}_2)\cdot[\vec{k}'\times\delta(\vec{r}_1-\vec{r}_2)\vec{k}], \end{aligned} \tag{3.2}$$

where $t_{0,1,2,3}$, $x_{0,1,2,3}$, α and W_0 are parameters to be adjusted. The first term is the so-called central term. The second and third terms are the velocity-dependent terms. The fourth term is the density-dependent term and the last term represents the spin-orbit contribution. It has to be noted that the density-dependent term, that is proportional to ρ^α, provides the variation with the density of the underlying microscopic effective interaction or of the energy [70]. If the parameter $\alpha = 1$, this density-dependent force exactly describes a three-body term, as for example, in the parametrization SIII [71].

The density-dependent term is of particular importance since it provides the appropriate saturation point and thus secures the success of the Skyrme-HF model in the description of finite nuclei. Chang [72] showed that the Skyrme interaction with the original three-body force provides unstable spin-saturated Hartree-Fock ground states in nuclear matter. He suggested that this difficulty may be removed by replacing the three-body force by the density-dependent force (which is more stable).

However, there are some drawbacks of the density-dependent interactions. Stone and Reinhard [73] and many others have argued that density-dependent interactions may lead to some inconsistencies since the variationally derived two-body interaction is not identical to the initially given interaction from which the energy was computed as expectation value. What is done in practice, is to compute the total energy as expectation value of the interaction first and then derive the HF equations and solve them using the standard variational procedure. This is precisely the concept of an effective EDF. The EDF concept is currently employed in nuclear physics. It has some common points and several differences with the density functional theory (DFT) concept, used in solid-state physics and in chemistry.

3.4 DFT

The DFT model is a powerful tool that greatly extends the range of applicability of many-body calculations by allowing to treat large systems in a simple self-consistent manner. It also provides a useful balance between accuracy and computational cost. In DFT, the particle density function $\rho(r)$ plays a central role rather than the many-body wave function. Indeed, in 1964, Hohenberg and Kohn proved that the total energy of a many-fermion system is a universal density functional of the local density distribution $\rho(r)$. This local density is a simple quantity which depends on a spatial coordinate only, has a clear physical meaning, and can be measured experimentally.

3.4.1 Hohenberg-Kohn theorems

The first theorem of Hohenberg and Kohn states that the ground state density $\rho(r)$ of a bound system of interacting particles in some external potential $v(r)$ determines this potential uniquely up to an additive constant. Consequently, it provides the ground-state wave function Ψ_0 [74].
This means that the knowledge of the ground-state density for any system uniquely determines the system. In other words, the ground state Ψ_0 is a functional of the density ρ_0 and consequently all the observables associated to Ψ_0 are a functional of ρ_0.
According to this theorem, for each system in an external potential $v(r)$, there exists an energy functional $E[\rho(r)]$ which is minimized by ρ_0 and thus by Ψ_0. This means that the ground-state energy is equal to $E_0 = E[\rho_0]$.
The second theorem states that for a density ρ that is different from the ground-state density ρ_0, the associated wave function Ψ is different from the ground-state wave function Ψ_0 and the energy density functional $E[\rho]$ is lower bounded by E_0.
In other words, given a density ρ_0 such that $\rho \neq \rho_0$, $\Longrightarrow E[\rho] \geq E[\rho_0] = E_0$.
Based on the Hohenberg-Kohn theorems, the Kohn-Sham equations have been derived to solve the many-body problem [75].

3.5 The EDF model in nuclear physics

The DFT concepts cannot be applied directly to nuclei because nuclei are self-bound systems. The basic theorems of DFT are demonstrated for many-body systems in an external potential. The nuclear EDF remains the only microscopic method that can be applied across the entire table of nuclides [76, 77]. It can be formulated in terms of low-energy effective theories in which high-energy effects are taken into account through the adjustment of parameters [78]. One of the goals of the EDF theory is to gather together the current phenomenological models of nuclear structure and reactions to lead to a well-founded microscopic theory with a maximum predictive power [79]. However, besides this great success, the EDF theory suffers from various deficiencies. For example, existing nuclear functionals remain rather poorly constrained with limited predictive power when extrapolating nuclear masses away

from the regions where experimental data are available [76]. A lot of efforts have recently been devoted to implementations of this aspect [80].
From a DFT- like point of view, the challenges by the EDF roadmap are three-fold:

1. Which mathematical form $E = E(\rho)$ should an energy functional take, so that it can provide a correct description of the system in its ground state?
   Let us write the functional as the sum of the kinetic energy part estimated with a Slater determinant and a term that corresponds to the contribution from the potential:

   $$E(\rho) = E_{kin}(\rho) + E_{pot}(\rho).$$

   What would be the expression of $E_{pot}(\rho)$? Is it a polynomial expansion in powers of the density ρ? $E_{pot}(\rho) = a_1\rho + a_2\rho^2 + \cdots$.

2. Given the mathematical form, how can one optimize the functional parameters to a set of experimental data, or to some reference curves or both?

3. How can one compute the properties of all atomic nuclei within a reasonable timescale and with a high predictive power?

3.5.1 Skyrme functional

Historically, the first nuclear energy density functional appeared in the context of the mean-field with Skyrme zero-range, density-dependent interactions. The Skyrme functional depends on densities and currents (and their derivatives) representing distributions of nucleonic matter, spins, momentum, and kinetic energy. By using the standard form of the Skyrme interaction, Eq. (3.2), the total binding energy can be expressed using a Hamiltonian density functional $\mathcal{H}(r)$:

$$E = \langle\Psi|H(\rho)|\Psi\rangle = \int \mathcal{H}(r)d^3r.$$

The density functional $\mathcal{H}(r)$, can be splitted into a sum of terms associated to the different parts of the force:

$$\mathcal{H} = \mathcal{K} + \mathcal{H}_0 + \mathcal{H}_3 + \mathcal{H}_{eff} + \mathcal{H}_{fin} + \mathcal{H}_{so} + \mathcal{H}_{sg} + \mathcal{H}_{Coul},$$

where $\mathcal{K} = \frac{\hbar^2}{2m}\tau$ comes from the kinetic energy term, $\mathcal{H}_0$ from the zero-range term, $\mathcal{H}_3$ from the density-dependent term, $\mathcal{H}_{eff}$ is an effective-mass term, $\mathcal{H}_{fin}$ comes from the velocity-dependent terms, $\mathcal{H}_{so}$ is related to the spin-orbit term and $\mathcal{H}_{sg}$ is a term due to the tensor coupling with spin and gradient. To specify the notation used, let us write the analytical

expressions for those terms:

$$\begin{aligned}
\mathcal{H}_0 &= \frac{1}{4}t_0\left[(2+x_0)\rho^2-(2x_0+1)(\rho_p^2+\rho_n^2)\right];\\
\mathcal{H}_3 &= \frac{1}{24}t_3\rho^\alpha\left[(2+x_3)\rho^2-(2x_3+1)(\rho_p^2+\rho_n^2)\right];\\
\mathcal{H}_{eff} &= \frac{1}{8}\left[(2+x_1)t_1+(2+x_2)t_2\right]\rho\tau+\frac{1}{8}\left[(1+2x_2)t_2-(1+2x_1)t_1\right](\rho_p\tau_p+\rho_n\tau_n);\\
\mathcal{H}_{fin} &= \frac{1}{32}\left[3(2+x_1)t_1-(2+x_2)t_2\right](\nabla\rho)^2+\frac{1}{32}\left[(1+2x_2)t_2-3(1+2x_1)t_1\right]\left[(\nabla\rho_p)^2+(\nabla\rho_n)^2\right];\\
\mathcal{H}_{so} &= \frac{1}{2}W_0\left[J\cdot\nabla\rho+J_p\cdot\nabla\rho_p+J_n\cdot\nabla\rho_n\right];\\
\mathcal{H}_{sg} &= -\frac{1}{16}\left[t_1x_1+t_2x_2\right]J^2+\frac{1}{16}\left[t_1-t_2\right](J_p^2+J_n^2).
\end{aligned}$$

The densities ρ, τ and J are defined in terms of the corresponding densities for protons and neutrons. i.e. $\rho=\rho_p+\rho_n$, $\tau=\tau_p+\tau_n$ and $J=J_p+J_n$.
If we identify the isospin label ($q=n,\ p$), then the corresponding matter, kinetic and spin densities are given by, respectively :

$$\begin{aligned}
\rho_q(r) &= \sum_{i,s}|\phi_i^q(r,s)|^2n_i^q,\\
\tau_q(r) &= \sum_{i,s}|\nabla\phi_i^q(r,s)|^2n_i^q,\\
J_q(r) &= \sum_{i,s,s'}\phi_i^{q*}(r,s')\nabla\phi_i^q(r,s)\times\langle s'|\sigma|s\rangle n_i^q,
\end{aligned}$$

where $\phi_i^q(r,s)$ and n_i^q are the single-particle wave function and the occupation number of the corresponding state with orbital, spin and isospin quantum numbers, i, s and q respectively. The Coulomb term $\mathcal{H}_{Coul}$ represents the finite-range Coulomb interaction between protons. A local-density approximation called the Slater approximation [14, 81, 82] is after used for expressing the Coulomb exchange contribution to the total energy. This contribution to the HF energy may be written as:

$$E_C^{ex}=-\frac{3e^2}{4}\left(\frac{3}{\pi}\right)^{\frac{1}{3}}\int\ \rho_p^{\frac{4}{3}}(r)d^3r,$$

where e is the elementary electric charge carried by a single proton, $e=1.602\times10^{-19}$ C (Coulomb). Since the Coulomb interaction does not have any effect in infinite nuclear matter, the accuracy of the Slater approximation has to be checked in finite nuclei. In 1974, Titin-Schnaider and Quentin [83] have checked this approximation in nuclear HF calculations and they found it rather good. In the EDF framework, the one-body Coulomb contribution is also written as a functional of the proton density as:

$$\mathcal{H}_{Coul}(r)=\frac{e^2}{2}\rho_p(r)\int\ \frac{\rho_p(r')}{|r-r'|}d^3r'-\frac{3e^2}{4}\left(\frac{3}{\pi}\right)^{\frac{1}{3}}\rho_p^{\frac{4}{3}}(r).$$

It has to be noted that some authors define the Coulomb potential by using the charge density, whereas most Skyrme interactions have been fitted by considering the point-proton density.

3.6 Infinite nuclear matter

Let us say some words about nuclear matter because we are going to present several applications done to matter. Infinite nuclear matter is an ideal system composed of nucleons and characterized by a fixed ratio of neutron to proton number, also defined by the isospin asymmetry factor $\delta = \frac{N-Z}{A}$. By construction, it possesses many properties:

1. It is a homogeneous medium with constant density ρ;
2. It is an infinite medium, i.e., without surface effects;
3. It is translational invariant, i.e., the wave functions are plane waves;
4. It does not have Coulomb interaction between protons.

In a sense, nuclear matter can be thought as a very large nucleus and, even though nuclear matter itself is not present in the universe, one expects it to describe qualitatively the interior of heavy nuclei and some regions of neutron stars [84]. Indeed, there are some properties of nuclear matter which are well known from the nuclear physics phenomenology.
In infinite nuclear matter, there are several fundamental properties, for instance, the binding energy per nucleon E/A at the saturation density ρ_0, the compression modulus or the incompressibility K_∞ (that determines the stellar evolution and supernova explosion in the extra terrestrial domain, and is related to the monopole excitation modes in nuclei), and the symmetry energy. Although these properties cannot be measured directly, they can be be extracted in a consistent manner from the properties of finite nuclei through appropriate models.

3.6.1 Saturation density

It is found that the central density of heavy nuclei corresponds to the saturation density of nuclear matter, independently of the nucleus. This feature is due to the saturation properties of the nuclear interaction that are generated by the combination of the Pauli and the uncertainty principles [85]. For example, C. S. Wang et al. [86] calculated the nuclear central density from the nuclear charge-density parameters measured by elastic electron scattering and muonic atom spectroscopy. By using many data, the authors extracted a value for the nuclear matter density ρ_0 equal to 0.1607 fm^{-3} and an A dependence for the central density of finite nuclei. In general, one can assume the following saturation properties of nuclear matter [87]: $\rho_0 = 0.16 \pm 0.002$ fm^{-3} and $E/A(\rho_0) = -16.0 \pm 0.2$ MeV.

3.6.2 Incompressibility

As we have already mentioned, the nuclear incompressibility contains important information about the EoS of nuclear matter. It is related to the curvature of the EoS and it may be constrained from experiments. The nuclear compressibility plays an important role in the static and dynamical description of nuclei, supernovae explosions (the strength of the shock wave), neutron stars, and heavy ion collisions. There are several procedures to extract its value from the properties of finite nuclei [84]. Two methods for its determination from experiment have been followed in this regard:

1. A semi-empirical macroscopic approach, based on a liquid-drop model approach. The compression modulus K_∞ of a nucleus is extracted from its finite nuclear value K_A [88, 89]:
$$K_A = K_v + K_s A^{-1/3} + K_c A^{-2/3} + K_{Cou} Z^2 A^{-4/3} + K_\delta \delta^2,$$
where δ is the asymmetry factor.
The nuclear breathing mode or isoscalar giant monopole resonance (GMR) determines the finite nuclear compression modulus K_A. By making an adjustment, the volume coefficient K_v is extracted and is identified with K_∞. However, the macroscopic approach presents several ambiguities because the formula is based on the assumption that the breathing mode is a small amplitude vibration.

2. A microscopic approach based on the calculations of the GMR in the framework of the HF plus the RPA methods with a series of effective interactions for many finite nuclei. Following the microscopic approach, Blaizot [90] was able to extract the value of the nuclear compressibility $K_\infty = 210 \pm 30$ MeV using the GMR data of the two closed-shell nuclei ^{40}Ca and ^{208}Pb. More recently, several studies have been performed to better understand and constrain the nuclear incompressibility (see for instance, Ref. [91]). We mention for example a work where the effect of pairing on the incompressibility has been analyzed [92].

3.6.3 Symmetry energy

Another important quantity that encodes useful information about the EoS of nuclear matter is the symmetry energy. The nuclear symmetry energy a_I is defined as the coefficient of the leading term of isospin asymmetry parameter δ, in the expression of the EoS of asymmetric nuclear matter:
$$a_I = \frac{1}{2}\frac{\partial^2}{\partial \delta^2}\left[\frac{E}{A}(\rho)\right].$$

1. The determination of the symmetry energy a_I is considered as a key objective of nuclear physics to understand for example dense matter in neutron stars.

2. It constrains the nuclear force on the neutron-proton asymmetry in a nuclear system. Its slope at saturation density provides the dominant baryonic contribution to the pressure in neutron stars [93].

3. It reduces the nuclear binding energy in nuclei and is critical for understanding properties of nuclei including the existence of rare isotopes with extreme proton to neutron ratios [94].

From their analysis of experimental data, Möller, Myers and Swiatecki [95] provided the following value for this coefficient:

$$a_I = 32.05 \pm 0.5 \quad \text{MeV}.$$

3.6.4 EoS in infinite nuclear matter

The knowledge of the EoS is one of the fundamental goals in nuclear physics which has not yet been fully achieved [96]. The EoS represents an important ingredient for modeling heavy ion collisions, at intermediate and relativistic energies. Moreover, it may play an important role in the structure of neutron stars, supernova explosions, neutrino-matter dynamics [96, 97, 98]. It can be computed by means of many-body theories, for example, using effective density-dependent interactions, such as the Skyrme forces [99]. The nuclear EoS, which is the energy per nucleon E/A of nuclear matter as a function of nucleonic density ρ, can be used to obtain the properties of nuclear matter such as the nuclear incompressibility, the symmetry energy, the pressure, the velocity of sound in the nuclear medium [87, 100].

3.6.4.1 Symmetric nuclear matter

The EoS of nuclear matter is considered as an important ingredient in the study of properties of nuclei at and far from stability and structures of compact astrophysical objects, such as neutron stars and core-collapse supernovae.
An example of infinite nuclear matter is the symmetric nuclear matter which is characterized by an equal number of protons and neutrons ($N = Z$ or $\delta = 0$). The scalar and kinetic densities of nucleons can be expressed as function of the total density ρ according to: $\rho_p = \rho_n = \rho/2 \quad$ and $\quad \tau_n = \tau_p = \tau/2$.
Therefore all quantities containing gradients are equal to zero and as a consequence, only $\mathcal{H}_0$, $\mathcal{H}_3$ and $\mathcal{H}_{eff}$ do not cancel out. To treat infinite systems, we consider a Slater determinant occupying lowest momentum up to k_F with periodic boundary condition. In this case, $\mathcal{H}(r) = \mathcal{H}$ becomes independent of r.
For a zero-range Skyrme force (3.2), the density functional gives the following energy per nucleon for symmetric nuclear matter:

$$\frac{E}{A}(\rho) = \frac{3\hbar^2}{10m}\left(\frac{3\pi^2}{2}\rho\right)^{\frac{2}{3}} + \frac{3}{8}t_0\rho + \frac{1}{16}t_3\rho^{\alpha+1} + \frac{3}{80}\left(\frac{3\pi^2}{2}\right)^{\frac{2}{3}}\rho^{\frac{5}{3}}\Theta_s,$$

where the coefficient Θ_s is expressed as a combination of parameters: $\Theta_s = 3t_1 + t_2(5 + 4x_2)$.
In Fig. 3.1, we show as an illustration the EoS for symmetric nuclear matter as a function of the total density ρ using the SLy5 parametrization [100].
The pressure in the nuclear fluid is related to the first derivative of the energy per particle

with respect to the density ρ: $P = \rho \frac{\partial \frac{E}{A}(\rho)}{\partial \rho}$. This pressure, which must be equal to zero at the saturation point, is given by:

$$P(\rho) = \rho \left[\frac{\hbar^2}{5m} \left(\frac{3\pi^2}{2} \rho \right)^{\frac{2}{3}} + \frac{3}{8} t_0 \rho + \frac{1}{16} (\alpha + 1) t_3 \rho^{\alpha+1} + \frac{1}{16} \left(\frac{3\pi^2}{2} \right)^{\frac{2}{3}} \rho^{\frac{5}{3}} \Theta_s \right]. \tag{3.3}$$

At saturation, the incompressibility coefficient K_∞ is defined as the second derivative of the energy per particle with respect to the density ρ at the equilibrium density ρ_0:

$$K_\infty = 9\rho_0^2 \frac{\partial^2}{\partial^2 \rho} \left[\frac{E}{A}(\rho) \right] \Bigg|_{\rho=\rho_0}.$$

At saturation, the incompressibility coefficient K_∞ can be written with the Skyrme force as:

$$K_\infty = 9\rho_0^2 \frac{\partial^2}{\partial^2 \rho} \left[\frac{E}{A}(\rho) \right] |_{\rho=\rho_0} = \frac{-3\hbar^2}{5m} \left(\frac{3\pi^2}{2} \rho \right)^{\frac{2}{3}} + \frac{9}{16} \alpha (\alpha + 1) t_3 \rho^{\alpha+1} + \frac{3}{8} \left(\frac{3\pi^2}{2} \right)^{\frac{2}{3}} \rho^{\frac{5}{3}} \Theta_s. \tag{3.4}$$

Finally, the isoscalar effective mass is written as:

$$\frac{m^*}{m} = \left(1 + \frac{1}{8} \frac{m}{\hbar^2} \rho_0 \Theta_s \right)^{-1}.$$

It has to be noted that the effective mass m^* is different from the bare mass m because the nucleons are interacting inside the nuclear medium. The empirical accepted value for the effective mass is $m^*/m = 0.8 \rightarrow 0.9$.

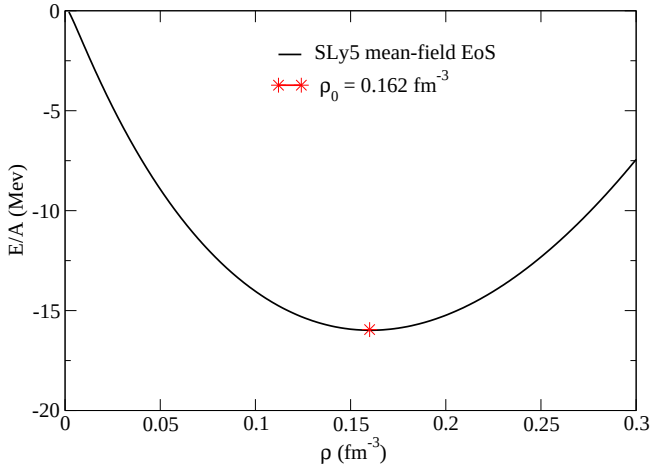

Figure 3.1: Mean-field EoS for symmetric nuclear matter with the SLy5 parametrization.

3.6.4.2 Asymmetric nuclear matter

The EoS of isospin asymmetric nuclear matter has a great interest in the investigations of exotic nuclei, supernovae and properties of neutron stars and other interesting topics in nuclear physics and astrophysics. The study of asymmetric nuclear matter represents one of the first steps for a microscopic theory of the structure of nuclei far from the valley of beta stability.
However, our knowledge on asymmetric nuclear matter is very limited because of our inadequate understanding of the symmetry energy [101], unlike the EoS of symmetric nuclear matter which has been determined over a wider range of densities [101].
The Skyrme EoS for asymmetric nuclear matter associated with the standard form of Skyrme interaction, (3.2), may be written as a function of the total density ρ and the isospin asymmetry parameter δ:

$$\begin{aligned}\frac{E}{A}(\delta,\rho) &= \frac{3\hbar^2}{10m}\left(\frac{3\pi^2}{2}\rho\right)^{\frac{2}{3}} G_{5/3} + \frac{t_0}{8}\rho[2(2+x_0)-(1+2x_0)G_2] + \frac{t_3}{48}\rho^{\alpha+1}[2(2+x_3)-(1+2x_3)G_2] \\ &+\frac{3}{40}\left(\frac{3\pi^2}{2}\right)^{\frac{2}{3}}\rho^{\frac{5}{3}}\left[\Theta_v G_{5/3}+\frac{1}{2}(\Theta_s-2\Theta_v)G_{8/3}\right], \end{aligned} \tag{3.5}$$

where G_β is given by

$$G_\beta = \frac{1}{2}\left[(1+\delta)^\beta + (1-\delta)^\beta\right],$$

and Θ_v is given in terms of the parameters of the nuclear Skyrme interaction:

$$\Theta_v = t_1(2+x_1) + t_2(2+x_2).$$

Moreover, the nuclear symmetry energy is expressed as a function of the total density ρ as:

$$a_I = \frac{1}{2}\frac{d^2}{d\delta^2}\left[\frac{E}{A}(\rho,\delta)\right]\Bigg|_{\delta=0}.$$

Consequently, using Eq. (3.5), one can write the Skyrme symmetry energy as follows:

$$a_I(\rho) = \frac{\hbar^2}{6m}\left(\frac{3\pi^2}{2}\rho\right)^{\frac{2}{3}} - \frac{1}{8}t_0\rho\left(2x_0+1\right) - \frac{1}{48}t_3\rho^{\alpha+1}\left(2x_3+1\right) - \frac{1}{24}\left(\frac{3\pi^2}{2}\right)^{\frac{2}{3}}\rho^{\frac{5}{3}}\left(3\Theta_v-2\Theta_s\right).$$

In Fig. 3.2, we show an example of EoS for asymmetric nuclear matter as a function of the total density ρ using the SLy5 parametrization.

3.6.4.3 Pure neutron matter

The investigations of the EoS for highly isospin asymmetric nuclear matter (or neutron-rich nuclear matter) can be done in nuclei far from the stability line and in the surface regions of nuclei exhibiting neutron skins (this provides information about low-density asymmetric

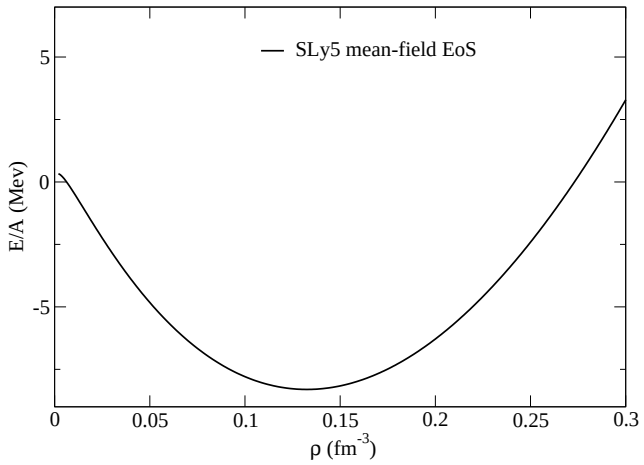

Figure 3.2: Mean-field EoS for asymmetric nuclear matter ($\delta = 0.5$) with the SLy5 parametrization.

matter). Pure neutron matter is an extreme case where only neutrons are present. It is very important for the studies of the properties of neutron stars [102].
The EoS of pure neutron matter is obtained from the EoS of asymmetric nuclear matter by setting the isospin asymmetry parameter $\delta = 1$. Starting from Eq. (3.5), the energy density functional gives the following energy per nucleon for pure neutron matter with a zero-range Skyrme force (3.2):

$$\frac{E}{A}(\rho) = \frac{3\hbar^2}{10m}\left(3\pi^2\rho\right)^{\frac{2}{3}} + \frac{1}{4}t_0\rho[1-x_0] + \frac{1}{24}t_3\rho^{\alpha+1}[1-x_3] + \frac{3}{40}\left(3\pi^2\right)^{\frac{2}{3}}\rho^{\frac{5}{3}}(\Theta_s - \Theta_v).$$

It has to be noted that the EoS of pure neutron matter is always positive. Moreover, the neutron matter does not have a saturation region unlike the case of symmetric nuclear matter. In Fig. 3.3, we show the EoS for pure neutron matter as a function of the total density ρ using the SLy5 parametrization.

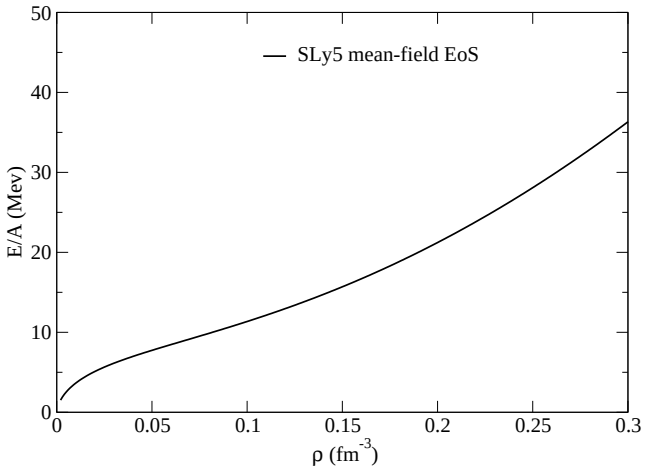

Figure 3.3: Mean-field EoS for pure neutron matter with the SLy5 parametrization.

Chapter 4

Higher-order corrections beyond the mean-field level

4.1 Introduction

The SCMF approaches provide the lowest-order nuclear binding energies and successfully reproduce the nuclear bulk properties throughout the chart of nuclei, especially for medium mass and heavy nuclei. For example, such models reproduce with a remarkable accuracy [14, 45, 103, 104] the nuclear masses (total energies) using the HFB method. Although the SCMF models are microscopic systematic approaches to study the ground and excited states of medium mass and heavy nuclei, it is known, for example, that the spectroscopic factors and the fragmentation of the single-particle states are not well reproduced. A possible way to overcome this limitation is to go beyond the mean-field level and consider correlations to better describe nuclear observables, achieve a higher precision and increase the predictive power of the models in exotic regions of the nuclear chart.

4.2 Beyond-mean-field approaches. Some examples

In the domain of the many-body nuclear physics, there are various methods to include correlations in order to achieve higher precision and better describe nuclear properties. We provide below some examples of theories and procedures that can be formulated to go beyond the mean-field approximation.

4.2.1 Particle-vibration coupling

The fluctuations of the mean-field nuclear potential associated with the collective vibrations provide a coupling between the vibrational degrees of freedom and those of the individual particles [105]. This coupling is called the PVC in spherical nuclei or particle-rotation coupling in deformed systems.
The PVC in nuclear physics is analogous to the coupling models employed in condensed

matter and atomic physics, for example, the electron-phonon coupling in metals [106] and the particle-phonon coupling in $^3\mathrm{He} - {}^4\mathrm{He}$ mixtures [107].
By including such couplings, the average nuclear potential acquires a dynamical content and it becomes nonlocal in time or energy-dependent [108, 109]. This dynamical part of the mean-field potential that arises from the vibrational coupling is a correction to the self energy and denoted by $\Sigma(\omega)$ where ω represents the frequency.
Calculations of PVC have been performed for many decades by using the nonrelativistic Skyrme Hamiltonian [108, 109, 110, 111] or the relativistic mean-field (RMF) Lagrangians [112, 113].
Following the non-relativistic formalism, Coló et al. perform the PVC calculations [111] by using the second-order perturbation theory. They express the corrected (dressed) single-particle energy of the state i in terms of the unperturbed HF energy and the self-energy $\Sigma(\omega)$ as follows:

$$\epsilon_i = \epsilon_i^{(0)} + \Sigma_i(\omega = \epsilon_i^{(0)}).$$

In this approach, the single-particle properties of the system are associated with the single-particle Green's function, which is a solution of the Dyson equation including the self-energy. For more details, see Chapter 7.
In this way, one may be able to describe the fragmentation and the related spectroscopic factors of the single-particle states, their density (which is proportional to the effective mass $m^\star$ near the Fermi energy), and the imaginary component of the optical potential [110, 114].

4.2.2 The generator coordinate method

The generator coordinate method (GCM) [35, 87, 115, 116, 117, 118, 119] is one of the methods to go beyond the mean-field approximation by including correlations that arise in nuclei. The GCM is a very powerful and successful variational quantum method used to describe microscopically large amplitude collective motion such as vibrations, shape co-existence and shape transitions, and the restoration of symmetries. The GCM has many attractive features:

1. It extends the configuration-mixing formalism to the case of a continuous collective variable, that is the generating coordinate.

2. Its basic idea is to do a linear superposition of mean-field wave functions that are optimized variationally.

3. It accounts for long-range ground-state correlations and provides excitation spectra and matrix elements that are successfully compared with data.

4. An example of GCM is the angular momentum projected GCM that uses the quadrupole moment as generating coordinate.

4.2.3 Projection methods

The SCMF wave function breaks several symmetries of the nuclear Hamiltonian, for example, the translational and rotational invariance. A superposition of wave functions should be done in order to restore the symmetry. Projection methods are a special case of the GCM. There are many projection methods, for example, the particle number projection: The violation of the particle-number in the BCS wave function is a good example of symmetry violation that can be treated by projection methods. It can be formulated for density-dependent forces like Skyrme and Gogny forces [50, 51, 115, 120, 121].
Several problems have been discussed in the last decade related to some inconsistencies of the usually employed projection methods [51]. These problems may lead to divergences and irregularities as well be discussed later.

4.2.4 Variational multiparticle-multihole configuration mixing

The multiparticle-multihole (mp-mh) configuration mixing [122, 123, 124] is a variational method that is used to describe pairing correlations as well as other kinds of long-range correlations such as those associated with collective vibrations. In this approach:

1. The wave function is assumed to be a superposition of a finite set of Slater determinants which includes a HF-type state together with multiple particle-hole excitations of this state.

2. The configuration mixing coefficients and the single-particle states are determined in a self-consistent way.

3. The mp-mh approach preserves the particle number and never violates the Pauli principle in contrary to the RPA and quasi particle RPA methods.

4. This method is a kind of mixing of mean-field concepts and shell-model procedures.

4.2.5 Second RPA

The second RPA [125, 126, 127, 128, 129] is a natural extension of RPA where the 2 particle - 2 hole excitations are included together with the usual RPA 1 particle - 1 hole configurations providing in this way a richer description of the excitation modes. This method also allows one to describe the fragmentation and the width of the excited states.

4.2.6 Extensions of RPA

There are various methods dealing with correlations that are explicitly included in the ground state. Several extensions of RPA are based on the introduction of an explicitly correlated ground state with occupation numbers different from 1 (hole states) and 0 (particle states). This formulation cures the violation of the Pauli principle that characterizes the RPA theory.

Several examples of RPA extensions have been discussed in the past decades (see, e.g., [128] and references therein).

4.3 Conceptual problems

It has been already mentioned that one of the reasons to go beyond the mean-field level is to better describe and reproduce nuclear observables. However, there are some subtle conceptual problems when computing long- and short-range correlations in this framework: for example, problems of double counting, of irregularities and of UV divergences.

4.3.1 The problem of double counting

The first question that one should address before adding correlations is: What are the many-body correlations that are already effectively included implicitly in the mean-field approach? In fact, the energy functionals that we use are specially designed for SCMF calculations. Since the parameters are adjusted to reproduce observables, the functionals certainly contain in an implicit way various correlation effects. Using these functionals to compute correlations in beyond SCMF methods looks like double counting because certain correlations will be overtaken into account [130].

4.3.2 The problem of irregularities

It is clear that, when going beyond the mean-field approximation by including correlations, one gets an improved description of a many-body system. Some ways to go beyond the mean-field approximation have been discussed in the previous section.
It has been noticed that the particle-number projection technique might exhibit divergences [51, 131, 132] and finite steps [133] whenever a single-particle level crosses the Fermi energy as a function of a collective coordinate. This problem is particular to energy density functionals but absent in approaches based on the use of a genuine Hamiltonian and a correlated wave function [48]. As pointed out by Anguiano et al. in Refs. [51, 132], the exchange terms are considered important and their neglection leads to divergences. The authors showed that as long as all terms are taken into account and exactly the same terms are used in the mean-field and in the pairing channel, no divergences appear in the particle-number projection. Later, Lacorix et al. [48, 49] pointed out that problematic terms are still present if one uses a density-dependent two-body force under the form of a noninteger power of the density matrix. They proposed a regularization method [50] that enables to remove the divergent terms from the energy density functional. This procedure applies to any symmetry-restoration- and/or generator-coordinate-method-based configuration mixing calculation.

4.3.3 The problem of the UV divergences

The UV divergences appear in perturbative quantum field theory (QFT) [134] and in simple quantum mechanical models, as well as in nuclear and in atomic physics. UV divergences in QFT can be viewed as a consequence of writing the theory with local interactions imposed by the principles of relativity, unitarity, and causality. This generally leads to theories with UV divergences, such as quantum electrodynamics (QED). In the domain of nuclear physics, UV divergences may appear for instance when one uses models beyond the mean-field level with zero-range interactions. For example, UV divergences appears in the so-called Bogoliubov-de Gennes or HFB theories if a zero-range interaction is employed in the pairing channel to treat a superfluid many-fermion system [135, 136]. It was believed by many physicists, in the 1930s, that the fundamental principles of physics had to be changed in order to get rid of such divergences.
A major breakthrough occurred, in the late 1940s, when Bethe, Feynman, Schwinger, Tomonaga, Dyson, and other physicists proposed a program of "renormalization" that gave finite and physically meaningful results by absorbing the divergences into redefinitions of physical quantities. Moreover, in the 1970s, K. Wilson defined renormalization as nothing more than parameterizing the sensitivity of low-energy physics to high-energy physics [36, 52]. Due to the uncertainty principle, the high-energy virtual states will propagate over distances for a very-short time and consequently their effects on low-energy processes can be simulated by local interactions [36].

4.4 Regularization and renormalization schemes

In order to have a well-defined theory, one must modify the short-distance behavior (high-momentum) of the theory so that all the divergent momentum integrals become finite. This is called regularization. A regularization parameter is introduced so that all the divergences of the integrals appear as singularities in this parameter.
There are various possible regularization procedures: Momentum Cutoff (MC) Λ regularization [36], Pauli-Villars regularization [137], Zeta regularization [138] and the techniques of the DR [139].
Although the regulators have unphysical features at high momentum scales, it remains possible to extract the finite part of the regularized divergent integrals in such a way it has physical meaning. Moreover, physical observables are sensitive to physics at very short distances only through the values of renormalized coupling constants. This is what is called the renormalization group equation.

4.4.1 Momentum Cutoff Λ regularization

The general ideas underlying the MC Λ regularization [36] may be summarized as follows:

- A momentum cutoff Λ is introduced as an upper limit on the momentum of the intermediate virtual states. In other words, the states with momentum greater than

the cutoff Λ are discarded from the theory. The cut-off theory can then be used for processes involving momenta p smaller than Λ.

- A new set of local interactions is added in order to account for the discarded states. These interactions take the form of a polynomial of the fields and their derivatives. In nuclear physics and in the language of EFT, local interactions mean Dirac-delta interactions with their derivatives.

- It has to be noted that the structure of these local interactions does not depend on the details of the short-range dynamics. Only the numerical values of the coefficients of these interactions depend on the details of the short-range dynamics. These parameters are usually adjusted to experimental data.

- Power counting and dimensional analysis tell us that one needs only a few number of local interactions when working at a particular order in p/Λ, where p is a typical momentum of the process under study.

A drawback of the momentum cutoff Λ regularization is that it breaks symmetries like Lorentz and gauge invariance.

4.4.2 DR

The DR technique is an elegant and powerful tool of handling the divergences that arise in perturbation theory. The original formulation of DR is due to 't Hooft and Veltman [139] who invented this procedure in order to regularize non-abelian gauge theories where all previous cutoff methods failed.
There are several favorable qualities and attractive features of the DR technique that motivate physicists to use such regularization:

1. It respects gauge and Lorentz invariance unlike the MC regularization.

2. It is used by physicists because of its simplicity although the meaning of physics in a complex $d-$dimensional space-time is rather opaque.

3. It allows one an easy identification of the divergences as poles around the physical space-time dimension d.

4. It allows one to handle both UV and infrared divergences in the same manner. The latters appear in massless theories.

The basic idea behind DR is that we regularize the divergent integrals in such a way that the measure of integration d or the dimension of the physical space-time becomes an external parameter that can be varied in the complex plane $\mathbb{C}$. The analytic extrapolation to non-integer dimension will be based on the extrapolation of the factorial of integer numbers to real numbers by the Gamma function.
The regularized integrals become convergent and analytic in an interval d. This function

can be continued meromorphically to all $\mathbb{C}$. It can be proved that the UV divergences of Feynman graphs appear as poles at isolated values of the physical space-time dimension d [140, 141].
Finally, the finite part or the regularized value cannot depend on the employed regulator. It is obtained by introducing a subtraction scheme that controls the process of absorbing the regulator into the physical quantities.
Some of the more common subtraction schemes are: the MS, where one subtracts only the divergent parts that are proportional to powers of $\frac{1}{\epsilon}$ where $\epsilon = d_0 - d$ and $d_0 = 3$ or 4; the modified minimal subtraction ($\overline{MS}$), where one subtracts certain additional finite terms from the MS scheme, and the Power Divergent Subtraction (PDS) scheme.

4.4.2.1 DR with Minimial Subtraction Scheme

Over the years, field theorists invented several types of renormalization schemes. Since 40 years, the most popular schemes are the MS technique and its close cousin $\overline{MS}$. DR/MS and DR/$\overline{MS}$ have been widely used in quantum field theory and also in the domain of EFT for treating dilute Fermi systems in their normal ground state [52, 142]. The DR/MS scheme was constructed to subtract UV power divergences and takes care only of the logarithmic-type divergences. Here are the main steps for the MS scheme:

1. We introduce an auxiliary parameter μ, which is a renormalization scale, to make sure that the calculated observable has the correct physical dimensions:

$$\frac{d^3p}{(2\pi)^3} \longrightarrow \mu^{3-d}\frac{d^dp}{(2\pi)^d}.$$

2. The UV divergences of some $L-$loop integrals will be polynomials of degree-L in $1/\epsilon$ with $\epsilon = 3 - d$ as follows:

$$g^{2L}\left(\sum_{j=1}^{L}\frac{A_j}{\epsilon^j} + A_0 + f(p^2) + \mathcal{O}(\epsilon)\right), \tag{4.1}$$

   where g is the coupling strength and $A_j,\ j = 0, \cdots L$ are constants.

3. To cancel the divergences, we subtract the pole parts which are called the counter terms that appear in the Laurent expansion, Eq. (4.1). Therefore, we need a $L-$loop order counter term:

$$\delta_L g \propto g^{2L}\left(\sum_{j=1}^{L}\frac{A_j}{\epsilon^j}\right).$$

This is called MS because the minimum number of counter terms needed to do the renormalization procedure is the number of poles that exist for $\epsilon \to 0$. It has to be noted that the counter terms are completely determined by the UV divergence of the $L-$loop diagrams,

whereas the finite free term A_0 is not: it is produced by the renormalization scheme of the loop diagrams and the counter terms do not contribute to it.
There some disadvantages of using DR/MS:

1. DR/MS tends to produce some large coefficients in the perturbation expansion like $[\ln(4\pi) - \gamma_E] \sim 1.95$. Thus, it has become more conventional to use a modified scheme, called the $\overline{MS}$ scheme [143, 144]. The auxiliary parameter $\bar{\mu}$ of the $\overline{MS}$ scheme is given by:
$$\bar{\mu} = \mu\sqrt{4\pi\ e^{-\gamma_E}} \approx 2.63\mu.$$

2. The use of DR/MS can obfuscate the renormalization process because it subtracts automatically the power divergent parts.

4.4.2.2 DR with Power Divergence Subtraction Scheme

The PDS scheme, adopted for example by Kaplan, Savage, and Wise (KSW) [39], is a generalization of the DR/MS (the DR/MS scheme is recovered by taking $\mu = 0$). KSW introduced the PDS scheme to provide a consistent power counting in the two body-problem when the scattering length a_s is unnaturally large [145]. A key feature of the PDS renormalization scheme is that it keeps track of power divergences by giving to the coefficients of the contact interactions a power-law dependence on the renormalization scale. Therefore, one can verify that, by using PDS, the problem will be renormalized successfully up to a given order by observing the cancellation of μ between the couplings and loop integrals.
One disadvantage of the PDS scheme, is that the power counting is no longer clear for $\mu \geq$ 300 MeV, and KSW conclude that the application of the theory is restricted to momenta less than 300 MeV. An alternative solution for that problem is a momentum subtraction scheme proposed by Gegelia [146].

Chapter 5

The nuclear many-body problem and second-order corrections in nuclear matter. Results

5.1 Introduction

In Chapter 3, we have mentioned that SCMF models are widely employed to describe satisfactorily the nuclear bulk properties throughout the nuclear chart. Moreover, they are designed to analyze a large variety of many-body systems where an independent-particle picture can be adopted. Since these approaches provide the lowest-order nuclear binding energy [115], it would be very interesting to go beyond this approximation and introduce higher-order energy corrections in the nuclear many-body problem.

5.2 Why do we deal with $2^{nd}-$ order in nuclear matter?

An example of nuclear many-body theories in finite systems (for example spherical or deformed nuclei) is the previously mentioned PVC approach which is the model where the coupling between the individual and the collective degrees of freedom of the nucleons is taken into account. This is an example of beyond-mean-field models. In Chapter 4, we have learned that the inclusion of higher-order corrections may imply a double counting problem and UV divergences when a zero-range force is used. In particular, in the framework of PVC, we encounter the following problems:

1. Diagrams that are counted twice (second-order corrections) should be subtracted in order to get rid of this double counting.

2. Moreover, such diagrams diverge if a zero-range interaction is employed in such approach. Techniques to treat the UV divergences were introduced in Chapter 4.

3. When one uses phenomenological interactions that are adjusted at the mean-field level, the problem of the double counting of correlations (that are implicitly contained to some extent in the parameters) should be addressed.

Due to the complexity of nuclear systems, the nuclear many-body problem is extremely difficult and requires the use of approximations. Nuclear matter can be viewed as a trial system that allows one to achieve simplicity and analyticity. In the framework of my thesis, we have decided to study the nuclear many-body problem in nuclear matter as a preparatory work and a first step to treat afterward nuclei within the PVC approach. In this perspective, the many-body problem in nuclear matter is truncated at the second order in perturbation theory.

5.3 Second-order energy diagrams

The Green's function (or propagator) is defined as the expectation value of the Heisenberg field operators taken between the exact interacting ground-state [46]:

$$iG_{\alpha\beta}(x,y) = \frac{\langle\Phi_0|T\left[\hat{\psi}_{H\alpha}(x)\hat{\psi}^{\dagger}_{H\beta}(y)\right]|\Phi_0\rangle}{\langle\Phi_0|\Phi_0\rangle}, \tag{5.1}$$

where the labels α and β represent the component of the field operators and Φ_0 is the Heisenberg ground state in the interacting representation. We define the $T-$product as follows:

$$T\left[\hat{\psi}_{H\alpha}(x)\hat{\psi}^{\dagger}_{H\beta}(y)\right] = \begin{cases} \hat{\psi}_{H\alpha}(x)\hat{\psi}^{\dagger}_{H\beta}(y) & \text{if } t_x > t_y, \\ \pm\hat{\psi}^{\dagger}_{H\beta}(y)\hat{\psi}_{H\alpha}(x) & \text{if } t_x < t_y, \end{cases}$$

where $x = (\vec{x}, t_x)$ and $y = (\vec{y}, t_y)$. In the case $t_x < t_y$, the sign is + (-) for bosons (fermions). The Green's functions play a fundamental role in the treatment of the many-body problem because:

1. The Feynman rules for calculating the n^{th} order contribution in perturbation theory are simpler for Green's functions than for any other combination of field operators.

2. They allow us to evaluate the expectation value of any single-particle operator in the ground state, the ground-state energy of the system, the excitation spectrum of the system through the Lehmann representation [147].

3. All one-particle quantities of the system, such as the kinetic energy, may be computed from the one-particle Green's function;

4. From the two-particle Green's function we can compute the potential energy due to two-body forces, etc.

By using Wick's theorem [148], the exact expression of the Green's function derived from perturbation theory is given by:

$$iG_{\alpha\beta}(x,y) = \sum_{m=0}^{\infty} \left(\frac{-i}{\hbar}\right)^m \frac{1}{m!} \int_{-\infty}^{\infty} dt_1 \cdots dt_m \, \langle \Phi_0 | T \left[\hat{H}_1(t_1) \cdots \hat{H}_1(t_m) \hat{\psi}_\alpha(x) \hat{\psi}^\dagger_\beta(y) \right] | \Phi_0 \rangle_{connected},$$

where $\hat{H}_1$ denotes the interaction Hamiltonian and U is the interacting potential:

$$\hat{H}_1 = \frac{1}{2!} \sum_{\substack{\alpha\beta\alpha'\beta' \\ \gamma\mu\gamma'\mu'}} \int d^4r \, d^4r' \, \hat{\psi}^\dagger_{\alpha;\gamma}(\mathbf{r}) \hat{\psi}^\dagger_{\beta;\mu}(\mathbf{r}') U(r,r')_{\substack{\alpha\alpha',\beta\beta' \\ \gamma\gamma',\mu\mu'}} \hat{\psi}_{\beta';\mu'}(\mathbf{r}') \hat{\psi}_{\alpha';\gamma'}(\mathbf{r}). \tag{5.2}$$

The exact expression of the Green's function consists of the unperturbed Green's function G^0 plus all connected terms with a free Green's function G^0 at each end. The corresponding analytical expression is given by Dyson's equation [149]:

$$G_{\alpha\beta}(x,y) = G^0_{\alpha\beta}(x,y) + \sum_{\gamma\mu} \int d^4u \int d^4v \, G^0_{\alpha\gamma}(x,u) \Sigma(u,v)_{\gamma\mu} \, G^0_{\mu\beta}(v,y). \tag{5.3}$$

The general structure of the Green's function can be represented graphically by means of diagrams as shown in Fig. 5.1:

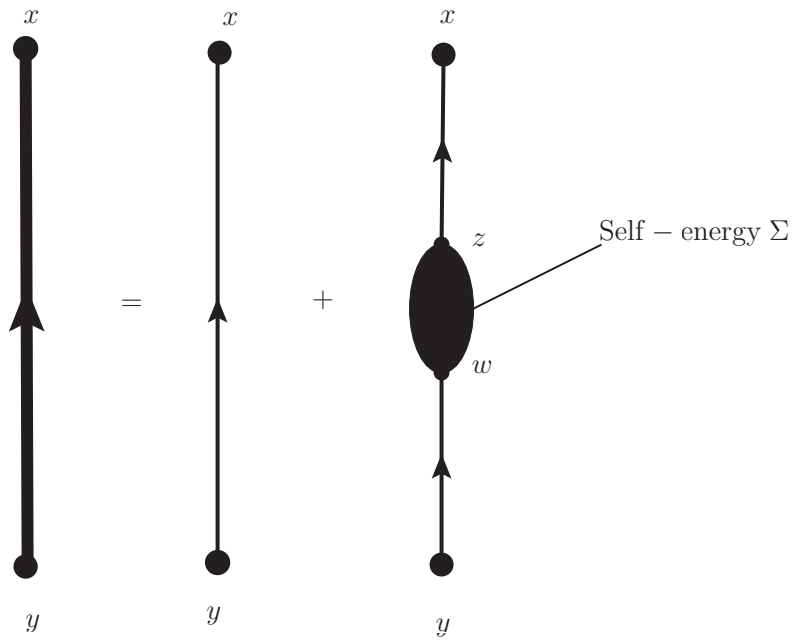

Figure 5.1: General structure of $G_{\alpha\beta}(x,y)$.

In Fig. 5.1, the thick lines represent G and the thin lines represent G^0. The term $\Sigma(u,v)_{\gamma\mu}$ in Eq. (5.3) is called the self-energy (a part of a diagram that is connected to the rest of the diagram by one line in and one line out).
The proper self-energy $\Sigma^\star$ is defined as a self-energy insertion that cannot be separated into two parts by cutting only a single-particle line. By using Σ^*, Eq. (5.3) becomes:

$$G_{\alpha\beta}(x,y) = G^0_{\alpha\beta}(x,y) + \int d^4z \int d^4w \; G^0_{\alpha\lambda}(x,z)\Sigma^*(z,w)_{\lambda\mu}G_{\mu\beta}(w,y). \tag{5.4}$$

The above equation can be represented graphically by means of diagrams as shown in the Fig. 5.2:

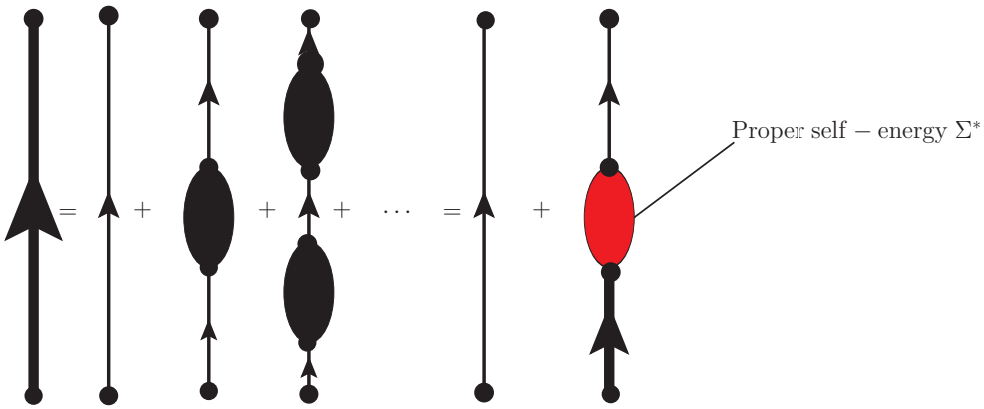

Figure 5.2: Dyson's equation for $G_{\alpha\beta}(x,y)$.

To lowest order the proper self-energy consists only of one direct and one exchange term, whose graphical representation is given by:

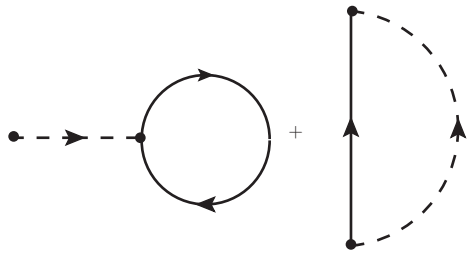

Figure 5.3: Direct (left) and exchange (right) first-order contributions to the proper self-energy Σ^*.

To obtain the the self-consistent proper self-energy in the Hartree-Fock approximation, one replaces the free Green's function by the exact Green's function as shown in Fig. 5.4.

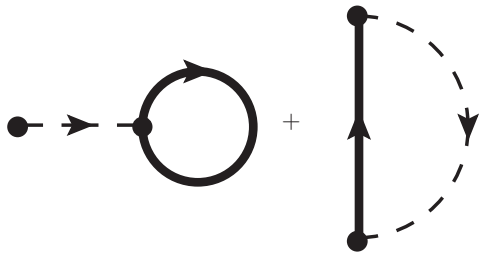

Figure 5.4: Self-consistent proper self-energy in the Hartree-Fock approximation.

The second-order proper self-energy $\Sigma^{(*2)}$ is represented by Fig. 5.5.

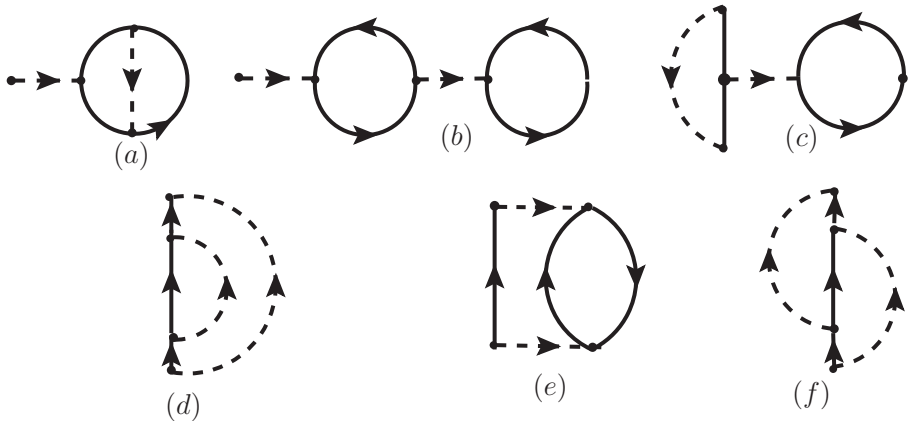

Figure 5.5: Second-order contributions to the proper self energy Σ^*.

5.3.1 Goldstone's theorem

The application of quantum field theory to the many-body problem was started by Goldstone in 1957 [150]. He proved the cancellation of the disconnected diagrams to all orders, and derived the following expression for the energy shift of the ground state:

$$E = E_0 + \langle\Phi_0|H_1 \sum_{n=0}^{\infty} \left(\frac{1}{E_0 - H_0} H_1\right)^n |\Phi_0\rangle_{connected}, \tag{5.5}$$

where E_0 is the energy of the unperturbed system and H_1 is the interacting Hamiltonian given in Eq. (5.2). The Goldstone's theorem was originally stimulated by Brueckner theory of strongly interacting Fermi systems [33]. It is an exact restatement (to all orders) of the

familiar time-independent perturbation expression for the ground-state energy:

$$E = E_0 + \langle\Phi_0|H_1|\Phi_0\rangle + \sum_{m\neq 0} \frac{\langle\Phi_0|H_1|\Phi_m\rangle\langle\Phi_m|H_1|\Phi_0\rangle}{E_0 - E_m} + \cdots .$$

In Appendices A and B, we make a proof of Goldstone's theorem and show that the only diagrams that contribute at the first and the second orders are shown in Fig. 5.6.

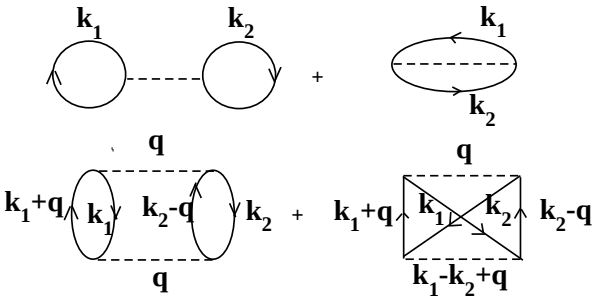

Figure 5.6: Direct (left) and exchange (right) first-order (upper line) and second-order (lower line) contributions to the total energy.

5.3.2 Remarks

In the PVC models, we introduce the coupling of a single-particle to particle-hole (p-h) vibrations of the core. The p-h vibrations will be described in the framework of RPA (see Chapter 7).
However, the use of RPA excitations or phonons to evaluate the graphs leads to problems of double counting in the self-energy and one has to subtract out the second-order contributions of Fig. 5.6 to obtain the correct counting:

$$\Sigma = \Sigma^{HF} + \Sigma^{RPA} - \Sigma^{(2)},$$

where Σ^{RPA} is represented by Fig. 5.7 (a) and (b) and $\Sigma^{(2)}$ is represented by Fig. 5.7 (c) and (d). Since our long-term objective is to cure the drawbacks of the PVC model, we first deal with the second-order contributions that have to be subtracted from the RPA contribution. Bertsch et al. [151] showed that the particle-particle (p-p) vibrations contribute much less than the p-h vibrations to the imaginary part of the self-energy, i.e., the damping widths of the excited states.

5.4 Second-order energy correction in nuclear matter

Since the nuclear many-body problem is very complicated, we are going to calculate the nuclear binding energy in nuclear matter using the Skyrme energy-density functional introduced in Sect. 3.5.1 because this functional simplifies the calculations and leads to elegant

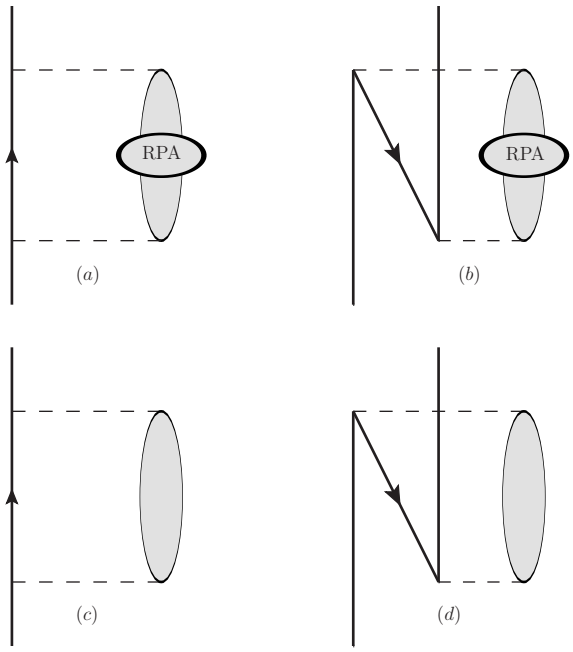

Figure 5.7: Processes contributing the self-energy. (a) and (b) particle-hole RPA contributions; (c) and (d) second-order contributions.

analytical expressions.
In this chapter, we are going to deal with the second-order energy corrections to the EoS in nuclear matter as an example to go beyond the mean-field approximation. First of all, we derive the EoS up to the second order of symmetric nuclear matter with the simplified Skyrme interaction known as $t_0 - t_3$ model. Then we extend our work to the full Skyrme interaction by including the velocity-dependent terms and to asymmetric matter. In all cases, a double counting problem arises at this level because the Skyrme parametrization was designed to be used at the mean-field level. For that reason, a readjustment of the Skyrme parameters is performed using a χ^2-minimization. Moreover, the UV divergences are visible at the second order and thus divergent integrals are regularized via the the cutoff scheme.
As a first step, we will restrict our study to the case of symmetric nuclear matter and use the simple contact force that is proportional to a $\delta-$ function without the velocity-dependent terms.

5.4.1 With the simplified $t_0 - t_3$ Skyrme model.

All the results presented in this subsection have been published in Ref. [9].
Let us define a phenomenological zero-range force characterized by two dimensional parameters t_0 (Mev fm^3) and t_3 (Mev fm$^{3+3\alpha}$) and one dimensionless parameter α:

$$V(\mathbf{r}_1, \mathbf{r}_2) = t_0\delta(\mathbf{r}_1 - \mathbf{r}_2) + \frac{t_3}{6}\rho^\alpha\delta(\mathbf{r}_1 - \mathbf{r}_2). \tag{5.6}$$

For simplicity, let us introduce the density-dependent field strength $g(\rho)$, defined by $g(\rho) = t_0 + \frac{t_3}{6}\rho^\alpha$. Consequently, our zero-range interaction becomes:

$$V(\mathbf{r}_1, \mathbf{r}_2) = g(\rho)\delta(\mathbf{r}_1 - \mathbf{r}_2).$$

This corresponds to the so-called $t_0 - t_3$ model. This model is a simplification of the usual Skyrme model where the spin-dependent, velocity-dependent, and spin-orbit terms are dropped. In next section, we are going to take into considerations some of these neglected terms.
After defining the zero-range phenomenological interaction, let us now go beyond the mean-field level by introducing the second-order energy correction in infinite nuclear matter. This second-order correction normalized within a box of volume Ω is given by (the corresponding direct and exchange diagrams are shown in the lower line of Fig. 5.6):

$$\Delta E = d\frac{\Omega^3}{(2\pi)^9}\int_{C_I} d^3\mathbf{q}\, d^3\mathbf{k}_1\, d^3\mathbf{k}_2\, \frac{V^2(\mathbf{q})}{\epsilon_{\mathbf{k}_1} + \epsilon_{\mathbf{k}_2} - \epsilon_{\mathbf{k}_1+\mathbf{q}} - \epsilon_{\mathbf{k}_2-\mathbf{q}}}. \tag{5.7}$$

The parameter d is expressed in terms of the level of degeneracy n as:

$$d = \frac{n^2 - n}{2}, \quad n = 4 \text{ in the case of symmetric nuclear matter.}$$

The term $V(\mathbf{q})$ is the momentum representation (i.e., the Fourier transform) of the zero-range force represented in coordinate space by Eq. (5.6). In other words, the expression of $V(\mathbf{q})$ in a box of volume Ω is given by:

$$V(\mathbf{q}) = \frac{g(\rho)}{\Omega}.$$

The domain of integration C_I represents the intersection of the inner region of a sphere of radius k_F (that represents hole states) where k_F is the Fermi momentum, and the outer region of another sphere of radius k_F (that represents particle states):

$$C_I = \begin{cases} |\mathbf{k}_1| < k_F, & |\mathbf{k}_1 + \mathbf{q}| > k_F \\ |\mathbf{k}_2| < k_F, & |\mathbf{k}_2 - \mathbf{q}| > k_F. \end{cases} \tag{5.8}$$

This means that $\mathbf{k}_1$ and $\mathbf{k}_2$ represent hole states whereas $\mathbf{k}_1 + \mathbf{q}$ and $\mathbf{k}_2 - \mathbf{q}$ represent particle states. Moreover, the terms that appear in the denominator of Eq. (5.7) are the non-relativistic energies for the nucleons and they are expressed in terms of the corresponding momenta and the effective mass m^*: $\epsilon_k = \frac{\hbar^2 k^2}{2m^*}$. By performing the following change of variables:

$$\mathbf{q} \to \frac{\mathbf{q}}{k_F}, \quad \mathbf{k}_1 \to \frac{\mathbf{k}_1}{k_F} \quad \text{and} \quad \mathbf{k}_2 \to \frac{\mathbf{k}_2}{k_F},$$

and using Shwinger's proper time representation, our propagator can be written as:

$$\frac{1}{\mathbf{q}^2 + \mathbf{q}\cdot(\mathbf{k}_1 - \mathbf{k}_2)} = \int_0^\infty d\alpha\, e^{-\alpha\left[\mathbf{q}^2 + \mathbf{q}\cdot(\mathbf{k}_1 - \mathbf{k}_2)\right]}.$$

The second-order energy correction in Eq. (5.7) becomes:

$$\Delta E \;=\; -d\frac{\Omega^3}{(2\pi)^9}\left(\frac{m^*}{\hbar^2}\right)k_F^7\int_{|\mathbf{q}|>0} d^3\mathbf{q}\; V^2(q)\; G(q), \tag{5.9}$$

where the expression of $G(|\mathbf{q}|)$ is given by:

$$G(|\mathbf{q}|) = \int_0^\infty d\alpha\; e^{-\alpha\mathbf{q}^2}\int_{\substack{|\mathbf{k}_1|<1\\ |\mathbf{k}_1+\mathbf{q}|>1}} d^3\mathbf{k}_1\; e^{-\alpha\mathbf{q}\cdot\mathbf{k}_1}\int_{\substack{|\mathbf{k}_2|<1\\ |\mathbf{k}_2-\mathbf{q}|>1}} d^3\mathbf{k}_2\; e^{\alpha\mathbf{q}\cdot\mathbf{k}_2}.$$

The last two integrals in the above expression are symmetric under the change of variable $\mathbf{k}_1 \to -\mathbf{k}_2$; hence, the expression of $G(|\mathbf{q}|)$ reduces to:

$$G(|\mathbf{q}|) = \int_0^\infty d\alpha\; e^{-\alpha\mathbf{q}^2}\left[\int_{\substack{|\mathbf{p}|<1\\ |\mathbf{p}+\mathbf{q}|>1}} d^3\mathbf{p}\; e^{-\alpha\mathbf{q}\cdot\mathbf{p}}\right]^2.$$

In order to calculate analytically the expression of $G(|\mathbf{q}|)$, one needs to set up the domain of integration. This domain can be splitted into two parts according to the values of $|\mathbf{q}|$:

1. **High-energy region ($|\mathbf{q}| > 2$):** In this region, the particle states can take arbitrarily large values of momenta from $2k_F$ up to infinity. This region contains the UV divergences due to the zero-range character of the interaction.
   In this case: for $|\mathbf{q}| > 2$, $|\mathbf{p}+\mathbf{q}| > 1$ is always satisfied whenever $|\mathbf{p}| < 1$. In other words, the domain of integration becomes: $(|\mathbf{q}| > 2) \cap (|\mathbf{p}+\mathbf{q}| > 1) \cap (|\mathbf{p}| < 1) = |\mathbf{p}| < 1$.
   In this region, the expression of $G(|\mathbf{q}|)$ reduces to:

   $$G(|\mathbf{q}|) = \int_0^\infty d\alpha\; e^{-\alpha\mathbf{q}^2}\left[\int_{|\mathbf{p}|<1} d^3\mathbf{p}\; e^{-\alpha\mathbf{q}\cdot\mathbf{p}}\right]^2.$$

   After introducing the polar coordinates in the second integral and performing the integration over α, one obtains an elegant closed form of $G(u)$ by taking $u = \frac{|\mathbf{q}|}{2}$ (see Appendix C):

   $$\begin{aligned} G\,(u) \;=\; & \frac{(2\pi)^2}{30u}[(4-20u^2-20u^3+4u^5)\log(u+1)+(-4+20u^2-20u^3+4u^5)\log(u-1) \\ & +22u+4u^3+(40u^3-8u^5)\log(u)]. \end{aligned}$$

2. **Low-energy region ($0 < |\mathbf{q}| < 2$):** In this region, there are no UV divergences because all the momenta are upper-bounded by the value of $2k_F$. In this case, all the momentum integrals are finite and convergent.
   To simplify the domain of integration, we will apply the techniques presented in Ref. [152], with the following change of variables $x = \hat{\mathbf{q}}\cdot\mathbf{n}$, where $\mathbf{n}$ is a unit vector $\mathbf{n} = \mathbf{p} + \alpha\mathbf{q}$:

   $$\int_{D(p)} d^3\mathbf{p}\; f(\mathbf{p},\mathbf{q}) = q\int_0^{2\pi} d\Phi\int_0^1 d\alpha\int_{q\alpha/2}^1 x\; f(\mathbf{n}-\alpha\mathbf{q},\mathbf{q})\; dx.$$

Let us use $D(\mathbf{p}) = (|\mathbf{p}| < 1) \cap (|\mathbf{p}+q| > 1)$ and $f(\mathbf{p},\mathbf{q}) = e^{-\alpha \mathbf{q}\cdot\vec{\mathbf{p}}}$; we have:

$$\int_{\substack{|\mathbf{p}|<1 \\ |\mathbf{p}+q|>1}} d^3\vec{\mathbf{p}}\; e^{-\alpha\vec{q}\cdot\vec{\mathbf{p}}} \;=\; 2\pi|q| \int_0^1 d\beta\; e^{\alpha\beta q^2} \int_{\frac{|q|\beta}{2}}^1 dx\; x\; e^{-\alpha|q|x}.$$

By performing an integration by parts to the last integral, we get:

$$\int_{\substack{|\mathbf{p}|<1 \\ |\mathbf{p}+q|>1}} d^3\vec{\mathbf{p}}\; e^{-\alpha\vec{q}\cdot\vec{\mathbf{p}}} \;=\; \frac{(2\pi)}{(\alpha|q|)^3}\left[\alpha q^2\; e^{\frac{\alpha q^2}{2}} + (1+\alpha|q|)\; e^{-\alpha|q|} - (1+\alpha|q|)\; e^{\alpha|q|(|q|-1)}\right].$$

After straight-forward calculations (see Appendix C), the expression of $G(u)$, with $u = \frac{|q|}{2}$, becomes:

$$\begin{aligned} G(u) \;=\; & \frac{(2\pi)^2}{30u}[(4+\frac{15}{2}u - 5u^3 + \frac{3}{2}u^5)\log(1+u) + (4 - \frac{15}{2} + 5u^3 - \frac{3}{2}u^5)\log(1-u) \\ & +29u^2 - 3u^4 - 40u^2\log 2]. \end{aligned}$$

Finally, the energy contributions due to the low- and high-energy regions can be summed up and we get:

$$\Delta E \;=\; -d\frac{\Omega^3}{(2\pi)^9}\left(\frac{m^*}{\hbar^2}\right) k_F^7 \left[\int_{|0<|\mathbf{q}|<2} d^3\mathbf{q}\; V^2(q)\; G(q) + \int_{|\mathbf{q}|>2} d^3\mathbf{q}\; V^2(q)\; G(q)\right].$$

By performing the change of variable $\mathbf{q} = 2\mathbf{u}$ and integrating over the solid angle, the second-order energy correction in infinite nuclear matter becomes:

$$\Delta E \;=\; -\,(32\pi\; d)\; \frac{\Omega^3}{(2\pi)^9}\left(\frac{m^*}{\hbar^2}\right) k_F^7 \left[\int_0^1 u^2\; V^2(u)\; G(u)\; du + \int_1^\infty u^2\; V^2(u)\; G(u)\; du\right].$$

In symmetric nuclear matter with the simplified Skyrme interaction ($t_0 - t_3$ model), the value of d is equal to 6. This means that the energy exchange contribution is one-fourth of the direct energy contribution. Moreover, the effective mass m^* within the $t_0 - t_3$ model is equal to the nucleonic mass m.
Using the above simplifications, the energy per particle in symmetric nuclear matter reduces to:

$$\frac{\Delta E}{A}(k_F) \;=\; -\frac{9}{4\pi^4}\left(\frac{m}{\hbar^2}\right) k_F^4\; g^2(k_F) \left[\int_0^1 u^2\; G(u)\; du + \int_1^\infty u^2\; G(u)\; du\right].$$

As we have already mentioned, the second integral is divergent due to the high-energy processes involved. In order to make our integrals convergent and finite, we are going to introduce a momentum cutoff Λ and separate the high-energy region from the low-energy one:

$$\frac{\Delta E}{A}(k_F) \;=\; -\frac{9}{4\pi^4}\left(\frac{m}{\hbar^2}\right) k_F^4\; g^2(k_F) \left[\int_0^1 u^2\; G(u)\; du + \int_1^{\frac{\Lambda}{2k_F}} u^2\; G(u)\; du\right].$$

When the cutoff Λ is introduced, the last integral has $\frac{\Lambda}{2k_F}$ as upper limit and the corresponding quantity is denoted by $I(\rho,\Lambda)$. To simplify the above expression, we will introduce the following notation:

$$\frac{\Delta E}{A}(k_F) \;=\; -\frac{9}{8\pi^4}\left(\frac{m^*}{\hbar^2}\right)\, k_F^4\, g^2(k_F)\, I\left(\frac{\Lambda}{k_F}\right),$$

where the expression of I is given by:

$$I\left(\frac{\Lambda}{k_F}\right) \;=\; 2\left[\int_0^1 u^2\, G(u)\, du + \int_1^{\frac{\Lambda}{2k_F}} u^2\, G(u)\, du\right].$$

After straight-forward calculations, the analytical expression of $I(\frac{\Lambda}{k_F})$ is:

$$\begin{aligned} I\left(\frac{\Lambda}{k_F}\right) \;=\; & \frac{1}{105}(-11+2\ln 2) + \frac{\Lambda}{35k_F} + \frac{11\Lambda^3}{210k_F^3} + \frac{\Lambda^5}{840k_F^5} + \left(\frac{\Lambda^5}{60k_F^5} - \frac{\Lambda^7}{1680k_F^7}\right)\ln\left(\frac{\Lambda}{k_F}\right) \\ & + \left(\frac{1}{35} - \frac{\Lambda^2}{30k_F^2} + \frac{\Lambda^4}{48k_F^4} - \frac{\Lambda^5}{120k_F^5} + \frac{\Lambda^7}{3360k_F^7}\right)\ln\left(-2+\frac{\Lambda}{k_F}\right) \\ & - \left(\frac{1}{35} - \frac{\Lambda^2}{30k_F^2} + \frac{\Lambda^4}{48k_F^4} + \frac{\Lambda^5}{120k_F^5} - \frac{\Lambda^7}{3360k_F^7}\right)\ln\left(2+\frac{\Lambda}{k_F}\right). \end{aligned}$$

5.4.1.1 Counter terms

Let us show which kind of counter terms one should include to remove the UV divergences at second order. In other words: is it possible to find counter terms that remove the UV divergences in the present $t_0 - t_3$ model?
The behavior of $I\left(\frac{\Lambda}{k_F}\right)$ for large values of the cutoff Λ (asymptotic behavior) can be approximated as:

$$I\left(\frac{\Lambda}{k_F}\right) \approx \frac{\Lambda}{9k_F} + \frac{1}{105}(-11+2\ln 2) + O\left(\frac{k_F}{\Lambda}\right).$$

For the sake of simplicity, let us take $\alpha = 1$ that corresponds to a phenomenological three-body force. From the above expression, the asymptotic behavior of the second-order energy correction (for $\Lambda >> M$ where M is a hard-mass scale) diverges linearly with Λ:

$$\begin{aligned} \frac{E}{A}(k_F,\Lambda >> M) \;=\; & \frac{3\hbar^2}{10m}k_F^2 + \frac{1}{4\pi^2}\left[t_0 - \frac{m\Lambda}{2\pi^2\hbar^2}t_0^2\right]k_F^3 + \frac{1}{36\pi^4}\left[t_3 - \frac{m\Lambda}{\pi^2\hbar^2}t_0 t_3\right]k_F^6 \\ & + \left(\frac{9m}{8\pi^4\hbar^2}\right)\left(t_0 + \frac{t_3}{6}\rho\right)^2\left[\frac{11-2\ln 2}{105}\right]k_F^4 - \left(\frac{m\Lambda}{648\pi^8\hbar^2}t_3^2\right)k_F^9. \end{aligned}$$

Some comments can be drawn:

1. The terms in green can be regrouped with the contributions from the mean field by redefining the parameters t_0 and t_3 as follows:

$$t_0^R = t_0(\Lambda) - \frac{m\Lambda}{2\pi^2\hbar^2} t_0^2(\Lambda) \quad \text{and} \quad t_3^R = t_3(\Lambda) - \frac{m\Lambda}{\pi^2\hbar^2} t_0(\Lambda) t_3(\Lambda).$$

2. However, it is not possible to absorb the divergent term (in red) unless we add a four-body force, treated perturbatively at the mean-field level, to the simplified Skyrme interaction:

$$V(r_1, r_2, r_3, r_4) = t_4 \; \delta(r_1 - r_2)\delta(r_2 - r_3)\delta(r_3 - r_4),$$

   where t_4 is a parameter to be fitted to some data. This analysis of counter terms is addressed in detail in Ref. [153].

3. Of course, by adding such counter term, the Skyrme interaction becomes more complicated and thus applications to finite nuclei are more difficult. In this case, the Skyrme interaction would be made up of a two-body, three-body (the two-body density-dependent part with $\alpha = 1$) and four-body term. Then, an important question should be addressed at this level: Is there any systematic expansion that controls the hierarchy of this interaction? (see Chapter 6).

4. This means that it is already extremely difficult to use the techniques of adding counter terms with the present $t_0 - t_3$ interaction, even in the simpler case where $\alpha = 1$.

To get rid of such divergent term (the term in red), one may follow two directions:

1. The first direction is to absorb the divergence by readjusting the parameters of the Skyrme interaction in order to have a reasonable EoS at second order.

2. Another direction is to use the techniques of DR/MS that automatically cancel all power-divergent integrals (for more details, see Chapter 6).

5.4.1.2 Analyzing the divergence

In the case of effective interactions between point-nucleons, the cutoff Λ must certainly be smaller than the momentum associated with the nucleon size, i.e., $\Lambda \leq 2$ fm^{-1} . Moreover, the energy scale of low-energy nuclear phenomena in finite nuclei is much lower (see, for instance, Ref. [154]). In fact, to describe giant resonances or rotational bands of nuclei, the scale should be even smaller, perhaps around 0.5 fm^{-1} .
In Fig. 5.8(a), the EoS $E/A + \Delta E/A$ (first- plus second-order) for symmetric nuclear matter with the simplified $t_0 - t_3$ Skyrme interaction is plotted for different values of the cutoff Λ (from 0.5 to 2 fm^{-1}) and compared with the SkP [155] mean-field curve (solid black line). The second-order correction $\Delta E/A$ is also shown in Fig. 5.8(b). In fact, we have chosen as a reference the SkP mean-field EoS because it represents a reasonable EoS where only the terms t_0 and t_3 terms do contribute at the mean-field level due to the choice of the SkP

parametrization.
All the curves are calculated using the SkP parameters (cf. Table 5.1). It has to be noted that the UV divergence is clearly visible in the figure. For $\Lambda = 1.5$ fm^{-1}, the maximum correction is already comparable with the energy per particle at the saturation point, i.e., $\approx$ 15 MeV.

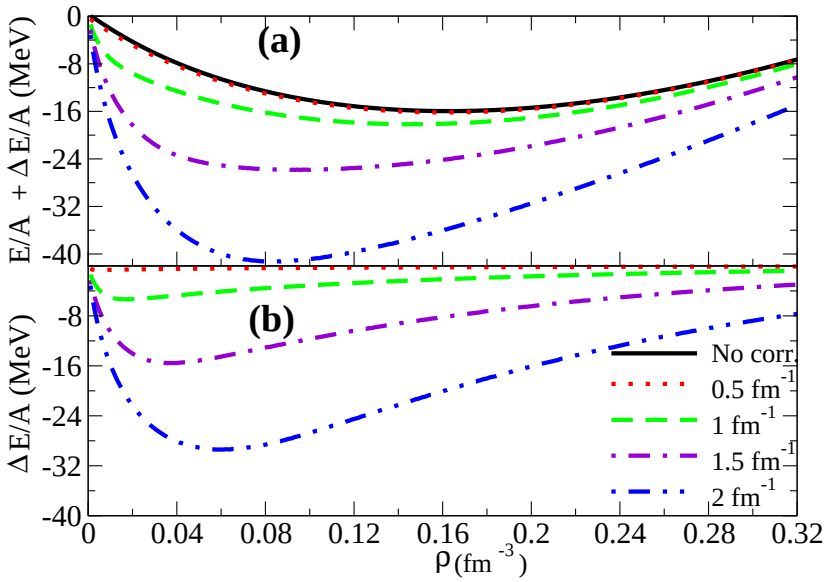

Figure 5.8: (a) $E/A + \Delta E/A$ as a function of the density and for different values of the cutoff Λ. The SkP mean-field EOS (solid black line) is shown for comparison. (b) Correction $\Delta E/A$ for different values of Λ.

5.4.1.3 Adjustment of the Skyrme parameters

Our objective is to treat the UV divergence that is generated at the second-order in the expression of the EoS for symmetric nuclear matter. Since the technique of adding counter terms has been previously rejected for this case, we will follow a phenomenological approach by which the divergence is absorbed by adjusting the parameters of the Skyrme interaction. For each value of Λ we can perform a least-square fit to determine a new parameter set SkP$_\Lambda$, such that the EoS including the second-order correction matches the one obtained with the original force SkP at the mean-field level. This result is illustrated in Fig. 5.9.
The SkP EoS is chosen as our reference on which we perform the fit. Of course, we could have chosen any other reasonable EoS for nuclear matter as a reference. The refitted parameters are listed in Table 5.1 together with the obtained saturation density and binding energy at saturation. In Fig. 5.9(b) we display, for purely mathematical illustration, the refit done with the extreme value of $\Lambda = 350$ fm^{-1} to show that the procedure works even with an

unphysical value of the cutoff.

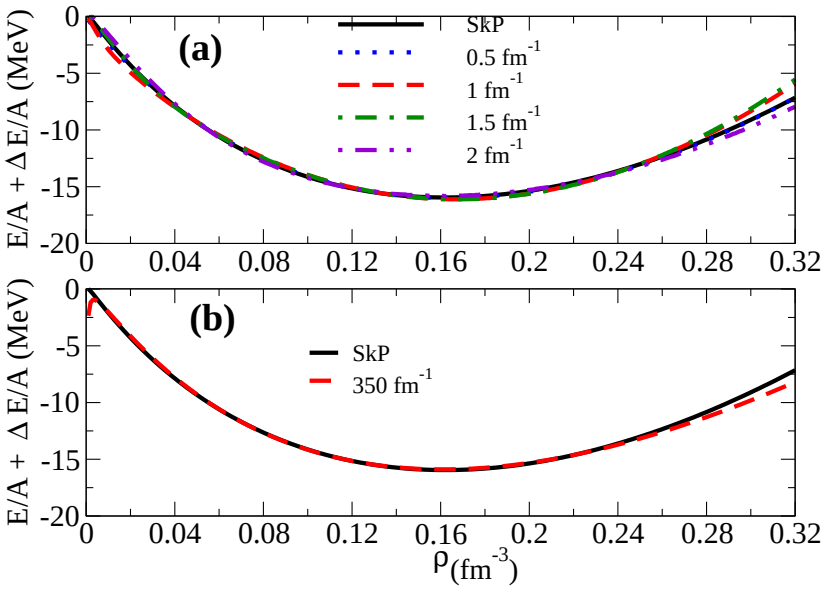

Figure 5.9: (a) Second-order-corrected and refitted equations of state compared with the reference EoS (SkP at mean-field level). (b) Extreme case of $\Lambda = 350$ fm^{-1}.

Table 5.1: From the second line, columns 2, 3 and 4: parameter sets obtained in the fits associated with different values of the cutoff Λ compared with the original set SkP (first line). In the fifth column the χ^2-value (χ^2 divided by the number of fitted points) associated to each fit is shown. In columns 6 and 7 the saturation points and the binding energies are shown.

	t_0 (MeV fm^3)	t_3 (MeV fm$^{3+3\alpha}$)	α	χ^2/N	ρ_0 (fm^{-3})	$E/A(\rho_0)$ (MeV)
SkP	-2931.70	18708.97	1/6		0.16	-15.95
$\Lambda = 0.5$ fm^{-1}	-2352.900	15379.861	0.217	0.00004	0.16	-15.96
$\Lambda = 1$ fm^{-1}	-1155.580	9435.246	0.572	0.00142	0.17	-16.11
$\Lambda = 1.5$ fm^{-1}	-754.131	8278.251	1.011	0.00106	0.17	-16.09
$\Lambda = 2$ fm^{-1}	-632.653	5324.848	0.886	0.00192	0.16	-15.82
$\Lambda = 350$ fm^{-1}	-64.904	360.039	0.425	0.00042	0.16	-15.88

We have thus shown that, for any value of the cutoff Λ, it is possible to find a new refitted interaction that can be used to take into account the mean-field contribution plus the second-order corrections. The quality of the fits, that can be judged from Fig. 5.9, demonstrates that the refitted interactions can describe satisfactorily the empirical EoS for

the case of symmetric nuclear matter treated with a simplified contact force. The quality of the fit is also clearly indicated by the values of χ^2 (Table 5.1), defined as :

$$\chi^2 = \frac{1}{N-1}\sum_{i=1}^{N}\left(\frac{E_i - E_{i,ref}}{E_{i,ref}}\right)^2, \tag{5.10}$$

where N is the number of fitted points.

5.4.2 With the full Skyrme interaction.

All the results presented in this and the following subsections have been published in Ref. [10].
As was done in the previous section, we treat the EoS of nuclear matter by adding the second-order correction to the first-order mean-field energy. This time, we use the standard Skyrme interaction in its complete form where only the spin-orbit term is obviously neglected because we deal with matter. This interaction was introduced in Chapter 3:

$$\begin{aligned} V(\vec{r}_1,\vec{r}_2) &= t_0(1+x_0P_\sigma)\delta(\vec{r}_1-\vec{r}_2) + \frac{1}{2}t_1(1+x_1P_\sigma)[\vec{k}'^2\delta(\vec{r}_1-\vec{r}_2)+\delta(\vec{r}_1-\vec{r}_2)\vec{k}^2] \\ &+ t_2(1+x_2P_\sigma)\vec{k}'\cdot\delta(\vec{r}_1-\vec{r}_2)\vec{k} + \frac{1}{6}t_3(1+x_3P_\sigma)\rho^\alpha(\vec{R})\delta(\vec{r}_1-\vec{r}_2). \end{aligned}$$

The second-order contribution in nuclear matter is due to the neutron-neutron, the proton-proton and the neutron-proton contributions. We can define thus the second-order correction $\Delta E^{(2)}$ as:

$$\Delta E^{(2)} = (\Delta E + \Delta E^x)_{nn} + (\Delta E + \Delta E^x)_{pp} + \Delta E_{np}. \tag{5.11}$$

In the above compact notation, we denote by ΔE the second-order energy correction due to the direct diagrams and by ΔE^x the second-order energy correction due to the exchange diagrams.

5.4.2.1 $nn - pp$ channels

The direct ΔE and the exchange ΔE^x contributions for the neutron-neutron (nn) and proton-proton (pp) channels normalized in a box of volume Ω are given by:

$$\begin{aligned} \Delta E_{ii} &= \frac{1}{2}\frac{\Omega^3}{(2\pi)^9}\int_{C_I} d^3\mathbf{k}_1\, d^3\mathbf{k}_2\, d^3\mathbf{q}\, \frac{v^2(\mathbf{q})}{\epsilon_{\mathbf{k}_1}+\epsilon_{\mathbf{k}_2}-\epsilon_{\mathbf{k}_1+\mathbf{q}}-\epsilon_{\mathbf{k}_2-\mathbf{q}}}, \\ \Delta E^x_{ii} &= -\frac{1}{2}\frac{\Omega^3}{(2\pi)^9}\int_{C_I} d^3\mathbf{k}_1\, d^3\mathbf{k}_2\, d^3\mathbf{q}\, \frac{v(\mathbf{q})v(\mathbf{k}_1-\mathbf{k}_2+\mathbf{q})}{\epsilon_{\mathbf{k}_1}+\epsilon_{\mathbf{k}_2}-\epsilon_{\mathbf{k}_1+\mathbf{q}}-\epsilon_{\mathbf{k}_2-\mathbf{q}}}. \end{aligned} \tag{5.12}$$

In the nn and pp channels, the $\mathbf{k}_1$ and $\mathbf{k}_2$ momenta appearing in the integrals of Eq. (5.12) refer either both to neutrons or both to protons.
The integration domain C_I is given by:

$$C_I = \begin{cases} |\mathbf{k}_1| < k_F^{(i)}, & |\mathbf{k}_1+\mathbf{q}| > k_F^{(i)} \\ |\mathbf{k}_2| < k_F^{(i)}, & |\mathbf{k}_2-\mathbf{q}| > k_F^{(i)} \end{cases},$$

where the Fermi momentum $k_F^{(i)}$ in C_I refers either to the proton or to the neutron Fermi momentum if k_1 and k_2 represent both protons or both neutrons. The two Fermi momenta k_F^n and k_F^p are defined as:

$$k_F^n = \left(\frac{3}{2}\pi^2\rho_n\right)^{1/3} = \left[\frac{3}{4}\pi^2\rho(1+\delta)\right]^{1/3}, \tag{5.13}$$

$$k_F^p = \left(\frac{3}{2}\pi^2\rho_p\right)^{1/3} = \left[\frac{3}{4}\pi^2\rho(1-\delta)\right]^{1/3}. \tag{5.14}$$

We introduce the parameter a depending on k_n and k_p as,

$$a = \frac{k_p}{k_n} = \left(\frac{1-\delta}{1+\delta}\right)^{1/3} \leq 1. \tag{5.15}$$

In Eq. (5.12) the energies ϵ are expressed as $\epsilon_k = \frac{\hbar^2 k^2}{2m^*_{n,p}}$, where $m^*_{n,p}/m$ is the effective mass for neutrons or protons that we have taken equal to its mean-field value (see, for instance, Ref. [100]):

$$\frac{m}{m^*_{n,p}} = 1 + \frac{m}{4\hbar^2}(\rho_n+\rho_p)\Theta_v + \frac{m}{4\hbar^2}\rho_{n,p}(\Theta_s - 2\Theta_v).$$

By expressing the neutron and proton densities in terms of the total density via,

$$\rho_n = \frac{1+\delta}{2}\rho, \quad \rho_p = \frac{1-\delta}{2}\rho \quad \text{and} \quad \rho = \rho_n + \rho_p,$$

the ratio of the nucleonic mass to the effective mass $m^*_{n,p}$ becomes:

$$\frac{m}{m^*_{n,p}} = 1 + \frac{m}{4\hbar^2}\rho\Theta_v + \frac{m}{4\hbar^2}\frac{\rho(1+\omega_{n,p}\delta)}{2}(\Theta_s - 2\Theta_v), \tag{5.16}$$

where $\omega_n = 1$ and $\omega_p = -1$. The mean-field isoscalar effective mass m^*_s/m can be deduced from Eq. (5.16) by setting $\delta = 0$, i.e., by restricting to the case of equal number of protons and neutrons. It is given by the following formula:

$$\left(\frac{m}{m^*_s}\right) = 1 + \frac{1}{8}\frac{m}{\hbar^2}\Theta_s\rho.$$

To simplify the notation, let us introduce two parameters b and c:

$$b = \frac{m^*_s}{m^*_n}, \qquad c = \frac{m^*_s}{m^*_p} \qquad \text{[Note that: } b + c = 2\text{]}$$

In Eq. (5.12), the numerators $v^2(\vec{q})$ and $v(\vec{q})v(\vec{k}_1 - \vec{k}_2 + \vec{q})$ are calculated after summing over spin and isospin indices. To perform the sum, we have used the following properties:

1. The Pauli spin matrices are traceless, i.e.,

$$\sum_{\sigma_1,\sigma_2} \langle \sigma_1, \sigma_2 | \sigma_1 \cdot \sigma_2 | \sigma_1, \sigma_2 \rangle = 0.$$

2. The operators P_σ and P_τ satisfy the following relation: $P_\sigma^2 = 1$ and $P_\tau^2 = 1$.

3. After straight-forward calculations, the terms $v^2(\vec{q})$ and $v(\vec{q})v(\vec{k}_1 - \vec{k}_2 + \vec{q})$ can be written as:

$$\begin{aligned} v^2(\vec{q}) &= 4(\gamma_1 + \gamma_2) + (8\gamma_3 + 4\gamma_4)q^2 + 4(\gamma_5 + \gamma_6)q^4, \\ v(\vec{q})v(\vec{k}_1 - \vec{k}_2 + \vec{q}) &= (2\gamma_1 + 8\gamma_2) + (2\gamma_3 + 4\gamma_4)\left[q^2 + (\vec{k_1} - \vec{k_2} + \vec{q})^2\right] \\ &\quad + (8\gamma_5 + 2\gamma_6)\, q^2(\vec{k_1} - \vec{k_2} + \vec{q})^2. \end{aligned} \tag{5.17}$$

The parameters γ_i in Eq. (5.17) are listed in the following table,

γ_1	γ_2	γ_3	γ_4	γ_5	γ_6
$t_{03}^2 + x_{03}^2$	$t_{03}\, x_{03}$	$t_{03}t_{12} + x_{03}x_{12}$	$t_{03}x_{12} + x_{03}t_{12}$	$t_{12}\, x_{12}$	$t_{12}^2 + x_{12}^2$

where the following notation has been adopted,

t_{03}	x_{03}	t_{12}	x_{12}
$t_0 + \frac{t_3}{6}\rho^\alpha$	$t_0x_0 + \frac{t_3x_3}{6}\rho^\alpha$	$t_1 + t_2$	$t_1x_1 + t_2x_2$

After some manipulations, the pp and nn contributions can be written as the sum of ten terms that are functions of the density ρ, of the asymmetry parameter δ and of the momentum cutoff Λ:

$$\sum_{i=n,p} \frac{\Delta E_{ii} + \Delta E_{ii}^x}{A}(\delta, \rho, \Lambda) = \sum_{j=1}^{10} \chi_j(\delta, \rho) I_j(\delta, \rho, \Lambda). \tag{5.18}$$

The first 5 terms describe the nn channel and the last 5 terms describe the pp channel. Let us first consider the nn case.

• The integrals I_j in Eq. (5.18) are given by:

$$I_j(\delta, \rho, \Lambda) = \Gamma_j \int_0^{\frac{\Lambda}{2k_n}} du\; f_j(u)\; [\Theta(1-u)\; F_1^j(u) + \Theta(u-1)\; F_2^j(u)], \qquad j = 1, \ldots, 5, \tag{5.19}$$

where the five coefficients Γ_i and the five functions f_i are listed in the following table:

Γ_1	Γ_2	Γ_3	Γ_4	Γ_5	$f_1(u)$	$f_2(u)$	$f_3(u)$	$f_4(u)$	$f_5(u)$
1/15	1/15	-1	4/15	1/15	u	u^2	u^2	u^4	u^4

The expressions of the ten functions $F_1^j(u)$, $F_2^j(u)$ (with j running from 1 to 5) are provided in Appendix D.1.

• The coefficients χ_j appearing in Eq. (5.18) (for $j = 1, \ldots, 5$) are written as follows:

$$\begin{aligned}
\chi_1(\delta,\rho) &= 8\pi^3 C_{\Delta E} m_n^* k_n^7 (t_{03} - x_{03})^2, \\
\chi_2(\delta,\rho) &= 32\pi^3 C_{\Delta E} m_n^* k_n^9 (t_{03}t_{12} + x_{03}x_{12}), \\
\chi_3(\delta,\rho) &= 64\pi^3 C_{\Delta E} m_n^* k_n^9 (t_{03}x_{12} + x_{03}t_{12}), \\
\chi_4(\delta,\rho) &= 64\pi^3 C_{\Delta E} m_n^* k_n^{11} t_{12}x_{12}, \\
\chi_5(\delta,\rho) &= 64\pi^3 C_{\Delta E} m_n^* k_n^{11} (t_{12}^2 + x_{12}^2),
\end{aligned} \tag{5.20}$$

where the following notation has been introduced: $C_{\Delta E} = -\frac{8}{(2\pi)^9}\frac{1}{\hbar^2\rho}$.

The integral I_1 in Eq. (5.18) has already been encountered in the $t_0 - t_3$ model treated in Subsec. 5.4.1, whereas the additional four integrals $I_{2,3,4,5}$ appear when the velocity-dependent terms are considered.

The last five terms in Eq. (5.18) correspond to the *pp* channel. They are equal to the first five terms with the replacements $m_n^* \to m_p^*$ and $k_n \to k_p$ in the coefficients χ.

The replacement $k_n \to k_p$ is also done in the upper limit of the integral in Eq. (5.19). The coefficients Γ_i and the functions f_i and $F_{1,2}^i$, with i running from 6 to 10, are equal to those already written for i running from 1 to 5.

5.4.2.2 $np - pn$ channel

The second-order contribution in the $np - pn$ channel normalized in a box of volume Ω is given by:

$$\Delta E_{np} = \frac{\Omega^3}{(2\pi)^9} \int_{C_I} d^3\mathbf{k}_1 \, d^3\mathbf{k}_2 \, d^3\mathbf{q} \frac{2v^2(\mathbf{q})}{\epsilon_{\mathbf{k}_1} + \epsilon_{\mathbf{k}_2} - \epsilon_{\mathbf{k}_1+\mathbf{q}} - \epsilon_{\mathbf{k}_2-\mathbf{q}}}, \tag{5.21}$$

where $v^2(\mathbf{q})$ is explicitly written in Eq. (5.17).

The factor 2 in Eq. (5.21) comes from the sum of the *np* and *pn* channels. The momentum $\mathbf{k}_1$ ($\mathbf{k}_2$) is associated to a neutron (proton). That means that, in the integration domain C_I that we write formally in the same way as for the *nn* and *pp* cases, the k_F associated to the k_F^i of the neutron (proton) represents the neutron (proton) Fermi momentum.

In this channel we divide the region of integration into three parts:

1. **Low-energy region ($0 < |\mathbf{q}| < 2k_p$):** In this region, momentum integrals are finite and convergent since the momenta are restricted to an upper value equal to $2k_p$. Therefore, there are no UV divergences.

2. **Intermediate region ($2k_p < |\mathbf{q}| < 2k_n$):** In this region, the momenta of the states have a lower bound equal to $2k_p$ and an upper bound equal to $2k_n$. In other words, all momentum integrals are convergent and there is no need to do any regularization procedure.

3. **High-energy region ($|q| > 2k_n$):** In this region, the particle states can take arbitrarily large values of momenta from $2k_n$ up to infinity. The integration over the momentum $|\mathbf{q}|$ in Eq. (5.21) diverges because of the high-energy processes involved in this region. In principle, one should regularize this integral and absorb the divergence by adding a counter term to the Skyrme interaction.

We derive the second-order energy correction, Eq. (5.21), in the $np-pn$ channel by summing up the contributions from the above three regions and we obtain:

$$\frac{\Delta E_{np}}{A} = \frac{16\pi^3 C_{\Delta E} k_n^7}{15} \frac{m_s^*}{(bc)^3} D_{abc}(\infty).$$

The expression $D_{abc}(\infty)$, which depends on the total density ρ and the isospin parameter δ, diverges in the high-energy region ($u > 1$) where $u = |\mathbf{q}|/2k_n$:

$$D_{abc}(\infty) = \int_0^a du\ u\ v^2(2k_n u) F_1^{abc}(u) + \int_a^1 du\ u\ v^2(2k_n u)\ F_3^{abc}(u) + \int_1^\infty du\ u\ v^2(2k_n u)\ F_2^{abc}(u),$$

where:

$$v^2(2k_n\ u) = 4(\gamma_1+\gamma_2) + (8\gamma_3+4\gamma_4)(2k_n\ u)^2 + 4(\gamma_5+\gamma_6)(2k_n\ u)^4.$$

The expressions of the three functions $F_1^{abc}(u)$, $F_2^{abc}(u)$ and $F_3^{abc}(u)$ are provided in Appendix D.2.

In order to have for $D_{abc}(\infty)$ a finite integral, we introduce a momentum cutoff Λ so that the integrand in the region $(1 < u < \infty)$ becomes $(1 < u < \frac{\Lambda}{2k_n})$:

$$D_{abc}(\Lambda) = \int_0^a du\ u\ v^2(2k_n u) F_1^{abc}(u) + \int_a^1 du\ u\ v^2(2k_n u)\ F_3^{abc}(u) + \int_1^{\frac{\Lambda}{2k_n}} du\ u\ v^2(2k_n u)\ F_2^{abc}(u).$$

To summarize, let us write the second-order energy correction in all the channels in a compact form as follows:

$$\frac{\Delta E_{np}}{A}(\delta,\rho,\Lambda) = \sum_{j=11}^{15} \chi_j(\delta,\rho) I_j(\delta,\rho,\Lambda),$$

where the last five terms refer to the $np-pn$ channel and the first ten terms have been already introduced for the $nn-pp$ channel. For the last five terms, the cutoff-dependent integrals $I_j(\delta,\rho,\Lambda)$ are given by:

$$I_j(\delta,\rho,\Lambda) = \frac{1}{15}\int_0^{\frac{\Lambda}{2k_n}} du\ f_j(u)\ F_{total}^{abc}(u,\rho,\delta). \tag{5.22}$$

The function $F_{total}^{abc}(u,\rho,\delta)$ is the sum of three functions in different domains according to the values of u:

$$F_{total}^{abc}(u,\rho,\delta) = \frac{1}{(bc)^3}\left[\Theta(a-u)F_1^{abc}(u) + \Theta(u-a)\Theta(1-u)F_3^{abc}(u) + \Theta(u-1)F_2^{abc}(u)\right] \tag{5.23}$$

The five values of f_j for $11 \leq j \leq 15$ are reported in the following table:

$f_{11}(u)$	$f_{12}(u)$	$f_{13}(u)$	$f_{14}(u)$	$f_{15}(u)$
u	u^3	u^3	u^5	u^5

The last 5 coefficients χ_j are equal to

$$\begin{aligned}
\chi_{11}(\delta,\rho) &= 32\pi^3 C_{\Delta E} m_s^* k_n^7 (t_{03}^2 + x_{03}^2 + t_{03}x_{03}),\\
\chi_{12}(\delta,\rho) &= 256\pi^3 C_{\Delta E} m_s^* k_n^9 (t_{03}t_{12} + x_{03}x_{12}),\\
\chi_{13}(\delta,\rho) &= 128\pi^3 C_{\Delta E} m_s^* k_n^9 (t_{03}x_{12} + x_{03}t_{12}),\\
\chi_{14}(\delta,\rho) &= 512\pi^3 C_{\Delta E} m_s^* k_n^{11} t_{12}x_{12},\\
\chi_{15}(\delta,\rho) &= 512\pi^3 C_{\Delta E} m_s^* k_n^{11} (t_{12}^2 + x_{12}^2).
\end{aligned} \tag{5.24}$$

Finally, the Skyrme EoS up to second order is written as

$$\begin{aligned}
\frac{E}{A}(\delta,\rho,\Lambda) &= \frac{3\hbar^2}{10m}\left(\frac{3\pi^2}{2}\rho\right)^{\frac{2}{3}} G_{5/3} + \frac{1}{8}t_0\rho[2(2+x_0) - (1+2x_0)G_2]\\
&+\frac{1}{48}t_3\rho^{\alpha+1}[2(2+x_3) - (1+2x_3)G_2]\\
&+\frac{3}{40}\left(\frac{3\pi^2}{2}\right)^{\frac{5}{3}}\rho^{\frac{5}{3}}\left[\Theta_v G_{5/3} + \frac{1}{2}(\Theta_s - 2\Theta_v)G_{8/3}\right]\\
&+\sum_{j=1}^{15}\chi_j(\delta,\rho)I_j(\delta,\rho,\Lambda).
\end{aligned} \tag{5.25}$$

5.4.2.3 Analyzing the divergence

Starting from Eq. (5.25) the asymptotic behavior of the second-order energy contribution can be obtained by taking its asymptotic expansion. It can be shown that this leads to:

$$\begin{aligned}
\frac{\Delta E^{(2)}}{A}(\delta,\rho) &= k_F^3\left[a_0(\delta)\Lambda + a_1(\delta)\Lambda^3 + a_2(\delta)\Lambda^5\right] + k_F^5\left[b_0(\delta)\Lambda + b_1(\delta)\Lambda^3\right] + k_F^{3+3\alpha}\left[c_1(\delta)\Lambda + c_2(\delta)\Lambda^3\right]\\
&+k_F^7\left[c_0(\delta)\Lambda\right] + k_F^{3+6\alpha}\left[c_3(\delta)\Lambda\right] + k_F^{5+3\alpha}\left[c_4(\delta)\Lambda\right],
\end{aligned} \tag{5.26}$$

where the coefficients a^i, b^i and c^i depend on δ and ρ. Some comments can be drawn:

1. We observe that the energy correction diverges as Λ^5 for large values of Λ and that this divergence is much stronger than the linear divergence of the $t_0 - t_3$ model.

2. Which counter terms should be added? Let us consider the simple example that corresponds to $\alpha = 1$:

   (a) The three terms in green can be regrouped with the mean-field contributions by redefining the parameters.

   (b) However, the first term in red $k_F^7\left[c_0(\delta)\Lambda\right]$ can be absorbed only by adding to the original Skyrme interaction the two-body term: $\nabla^4\delta(r_1 - r_2)$.

(c) The second red term: $k_F^9\,[c_3(\delta)\Lambda]$ can be absorbed only by adding to the original Skyrme interaction a contact four-body force proportional to $\delta(r_1 - r_2)\delta(r_2 - r_3)\delta(r_3 - r_4)$;

(d) Finally, the last term $k_F^8\,[c_4(\delta)\Lambda]$ can be absorbed by adding to the original Skyrme interaction a contact three-body velocity dependent term proportional to: $\nabla^2\delta(r_1 - r_2)\delta(r_2 - r_3)$.

(e) (a), (b), (c) and (d) are discussed in Ref. [153].

3. By adding these counter terms, applications to finite nuclei would become extremely complicated. Two possible alternative directions can be followed:

   (a) The first direction is to absorb the divergence by readjusting the parameters of Skyrme interaction in order to have a reasonable EoS at second order at each value of the cutoff.

   (b) Another direction is to use the techniques of DR/MS that automatically cancels all power-divergent integrals (for more details, see Chapter 6).

5.4.3 Applications with the full Skyrme interaction: symmetric nuclear matter

Symmetric nuclear matter corresponds to equal number of protons and neutrons ($N = Z$). Consequently, the EoS for symmetric matter evaluated at the second order is obtained from Eq. (5.25) by setting the isospin asymmetry $\delta = 0$. In Fig. 5.10 we show a plot of the EoS as a function of the density ρ for different values of the cutoff Λ, computed with the parameter of the SLy5 Skyrme force and compared with SLy5 mean-field EoS. The parametrization SLy5 is chosen this time as a reference. Of course, any other reasonable reference EoS could have been chosen.

In the upper panel of Fig. 5.10, the first- plus second-order EoS obtained for different values of the cutoff Λ (see legend) is plotted, from 0.5 up to 2 fm^{-1}. The different equations of state are calculated by using the SLy5 Skyrme parameters and are compared with the reference mean-field SLy5 EoS [solid line in panel (a)]. In panel (b), the second-order correction is plotted for the same values of the cutoff.

- The dependence on the cutoff appears in the second-order corrections.
- For example, we observe that for a cutoff value equal to 2 fm^{-1} the correction to the energy at the saturation point of nuclear matter, $\rho = 0.16$ fm^{-3}, is already very large and is equal to -80 MeV.
- This is due to the UV divergence that appears at second order.

Two important properties of symmetric nuclear matter are the pressure P and the incompressibility modulus K_∞ at saturation. From Eq. (5.25), one can calculate the first-order

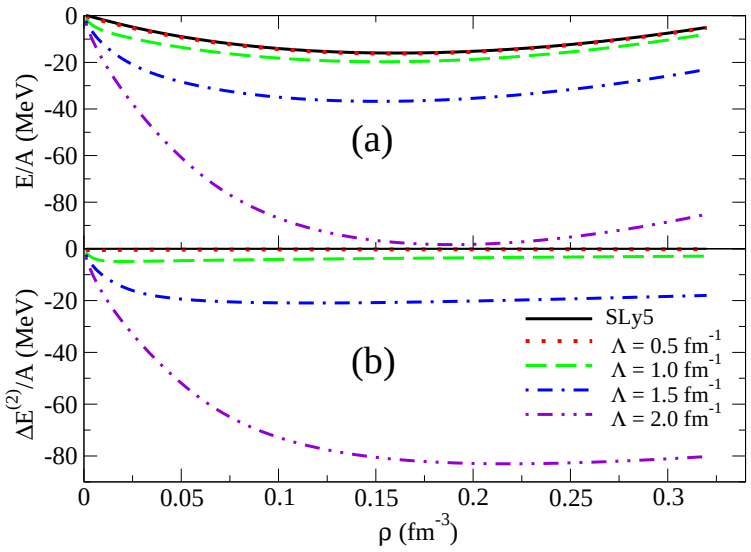

Figure 5.10: (a) Second-order EoS for different values of the cutoff Λ and (b) second-order correction for symmetric nuclear matter calculated with the SLy5 parameters. The SLy5 mean-field EoS is also plotted in (a) (solid line).

and second-order derivatives of the energy per particle with respect to the density ρ in order to get the expressions for the pressure P and the incompressibility modulus K_∞ at the second-order level.
The total pressure can be expressed as the sum of the first-order mean-field pressure and the second-order contribution as follows:

$$P(\rho,\Lambda) \;=\; \rho^2 \frac{d}{d\rho}\frac{E}{A}(\rho,\Lambda) = P^{(1)}(\rho) + P^{(2)}(\rho,\Lambda). \tag{5.27}$$

The expression of the first-order pressure is given in Eq. (3.3) whereas the second-order pressure of symmetric nuclear matter is given by:

$$P^{(2)}(\rho,\Lambda) \;=\; \rho^2 \left[\sum_{j=1}^{15}\left(\chi_j^{'}(\delta,\rho) I_j(\delta,\rho,\Lambda) + \chi_j(\delta,\rho) I_j^{'}(\delta,\rho,\Lambda)\right)\right]_{\delta=0}. \tag{5.28}$$

The incompressibility modulus K_∞ can also be splitted into two parts: a mean-field part plus a second-order term:

$$K_\infty(\rho,\Lambda) \;=\; 9\rho^2 \frac{d^2}{d\rho^2}\frac{E}{A}(\rho,\Lambda) = K_\infty^{(1)}(\rho) + K_\infty^{(2)}(\rho,\Lambda). \tag{5.29}$$

The mean-field part of the incompressibility is given in Eq. (3.4) and the second-order correction is given below:

$$K_\infty^{(2)}(\rho,\Lambda) = 9\rho^2 \left[\sum_{j=1}^{15} \chi_j^{''}(\delta,\rho) I_j(\delta,\rho,\Lambda) + 2\chi_j^{'}(\delta,\rho) I_j^{'}(\delta,\rho,\Lambda) + \chi_j(\delta,\rho) I_j^{''}(\delta,\rho,\Lambda)\right]_{\delta=0} \tag{5.30}$$

The $'$ notation in Eqs. (5.28) and (5.30) denotes the derivative with respect to the total density ρ.
By using the same values of the cutoff Λ and the SLy5 parameters, the second-order pressure and the second-order incompressibility modulus are displayed in Fig. 5.11. One may observe how strongly the UV divergence affects the pressure and the incompressibility modulus for large values of the cutoff Λ. The incompressibility is strongly enhanced by the second-order correction and is equal to ~ 625 MeV at the saturation point of matter for $\Lambda = 2$ fm^{-1}.

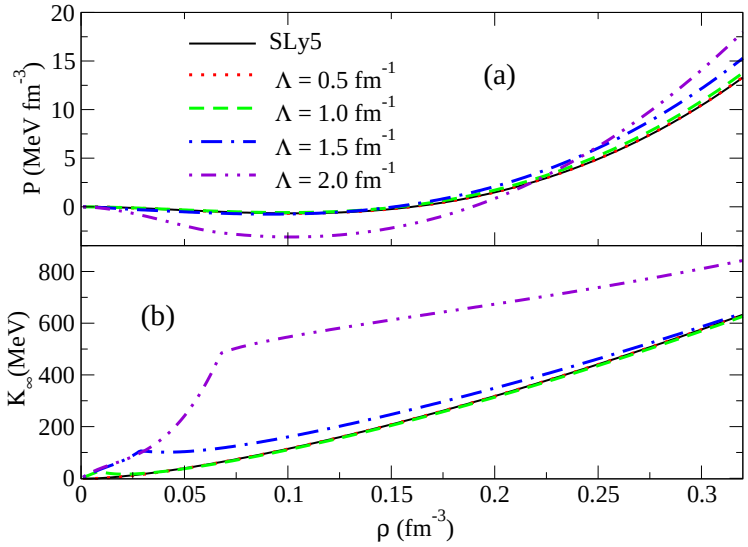

Figure 5.11: Second-order pressure (a) and incompressibility modulus (b) calculated with the SLy5 parameters for different values of the cutoff. The mean-field SLy5 curves are also plotted in both panels (solid lines).

5.4.3.1 Adjustment of the Skyrme parameters

As was mentioned in Chapter 4, the introduction of the second-order contributions would in principle imply a double counting problem. In our attitude, we are dealing with phenomenological interactions where their corresponding parameters can be adjusted according to which diagrams are explicitly introduced. We have seen in Subsection 5.4.2.3 that, if one wants to renormalize the problem, counter terms like 4-derivative two-body, 2-derivative three body and a four-body force, should in principle be added to the original Skyrme interaction. However, adding such counter terms would strongly complicate the calculations, especially in the perspective of doing applications to finite nuclei. Therefore, we first employ a simple procedure and absorb the UV divergences by adjusting the parameters of Skyrme in order to have a reasonable second-order EoS (as we have already done for the $t_0 - t_3$ model).

χ^2 minimization:

We have adjusted the nine parameters of the Skyrme interaction entering in the expression of the EoS to reproduce the reference SLy5 mean-field EoS (again, we could have chosen any other reasonable EoS). We have chosen $N = 15$ equidistant reference points for densities ranging from 0.02 fm^{-3} to 0.30 fm^{-3}. All the parameters are kept free in the adjustment procedure by neglecting for the moment the existing correlations between the parameters. The minimization has been performed using the following definition for the χ^2,

$$\chi^2 = \frac{1}{N-1} \sum_{i=1}^{N} \frac{(E_i - E_{i,ref})^2}{\Delta E_i^2}. \tag{5.31}$$

The errors or *adopted* standard deviations, ΔE_i, in Eq. (5.31) are chosen equal to 1% of the reference SLy5 mean-field energies $E_{i,ref}$. This choice is arbitrary since we are fitting a theoretical EoS where a standard deviation for this quantity has not been estimated. However, the magnitude of the χ^2 defined in Eq. (5.31) has a clear and reasonable meaning: if it is smaller or equal to one, the reference EoS is reproduced within one standard deviation, i.e., within a 1% average error, by our second-order EoS. The corresponding curves obtained with the adjusted parameters are shown in Fig. 5.12 for different values of Λ. The quantities which are displayed in this figure are the differences between the refitted EoS and the reference SLy5 mean-field EoS for different values of the cutoff Λ. We observe that the deviations are extremely small except at very low densities where they are anyway not larger than 0.06 MeV. In the inset of the figure the refitted EoS are plotted and compared with the SLy5 mean-field EoS (solid line). Due to the scale, the curves in the inset are practically indistinguishable. The obtained sets of parameters and the χ^2 values are shown in Table 5.2 for each value of the cutoff Λ. The χ^2 values are always extremely small indicating that, on average, the fitted points are deviating much less than 1 % (according to the adopted expression for χ^2, Eq. (5.31)) with respect to the reference EoS.

We have noticed that, for the four refitted interactions, the saturation density ρ_0 and the incompressibility modulus are equal in all cases to 0.16 fm^{-3} and 229.9 MeV, respectively.

The pressure and the incompressibility, Eqs. (5.27) and (5.29), evaluated by using the parameters listed in Table 5.2, are plotted in the two panels of Fig. 5.13. Again, what is plotted is the deviation with respect to the SLy5 mean-field reference values. In the two insets, the absolute values are displayed together with the SLy5 mean-field curves (solid lines). We stress that the pressure and the incompressibility do not enter in the fits. In spite of this, small deviations from the SLy5 reference curves are observed, only at large densities.

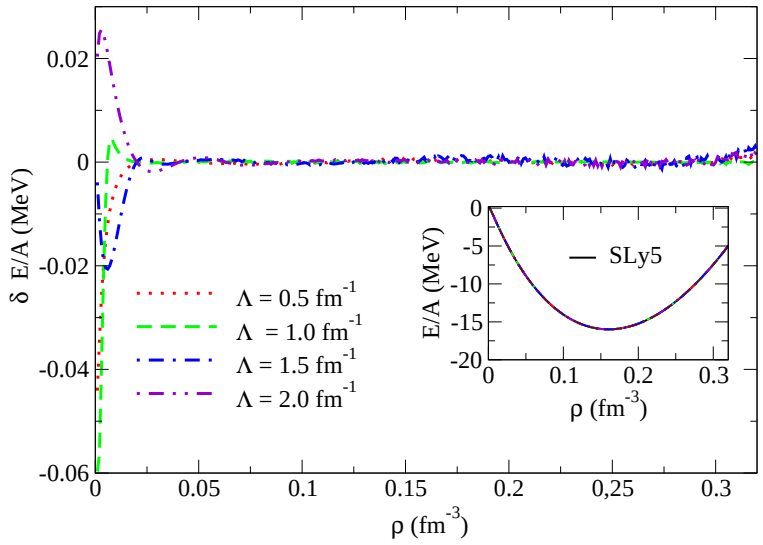

Figure 5.12: Deviations between the refitted second-order EoS (for different values of the cutoff) and the SLy5 mean-field curve for symmetric nuclear matter. In the inset the absolute values are plotted and compared with the SLy5 mean-field EoS (solid line).

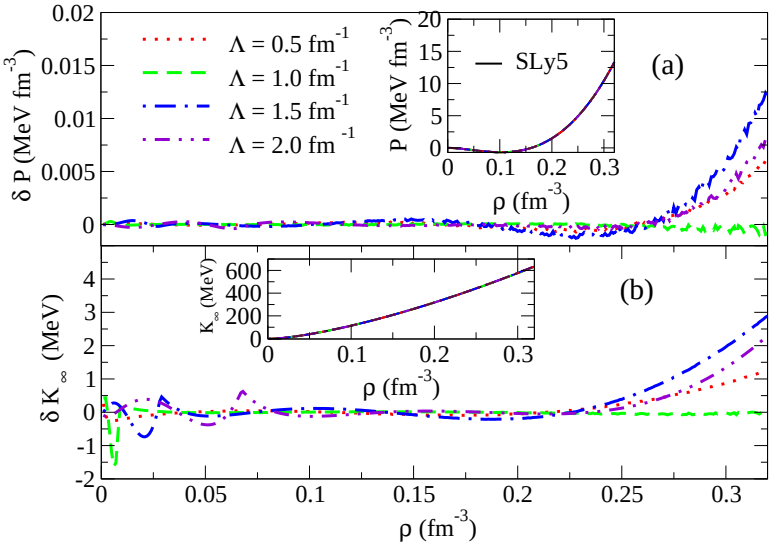

Figure 5.13: Deviations of the pressure (a) and of the incompressibility (b) (calculated with the refitted parameters for symmetric nuclear matter) with respect to the mean-field SLy5 values. In the insets the absolute values are displayed and compared with the SLy5 mean-field curves (solid lines).

Table 5.2: Parameter sets obtained in the fit of the EoS of symmetric matter for different values of the cutoff Λ compared with the original set SLy5. In the last column the χ^2 values are shown.

	t_0 (MeV fm^3)	t_1 (MeV fm^5)	t_2 (MeV fm^5)	t_3 (MeV fm$^{3+3\alpha}$)	x_0	x_1	x_2	x_3	α	
SLy5	-2484.88	483.13	-549.40	13763.0	0.778	-0.328	-1.0	1.267	0.16667	
Λ(fm^{-1})										χ^2
0.5	-1817.280	646.948	4373.135	10101.307	-0.0002	-3.464	-1.314	6.233	0.246	6.2e-06
1.0	-1132.001	807.361	-323.413	7555.400	0.733	1.201	0.644	5.012	0.457	4.9e-07
1.5	-608.125	71.647	241.517	-3920.616	1.565	-2.376	1.655	6.111	0.834	7.2e-06
2.0	-331.658	660.677	-695.979	-90.060	3.000	-0.803	-1.120	164.031	0.754	3.3e-06

5.4.4 Applications with the full Skyrme interaction: pure neutron matter

The EoS (mean-field plus second-order) for pure neutron matter is obtained by setting the isospin parameter $\delta = 1$ in Eq. (5.25). We plot in Fig. 5.14 the EoS for pure neutron matter evaluated at the second-order (a) and the second-order correction (b) as function of the density ρ for different values of the cutoff Λ, from 0.5 fm^{-1} to 2 fm^{-1}. In the upper panel the reference SLy5 mean-field EoS is also plotted (solid line).

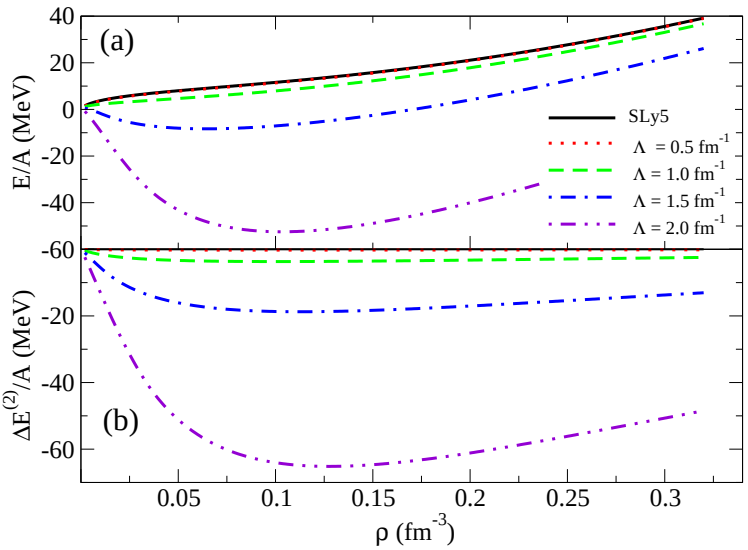

Figure 5.14: As in Fig. 5.10 but for pure neutron matter.

Some comments can be drawn from the above figure:

- The EoS for pure neutron matter depends on the cutoff Λ. Moreover, the UV divergences are visible in Fig. 5.14 and are very strong as expected from Eq. (5.26).

- The reference SLy5 mean-field EoS (solid line) for pure neutron matter is always positive, whereas the total EoS at the second-order is negative for $\Lambda \geq 1.5$ fm^{-1}.
- Starting from the cutoff value $\Lambda = 1.5$ fm^{-1}, it is clear from Fig. 5.14 that the corrected EoS of pure neutron matter has an equilibrium point which is unphysical and artificial since the UV divergences are not suppressed. The appearance of such an equilibrium point at the second-order shows how the UV divergence is responsible for generating artificial and unphysical strong correlations in the system. This *anomaly* can be cured by the adjustment of the parameters.

5.4.4.1 Adjustment of the Skyrme parameters

We have performed also in this case the adjustment of the nine parameters of the Skyrme interaction with the same definition of χ^2 as above, Eq. (5.31). The fitted points are the same as in the previous case. In Fig. (5.15) the deviations with respect to the SLy5 mean-field EoS are shown. Again, the deviations are extremely small and are larger at very low densities. In the inset the absolute curves are plotted. The obtained parameters and the χ^2 values per point are listed in Table 5.3. The χ^2 values are extremely small also in this case and not larger than 10^{-6}.

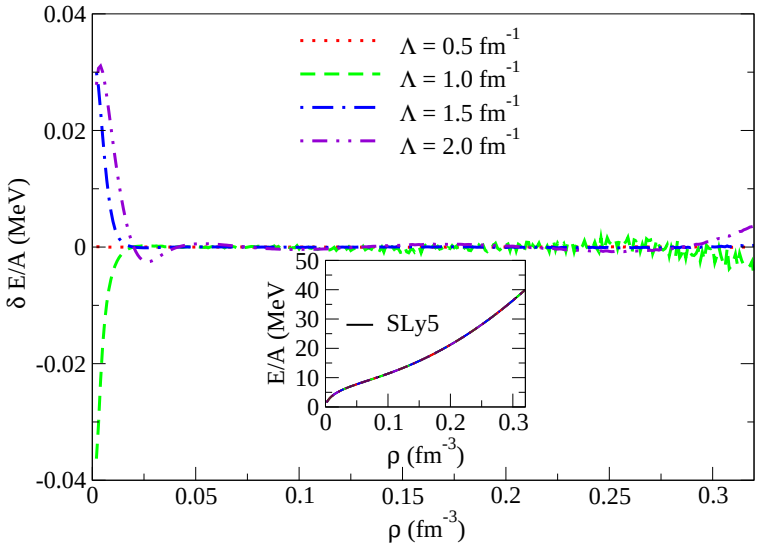

Figure 5.15: Deviations of the refitted EoS for pure neutron matter with respect to the SLy5 mean-field EoS. In the inset the absolute curves are displayed with the SLy5 mean-field EoS (solid line).

Table 5.3: Parameter sets obtained in the fit of the EoS of neutron matter for different values of the cutoff Λ compared with the original set SLy5. In the last column the χ^2 values are shown.

	t_0 (MeV fm^3)	t_1 (MeV fm^5)	t_2 (MeV fm^5)	t_3 (MeV fm$^{3+3\alpha}$)	x_0	x_1	x_2	x_3	α	
SLy5	-2484.88	483.13	-549.40	13736.0	0.778	-0.328	-1.0	1.267	0.16667	
Λ(fm^{-1})										χ^2
0.5	-535.222	403.303	1660.746	42905.115	0.094	-0.970	-1.031	1.094	0.144	9.1e-09
1.0	-1941.276	92.989	393.422	-137583.116	0.609	-0.502	-1.010	1.057	0.613	1.5e-06
1.5	-18033.283	319.198	-186.907	110184.232	1.846	-1.113	-0.929	1.893	0.006	4.7e-08
2.0	-218.464	598.755	-538.604	496.206	0.015	-0.885	-0.745	14.793	0.205	6.6e-06

5.4.5 Application with the full Skyrme interaction: Asymmetric nuclear matter: $\delta = 0.5$ as an example

In this subsection, we take the asymmetry value $\delta = 0.5$ as an example of asymmetric nuclear matter. The value of $\delta = 0.5$ means that the neutron density is equal to $3\rho/4$ and the proton density is equal to $1/4\rho$. We proceed as in the previous subsections and plot in the upper and lower panels of Fig. 5.16, the corrected second-order EoS for asymmetric nuclear matter and the second-order correction, respectively, as a function of the density and the cutoff Λ. From Fig. 5.16, the UV divergences are visible due to the behavior of the EoS at large values of the cutoff Λ.

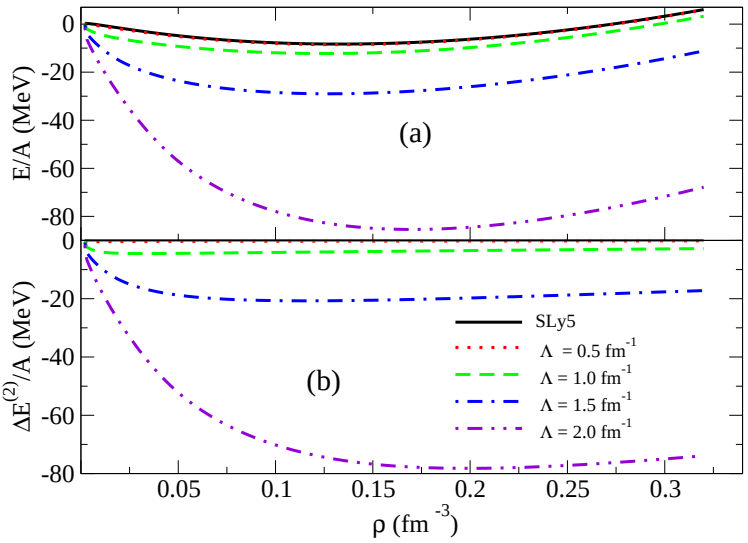

Figure 5.16: As in Fig. 5.10 but for asymmetric nuclear matter in the case $\delta = 0.5$.

5.4.5.1 Adjustment of the Skyrme parameters

We use here the same definition of χ^2 and the same number of fitted points as for the previous two cases. The results of the fit are shown in Fig. 5.17 whereas the sets of parameters are listed in Table 5.4. The quality of the fit is very good also in this case as indicated by the low values of χ^2. These values have increased with respect to the two previous adjustments but they still remain much lower than 1.

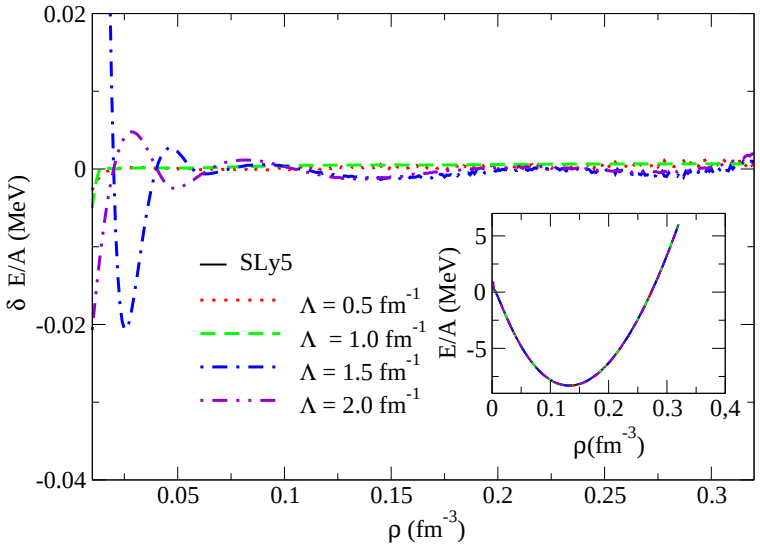

Figure 5.17: As in Fig. 5.15 but for asymmetric matter ($\delta = 0.5$).

Table 5.4: Parameter sets obtained in the fit of the EoS of asymmetric matter ($\delta = 0.5$) matter for different values of the cutoff Λ compared with the original set SLy5. In the last column the χ^2 values are shown.

	t_0 (MeV fm^3)	t_1 (MeV fm^5)	t_2 (MeV fm^5)	t_3 (MeV fm$^{3+3\alpha}$)	x_0	x_1	x_2	x_3	α	
SLy5	-2484.88	483.13	-549.40	13763.0	0.778	-0.328	-1.0	1.267	0.16667	
Λ(fm^{-1})										χ^2
0.5	-2691.295	2227.930	-275.173	19875.288	1.109	-1.510	4.268	2.790	0.116	2.5e-04
1.0	-4139.692	771.130	1079.952	20372.212	-1.159	2.114	-1.047	-1.790	0.027	7.0e-04
1.5	-1005.707	651.553	-297.441	202.122	1.357	0.708	-1.306	2.657	-0.434	3.5e-04
2.0	-2795.987	699.587	-563.067	11780.236	5.252	-0.515	-0.939	7.119	-0.007	2.1e-04

5.4.6 Global fit with the full Skyrme interaction: Cutoff Dependence

In this Subsection, we do a unique and global fit to readjust the three mean-field plus second-order EoS's for symmetric, asymmetric ($\delta = 0.5$) and pure neutron matter to reproduce the corresponding SLy5 mean-field curves.
As was done in the previous fits, we use a chi-square minimization with the same definition of χ^2, Eq. (5.31). In this case, the χ^2 is composed by the three contributions as calculated in the previous cases and the final value is divided by three in order to make our different results comparable:

$$\chi^2 = \frac{1}{3}\left[\chi^2(\delta = 0) + \chi^2(\delta = 0.5) + \chi^2(\delta = 1)\right].$$

The obtained sets of parameters are reported in Table 5.5. The three refitted EoS's are plotted in Fig. 5.18 as a function of the density ρ and for different values of the cutoff Λ from 0.5 fm^{-1} to 2 fm^{-1}. Moreover, the deviations from the Sly5 mean-field curves are shown in Fig. 5.19. These deviations are small, especially at low densities and around saturation density.
Since we have included the EoS of symmetric nuclear matter in the global fit, it would be interesting to plot the pressure and incompressibility modulus with the refitted parameters. The plots are shown in Fig. 5.20 and their deviations with respect to the SLy5 mean-field values are presented in Fig. 5.21. The values of the saturation density ρ_0 and of the incompressibility modulus $K_\infty(\rho_0)$ for symmetric matter resulting from the global fit are displayed in Table 5.6 for the four values of the cutoff Λ.
Globally, as one can see from the χ^2 values, the quality of the fit is deteriorated with respect to that found for each separate case. However, the fit is still of good quality. Specifically, the χ^2 values are still less than 1 up to $\Lambda = 1$ fm^{-1}. Values between 1 and 2 (to be judged by considering the adopted choice of the errors in the expression of χ^2) are found for larger values of the cutoff meaning that the fit is still reasonably good.
Finally, for the case of the global fits (that constitutes our more demanding test for the second-order EoS) we have estimated the standard deviation σ of the fitted parameters [156]. This analysis allows one to asses how well the used reference data together with the adopted errors constrain the parameters of our model. In particular, the standard deviation associated to such parameters are displayed in Table 5.5.

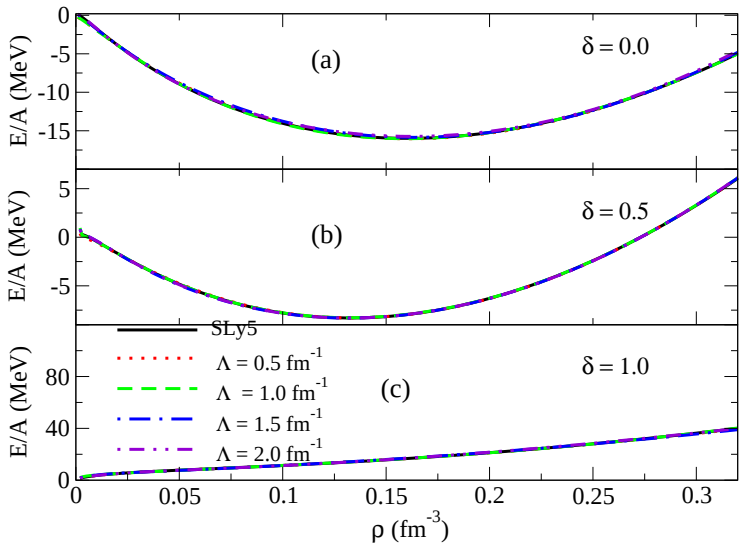

Figure 5.18: Refitted EoS (global fit) for symmetric (a), asymmetric with $\delta = 0.5$ (b) and pure neutron (c) matter. The reference SLy5 mean-field curves are also plotted in the 3 panels (solid lines).

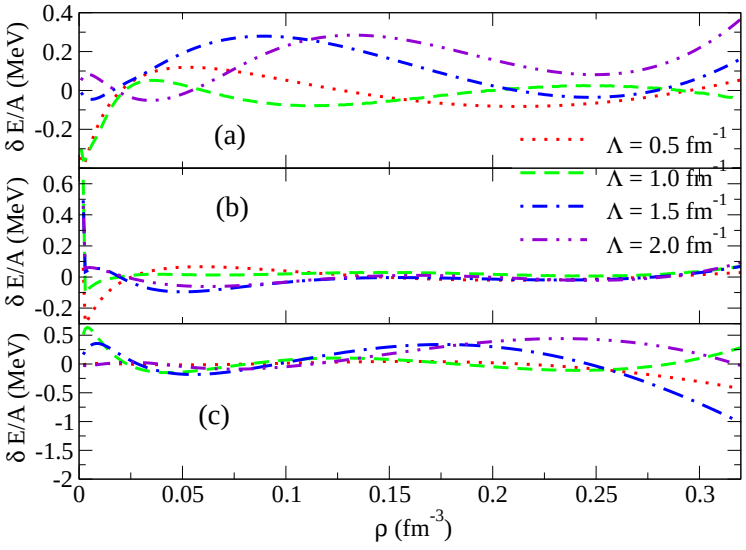

Figure 5.19: Deviations of the refitted EoS (global fit) for symmetric (a), asymmetric with $\delta = 0.5$(b) and pure neutron (c) matter with respect to the mean-field SLy5 values.

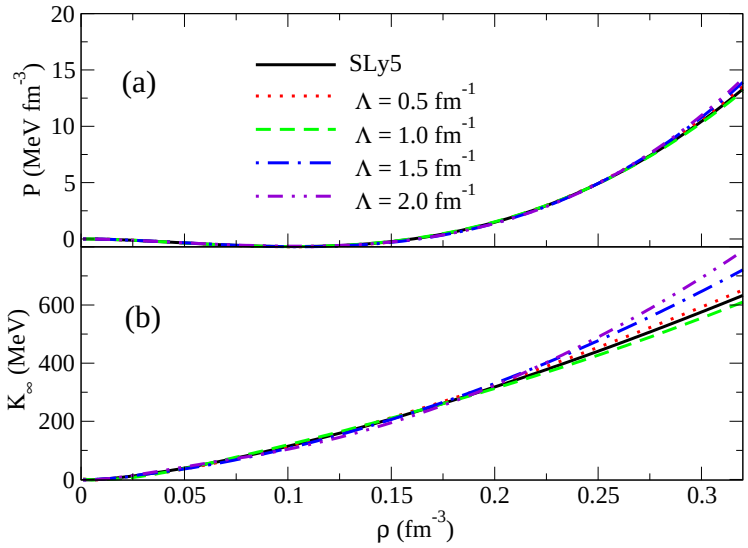

Figure 5.20: Pressure (a) and incompressibility (b) evaluated with the parameters obtained with the global fit.

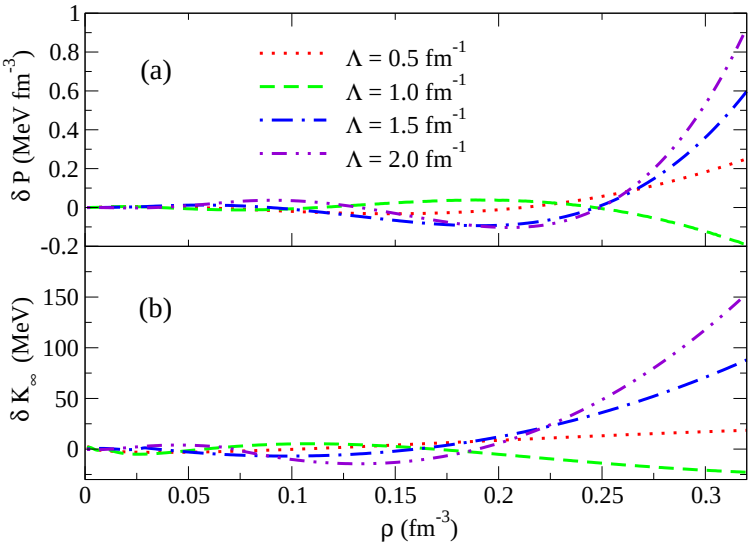

Figure 5.21: Deviations of the pressure (a) and of the incompressibility (b) (evaluated with the parameters obtained with the global fit) with respect to the mean-field SLy5 curves.

Table 5.5: Parameter sets obtained in the fit of the EoS of symmetric, asymmetric and pure neutron matter for different values of the cutoff Λ compared with the original set SLy5. The standard deviation, σ, estimated for the different parameters is also given. In the last column the χ^2 values are shown.

	t_0	t_1	t_2	t_3	x_0	x_1	x_2	x_3	α	
	σ_{t_0}	σ_{t_1}	σ_{t_2}	σ_{t_3}	σ_{x_0}	σ_{x_1}	σ_{x_2}	σ_{x_3}	σ_α	
	(MeV fm^3)	(MeV fm^5)	(MeV fm^5)	(MeV fm$^{3+3\alpha}$)						
SLy5	-2484.88	483.13	-549.40	13736.0	0.778	-0.328	-1.0	1.267	0.16667	
Λ(fm^{-1})										χ^2
0.5	-2022.142	290.312	1499.483	12334.459	0.481	-5.390	-1.304	0.880	0.259	0.411
	0.49	0.212	1.75	4.5	0.001173	0.00657	0.00020	0.001632	0.000280	
1.0	-627.078	83.786	-971.384	186.775	3.428	-1.252	-1.620	200.360	0.338	0.540
	1.668	0.2740	0.782	0.078	0.00260	0.01927	0.00026	0.082	0.000314	
1.5	-743.227	112.246	-42.816	5269.849	1.013	3.478	-2.114	0.189	0.814	1.733
	0.306	0.685	0.2972	5.4	0.01415	0.01309	0.00519	0.045037	0.000784	
2.0	-718.397	573.884	-497.766	6179.243	0.391	-0.393	-0.574	0.785	1.051	1.313
	0.343	0.251	0.261	8.33	0.005876	0.001850	0.000597	0.017475	0.00104	

Table 5.6: Saturation density and incompressibility modulus resulting from the global fit for symmetric nuclear matter.

Λ (fm^{-1})	ρ_0 (fm^{-3})	K_∞ (MeV)
0.5	0.16	236.36
1.0	0.16	230.52
1.5	0.16	236.28
2.0	0.16	222.76

5.5 Conclusions

In this chapter, we have solved the nuclear many-body problem with a zero-range effective interaction in nuclear matter by including second-order energy corrections. The zero-range character of the interaction generates UV divergences in this beyond-mean-field example. It was first found that the second-order EoS of symmetric nuclear matter with the simplified t_0-t_3 Skyrme interaction diverges linearly with the cutoff Λ (i.e. $\sim \Lambda$) if a momentum cutoff regularization is used [9].

Then, we have extended our work to the case of full Skyrme interaction by including the velocity-dependent terms. In this case, we have considered both symmetric and asymmetric matter, including the extreme case of pure neutron matter. We have derived analytically the second-order correction to the EoS and its asymptotic behavior for large values of the cutoff Λ shows a strong divergence ($\sim \Lambda^5$) [10]. An adjustment of the Skyrme parameters is performed for the single cases of symmetric, neutron and asymmetric ($\delta = 0.5$) matter. The resulting fits are of extremely good quality. A global fit is finally performed simultaneously for the three EoS's. The results are still very satisfactory.

Two interesting conclusions may be drawn:

1. Even if the divergence is much stronger than in the simple $t_0 - t_3$ case, the fit of the parameters is still possible;

2. The three EoS's is be adjusted simultaneously and the problem of the appearance of an artificial equilibrium point for neutron matter can be always cured by the adjustment of the parameters.

The adjusted interactions display reasonable properties for nuclear matter. This opens new perspectives for future applications of this kind of interactions in beyond-mean-field models to treat finite nuclei. It is worth reminding that, so far, conventional phenomenological interactions (adjusted at the mean-field level) have been employed for nuclei in different beyond-mean-field calculations (see, for instance, Refs. [111, 123, 125]).
A drawback of the cutoff regularization adopted in Refs. [9, 10] is that for each momentum cutoff a different parametrization is generated. However, a unique set of parameters could be provided by applying the techniques of DR to the second-order EoS of nuclear matter (see next chapter).

Chapter 6

Towards an EFT approach to treat UV divergences at second order. Results

6.1 Introduction

In Chapter 5, we have derived the EoS of nuclear matter at the second order with the simplified Skyrme $t_0 - t_3$ model and with the full Skyrme interaction. In both cases, we have adopted a cutoff scheme to regularize the divergent momentum integrals and then an adjustment of parameters was performed to get rid of double counting problems and obtain EoS's with reasonable properties. We found that, for every value of the cutoff Λ, a different set of parameters can be generated and hence our model depends on the cutoff used. In this Chapter, we are going to use the techniques of DR introduced in Chapter 4 to derive the EoS with second-order corrections of nuclear matter. We start our work with symmetric nuclear matter and the simplified Skyrme $t_0 - t_3$ interaction and then we include the velocity-dependent terms to the Skyrme interaction.

6.2 2^{nd}-order energy correction with DR/MS

Let us consider the second-order correction beyond the mean-field EoS in the $t_0 - t_3$ model for symmetric nuclear matter [9]. As was discussed in Chapter 5, the second-order EoS for symmetric nuclear matter diverges linearly with the momentum cutoff Λ. In this section, we are going to use the techniques of DR to regularize the divergent integrals and use the MS scheme (that was already introduced in Chapter 4) to renormalize our problem.
The results presented in the following Sections have been published in Ref. [11].

6.3 With the simplified Skyrme interaction

We write the generalized expression of the second-order correction where we introduce a continuous dimension d in the integral and the auxiliary scale μ. In a box of volume Ω one has,

$$\Delta E = d\frac{\Omega^d}{(2\pi)^{3d}} \int_{C_I} d^d\mathbf{q}\; d^d\mathbf{k}_1\; d^d\mathbf{k}_2\; \frac{V^2(\mathbf{q})}{\epsilon_{\mathbf{k}_1} + \epsilon_{\mathbf{k}_2} - \epsilon_{\mathbf{k}_1+\mathbf{q}} - \epsilon_{\mathbf{k}_2-\mathbf{q}}}. \tag{6.1}$$

The domain of integration C_I is already defined in Eq. (5.8) and the momentum representation of the simplified $t_0 - t_3$ Skyrme interaction is given by: $V(\mathbf{q}) = \frac{g(\rho)}{\Omega}$.
By making some manipulations and by using the Schwinger's proper time representation of Feynman integrals, Eq. (6.1) becomes:

$$\Delta E = -\frac{D}{\mu^{3(d-3)}} \frac{\Omega^d}{(2\pi)^{3d}} \left(\frac{m}{\hbar^2}\right)\; k_F^{3d-2} \left[\int_{0\leq|\mathbf{q}|\leq 2} d^d\mathbf{q}\; V^2(\mathbf{q})\; G_d(\mathbf{q}) + \int_{|\mathbf{q}|\geq 2} d^d\mathbf{q}\; V^2(\mathbf{q})\; G_d(\mathbf{q})\right] \tag{6.2}$$

with the following definition of $G_d(\mathbf{q})$:

$$G_d(\mathbf{q}) = \int_0^\infty d\alpha\; e^{-\alpha\mathbf{q}^2} \left[\int_{\substack{|\mathbf{p}|<1 \\ |\mathbf{p}+\mathbf{q}|>1}} d^d\mathbf{p}\; e^{-\alpha\mathbf{q}\cdot\mathbf{p}}\right]^2. \tag{6.3}$$

In our case the regulator ϵ can be written in terms of the dimension d as $\epsilon = 3 - d$. When $\epsilon \to 0$, d returns to the integer value 3.
In dimension d, all mass-less integrals are regularized to zero [157, 158, 159]. For instance, it holds:

$$I = \int\; d^d\mathbf{q} \int_{|\mathbf{k}_1|<1} d^d\mathbf{k}_1 \int_{|\mathbf{k}_2|<1} d^d\mathbf{k}_2\; \frac{1}{\mathbf{q}^2} = 0. \tag{6.4}$$

By rewriting I as the sum of two integrals I_1 and I_2 (by splitting the integration in two regions),

$$\begin{aligned} I_1 &= \int_{|\mathbf{q}|>2} d^d\mathbf{q} \int_{|\mathbf{k}_1|<1} d^d\mathbf{k}_1 \int_{|\mathbf{k}_2|<1} d^d\mathbf{k}_2\; \frac{1}{\mathbf{q}^2}, \\ I_2 &= \int_{|\mathbf{q}|<2} d^d\mathbf{q} \int_{|\mathbf{k}_1|<1} d^d\mathbf{k}_1 \int_{|\mathbf{k}_2|<1} d^d\mathbf{k}_2\; \frac{1}{\mathbf{q}^2}, \end{aligned} \tag{6.5}$$

the second-order correction reads:

$$\Delta E = -\frac{D}{\mu^{3(d-3)}} \frac{\Omega^{d-2}}{(2\pi)^{3d}} \left(\frac{m}{\hbar^2}\right) k_F^{3d-2}\; g^2(\rho) \left[\left(\int_{0\leq|\mathbf{q}|\leq 2} d^d\mathbf{q}\; G_d(\mathbf{q}) - I_2\right) + \left(\int_{|\mathbf{q}|\geq 2} d^d\mathbf{q}\; G_d(\mathbf{q}) - I_1\right)\right].$$

Let us denote by $A(d)$ and $B(d)$ the two integrals in parenthesis on the r.h.s of the above equation; the second-order EoS becomes:

$$\Delta E = -\frac{D}{\mu^{3(d-3)}} \frac{\Omega^{d-2}}{(2\pi)^{3d}} \left(\frac{m}{\hbar^2}\right) k_F^{3d-2}\; g^2(\rho)\left[A(d) + B(d)\right]. \tag{6.6}$$

where we adopt the following definitions of $A(d)$ and $B(d)$:

$$A(d) = \int_{|\mathbf{q}|\geq 2} d^d\mathbf{q}\; G_d(\mathbf{q}) - I_1 \quad \text{and} \quad B(d) = \int_{0\leq|\mathbf{q}|\leq 2} d^d\mathbf{q}\; G_d(\mathbf{q}) - I_2.$$

The quantity B is finite for $|q| \leq 2$ when $d \to 3$ and one can show that its value is equal in this case to:

$$B = 64\pi^3 \left(\frac{59}{315} - \frac{46}{105}\ln 2\right). \tag{6.7}$$

It is shown in Appendix D.3 that the quantity $A(d)$ may be written in terms of a hypergeometric function [160] as follows:

$$A(d) = \frac{C(d)}{2-d}\left[{}_4\mathrm{F}_3\left(\frac{1+d}{2}, \frac{1}{2}, 1, \frac{2-d}{2}; 1+\frac{d}{2}, 1+d, \frac{4-d}{2}; 1\right) - 1\right].$$

Moreover, the limit of $A(d)$ when the dimension $d \to 3$ is finite and is equal to:

$$A(3) = \lim_{d\to 3} A(d) = \left(\frac{256\pi^3}{9}\right)\left(-\frac{23}{35} + \frac{36}{35}\ln 2\right). \tag{6.8}$$

$A(d)$ converges for $0 \leq d < 4$ (with a pole at $d = 4$) as shown in Fig. 6.1. For $d = 3$ the divergence has been removed by the regularization procedure.

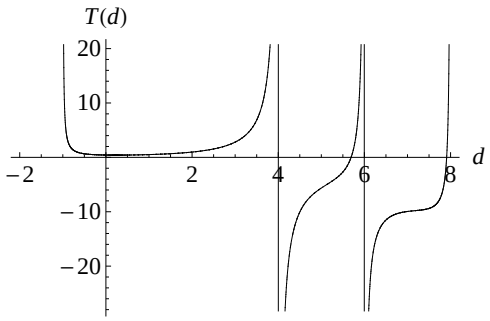

Figure 6.1: $A(d)$ as a function of the space-dimension d.

In symmetric nuclear matter, the value of D is equal to 6, hence the second-order correction in Eq. (6.6) becomes:

$$\Delta E \;=\; -D\frac{\Omega}{(2\pi)^9}\left(\frac{m}{\hbar^2}\right)k_F^7\; g^2(\rho)\,[A(3)+B] = -\frac{9}{8\pi^4}\left(\frac{m}{\hbar^2}\right)k_F^4\; g^2(\rho)\left[\frac{-11+2\ln 2}{105}\right].$$

Consequently, the EoS for symmetric nuclear matter at the second-order is given by:

$$\frac{E}{A}(\rho) = \frac{3\hbar^2}{10m}\left(\frac{3\pi^2}{2}\rho\right)^{\frac{2}{3}} + \frac{3}{8}\rho\; g(\rho) + \frac{9}{8\pi^4}\left(\frac{m}{\hbar^2}\right)k_F^4\; g^2(\rho)\left[\frac{11-2\ln 2}{105}\right] + \mathcal{O}\left[(g^3(\rho)\right]. \tag{6.9}$$

6.3.1 Discussion

The EoS (first + second-order) for symmetric nuclear matter is plotted in Fig. 6.2 as a function of the density ρ and compared with the reference SkP mean-field EoS (a). In panel (b) only the second-order corrective term is plotted.

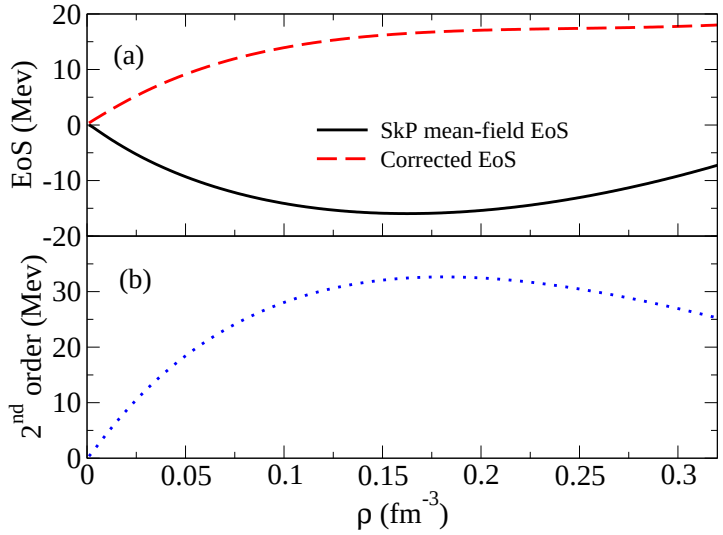

Figure 6.2: (a) SkP mean-field EoS (full line) and mean-field + second-order EoS calculated with the SkP parameters (dashed line) for the $t_0 - t_3$ model in symmetric matter. (b) Second-order correction.

Some comments can be drawn:

- We observe from Eq. (6.9) that the power-law divergent terms have been removed automatically by the MS scheme and do not appear in the final expression as powers of the auxiliary parameter μ.
- The independence on μ shows that the UV divergences are hidden in the 4−dimension space. Hence, the DR/MS procedure can obscure the renormalization process.
- One can notice that the regularized second-order correction is always positive and has the opposite curvature with respect to the first-order EoS.
- The second-order correction has its maximum value (due to the change of curvature, the second-order term has a maximum) around the equilibrium density for matter. The corrected EoS is strongly modified with respect to the mean-field EoS calculated with the same parameters and, in particular, the curvature is changed because the second-order correction is dominant.
- Due to the difference of curvature it turns out that the adjustment of the corrected EoS to a reasonable reference EoS (we have chosen the SkP mean-field EoS as a reference)

is not feasible. This means that a χ^2- minimization does not lead to any result: the parameters can not be adjusted in this case .

6.4 With the full Skyrme interaction

We have seen in Subsec. 6.3.1, that an adjustment of parameters is not possible in the t_0-t_3 case and hence the second-order EoS does not represent a reasonable EoS in that case when the DR technique is used to remove the UV divergence.
In this section, we include the velocity-dependent terms of the Skyrme interaction that were neglected in the t_0-t_3 model. By following the same procedure done in the previous section and using the fact that massless integrals vanish in $d-$dimension when using DR/MS, it is possible to regularize the second-order corrections of the EoS of symmetric nuclear matter for the full Skyrme interaction which contains nine parameters to be adjusted: $t_{0,1,2,3}$, $x_{0,1,2,3}$ and α.

6.4.1 Symmetric nuclear matter

The EoS of symmetric nuclear matter with the full Skyrme interaction evaluated at the second order is expressed as the sum of the mean-field term (first-order) and the second-order terms. By using the DR/MS technique we can derive the following expression:

$$\frac{E}{A}(\rho)=\frac{3\hbar^2}{10m}\left(\frac{3\pi^2}{2}\rho\right)^{\frac{2}{3}}+\frac{3}{8}t_0\rho+\frac{1}{16}t_3\rho^{\alpha+1}+\frac{3}{80}\left(\frac{3\pi^2}{2}\right)^{\frac{2}{3}}\rho^{\frac{5}{3}}\Theta_s+\frac{\Delta E^S}{A}(\rho),$$

where S stands for symmetric matter. Moreover, the expression of the second-order correction is given by:

$$\frac{\Delta E^S}{A}(\rho)=\frac{2\ln 2-11}{105}\,\chi_1^S(\rho)+\frac{24\ln 2-167}{945}\,\chi_2^S(\rho)+\frac{312\ln 2-2066}{31185}\,\chi_3^S(\rho)+\frac{1236\ln 2-9997}{62370}\,\chi_4^S(\rho). \tag{6.10}$$

The four density-dependent coefficients $\chi^S_{1,2,3,4}$ have the following expressions as a function of the parameters of the interaction:

$$\begin{aligned}
\chi_1^S(\rho) &= 48\,\pi^3\,\tilde{C}\,m_S^*\,k_F^4(\rho)\left(t_{03}^2+x_{03}^2\right),\\
\chi_2^S(\rho) &= 64\,\pi^3\,\tilde{C}\,m_S^*\,k_F^6(\rho)\left(t_{03}\,t_{12}+x_{03}\,x_{12}\right)\\
\chi_3^S(\rho) &= 64\,\pi^3\,\tilde{C}\,m_S^*\,k_F^8(\rho)\left(t_{12}\,x_{12}\right),\\
\chi_4^S(\rho) &= 64\,\pi^3\,\tilde{C}\,m_S^*\,k_F^8(\rho)\left(t_{12}^2+\,x_{12}^2\right),
\end{aligned} \tag{6.11}$$

with $\tilde{C}=-\frac{1}{\hbar^2}\frac{3}{(2\pi)^7}$. The expressions of t_{03}, x_{03}, x_{12} and t_{12} have been already introduced previously. One can notice the following:

1. It is clear from Eq. (6.11) that there is a different dependence of the different coefficients χ on the Fermi momentum k_F and consequently on the density ρ. Moreover,we note the implicit density dependence inside the expressions of t_{03} and x_{03} due to the density-dependent two-body force.

2. The first term in Eq. (6.11) corresponds to that obtained in the $t_0 - t_3$ model (See Eq. (6.9)). The $t_0 - t_3$ result for the second-order correction is recovered by considering the first term where the parameters x_0 and x_3 are taken equal to zero.

The corrected second-order EoS is plotted in Fig. 6.3 as a function of the density ρ and compared with the SLy5 reference mean-field EoS. One can observe the following:

- The correction is extremely large also in the case of the full Skyrme interaction.
- But the curvature is not modified in this case with respect to the mean-field EoS. This is due to the analytical expression of the second-order correction (in this case there is no simple dependence on the square of a coupling constant as in the $t_0 - t_3$ model).
- Since the SLy5 parametrization is designed to work well for Skyrme SCMF models, an adjustment of parameters is needed to avoid double counting problems and provide a reasonable EoS.

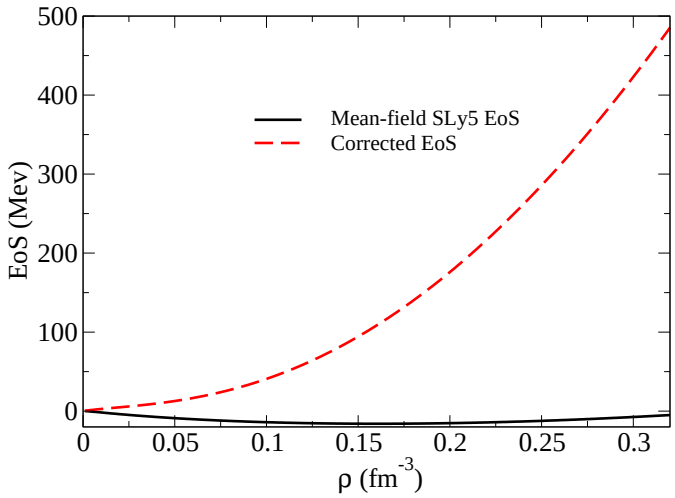

Figure 6.3: SLy5 mean-field EoS (full line) and mean-field + second-order EoS calculated with the SLy5 parameters (dashed line) for symmetric matter.

6.4.1.1 Adjustment of parameters

We have chosen the Sly5 mean-field EoS as our reference EoS to adjust the parameters of the Skyrme interaction at this beyond mean-field level. A χ^2-minimization is performed again using the expression of χ^2 defined in Eq. (5.31). In this fitting procedure, we have kept free the nine parameters of the Skyrme interaction, and first performed separate fits for the cases of symmetric, asymmetric and pure neutron matter. The number N of fitted points is 15 and the errors ΔE_i are chosen equal to 1% of the reference SLy5 mean-field energies

$E_{i,ref}$. The points are in the range of densities between 0.02 to 0.30 fm^{-3}. We have then done simultaneous fit of symmetric and pure neutron matter. The points are in this case in the range of densities between 0.1 and 0.3 fm^{-3}. We first present the results obtained for symmetric matter.
Since the number of parameters is large enough (compared to the simple $t_0 - t_3$ model), we were able this time to perform successfully the fit. The results are shown in Fig. 6.4. The refitted parameters and the corresponding χ^2 value are reported in the Table 6.1.

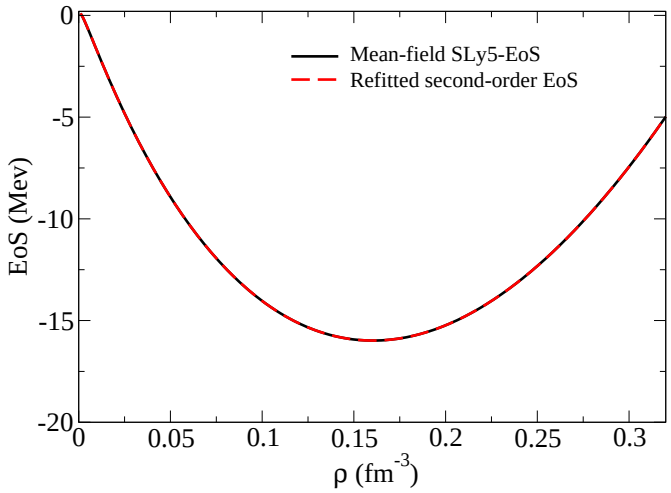

Figure 6.4: SLy5 mean-field EoS (full line) and refitted second-order EoS (dashed line) for symmetric matter.

Table 6.1: Parameter sets obtained in the fit of the EoS of symmetric matter compared with the original set SLy5. In the last column the χ^2 values are shown. In the last line the parameters correspond to the fit where an additional constraint on the symmetry energy value is added.

	t_0 (MeV fm^3)	t_1 (MeV fm^5)	t_2 (MeV fm^5)	t_3 (MeV fm$^{3+3\alpha}$)	x_0	x_1	x_2	x_3	α	χ^2
SLy5	-2484.88	483.13	-549.40	13763.0	0.778	-0.328	-1.0	1.267	0.16667	–
New	-2510.87	20239.43	-897.06	-1176280.24	0.065	-1.272	-21.775	-0.656	0.663	3.5×10^{-7}
New$_{a_I}$	-3401.65	28666.59	-970.62	-1938032.85	0.330	-1.563	-24.078	-0.819	0.666	4.6×10^{-3}

Using the refitted parameters from Table 6.1, the corresponding second-order pressure and compressibility are displayed in the upper and lower panels of Fig. 6.5. In particular, the incompressibility value at saturation density is equal to 229.5 MeV.
The quality of the fit is extremely good as one can deduce from the figures and from the

small value of the corresponding χ^2. We have then performed a final check with the refitted parameters: we have computed the symmetry energy a_δ by using the second derivative of the second-order EoS for asymmetric matter. We have obtained $a_I = 1643.3$ MeV, that is very far from the range of acceptable values. For this reason, we have added in the fitting procedure an additional constraint on the value of the symmetry energy by using as a reference the SLy5 mean-field value of a_I. We report in the fourth line of Table 6.1 the new parameters. We observe that the value of χ^2 is larger in this case than in the previous fit indicating that the inclusion of the new constraint slightly deteriorates the quality of the fit that is still anyway extremely good. The symmetry energy is now equal to 32.03 MeV (equal to the mean-field SLy5 value). The incompressibility value at saturation density is now equal to 228.5 MeV.

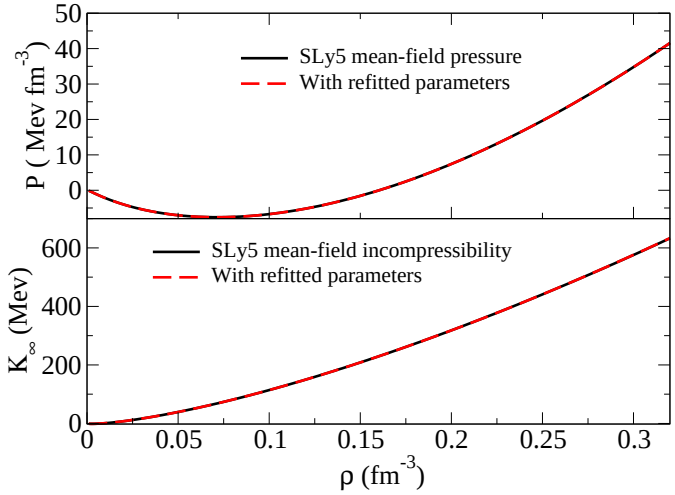

Figure 6.5: (a) Mean-field SLy5 pressure (full line) and second-order pressure obtained with the refitted parameters of Table I (dashed line). (b) Same as in (a) but for the incompressibility.

6.4.2 Pure neutron matter

By using the DR/MS technique, the EoS of pure neutron matter with the full Skyrme interaction evaluated at the second order is expressed as:

$$\frac{E}{A}(\rho) = \frac{3\hbar^2}{10m}\left(3\pi^2\rho\right)^{\frac{2}{3}} + \frac{1}{4}t_0\left(1-x_0\right)\rho + \frac{1}{24}\left(1-x_3\right)t_3\rho^{\alpha+1} + \frac{3}{40}\left(3\pi^2\right)^{\frac{2}{3}}\rho^{\frac{5}{3}}\left(\Theta_s - \Theta_v\right) + \frac{\Delta E^N}{A}(\rho),$$

where N stands for pure neutron matter. In this case, the second-order energy correction is given by:

$$\begin{aligned}\frac{\Delta E^N}{A}(\rho) &= \frac{2\ln 2 - 11}{105}\,\chi_1^N(\rho) + \frac{24\ln 2 - 167}{2835}\,\chi_2^N(\rho) + \frac{167 - 24\ln 2}{5670}\,\chi_3^N(\rho) \\ &+ \frac{461 - 24\ln 2}{31185}\,\chi_4^N(\rho) + \frac{516\ln 2 - 4021}{124740}\,\chi_5^N(\rho), \end{aligned} \tag{6.12}$$

and the five density-dependent coefficients χ^N are:

$$\begin{aligned}\chi_1^N(\rho) &= 8\,\pi^3\,\tilde{C}\,m_N^*\,k_N^4(\rho)\,(t_{03} - x_{03})^2\,, \\ \chi_2^N(\rho) &= 32\,\pi^3\,\tilde{C}\,m_N^*\,k_N^6(\rho)\,(t_{03}\,t_{12} + x_{03}\,x_{12})\,, \\ \chi_3^N(\rho) &= 64\,\pi^3\,\tilde{C}\,m_N^*\,k_N^6(\rho)\,(t_{03}\,x_{12} + x_{03}\,t_{12})\,, \\ \chi_4^N(\rho) &= 64\,\pi^3\,\tilde{C}\,m_N^*\,k_N^8(\rho)\,(t_{12}\,x_{12})\,, \\ \chi_5^N(\rho) &= 64\,\pi^3\,\tilde{C}\,m_N^*\,k_N^8(\rho)\left(t_{12}^2 + x_{12}^2\right). \end{aligned} \tag{6.13}$$

In Eq. (6.13), we take the neutron effective mass m_N^* equal to its mean-field value like in Ref. [10]. Moreover, the neutron Fermi momentum k_N is given as function of the Fermi momentum and the isospin parameter δ ($\delta = 1$ for pure neutron matter) according to the following formulas:

$$k_N(\rho) = k_F(\rho)(1+\delta)^{1/3}, \quad \text{and} \quad \delta = \frac{\rho_N - \rho_P}{\rho_N + \rho_P}.$$

We plot in Fig. 6.6, the second-order EoS calculated with the SLy5 parameters as a function of the density ρ and compared with the mean-field SLy5 EoS.

1. We observe that the correction is always positive and it is extremely large as compared to the SLy5 mean-field EoS. This means that an adjustment of parameters is required to get rid of double counting problems.

2. In the case of DR/MS, we see that the corrected EoS does not have any saturation region unlike the case with the cutoff scheme introduced in the previous chapter.

6.4.2.1 Adjustment of parameters

We choose the SLy5 mean-field EoS as a reference EoS to perform the fit and we perform a χ^2 minimization using Eq. (5.31). The result of the fit is displayed in Fig. 6.7 and the corresponding parameters are given in Table 6.2. It has to be noted also this time that the quality of the fit is extremely good because the value of the corresponding χ^2 is very small.

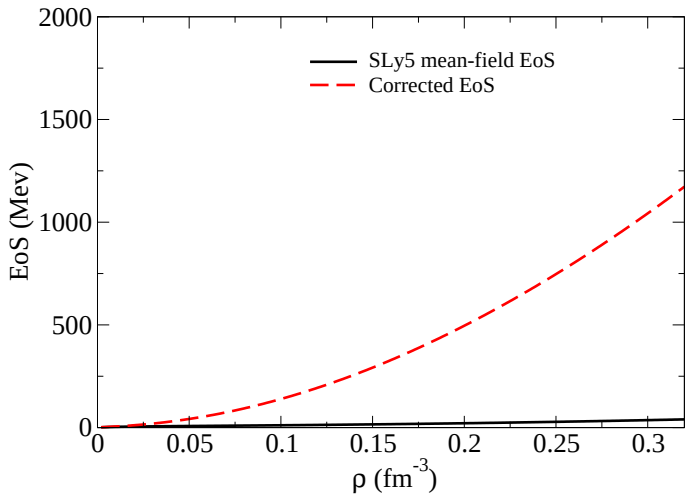

Figure 6.6: SLy5 mean-field EoS (full line) and mean-field + second-order EoS calculated with the SLy5 parameters (dashed line) for neutron matter.

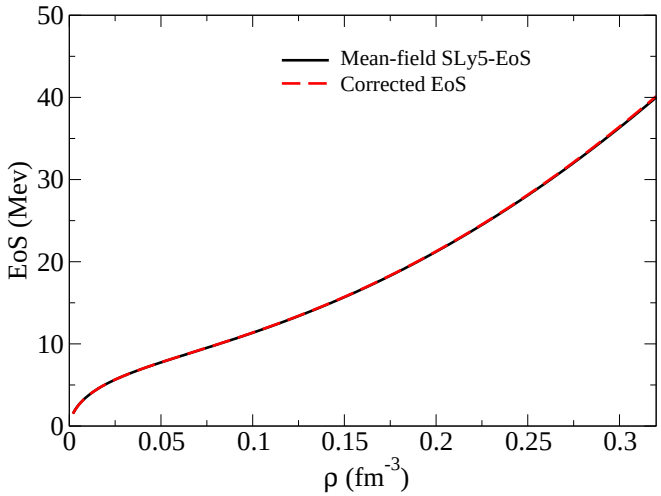

Figure 6.7: SLy5 mean-field EoS (full line) and refitted second-order EoS (dashed line) for neutron matter (parameters of Table 6.2).

Table 6.2: Parameter sets obtained in the fit of the EoS of pure neutron matter compared with the original set SLy5. In the last column the χ^2 value is shown.

	t_0 (MeV fm^3)	t_1 (MeV fm^5)	t_2 (MeV fm^5)	t_3 (MeV fm$^{3+3\alpha}$)	x_0	x_1	x_2	x_3	α	χ^2
SLy5	-2484.88	483.13	-549.40	13763.0	0.778	-0.328	-1.0	1.267	0.16667	–
New	-3287.287	2038.711	-459.159	109814.050	0.706	-1.645	-3.861	3.127	0.656	1.15×10^{-4}

6.4.3 Asymmetric nuclear matter

The EoS of asymmetric nuclear matter ($\delta = 0.5$ as an example) with the full Skyrme interaction evaluated at the second order is given by the following expression (if DR/MS technique is used):

$$\begin{aligned}\frac{E}{A}(\delta,\rho) &= \frac{3\hbar^2}{10m}\left(\frac{3\pi^2}{2}\rho\right)^{\frac{2}{3}} G_{5/3} + \frac{1}{8}t_0\rho[2(2+x_0)-(1+2x_0)G_2] \\ &+ \frac{1}{48}t_3\rho^{\alpha+1}[2(2+x_3)-(1+2x_3)G_2] + \frac{3}{40}\left(\frac{3\pi^2}{2}\right)^{\frac{2}{3}}\rho^{\frac{5}{3}}\left[\Theta_v G_{5/3} + \frac{1}{2}(\Theta_s - 2\Theta_v)G_{8/3}\right] \\ &+ \frac{\Delta E^{AS}(\delta,\rho)}{A}, \end{aligned} \tag{6.14}$$

where 'AS' stands for asymmetric and the expression G_β is given in terms of the asymmetry parameter δ according to: $G_\beta = \frac{1}{2}[(1+\delta)^\beta + (1-\delta)^\beta]$. The expression for $\Delta E^{AS}(\rho,\delta)/A$ is reported in Appendix D.4.

6.4.3.1 Adjustment of parameters

We perform a χ^2 minimization using again Eq. (5.31). The result of the fit is displayed in Fig. 6.8 and the corresponding parameters are given in Table 6.3. The value of the corresponding χ^2 is very small also this time.

Table 6.3: Parameter sets obtained in the fit of the EoS of asymmetric matter $\delta = 0.5$ compared with the original set SLy5. In the last column the χ^2 value is shown.

	t_0 (MeV fm^3)	t_1 (MeV fm^5)	t_2 (MeV fm^5)	t_3 (MeV fm$^{3+3\alpha}$)	x_0	x_1	x_2	x_3	α	χ^2
SLy5	-2484.88	483.13	-549.40	13763.0	0.778	-0.328	-1.0	1.267	0.16667	–
New	-2902.271	24500.821	-1052.111	-1591978.20	0.118	-1.683	-25.549	-0.734	0.661	1.17×10^{-4}

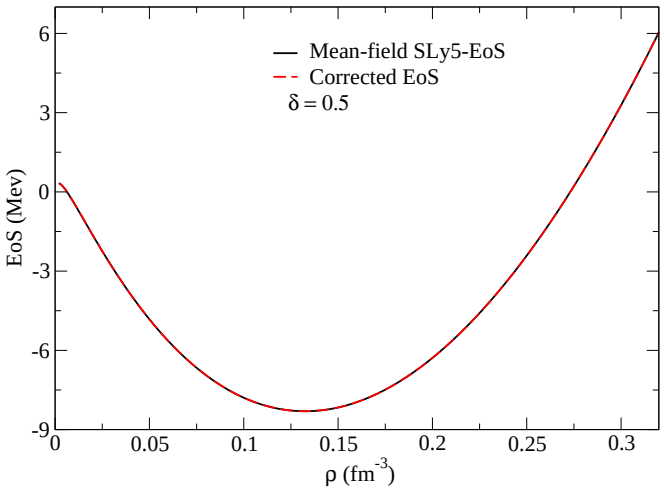

Figure 6.8: SLy5 mean-field EoS (full line) and refitted second-order EoS (dashed line) for asymmetric matter $\delta = 0.5$ (parameters of Table 6.3).

6.4.4 Results: Global fits

In the previous chapter, within the cutoff scheme, we have performed a global fit by including simultaneously three EoS's: symmetric, pure neutron matter, and also a case of asymmetric matter. We have tried also this time to perform the same kind of adjustment, but it turns out that the minimization of the χ^2 in this case does not provide any good result. We have thus performed global fits by including only two equations of state instead of three: symmetric and pure neutron matter. The results of the fit is displayed in Fig. 6.9 and the values of the refitted parameters are given in Table 6.4.

Table 6.4: Parameter sets obtained in the fit of the EoS of symmetric and pure neutron matter compared with the original set SLy5. In the last column the χ^2 value is shown.

	t_0 (MeV fm^3)	t_1 (MeV fm^5)	t_2 (MeV fm^5)	t_3 (MeV fm$^{3+3\alpha}$)	x_0	x_1	x_2	x_3	α	χ^2
SLy5	-2484.88	483.13	-549.40	13763.0	0.778	-0.328	-1.0	1.267	0.16667	–
New	-460.73	10403.66	-8485.73	-141558.6	1.460	-0.681	-0.641	-0.779	0.650	0.202

Moreover, the resulting pressure and incompressibility are plotted, in Fig. 6.10 as function of the density using the refitted parameters. At saturation, the incompressibility value is equal to 252.18 MeV.
The χ^2 value is larger than in the previous cases indicating that the quality of the fit has been deteriorated, but it still remains reasonably good. This can be seen also by looking at the plotted curves.

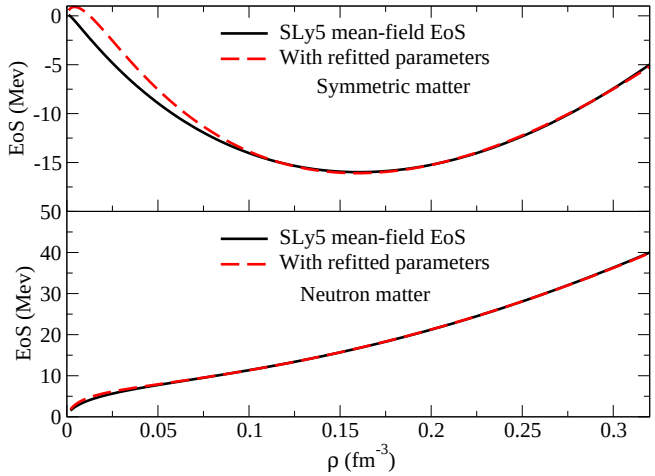

Figure 6.9: (a) SLy5 mean-field (full line) and refitted (dashed line) EoS for symmetric matter. (b) Same as in (a) but for neutron matter. The results are obtained by fitting simultaneously symmetric and neutron matter (parameters of Table 6.4).

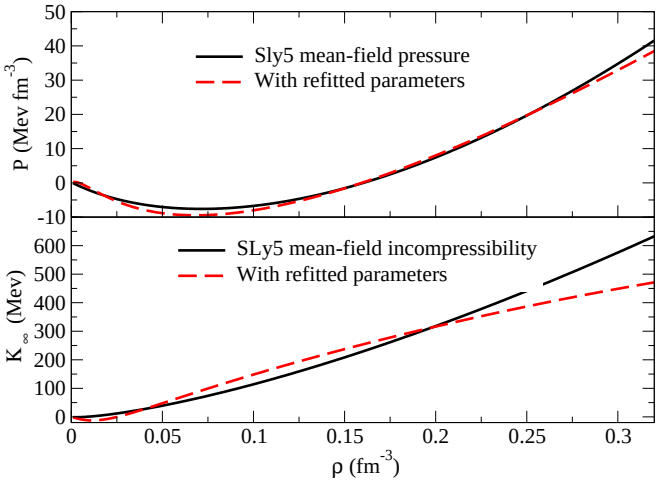

Figure 6.10: (a) Mean-field SLy5 pressure (full line) and second-order pressure obtained with the refitted parameters (dashed line). (b) Same as in (a) but for the incompressibility. The results are obtained by fitting simultaneously symmetric and neutron matter (parameters of Table 6.4).

We have computed also in this case the symmetry energy with the parameters of Table 6.4 and obtained the value of -7.5 MeV that is not acceptable. We have partially succeeded this time in adding also a constraint on the value of the symmetry energy: what we have found with this last fit is a value of 32.7 MeV for the symmetry energy and a value of 310.74 MeV for the incompressibility at the saturation point. However, the associated χ^2 is equal to 4.49, that indicates that the fit is much less good than in the previous cases. The fitted curves are of much lower quality than for the other fits and are not shown in the manuscript. We conclude that the global fit that includes symmetric and pure neutron matter does not provide satisfactory results: either it does not lead to a reasonable value for the symmetry energy or it is of quite low quality (when the constraint on the symmetry energy is explicitly introduced).
We have performed a new global fit by disregarding the case of pure neutron matter and by considering together symmetric and asymmetric matter (with $\delta = 0.5$). The results are shown in Fig. 6.11 and the parameters are listed in Table 6.5.

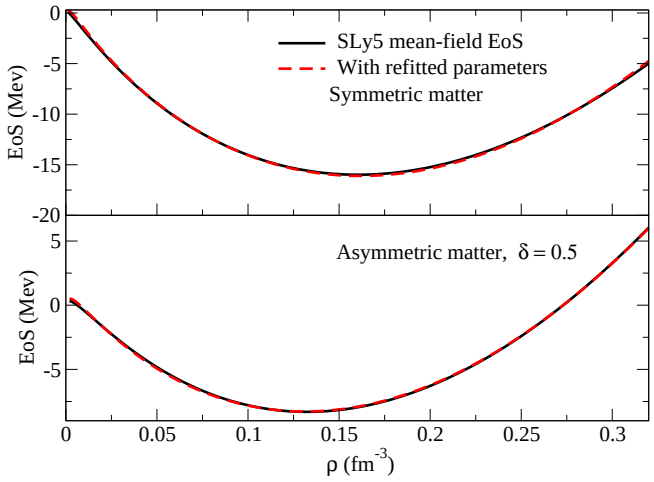

Figure 6.11: (a) SLy5 mean-field (full line) and refitted (dashed line) EoS for symmetric matter. (b) Same as in (a) but for neutron matter. The results are obtained by fitting simultaneously symmetric and asymmetric matter with $\delta = 0.5$ (parameters of Table 6.5).

The pressure and incompressibility values are plotted in Fig. 6.12. At saturation, the incompressibility is equal to 233.8 MeV and the symmetry energy is equal to 24.9 MeV. If we include in the fitting procedure an additional constraint on the symmetry energy value we obtain curves that are very similar to those already shown in Fig. 6.11, a value for the incompressibility at the saturation point equal to 233.9 MeV and a value for the symmetry energy equal to 32.00 MeV. The corresponding new parameters are reported in the last line of Table 6.5 and are not very different with respect to the previous set that is shown in the line above.

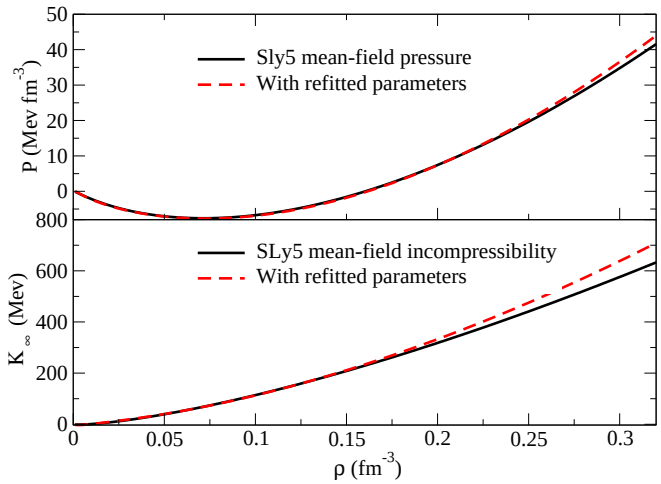

Figure 6.12: (a) Mean-field SLy5 pressure (full line) and second-order pressure obtained with the refitted parameters (dashed line). (b) Same as in (a) but for the incompressibility. The results are obtained by fitting simultaneously symmetric and asymmetric matter with $\delta = 0.5$ (parameters of Table 6.5).

Table 6.5: Parameter sets obtained in the fit of the EoS of symmetric and asymmetric matter compared with the original set SLy5. In the last column the χ^2 value is shown. In the last line the parameters correspond to the fit where an additional constraint on the symmetry energy value has been added.

	t_0 (MeV fm^3)	t_1 (MeV fm^5)	t_2 (MeV fm^5)	t_3 (MeV fm$^{3+3\alpha}$)	x_0	x_1	x_2	x_3	α	χ^2
SLy5	-2484.88	483.13	-549.40	13763.0	0.778	-0.328	-1.0	1.267	0.16667	–
New	-1653.09	10346.70	-698.66	-784064.9	0.716	-1.715	-14.9	-0.697	0.667	1.337
New$_{a_I}$	-1656.03	10526.54	-727.53	-795583.4	0.729	-1.783	-14.7	-0.725	0.667	1.341

6.5 Limits of the phenomenological approaches

To summarize:

- It is evident from Fig. 6.2 that the EoS for symmetric nuclear matter evaluated at the second-order in the $t_0 - t_3$ model is always positive and has the opposite curvature with respect to the SkP mean-field EoS. Moreover, it turns out that the adjustment of the corrected EoS to a reasonable reference EoS is not feasible. The minimization of a χ^2 does not lead to any result and this means that the parameters cannot be adjusted in this case.

- The second-order correction is greater than the first-order one and this means that the expansion parameter in the perturbation theory we are using is greater than 1 in this case.

- For the full Skyrme interaction, the situation is different and we are able to readjust the Skyrme parameters after having applied the DR techniques.
- There is a general problem related to the use of effective interactions and perturbative expansions to extract the leading (the mean-field level) and the subleading (beyond the mean-field level) contributions: we observe that the second-order contributions are not smaller with respect to the leading order.
- We have truncated at the second-order level by arguing that the third-, fourth-, $\cdots$,n^{th}-orders are small compared to the second-order contribution. However, it turns out that this may not be the case and that what we treat as a higher-order (beyond the mean-field level) contribution might be comparable to some of the leading-order contributions with the Skyrme interaction.
- This general problem will be addressed in my future work.

6.6 Conclusions

In this chapter, we have regularized the second-order divergent term of the EoS of nuclear matter evaluated with a zero-range Skyrme interaction. The DR/MS technique with minimal subtraction scheme has been used.
First of all, we have derived the EoS of symmetric nuclear matter with the simplified $t_0 - t_3$ Skyrme interaction. We have drawn the following conclusions:

1. We found that the corrected EoS is always positive and has a maximum: consequently, in this case, the equilibrium point does not exist.
2. This means that DR/MS shows the repulsive nature of the finite part unlike the case when a momentum cutoff is introduced [9, 161].
3. The adjustment of the corrected EoS to a reasonable reference EoS is not feasible because the χ^2-minimization does not lead to any result.

Then, we have included the velocity-dependent terms of the Skyrme interaction to increase the number of parameters. We have done some applications to different types of matter with the full Skyrme interaction.

1. It has been shown that a fit of the regularized EoS of symmetric, pure neutron and asymmetric matter, to a reference EoS is possible.
2. It is also shown that simultaneous fits of symmetric and neutron matter can be done with reasonable values of χ^2.
3. It has been verified that an additional constraint on the value of the symmetry energy can be added and satisfactory results are found in this way in the cases where only symmetric matter or symmetric and asymmetric matter (simultaneously) are fitted.

4. These encouraging results open new prospectives for future applications of dimensional regularized Skyrme-type effective interactions adjusted at a beyond mean-field level. These interactions would be well adapted to be used in the framework of beyond-mean-field approaches for finite nuclei.

Chapter 7

Towards finite nuclei. An example of beyond-mean-field model in finite systems: The PVC model. Formalism and first applications.

7.1 Introduction

In the HF approximation, the trial wave function is expressed as a Slater determinant, an antisymmetrized product of single-particle wave functions. This variational method allows us to interpret the many-body wave function in terms of the single-particle degrees of freedom, a static independent-particle picture is adopted and correlations are not included. Giant resonances are basic nuclear excitations which encode useful information on the nuclear structure and on the effective nucleon-nucleon interaction [35, 105, 162]. To describe quantitatively the nuclear collective excitations, the most currently used theoretical tool is the RPA approximation which is constructed on top of the HF single-particle particle-hole configurations including small-amplitude correlations [35, 163]. This approximation was introduced by Bohm and Pines [164] in the theory of plasma oscillations. The HF and the RPA individual and collective degrees of freedom are the constructing blocks of the PVC. Before introducing the PVC model, we present the main properties of the RPA model.

7.2 Random-phase approximation

The collective excitations of nuclei such as the giant resonances can be calculated in a consistent framework by extending the static mean-field approach to a time-dependent description in its small-amplitude limit leading to the RPA model.
In the framework of RPA, the ground state $|\mathrm{RPA}\rangle$, that will be defined later, is in principle correlated.

7.2.1 The RPA ground state

The collective states can be described by defining an excitation operator $Q_n^\dagger$ that creates the excited state $|n\rangle$ when it acts on the ground state:

$$Q_n^\dagger|\text{ground}-\text{state}\rangle = |\text{n}\rangle.$$

In the RPA formalism, the excitation operator $Q_n^\dagger$ can be written as a superposition of particle-hole elementary excitations:

$$Q_n^\dagger = \sum_{ph}\left(X_{ph}^n a_p^\dagger a_h - Y_{ph}^n a_h^\dagger a_p\right), \tag{7.1}$$

where the p and h particle and hole indices are defined by convention with respect to the HF ground state of the system. The $|\text{RPA}\rangle$ ground state is defined as the vacuum of Q_n, that is, $Q_n|\text{RPA}\rangle = 0$.

7.2.2 Derivation of RPA equations. Some examples

There are numerous formulations of the RPA model.

7.2.2.1 The Green's function method

The Green's function method [165] is used to derive an approximate expression for the two-particle Green's function by summing a restricted class of bubble diagrams in a perturbation expansion.

7.2.2.2 The equations-of-motion method using the quasiboson approximation

Equations of motion written by using the Shroedinger equation are the starting point. In these equations, after simple manipulations, matrix elements appear that should be calculated in the $|\text{RPA}\rangle$ ground state. The quasiboson approximation consists in replacing the $|\text{RPA}\rangle$ by the HF ground state $|\text{HF}\rangle$ in all the matrix elements. In the quasiboson approximation [166], the particle-hole pair operators are approximated as bosons. In other words, the commutators of particle-hole operators are replaced by their vacuum expectation values in the uncorrelated particle-hole state; a drawback of such approximation is thus that it implies a violation of the Pauli principle [35].

7.2.2.3 Time-dependent HF method

The time-dependent HF (TDHF) theory is an attempt to find an approximate solution of the time-dependent Schrödinger equation [35, 167]. This approach has nice applications to a wide range of phenomena, such as low-lying collective excitations, nuclear fission, and heavy-ion collisions at moderate energies [35]. In its small-amplitude limit the TDHF theory leads to the standard RPA equations.

7.2.2.4 RPA equations

The RPA equations are usually written in a compact form as:

$$\begin{pmatrix} A & B \\ -B^\star & -A^\star \end{pmatrix} \begin{pmatrix} X_{ph} \\ Y_{ph} \end{pmatrix} = \hbar\Omega_n \begin{pmatrix} X_{ph} \\ Y_{ph} \end{pmatrix}. \tag{7.2}$$

- The amplitudes X and Y appear in Eq. (7.1), Ω_n is the excitation energy of the excited state $|n\rangle$:

  $$\Omega_n = E_n - E_0,$$

  where E_n is the energy of the excited state $|n\rangle$ and E_0 is the ground-state energy.

- The matrices A and B are defined as:

$$\begin{aligned} A_{ph\,p'h'} &= \langle RPA| \left[a_h^\dagger a_p \left[H, a_{p'}^\dagger a_{h'}\right]\right] |RPA\rangle \\ B_{ph\,p'h'} &= -\langle RPA| \left[a_h^\dagger a_p \left[H, a_{h'}^\dagger a_{p'}\right]\right] |RPA\rangle. \end{aligned} \tag{7.3}$$

Within the quasiboson approximation, the $|\text{RPA}\rangle$ is replaced by $|\text{HF}\rangle$. If one ignores B, then one is simply diagonalizing H in a truncated basis; this is the Tamm-Dancoff approximation.

7.2.3 Sum rules

The sum rules constitute a very important piece in the theory of collective excitations. In many cases, they allow us a calculation of global properties in a simple way and are useful for testing different approximation schemes.

7.2.3.1 Energy-weighted sum rules

Given a one-body operator, Q, we define the k^{th} power of the RPA energy-weighted moments m_k by:

$$m_k = \sum_{n=0}^{\infty} (E_n - E_0)^k \left|\langle n|Q|HF\rangle\right|^2,$$

where $|n\rangle$ represents an excited state and E_n its corresponding energy.
If one assumes that the states are oscillator-like, then the excitation energy for the k^{th} harmonic collective oscillation corresponds to the ratio of energy-weighted moments

$$E_k \approx (m_k/m_{k-2})^{1/2}.$$

Thouless [168], Martorell et al. [169] and Lipparini et al. [170] found that the m_1 RPA moment can be expressed in terms of expectation values of well-defined operators in the HF ground state. It is possible to write:

$$m_1 = \frac{1}{2}\langle HF| \left[Q, [H, Q]\right] |HF\rangle.$$

Consequently, one arrives to the following identity that is called energy-weighted sum rules:

$$\boxed{\sum_{n=0}^{\infty}(E_n - E_0)\left|\langle n|Q|HF\rangle\right|^2 = \frac{1}{2}\langle HF|\left[Q,[H,Q]\right]|HF\rangle}. \tag{7.4}$$

Checking how much this identity is satisfied is an important test when RPA calculations are performed.

7.2.3.2 Spurious modes

When the operator Q commutes with the Hamiltonian H (i.e., Q is a symmetry of H) like the linear momentum and total angular momentum in spherical systems, the double commutator of the r.h.s of Eq.(7.4) vanishes.

$$[H,Q] = 0 \Longrightarrow \langle HF|\left[Q,[H,Q]\right]|HF\rangle = 0.$$

The l.h.s. must therefore be equal to zero:

$$\sum_{n=0}^{\infty}(E_n - E_{RPA})\left|\langle n|Q|RPA\rangle\right|^2 = 0.$$

Consequently, the excitation energies of the states generated by these operators acting on the ground state must be zero. This zero-energy state is called a spurious state (for example, the oscillation of the center of mass of the nucleons in the nuclear potential well).
For example, the isoscalar dipole excitation [171] in nuclei simply corresponds to a translation of the center of mass and is predicted at excitation energy equal to zero (if the adopted approximation method is good). If the problem is solved without a full self-consistency, the spurious mode is found at finite energy (not zero).

7.3 PVC model

We are going to describe and use a second-order perturbation version of the PVC model. The coupling of the single-particle degrees of freedom to the RPA particle-hole excitations has a graphical representation in Fig. 7.1 where the polarization graph is drawn on the left and the correlation graph on the right. The overcounting problem due to the use of the RPA to evaluate the contributions of Fig. 7.1 is solved by subtracting the second-order contributions of Fig. 7.2 that have been already analyzed for nuclear matter in this work.
Let us clarify how in practice the PVC is realized.

If we start with the one-body Green's function G_α of the state $|\alpha\rangle$, we can write it as:

$$G_\alpha(E) = \frac{1}{E - K_\alpha - M_\alpha(E)}, \tag{7.5}$$

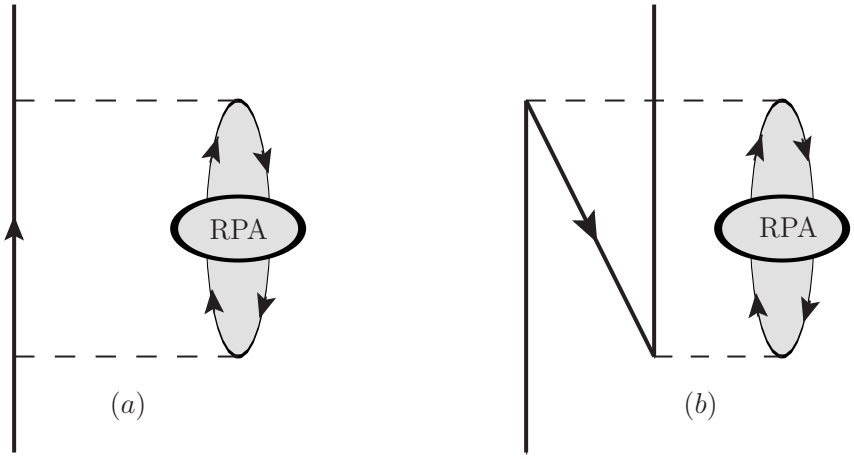

Figure 7.1: Particle-hole RPA contributions.

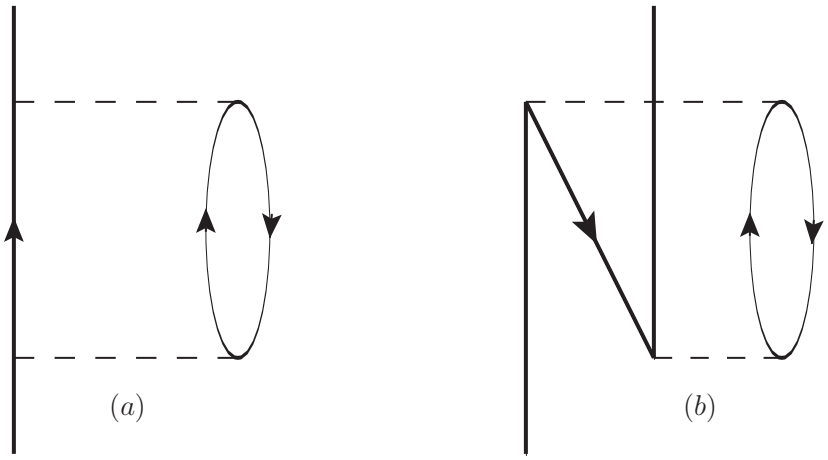

Figure 7.2: Second-order energy contributions.

where K_α represents the kinetic part and M_α is the mass operator. The poles of the G_α are:

$$E_\alpha = K_\alpha + M_\alpha(E_\alpha). \tag{7.6}$$

Let us interpret E_α as the energy of the main fragment of the state $|\alpha\rangle$. Close to E_α, one has:

$$G_\alpha(E) \sim \frac{S_\alpha}{E - E_\alpha}, \tag{7.7}$$

where S_α is what we call spectroscopic factor with:

$$S_\alpha = \left(1 - \frac{\partial M_\alpha}{\partial E}\right)^{-1}_{E=E_\alpha}. \tag{7.8}$$

In the specific case of the HF model, each state has a unique fragment at the HF single-particle energy ϵ_α of the state. The spectroscopic factor is thus just equal to 1 (no fragmentation). If one wants to describe some fragmentation, a model should be used where the mass operator has an energy dependence. PVC is an example.
The new mass operator, by taking into account the graphs of Figs. 7.1 and 7.2, is:

$$M(E) = M^{HF} + \Sigma(E). \tag{7.9}$$

- The term M^{HF} is the mass operator calculated at the mean-field level and it is represented in Fig. 7.3 by:

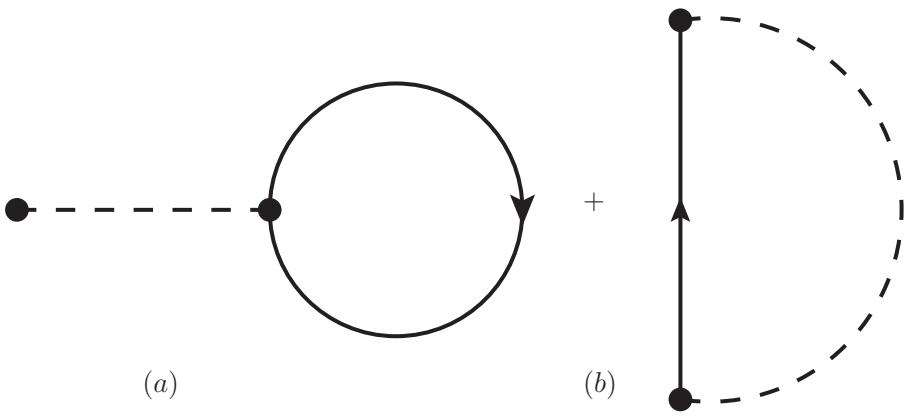

Figure 7.3: Mean-field contributions.

- The term $\Sigma(E)$ is the beyond mean-field contribution to the mass operator $M(E)$. Its expression is given by:

$$\Sigma(E) = \Sigma^{RPA} - \Sigma^{(2)}(E). \tag{7.10}$$

For each state $|\Psi_N\rangle$ of energy E_N and multipolarity L, we define a transition density ρ_N by:

$$\langle\Psi_0|\psi^\dagger(\hat{r})\psi(\hat{r})|\Psi_N\rangle \equiv \alpha_N\rho_N(\hat{r})Y_{LM}(\hat{r}), \tag{7.11}$$

where α_N is a given coefficient and $|\Psi_0\rangle$ is the ground state.
By using a partial wave expansion, the contribution $\Sigma^{\rm RPA}$ of the graphs shown in Fig. 7.1 can be expressed in terms of the RPA states and the residual interaction $\tilde{v}(r)$ as follows:

$$\begin{aligned}\Sigma^{\rm RPA}_{lj}(r,r',E) &= -\sum_N\sum_{L,l_\lambda,j_\lambda} \tilde{v(r)}\tilde{v(r')}\left|\alpha_N\langle lj|Y_L|l_\lambda j_\lambda\rangle\right|^2\rho_N(r)\rho_N(r') \\ &\times\left[\sum_{\lambda=p}\frac{R_\lambda(r)R_\lambda(r')}{\epsilon_\lambda-E+E_N-i\eta}+\sum_{\lambda=h}\frac{R_\lambda(r)R_\lambda(r')}{\epsilon_\lambda-E-E_N+i\eta}\right],\end{aligned} \tag{7.12}$$

where $R_\lambda(r)$ is the radial part of the HF wavefunction and ϵ_λ is the corresponding HF energy. Some comments could be drawn from Eq. (7.12):

1. The sum ($\lambda = p$) is unrestricted over all λ states. This means that Eq. (7.12) does not converge unless a cutoff is imposed on the intermediate energies and on the excitation energies E_N.

2. This is of course due to the fact that the Skyrme interaction is an effective force valid for low-energy calculations. UV divergences appear in such models.

3. For the residual interaction, a complete expression can be found in Ref. [172]. In the first applications that we perform here, we take only a $t_0 - t_3$ residual interaction, where:

$$\tilde{v}^{qq}_{res}(r) = \left[v_0^{qq}+v_\sigma^{qq}\sigma_1\cdot\sigma_2\right]\delta(r), \tag{7.13}$$

$$\tilde{v}^{qq'}_{res}(r) = \left[v_0^{qq'}+v_\sigma^{qq'}\sigma_1\cdot\sigma_2\right]\delta(r). \tag{7.14}$$

The expressions for v_0^{qq}, $v_0^{qq'}$, v_σ^{qq} and $v_\sigma^{qq'}$ are:

$$\begin{aligned}v_0^{qq} &= \frac{1}{2}t_0\left(1-x_0\right)+\frac{1}{16}t_3\left(2+\alpha\right)\left(1+\alpha\right)\rho^\alpha(r)-\frac{1}{12}t_3\left(x_3+\frac{1}{2}\right)\rho^\alpha(r) \\ &+ \frac{1}{48}t_3\alpha\left(1-\alpha\right)\left(1+2x_3\right)\rho^{\alpha-2}(r)\rho_-^2(r)-\frac{1}{12}t_3\alpha\left(1+2x_3\right)\rho^{\alpha-1}(r)\rho_-(r), \\ v_0^{qq'} &= \frac{1}{2}t_0\left(2+x_0\right)+\frac{1}{16}t_3\left(2+\alpha\right)\left(1+\alpha\right)\rho^\alpha(r)+\frac{1}{12}t_3\left(x_3+\frac{1}{2}\right)\rho^\alpha(r) \\ &+ \frac{1}{48}t_3\alpha\left(1-\alpha\right)\left(1+2x_3\right)\rho^{\alpha-2}(r)\rho_-^2(r), \\ v_\sigma^{qq}(r) &= \frac{1}{2}t_0\left(x_0-1\right)-\frac{1}{12}t_3\left(1-x_3\right)\rho^\alpha(r), \\ v_\sigma^{qq'}(r) &= \frac{1}{2}t_0x_0+\frac{1}{12}t_3x_3\rho^\alpha(r).\end{aligned}$$

In these formulas ρ_- stands for $\rho_n - \rho_p$.

4. In the simple calculation presented here we neglect unnatural-parity modes, that is, we drop the terms in $\sigma_1 \cdot \sigma_2$. Only v_0^{qq} and $v_0^{qq'}$ contribute. Furthermore, since our $t_0 - t_3$ model contains only the parameters t_0, t_3 and α, we take $x_0 = x_3 = 0$. The expressions for v_0^{qq}, $v_0^{qq'}$ become:

$$\begin{aligned} v_0^{qq} &= \frac{1}{2}t_0 + \frac{1}{16}t_3\,(2+\alpha)\,(1+\alpha)\,\rho^{\alpha}(r) - \frac{1}{24}t_3\rho^{\alpha}(r) + \frac{1}{48}t_3\alpha\,(1-\alpha)\,\rho^{\alpha-2}(r)\rho_-^2(r), \\ v_0^{qq'} &= t_0 + \frac{1}{16}t_3\,(2+\alpha)\,(1+\alpha)\,\rho^{\alpha}(r) + \frac{1}{24}t_3\rho^{\alpha}(r) + \frac{1}{48}t_3\alpha\,(1-\alpha)\,\rho^{\alpha-2}(r)\rho_-^2(r). \end{aligned}$$

The expression for the second-order contribution $\Sigma^{(2)}(r, r', E)$, represented by Fig. 7.2, is given by:

$$\begin{aligned} \Sigma_{lj}^{(2)}(r, r', E) &= -\frac{1}{2}\sum_{p,h}\sum_{L,l_\lambda,j_\lambda} \tilde{v(r)}\tilde{v(r')}\left|\langle lj|Y_L|l_\lambda j_\lambda\rangle\right|^2 \\ &\times \left(\frac{2j_h+1}{2L+1}\right)\left|\langle l_p j_p|Y_L|l_h j_h\rangle\right|^2 R_p(r)R_h(r)R_p(r')R_h(r') \\ &\times \left[\sum_{\lambda=p}\frac{R_\lambda(r)R_\lambda(r')}{\epsilon_\lambda - E + (\epsilon_p - \epsilon_h) - i\eta} + \sum_{\lambda=h}\frac{R_\lambda(r)R_\lambda(r')}{\epsilon_\lambda - E - (\epsilon_p - \epsilon_h) + i\eta}\right] \quad (7.15) \end{aligned}$$

1. Again, the sum ($\lambda = p$) is unrestricted over all λ states. This means that Eq. (7.15) does not converge unless a cutoff is imposed on the intermediate energies $\epsilon_p - \epsilon_h$ and ϵ_λ.

2. UV divergences appear.

7.4 First applications

We make here a first test of the interactions that we have introduced in the past chapters for nuclear matter. Our first question to answer is whether the regularization done for matter (at second order) has some effect on the results that we obtain for nuclei. To make a very simple test, we work with a $t_0 - t_3$ model and not with the full Skyrme interaction. To make self-consistent calculations, we use the $t_0 - t_3$ model in all the calculations: HF, RPA and PVC. Since the spin-orbit part has not been constrained in our calculations for nuclear matter, we include the spin-orbit contribution and we use in all cases described below the spin-orbit parameter of the interaction SkP.
For the $t_0 - t_3$ model, the DR technique does not provide any result (see Chapter 6). We thus use the MC-regularized interactions for these first test-calculations. We are of course aware that we do not expect in PVC exactly the same UV divergence as for the second-order contributions. Our first test has just the objective to verify if some effects of the performed regularization can be seen in the results obtained for nuclei, that is, to verify if the divergence

is at least reduced.
As already said, the PVC results are obtained by subtracting the second-order $\Sigma^{(2)}$ from the quantity $\Sigma^{\rm RPA}$. We can thus verify if the effect of the regularization can be seen at least in $\Sigma^{(2)}$.
To further simplify our test, we analyze only the PVC corrections to some single-particle energies (we do not analyze other quantities for the moment). In order to check if there is a mass dependence in our results, we consider three nuclei with different masses: ^{16}O, ^{48}Ca and ^{132}Sn.
We do not compare for the moment with experimental results because our calculations in the very simple $t_0 - t_3$ model do not have any quantitative predictive power.
We start our applications in finite nuclei by solving the HF equations in a radial mesh with a step equal to 0.1 fm. Once the HF solution is found, we solve the RPA equations in the usual matrix formulation:

1. For a given J^π value, where J denotes the multipolarity of the RPA phonon and π its parity, a N-dimensional basis of coupled p-h configuration associated with the $Q^\dagger$ operators of Eq. (7.1) is constructed. All possible occupied states (h) are considered together with all possible unoccupied states (p) lying below a cutoff energy.

2. We build the matrix elements A and B defined in Eqs. (7.3).

3. We diagonalize the RPA matrix (see Eq. (7.2)).

The continuum is discretized by imposing box boundary conditions on the eigenstates of the HF Hamiltonian. Consequently, in addition to occupied (hole) states denoted by h, we obtain unoccupied (particle) states that are labeled by an index p. Only the RPA phonons having energy smaller than the cutoff Λ are calculated.

7.4.1 Refitted interactions in nuclear matter

As was already discussed in Chap. 5, the cutoff Λ must certainly be smaller than the momentum associated with the nucleon size, i.e., $\Lambda \leq 2$ fm^{-1} = 394.6 MeV. Moreover, the energy scale of low-energy nuclear phenomena in finite nuclei is much smaller, perhaps around 0.5 fm^{-1} = 98.65 MeV.
In Chap. 5, we have derived the expression for the EoS for symmetric nuclear matter calculated at the second-order with the simplified $t_0 - t_3$ model. We adjusted the parameters of the interaction so that the SkP mean-field EoS is reproduced. Thus, we have generated new sets of effective interactions that lead to a reasonable EoS for each value of the cutoff Λ in symmetric nuclear matter. In Table 7.1, we report the values of the parameters t_0, t_3 and α that can be found for each value of the cutoff Λ from $\Lambda = 0.1$ fm^{-1} to $\Lambda = 0.3$ fm^{-1} (1 fm^{-1} = 197.3 MeV). We will take these values of the cutoff for our test calculations.

In Fig. 7.4, the EoS $E/A + \Delta E/A$ (first- plus second-order) for symmetric nuclear matter with the refitted $t_0 - t_3$ Skyrme interaction (see Table 7.1) is plotted for different values of

	t_0 (MeV fm^3)	t_3 (MeV fm$^{3+3\alpha}$)	α
SkP	-2931.700	18708.970	1/6
$\Lambda = 19.73$ MeV	-2931.367	18707.017	0.166
$\Lambda = 39.46$ MeV	-2926.404	18677.901	0.167
$\Lambda = 59.19$ MeV	-2905.302	18554.114	0.168

Table 7.1: Parameter sets obtained in the fits associated with different values of the cutoff Λ compared with the original set SkP (first line).

the cutoff Λ (from 19.73 MeV to 59.19 MeV) and compared with the SkP mean-field curve (solid black li `

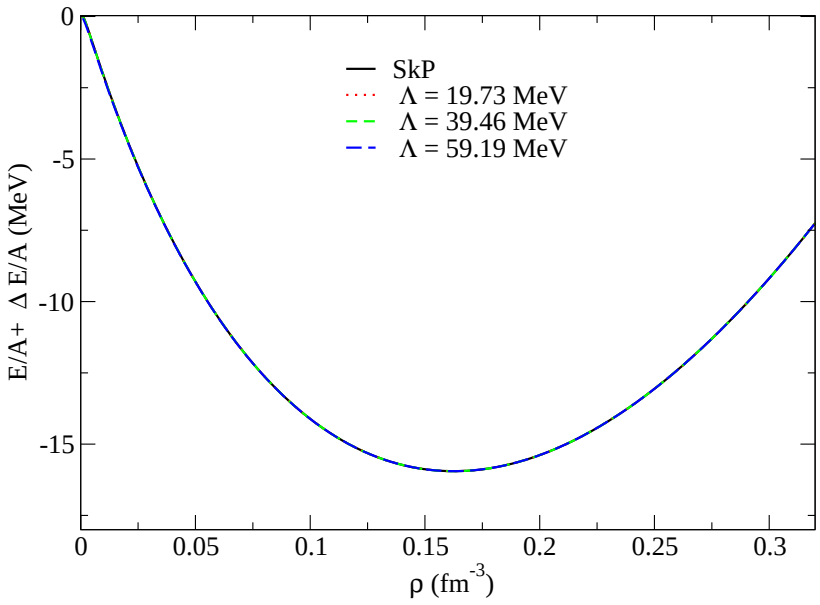

Figure 7.4: Second-order-corrected and refitted equations of state compared with the reference EoS (SkP at mean-field level) for different values of the cutoff Λ.

We analyze the following aspects:

1. Investigate whether these refitted interactions can be applied to finite nuclei and consequently reproduce not only the properties of nuclear matter but also provide single-particle energies that are stable with respect to the cutoff.

2. Compare the second-order contributions to the total PVC contributions. Indeed, it is often believed that the second-order corrections are negligible with respect to the main correction coming from Σ^{RPA}.

3. Check if the refitted interactions regularize at least the divergences that appear in the

second-order corrections.

7.4.2 Results: ^{16}O

In this section we take the nucleus ^{16}O as a simple test to perform the PVC calculations and in the next sections, we do applications to ^{48}Ca and ^{132}Sn.
We calculate the single-particle HF spectrum and then we perform self-consistent RPA calculations using the simplified $t_0 - t_3$ model by including the modes $L = 0^+$, 1^-, 2^+ and 3^-. For this nucleus, we consider as an illustration the neutron hole states $1p_{3/2}$ and $1p_{1/2}$ and the neutron particle state $1d_{5/2}$.
In Table. 7.2, we show the HF single-particle energies.

Nucleus	hole states [MeV]		particle states [MeV]	
^{16}O	$1p\frac{3}{2}$	-25.16	$1d\frac{5}{2}$	-11.54
	$1p\frac{1}{2}$	-17.69		

Table 7.2: Neutron single-particle energies in ^{16}O.

We perform the RPA calculations for each cutoff shown in Table 7.1. The HF+RPA calculations are first performed with the SkP $t_0 - t_3$ model for each cutoff (all the other parameters of the SkP interaction are put equal to zero). Then, a HF+RPA calculation is performed for each of the refitted interactions of Table 7.1 for the corresponding value of the cutoff (used for the RPA calculations). Calculations are thus self-consistent in all cases. The same cutoff is used each time in the PVC code. Results are shown in Fig. 7.5.

In Fig. 7.5, the black lines correspond to the HF energy for each single-particle state and the red dotted lines correspond to the single-particle energies calculated with the SkP parameters. The blue dash-dotted lines correspond to the single-particle energies calculated with the refitted parameters that are shown in Table 7.1.
Some comments could be drawn from Fig. 7.5:

1. First, we mention that the HF energies are almost the same when calculated with the SkP force and with the refitted interactions. This is why we show only one set of HF values in the figure.

2. We observe from Fig. 7.5 that the values of the single-particle energies obtained when using the SkP parametrization (red lines) almost coincide with those obtained when using the refitted parameters (blue lines) for the three values of the cutoff Λ.

3. The corrections to the single-particle energies increase when the value of Λ increases. This means that the UV divergences are present in the PVC model due to the short-range of the $t_0 - t_3$ interaction. For instance, for $\Lambda = 59.19$ MeV, the correction to the single-particle energy for the particle state $1d_{5/2}$ is equal to -2.320 MeV.

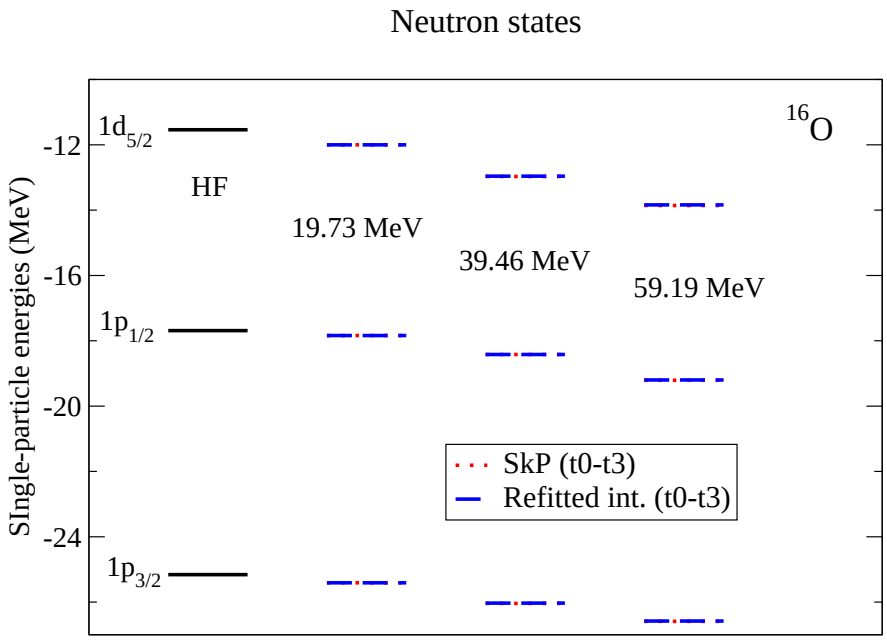

Figure 7.5: Single-particle energies calculated with different values of Λ.

4. The most important comment is that the cutoff dependence is not reduced when the refitted interactions are used with respect to the SkP case. The failure in using these refitted interactions in this case could be due for example to the fact the ^{16}O nucleus may not be a good candidate to perform such tests. This means that it would be better to perform calculations in medium and heavy nuclei, for example, ^{48} Ca and ^{132}Sn (because the refitted interactions have been introduced for matter). This will be checked in the next sections.

5. We see from Fig. 7.5 that, not only the particle states are shifted downwards by PVC corrections but also the hole states. This result contradicts what was commonly found for heavy nuclei, that the hole states are pushed upwards due to PVC corrections. Our result is coherent with what is published in Ref. [109].

7.4.3 Results: ^{48}Ca

Again, we start calculating the single-particle energies for the nucleus ^{48}Ca with HF. Then, we perform self-consistent RPA calculations using the simplified $t_0 - t_3$ model and include the modes $L = 0^+$, 1^-, 2^+ and 3^-. In Table. 7.3, we show the HF neutron single-particle energies in ^{48}Ca that we have chosen for our analysis: the hole states $1d_{3/2}$ and $1f_{7/2}$ and the particle state $2p_{3/2}$.

In Fig. 7.6, the black lines correspond to the HF energy for each single-particle state and the red dotted lines correspond to the single-particle energies calculated with SkP parameters. The blue dash-dotted lines correspond to the single-particle energies calculated with

Nucleus	hole states [MeV]		particle states [MeV]	
^{48}Ca	$1d\frac{3}{2}$	-18.82	$2p\frac{3}{2}$	-3.98
	$1f\frac{7}{2}$	-13.99		

Table 7.3: Neutron single-particle energies in ^{48}Ca.

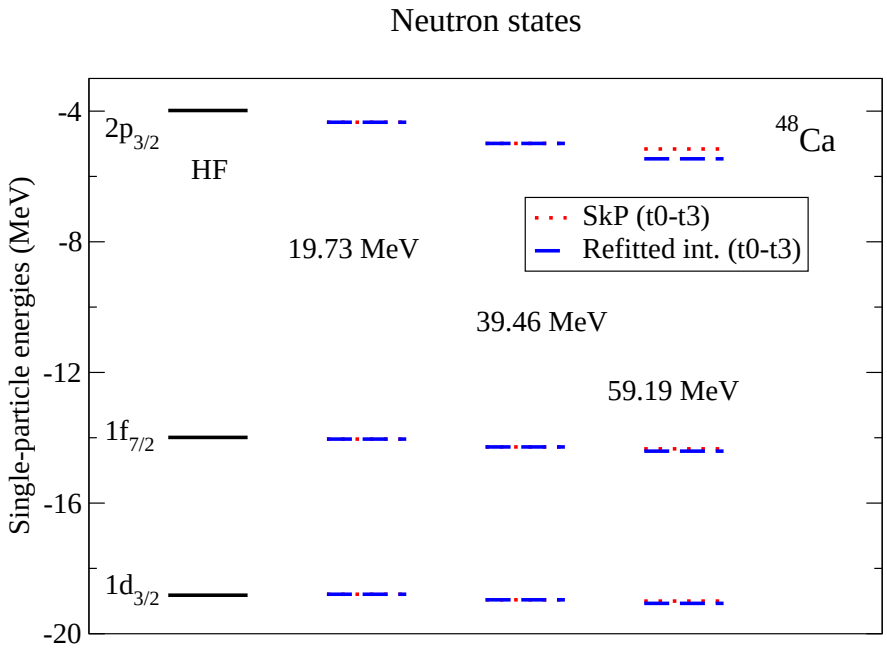

Figure 7.6: Single-particle energies in ^{48}Ca calculated with different values of Λ.

the refitted parameters that are shown in Table 7.1.
The same comments already done for the nucleus ^{16}O can be drawn here. We do not observe any effect due to regularization.
In this case, we have performed a more detailed test by separating the Σ^{RPA} and $\Sigma^{(2)}$ corrections. The results are plotted in Fig. 7.7 for the state $2p_{3/2}$. We can make two comments:

1. The corrections associated to $\Sigma^{(2)}$ (upper panel) are not 'better' regularized than the corrections coming from Σ^{RPA} (lower panel).

2. The second-order corrections are not at all negligible with respect to the corrections coming from Σ^{RPA}. These corrections cannot be disregarded.

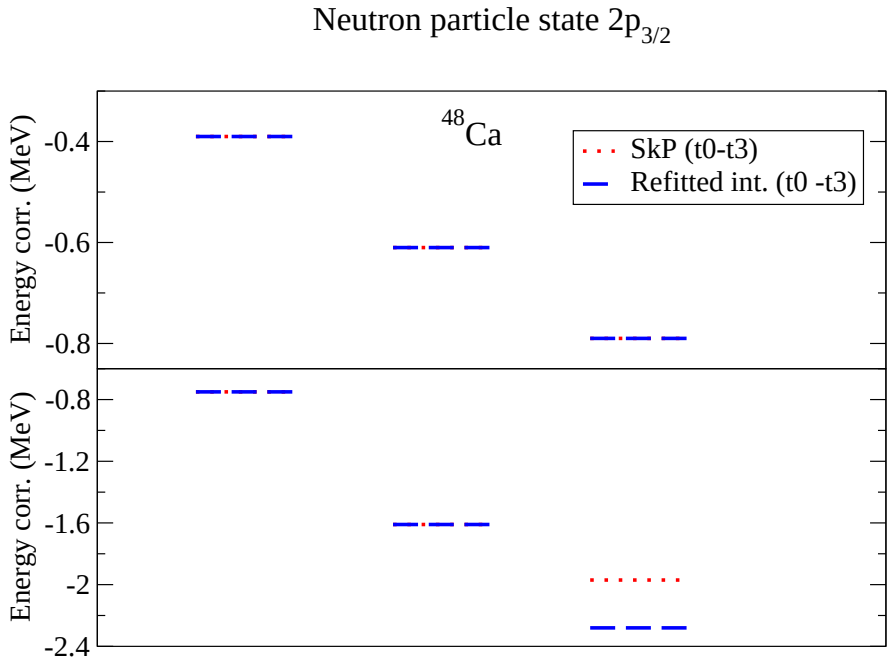

Figure 7.7: Upper panel: Second-order corrections to the single-particle energies for different values of Λ with the SkP parametrization (red lines) and with the refitted interactions (blue lines). Lower panel: Corrections coming from Σ^{RPA}.

7.4.4 Results: ^{132}Sn

We check now if the regularized interactions work better for a heavier nucleus. We calculate the single-particle HF spectrum and perform self-consistent RPA calculations using the simplified $t_0 - t_3$ model by including the modes $L = 0^+$, 1^-, 2^+ and 3^-. In Table. 7.4, we show the HF energies of the chosen neutron single-particle states in ^{132}Sn: the neutron hole states $3s_{1/2}$ and $2d_{3/2}$ and the particle state $1i_{13/2}$.

Nucleus	hole states [MeV]		particle states [MeV]	
^{132}Sn	$3s\frac{1}{2}$	-7.89	$1i\frac{13}{2}$	-3.04
	$2d\frac{3}{2}$	-7.86		

Table 7.4: Neutron single-particle energies in ^{132}Sn.

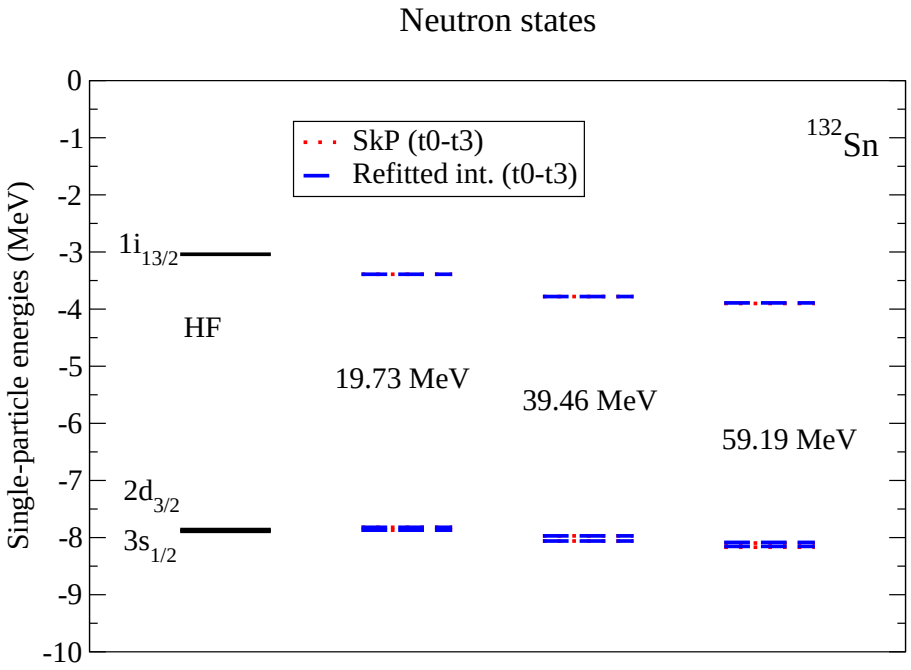

Figure 7.8: Single-particle energies in ^{132}Sn calculated with different values of Λ.

In Fig. 7.8, the black lines correspond to the HF energy for each single-particle state and the red dotted lines correspond to the single-particle energies calculated with the SkP parameters. The blue dash-dotted lines correspond to the single-particle energies calculated with refitted parameters that are shown in Table 7.1.
Also this time, the same comments already done for the previous cases may be repeated. We have not found any mass-dependence on the quality of the results concerning the refitted interactions.

7.5 Conclusions

In this chapter, we have dealt with a first test of the refitted interactions in the PVC model that go beyond the independent-particle picture. It is known that the PVC model enables one to gain better insight into the nuclear single-particle properties like the single-particle energies (spectroscopic factors and fragmentation of single-particle states).
We have calculated the single-particle energies in a self-consistent way using $t_0 - t_3$ Skyrme interactions. In this case, UV divergences appear in the PVC corrections because of the zero-range character of the $t_0 - t_3$ interaction. These divergences are still present also when we employ the interactions that have been regularized in nuclear matter. This occurs independently of the mass of the nucleus (applications have been done for ^{16}O, ^{48}Ca and ^{132}Sn).

1. The single-particle energies diverge as the cutoff Λ increases. This is due to the UV divergences that appear in this beyond-mean-field model.

2. The refitted parameters, regularized in nuclear matter, do not regularize the UV divergences not only in the total PVC corrections but also in the second-order corrections associated to $\Sigma^{(2)}$. This means that these refitted interactions do not provide any regularized behavior in applications to nuclei. We have tried a light nucleus like ^{16}O, a medium-mass nucleus ^{48}Ca and a heavy nucleus ^{132}Sn. The results are of the same type.

3. This negative result could be due to the fact that we are not dealing with the proper value of the cutoff when we make calculations for nuclei: the correspondence between the momentum cutoff in matter and the momentum cutoff in finite nuclei could not be so trivial as we have imagined in our first test applications. Work is in progress in this direction [174].

4. We also found that second-order corrections are not at all negligible compared to the PVC corrections as was currently believed. The second-order corrections have to be subtracted to get rid of double counting problems and they cannot be neglected.

5. It was commonly found for heavy nuclei that the particle states are shifted downwards and the hole states are pushed upwards by PVC corrections. In this work we have found that this is not always true. We have shown in this chapter that the hole states

can also be shifted downwards when the PVC corrections are taken into account. The same result has been also published in Ref. [109].

6. All the results of these first tests have been found for a $t_0 - t_3$ model. No effects of regularization are observed and this may be interpreted as a signal that perhaps we are not using the correct correspondence between the cutoff in matter and the cutoff in nuclei [174].
   To get rid of this cutoff problem, a clear and clean direction that can be pursued in my future work is to use the DR-regularized interaction (Chapter 6) where there is no cutoff dependence. This can be done only with the full Skyrme interaction (because we have shown that the $t_0 - t_3$ model does not provide any result) and thus requires heavier calculations.
   This is the direction I plan to follow in the next months, possibly by imagining to combine in the adjustments of the parameters constraints for matter and constraints for finite nuclei.

Chapter 8

Summary and outlook

This thesis work was undertaken to explore some techniques used in the nuclear many-body problem and the concept of beyond-mean-field models in nuclear matter with the objective of making first applications to nuclei. The beyond-mean-field models (the PVC model is used to make some first applications to nuclei in our case) enable one to gain better insight into nuclear properties like single-particle energies (spectroscopic factors and fragmentation of single-particle states), excited states and collectivity, spreading widths, $\cdots$.

In the framework of beyond-mean-field models, we have dealt with two technical and formal problems concerning the employed interaction that one may encounter: the problem of double counting, and the problem of UV divergences when zero-range interactions are used. The former problem was solved by performing an adjustment of the parameters of the interaction and the latter was solved by introducing a regularization scheme, for example the MC and DR schemes.

This thesis work sought to answer two questions:

1. Can we remove the UV divergences that appear in the expression of the EoS (at a beyond mean-field level) for nuclear matter by redefining the parameters of the used interaction?

2. Can we generate new effective interactions that can be employed to perform applications to nuclei?

In the first and most important part of this work [9, 10, 11], we have dealt with the many-body problem calculated at the second order in nuclear matter with the zero-range nuclear Skyrme interaction. This work sought to:

1. Derive an analytical expression for the corrected EoS for nuclear matter at the second-order.

2. Analyze the UV divergences which appear due to the zero-range character of the Skyrme interaction.

3. Generate effective interactions that are regularized and adjusted at this beyond mean-field level to provide an EoS for matter with reasonable features.

We have started with the simplified $t_0 - t_3$ model and derived the expression for the EoS for symmetric nuclear matter by introducing the second-order corrections. Two regularization techniques were being adopted to treat the UV divergence, the MC and the DR/MS schemes:

1. By using the MC scheme, we have found that the EoS for symmetric nuclear matter diverges linearly with the cutoff Λ. However, this linear UV divergence cannot be absorbed unless a four-body force is added to the interaction. Of course, by adding such counter term, the Skyrme interaction becomes much more complicated and thus applications to finite nuclei are more difficult [153]. We have thus absorbed this divergence by readjusting the parameters of the Skyrme interaction in order to have a reasonable EoS at second order [9]. Therefore, cutoff-dependent interactions were generated at this level (the cutoff becomes a parameter of the interaction).

2. In the case of DR/MS, we found that, although this scheme automatically cancels all power-divergent integrals, it was not possible to readjust the parameters of the simplified $t_0 - t_3$ interaction in order to have a reasonable EoS [11]. This occurs because the second-order EoS has the wrong curvature. We thus switch to the case of the full nuclear Skyrme interaction.

We have included the velocity-dependent terms to the Skyrme interaction and considered also asymmetric nuclear matter. We have repeated the same procedure done in the first work [9]. We have found the following results:

1. In the case of the MC scheme, the divergence becomes of order $\sim \Lambda^5$ due to the velocity-dependent terms (i.e., the non-local terms of the nuclear Skyrme interaction). In this case, the adjustment of the parameters is performed for both symmetric and asymmetric nuclear matter with different neutron-to-proton ratios [10]. Therefore, new effective interactions were generated with all the terms of the Skyrme interaction, except the spin-orbit part that does not contribute in matter.

2. In the case of DR/MS, the divergence is suppressed and the resulting EoS for nuclear matter at the second-order is independent of the used regulator. Thus, a unique set of parameters is obtained for the adjusted effective interaction [11].

In the second part of the work, we have dealt with an example of beyond-mean-field models applied to finite systems: the PVC model. In this model, the second-order corrections $\Sigma^{(2)}$ were subtracted from Σ^{RPA} in the calculation of the corrected single-particle energies to avoid problems of double counting. This part of the work is a very preliminary test performed to

have a first idea of what happens when the interactions designed for the second-order EoS in matter are used also for nuclei. This work sought to:

1. Investigate whether the cutoff-dependent interactions, that were generated and adjusted in nuclear matter, can be applied to finite nuclei and consequently provide single-particle energies that are stable with respect to the cutoff.

2. Test whether the second-order corrections are negligible with respect to the main correction coming from Σ^{RPA} and compare their to the total PVC contributions.

3. Check if the refitted interactions regularize at least the divergences that appear in the second-order corrections.

In this work, we have taken the simplified $t_0 - t_3$ interaction and used it self-consistently. The same interaction was employed in each case in HF, RPA and PVC calculations. We have performed applications to a light nucleus ^{16}O, a medium-mass nucleus ^{48}Ca and a heavy nucleus ^{132}Sn. We have focused our attention only on single-particle energies. We have found the following results:

1. The UV divergences appear in this beyond mean-field model due to the zero-range of the simplified $t_0 - t_3$ interaction. The corrected single-particle energies depend on the cutoff.

2. The regularized refitted interactions do not provide any regularized behavior in applications to nuclei. They do not regularize the UV divergences not only in the total PVC corrections but also in the second-order corrections associated to $\Sigma^{(2)}$. This unsatisfactory result could be due to the fact that we are not dealing with the proper value of the cutoff when we make calculations for nuclei. The correspondence between the cutoff in matter and the cutoff in finite nuclei perhaps should not be done in the way we have done. Work is in progress in this direction [174].

3. We have also found that second-order corrections cannot be neglected compared to the PVC corrections as was currently believed.

4. It was commonly found for heavy nuclei that the energies of the hole states are shifted upwards and those of the particle states are shifted downwards by the PVC corrections. We have shown that also the hole states can be shifted downwards when the PVC corrections are taken into account, for light and heavy nuclei. The same result has been also published in Ref. [109].

What we have done so far in these first tests applied to nuclei is using refitted interactions which are cutoff dependent. This cutoff dependence is due to the fact that we have not renormalized our problem yet; we have just absorbed the divergence by performing an adjustment of parameters.

A clear and clean direction that can be pursued in my future work is to:

1. Use the DR-regularized interaction, where there is no cutoff dependence. This can be done only with the full Skyrme interaction (because we have shown that the $t_0 - t_3$ model does not provide any result) and thus requires heavier calculations.

2. Analyze analytically the type of the divergence (whether it is ultraviolet or logarithmic) that appears in the framework of the PVC calculations.

3. Design a Skyrme force (by adjusting the parameters of the Skyrme interaction) that is well defined at this level and that can be eventually used also in other beyond-mean-field models.

Finally, I think that this is the direction I plan to follow in the next months, possibly by imagining to combine in the adjustments of the parameters constraints for matter and constraints for finite nuclei.

Moreover, it would be interesting to investigate the following issues:

1. Examine whether the higher-order corrections are small enough compared to the second-order terms, so that they can be neglected. In other words, examine the perturbativity of the problem when Skyrme-type interactions are used.

2. Investigate the hierarchy in our problem: what are the contributions that lead to the mean-field level and what are those that lead to the beyond mean-field level? Should we include other terms in the interaction to have a renormalizable theory order by order?

3. Since the Skyrme interaction is designed for mean-field calculations, it would be interesting to:

   (a) Investigate whether the velocity-dependent terms can be treated on equal footing with the $t_0 - t_3$ terms when we perform beyond-mean-field calculations.

   (b) Check whether the two-body density-dependent force should be replaced by a three-body force to better define the power counting when beyond-mean-field calculations are performed.

4. It would be interesting to be inspired by the chiral potentials that are introduced in the framework of EFT. They could be used as a benchmark.

Finally, by doing my thesis work I have learned that this domain is quite unexplored and has to be developed by establishing connections between the traditional EDF framework and the concepts and ideas that are currently discussed in the framework of EFT. I have started developing these links and connections with my work of the past years. This certainly opens many exciting and new perspectives in the developments of this research line that will be pursued in the following years.

Appendix A

First-order energy diagrams

In this appendix, we derive the expressions of the first-order energy corrections in infinite nuclear matter with a Dirac-delta interaction. We start our formalism from the Green's function and then we classify the Feynman diagrams into connected ones and disconnected ones.

A.1 Goldstone's theorem

The application of quantum field theory to the many-body problem was initiated by Goldstone in 1957 [150]. The Goldstone's theorem was originally stimulated by Bruckners theory of strongly interacting Fermi systems [33]. He proved the cancellation of the disconnected diagrams to all orders, and derived the following expression for the energy shift of the ground state:

$$E = \epsilon_k^{(0)} + \langle \Phi_0 | H_1 \sum_{n=0}^{\infty} \left(\frac{1}{\epsilon_k^{(0)} - H_0} H_1 \right)^n |\Phi_0\rangle_{connected}. \tag{A.1}$$

Another formula is due to Gell-Mann and Low [175], expresses the shift energy of the ground state as:

$$E - \epsilon_k^{(0)} = \sum_{m=0}^{\infty} (-i)^m \frac{1}{m!} \int_{-\infty}^{0} dt_1 \cdots dt_m \, \langle \Phi_0 | T \left[\hat{H}_1 \hat{H}_1(t_1) \cdots \hat{H}_1(t_m) \right] |\Phi_0\rangle_{connected}, \tag{A.2}$$

where the interacting Hamiltonian $\hat{H}_1$ can be written as:

$$H_1 = \frac{1}{2!} \sum_{\substack{\alpha\beta\alpha'\beta' \\ \gamma\mu\gamma'\mu'}} \int d^3\mathbf{r}\, d^3\mathbf{r}'\ \hat{\psi}^{\dagger}_{\alpha;\gamma}(\mathbf{r}) \hat{\psi}^{\dagger}_{\beta;\mu}(\mathbf{r}') V(\mathbf{r},\mathbf{r}')_{\substack{\alpha\alpha',\beta\beta' \\ \gamma\gamma',\mu\mu'}} \hat{\psi}_{\beta';\mu'}(\mathbf{r}') \hat{\psi}_{\alpha';\gamma'}(\mathbf{r}).$$

If we assume that $U(r,r') = V(\mathbf{r},\mathbf{r}')\delta(t-t')$, then

$$H_1 = \frac{1}{2!} \sum_{\substack{\alpha\beta\alpha'\beta' \\ \gamma\mu\gamma'\mu'}} \int d^4r\, d^4r'\ \hat{\psi}^{\dagger}_{\alpha;\gamma}(\mathbf{r}) \hat{\psi}^{\dagger}_{\beta;\mu}(\mathbf{r}') U(r,r')_{\substack{\alpha\alpha',\beta\beta' \\ \gamma\gamma',\mu\mu'}} \hat{\psi}_{\beta';\mu'}(\mathbf{r}') \hat{\psi}_{\alpha';\gamma'}(\mathbf{r}), \tag{A.3}$$

and $H_1(t)$ is the representation of H_1 in the interaction picture and given by:

$$H_1(t) = e^{iH_0 t} H_1 e^{-iH_0 t}.$$

From Eq. (A.2), one can write:

$$\begin{aligned} E &= \epsilon_k^{(0)} + \langle \Phi_0 | T\left[\hat{H}_1\right] | \Phi_0 \rangle_{connected} - i\int_{-\infty}^{0} dt_1 \langle \Phi_0 | T\left[\hat{H}_1 \hat{H}_1(t_1)\right] | \Phi_0 \rangle_{connected} + \cdots \\ &= \epsilon_k^{(0)} + E^{(1)} + E^{(2)} + \cdots . \end{aligned} \tag{A.4}$$

A.2 First-order energy diagrams

The first-order contributions to the total energy is given by:

$$E^{(1)} = \langle \Phi_0 | T\left[\hat{H}_1\right] | \Phi_0 \rangle_{connected}. \tag{A.5}$$

By using the expression of $\hat{H}_1$ from Eq. (A.3), the time-ordering of H_1 becomes:

$$T\left[\hat{H}_1\right] = \frac{1}{2!} \sum_{\substack{\alpha\beta\alpha'\beta' \\ \gamma\mu\gamma'\mu'}} U(r,r')_{\substack{\alpha\alpha',\beta\beta' \\ \gamma\gamma',\mu\mu'}} \int d^4r\, d^4r' T\left[\hat{\psi}^\dagger_{\alpha;\gamma}(\mathbf{r}) \hat{\psi}^\dagger_{\beta;\mu}(\mathbf{r}') \hat{\psi}_{\beta';\mu'}(\mathbf{r}') \hat{\psi}_{\alpha';\gamma'}(\mathbf{r})\right].$$

Wick's theorem requires us to sum over all possible contractions and the only non-vanishing contraction is between a field $\hat{\psi}$ and an adjoint field $\hat{\psi}^\dagger$ according to the following expressions:

$$\hat{\psi}_{a;b}(\mathbf{r}) \hat{\psi}^\dagger_{a';b'}(\mathbf{r}') = iG^0_{ab;a'b'}(\mathbf{r},\mathbf{r}') \text{ and } \hat{\psi}^\dagger_{a;b}(\mathbf{r}) \hat{\psi}_{a';b'}(\mathbf{r}') = -iG^0_{ba;b'a'}(\mathbf{r}',\mathbf{r}). \tag{A.6}$$

Consequently, the time-ordering becomes:

$$\begin{aligned} T\left[\hat{\psi}^\dagger_{\alpha;\gamma}(\mathbf{r}) \hat{\psi}^\dagger_{\beta;\mu}(\mathbf{r}') \hat{\psi}_{\beta';\mu'}(\mathbf{r}') \hat{\psi}_{\alpha';\gamma'}(\mathbf{r})\right] &= \hat{\psi}^\dagger_{\alpha;\gamma}(\mathbf{r}) :: \hat{\psi}_{\alpha';\gamma'}(\mathbf{r}) \hat{\psi}^\dagger_{\beta;\mu}(\mathbf{r}') :: \hat{\psi}_{\beta';\mu'}(\mathbf{r}') \\ &\quad - \hat{\psi}^\dagger_{\alpha;\gamma}(\mathbf{r}) :: \hat{\psi}_{\beta';\mu'}(\mathbf{r}') \hat{\psi}^\dagger_{\beta;\mu}(\mathbf{r}') :: \hat{\psi}_{\alpha';\gamma'}(\mathbf{r}). \end{aligned}$$

By using Eq. (B.3), we get:

$$T\left[\hat{\psi}^\dagger_{\alpha;\gamma}(\mathbf{r}) \hat{\psi}^\dagger_{\beta;\mu}(\mathbf{r}') \hat{\psi}_{\beta';\mu'}(\mathbf{r}') \hat{\psi}_{\alpha';\gamma'}(\mathbf{r})\right] = iG^0_{\alpha'\alpha;\gamma'\gamma}(\mathbf{r},\mathbf{r}) iG^0_{\beta'\beta;\mu'\mu}(\mathbf{r}',\mathbf{r}') - iG^0_{\beta'\alpha;\mu'\gamma}(\mathbf{r}',\mathbf{r}) iG^0_{\alpha'\beta;\gamma'\mu}(\mathbf{r},\mathbf{r}').$$

Therefore, we are able to write the first-order energy in a compact form by splitting it into two parts: direct and exchange part.

$$E^{(1)} = E^{(1)}_{direct} + E^{(1)}_{exchange}. \tag{A.7}$$

The expression for the direct-term is given by:

$$E^{(1)}_{direct} = \frac{1}{2!} \sum_{\substack{\alpha\beta\alpha'\beta' \\ \gamma\mu\gamma'\mu'}} \int d^4r\, d^4r' U(r,r')_{\substack{\alpha\alpha',\beta\beta' \\ \gamma\gamma',\mu\mu'}} \left[iG^0_{\alpha'\alpha;\gamma'\gamma}(\mathbf{r},\mathbf{r}) iG^0_{\beta'\beta;\mu'\mu}(\mathbf{r}',\mathbf{r}')\right]. \tag{A.8}$$

The expression for the exchange-term is given by:

$$E^{(1)}_{exchange} = \frac{1}{2!} \sum_{\substack{\alpha\beta\alpha^{'}\beta^{'} \\ \gamma\mu\gamma^{'}\mu^{'}}} \int d^4r \; d^4r^{'} U(r,r^{'})_{\substack{\alpha\alpha^{'},\beta\beta^{'} \\ \gamma\gamma^{'},\mu\mu^{'}}} \left[-iG^0_{\beta^{'}\alpha;\mu^{'}\gamma}(\mathbf{r}^{'},\mathbf{r}) iG^0_{\alpha^{'}\beta;\gamma^{'}\mu}(\mathbf{r},\mathbf{r}^{'}) \right]. \qquad \text{(A.9)}$$

We can now associate a picture to each of the terms appearing in Eq. (A.8) and Eq. (A.10). The unperturbed Green's function $G^0(x,y)$ is denoted by a straight with an arrow running from the second argument to the first as illustrated in Fig. A.1,

Figure A.1: The unperturbed Green's function $G^0_{\alpha\beta;\gamma\mu}(x,y)$.

and the interaction potential is denoted by a wavy line as in Fig. A.2

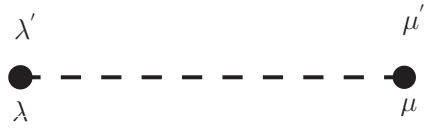

Figure A.2: The interaction $V_{\lambda\lambda^{'};\mu\mu^{'}}(x,x^{'})$.

By using the above pictures, we are able to draw the diagrammatic expression of Eq. (A.8) and Eq. (A.10) as follows:

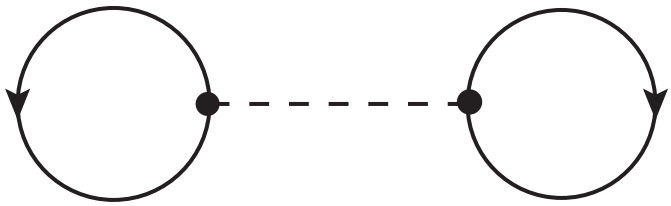

Figure A.3: First-order energy correction direct term.

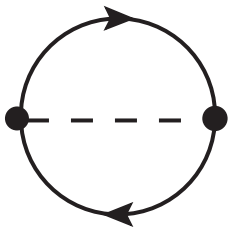

Figure A.4: First-order energy correction exchange term.

A.3 First-order energy corrections

Let us assume that the interaction V depends on the relative distance between the particles and does not depend on the spin space, i.e.,

$$U_{\substack{\alpha\alpha^{'},\beta\beta^{'}\\ \gamma\gamma^{'},\mu\mu^{'}}}(r,r^{'}) = \delta_{\alpha\alpha^{'}}\delta_{\beta\beta^{'}}\delta_{\gamma\gamma^{'}}\delta_{\mu\mu^{'}}V(\mathbf{r}-\mathbf{r}^{'})\delta(t-t^{'}).$$

Let us express the interaction in the momentum space as follows:

$$U(r-r^{'}) = \frac{1}{(2\pi)^4}\int d^4k\; e^{ik\cdot(r-r^{'})}U(k)$$

Moreover, in uniform and isotropic system, the Green's function takes the form [176]:

$$G^0_{ab;cd}(r,r^{'}) = \delta_{ab}\delta_{cd}G^0(r-r^{'}),$$

and consequently its Fourier transform becomes:

$$G^0(r,r^{'}) = \frac{1}{(2\pi)^4}\int d^4k\; e^{ik\cdot(r-r^{'})}G^0(k).$$

Eq. (A.11) becomes:

$$\begin{aligned} E^{(1)}_{exchange} &= \frac{1}{2!}\frac{1}{(2\pi)^{12}}\sum_{\substack{\alpha\beta\alpha^{'}\beta^{'}\\ \gamma\mu\gamma^{'}\mu^{'}}}\left[\delta_{\alpha\alpha^{'}}\delta_{\beta\beta^{'}}\delta_{\gamma\gamma^{'}}\delta_{\mu\mu^{'}}\right]\int d^4r_1\; d^4r_2\int d^4k_1\; d^4k_2\; d^4k_3\; e^{ik_1\cdot(r^{'}-r)} \\ &\quad \times e^{ik_2\cdot(r-r^{'})}\; e^{ik_3\cdot(r-r^{'})}U(k_3)\left[-iG^0_{\beta^{'}\alpha;\mu^{'}\gamma}(k_1)iG^0_{\alpha^{'}\beta;\gamma^{'}\mu}(k_2)\right]. \end{aligned}$$

After grouping the terms, we get:

$$\begin{aligned} E^{(1)}_{exchange} &= \frac{1}{2!}\frac{1}{(2\pi)^{12}}\sum_{\substack{\alpha\beta\alpha^{'}\beta^{'}\\ \gamma\mu\gamma^{'}\mu^{'}}}\left[\delta_{\alpha\alpha^{'}}\delta_{\beta\beta^{'}}\delta_{\gamma\gamma^{'}}\delta_{\mu\mu^{'}}\right]\int d^4k_1\; d^4k_2\; d^4k_3\left[\int d^4r_1\; d^4r_2\; e^{i(r-r^{'})\cdot(k_1-k_2+k_3)}\right]U(k_3) \\ &\quad \times\left[-iG^0_{\beta^{'}\alpha;\mu^{'}\gamma}(k_1)iG^0_{\alpha^{'}\beta;\gamma^{'}\mu}(k_2)\right]. \end{aligned}$$

It is to be noted that the integration over r and $r^{'}$ yields

$$\int d^4r\; d^4r^{'} e^{i(r-r^{'})\cdot(k_3+k_2-k_1)} = (2\pi)^4\delta^4(k_3+k_2-k_1)\;\Omega, \quad \text{where } \Omega \text{ is a unit volume,}$$

which conserves energy and momentum at each vertex. Therefore,

$$\begin{aligned} E^{(1)}_{exchange} &= \frac{1}{2!}\frac{\Omega}{(2\pi)^8}\sum_{\substack{\alpha\beta\alpha^{'}\beta^{'}\\ \gamma\mu\gamma^{'}\mu^{'}}}\left[\delta_{\alpha\alpha^{'}}\delta_{\beta\beta^{'}}\delta_{\gamma\gamma^{'}}\delta_{\mu\mu^{'}}\right]\int d^4k_1\; d^4k_2\; U(k_1-k_2)\left[-iG^0_{\beta^{'}\alpha;\mu^{'}\gamma}(k_1)iG^0_{\alpha^{'}\beta;\gamma^{'}\mu}(k_2)\right] \\ &= \frac{1}{2!}\frac{\Omega}{(2\pi)^8}\sum_{\alpha\beta\gamma\mu}\left[\delta_{\alpha\beta}\delta_{\gamma\mu}\right]\int d^4k_1\; d^4k_2\; U(k_1-k_2)\left[G^0(k_1)\;G^0(k_2)\right]. \end{aligned}$$

By performing the integration over k^0_1 and k^0_2, we get

$$\boxed{E^{(1)}_{exchange} = -\frac{g}{2!}\frac{\Omega}{(2\pi)^6}\int d^3k_1\; d^3k_2\; U(k_1-k_2)\;\theta(k_F-|\mathbf{k}_1|)\theta(k_F-|\mathbf{k}_2|),} \tag{A.10}$$

with $g = Tr\left[\delta_{\alpha\beta}\delta_{\gamma\mu}\right]$. Similarly,

$$\boxed{E^{(1)}_{direct} = \frac{g^2}{2!}\frac{\Omega}{(2\pi)^6}\int d^3k_1\; d^3k^{'}_2\; U(0)\;\theta(k_F-|\mathbf{k}_1|)\theta(k_F-|\mathbf{k}_2|),} \tag{A.11}$$

with $U(0) = \langle k_1, k_2|v|k_1, k_2\rangle$.

A.4 Application

Let take as an example the so-called simplified Skyrme interaction:

$$U(r_1,r_2) = V(\mathbf{r}-\mathbf{r}^{'})\delta(t-t^{'}) \quad \text{with} \quad V(\mathbf{r}-\mathbf{r}^{'}) = \left[t_0\delta(r_1-r_2) + \frac{t_3}{6}\rho^{\alpha}\delta(r_1-r_2)\right].$$

In this case: $U(0) = U(k_1-k_2) = \left(t_0 + \frac{t_3}{6}\rho^{\alpha}\right)$.
By using Eq. (A.11), the energy contribution due to direct diagrams becomes:

$$\begin{aligned} E^{(1)}_{direct} &= \frac{1}{2!}\frac{g^2}{(2\pi)^6}\left(t_0+\frac{t_3}{6}\rho^{\alpha}\right)\int d^3\mathbf{k}_1\; d^3\mathbf{k}_2\;\theta(k_F-|\mathbf{k}_1|)\theta(k_F-|\mathbf{k}_2|) \\ &= \frac{g^2}{72\pi^4}k_F^6\left(t_0+\frac{t_3}{6}\rho^{\alpha}\right) \quad \text{where} \quad g^2 = Tr\left[\delta_{\alpha\alpha^{'}}\delta_{\beta\beta^{'}}\delta_{\gamma\gamma^{'}}\delta_{\mu\mu^{'}}\right] = 16. \end{aligned} \tag{A.12}$$

Therefore, the binding energy per particle (direct term) evaluated with the $t_0 - t_3$ vertices is given by:

$$\boxed{\frac{E^{(1)}_{direct}}{A} = \left(\frac{g}{12\pi^2}\right)k_F^3\left(t_0+\frac{t_3}{6}\rho^{\alpha}\right).} \tag{A.13}$$

By using Eq. (A.10), the energy contribution due to the exchange diagrams becomes:

$$\begin{aligned} E^{(1)}_{exchange} &= -\frac{1}{2!}\frac{g}{(2\pi)^6}\int d^3\mathbf{k}_1\, d^3\mathbf{k}_2 V(\mathbf{k}_1-\mathbf{k}_2)\theta(k_F-|\mathbf{k}_1|)\theta(k_F-|\mathbf{k}_2|) \\ &= -\frac{g}{72\pi^4}k_F^6\left(t_0+\frac{t_3}{6}\rho^\alpha\right), \end{aligned}$$

where the notation $V(\mathbf{k}_1-\mathbf{k}_2)$ means that $V(\mathbf{k}_1-\mathbf{k}_2)=\langle k_1,k_2|v|k_2,k_1\rangle$.
Consequently, the energy contribution due to the exchange diagrams becomes:

$$\boxed{\frac{E^{(1)}_{exchange}}{A} = -\left(\frac{1}{12\pi^2}\right)k_F^3\left(t_0+\frac{t_3}{6}\rho^\alpha\right).}$$

As a result, the binding energy per particle (direct+exchange) evaluated at the first order with the (t_0-t_3) Skyrme interaction is given by:

$$\boxed{\frac{E^{(1)}}{A} = \left(\frac{g-1}{12\pi^2}\right)k_F^3\left(t_0+\frac{t_3}{6}\rho^\alpha\right).}$$

Appendix B

Second-order energy diagrams

In this appendix, we use the so-called Wick's theorem, Goldstone's theorem and Gell-Mann and Low theorem to find the expressions for the second-order energy corrections and their corresponding diagrams. For the sake of simplicity, we will ignore the isospin indices and label for example the Green's function as $G^0_{ab}(x,y)$. According to Eq. (A.2), the second-order energy correction is given by:

$$E^{(2)} = -i \int_{-\infty}^{0} dt_1 \langle \Phi_0 | T \left[\hat{H}_1 \hat{H}_1(t_1) \right] | \Phi_0 \rangle_{connected}, \tag{B.1}$$

where the expression for $\hat{H}_1 \hat{H}_1(t_1)$ is given by:

$$\begin{aligned} \hat{H}_1 \hat{H}_1(t_1) &= \frac{1}{4} \int d^4x \, d^4y \, d^4z \, d^4w \, \hat{\psi}^\dagger_a(x) \hat{\psi}^\dagger_b(y) U(x,y)_{ac,bd} \hat{\psi}_d(y) \hat{\psi}_c(x) \\ &\quad \times e^{iH_0 \, t_1} \left[\hat{\psi}^\dagger_\alpha(z) \hat{\psi}^\dagger_\beta(w) U(z,w)_{\alpha\gamma,\beta\mu} \hat{\psi}_\mu(w) \hat{\psi}_\gamma(z) \right] e^{-iH_0 \, t_1}. \end{aligned}$$

B.1 Feynman diagrams at second order

Using the above equation, the expression for the second-order energy correction becomes:

$$\begin{aligned} E^{(2)} &= \left(\frac{-i}{4} \right) \int d^4x \, d^4y \, d^4z \, d^4w \, \langle \Phi_0 | U(x,y)_{ac,bd} U(z,w)_{\alpha\gamma,\beta\mu} \times \\ &\quad T \left[\hat{\psi}^\dagger_a(x) \hat{\psi}^\dagger_b(y) \hat{\psi}_d(y) \hat{\psi}_c(x) \hat{\psi}^\dagger_\alpha(z) \hat{\psi}^\dagger_\beta(w) \hat{\psi}_\mu(w) \hat{\psi}_\gamma(z) \right] | \Phi_0 \rangle_c. \end{aligned}$$

Knowing that $U(x,y)_{ac,bd} = \delta_{ac} \delta_{bd} U(x,y)$, we get:

$$\begin{aligned} E^{(2)} &= \left(\frac{-i}{4} \right) \sum_{\substack{\alpha\beta\gamma\mu \\ abcd}} [\delta_{ac} \delta_{bd} \delta_{\alpha\gamma} \delta_{\beta\mu}] \int d^4x \, d^4y \, d^4z \, d^4w \, \langle \Phi_0 | U(x,y) U(z,w) \\ &\quad \times T \left[\hat{\psi}^\dagger_a(x) \hat{\psi}^\dagger_b(y) \hat{\psi}_d(y) \hat{\psi}_c(x) \hat{\psi}^\dagger_\alpha(z) \hat{\psi}^\dagger_\beta(w) \hat{\psi}_\mu(w) \hat{\psi}_\gamma(z) \right] | \Phi_0 \rangle_c. \end{aligned} \tag{B.2}$$

Let us concentrate on the following expression:

$$T\left[\hat{\psi}_a^\dagger(x)\hat{\psi}_b^\dagger(y)\hat{\psi}_d(y)\hat{\psi}_c(x)\hat{\psi}_\alpha^\dagger(z)\hat{\psi}_\beta^\dagger(w)\hat{\psi}_\mu(w)\hat{\psi}_\gamma(z)\right].$$

The expectation value of all the terms containing normal-ordered products of operators vanishes in the non-interacting ground state $|\Phi_0\rangle$, leaving only the fully contracted products of field operators. We have:

$$T\left[\hat{\psi}_a^\dagger(x)\hat{\psi}_b^\dagger(y)\hat{\psi}_d(y)\hat{\psi}_c(x)\hat{\psi}_\alpha^\dagger(z)\hat{\psi}_\beta^\dagger(w)\hat{\psi}_\mu(w)\hat{\psi}_\gamma(z)\right] = (1)+(2)+(3)+(4),$$

where the expressions of (1), (2), (3) and (4) are given below:

$$\begin{aligned}(1) = \psi_a^\dagger(x)\psi_d(y)\Big\{ & \quad \psi_b^\dagger(y)\psi_c(x)\left[\psi_\alpha^\dagger(z)\psi_\mu(w)\psi_\beta^\dagger(w)\psi_\gamma(z)+\psi_\alpha^\dagger(z)\psi_\gamma(z)\psi_\mu(w)\psi_\beta^\dagger(w)\right] \\ & + \psi_b^\dagger(y)\psi_\mu(w)\left[\psi_c(x)\psi_\alpha^\dagger(z)\psi_\beta^\dagger(w)\psi_\gamma(z)-\psi_c(x)\psi_\beta^\dagger(w)\psi_\alpha^\dagger(z)\psi_\gamma(z)\right] \\ & + \psi_b^\dagger(y)\psi_\gamma(z)\left[\psi_c(x)\psi_\alpha^\dagger(z)\psi_\mu(w)\psi_\beta^\dagger(w)+\psi_c(x)\psi_\beta^\dagger(w)\psi_\alpha^\dagger(z)\psi_\mu(w)\right]\Big\}.\end{aligned}$$

Expanding the above expression into six terms, we get:

$$\begin{aligned}(1) &= \psi_a^\dagger(x)\psi_d(y)\psi_b^\dagger(y)\psi_c(x)\psi_\alpha^\dagger(z)\psi_\mu(w)\psi_\beta^\dagger(w)\psi_\gamma(z) \\ &\quad +\psi_a^\dagger(x)\psi_d(y)\psi_b^\dagger(y)\psi_c(x)\psi_\alpha^\dagger(z)\psi_\gamma(z)\psi_\mu(w)\psi_\beta^\dagger(w) \\ &\quad +\psi_a^\dagger(x)\psi_d(y)\psi_b^\dagger(y)\psi_\mu(w)\psi_c(x)\psi_\alpha^\dagger(z)\psi_\beta^\dagger(w)\psi_\gamma(z) \\ &\quad -\psi_a^\dagger(x)\psi_d(y)\psi_b^\dagger(y)\psi_\mu(w)\psi_c(x)\psi_\beta^\dagger(w)\psi_\alpha^\dagger(z)\psi_\gamma(z) \\ &\quad +\psi_a^\dagger(x)\psi_d(y)\psi_b^\dagger(y)\psi_\gamma(z)\psi_c(x)\psi_\alpha^\dagger(z)\psi_\mu(w)\psi_\beta^\dagger(w) \\ &\quad +\psi_a^\dagger(x)\psi_d(y)\psi_b^\dagger(y)\psi_\gamma(z)\psi_c(x)\psi_\beta^\dagger(w)\psi_\alpha^\dagger(z)\psi_\mu(w) \\ &= (1)^a+(1)^b+(1)^c+(1)^d+(1)^e+(1)^f,\end{aligned}$$

where the expression of $(1)^a$, which is represented by Fig. B.1, is given by:

$$\begin{aligned}(1)^a &= \psi_a^\dagger(x)\psi_d(y)\psi_b^\dagger(y)\psi_c(x)\psi_\alpha^\dagger(z)\psi_\mu(w)\psi_\beta^\dagger(w)\psi_\gamma(z) \\ &= \left[-iG_{da}^0(y,x)\right]\left[-iG_{cb}^0(x,y)\right]\left[-iG_{\mu\alpha}^0(w,z)\right]\left[-iG_{\gamma\beta}^0(z,w)\right]\end{aligned}$$

The expression of $(1)^b$, which is represented by Fig. B.2, is given by:

$$\begin{aligned}(1)^b &= \psi_a^\dagger(x)\psi_d(y)\psi_b^\dagger(y)\psi_c(x)\psi_\alpha^\dagger(z)\psi_\gamma(z)\psi_\mu(w)\psi_\beta^\dagger(w) \\ &= \left[-iG_{da}^0(y,x)\right]\left[-iG_{cb}^0(x,y)\right]\left[-iG_{\gamma\alpha}^0(z,z)\right]\left[iG_{\mu\beta}^0(w,w)\right]\end{aligned}$$

The expression of $(1)^c$, which is represented by Fig. B.3, is given by:

$$\begin{aligned}(1)^c &= \psi_a^\dagger(x)\psi_d(y)\psi_b^\dagger(y)\psi_\mu(w)\psi_c(x)\psi_\alpha^\dagger(z)\psi_\beta^\dagger(w)\psi_\gamma(z) \\ &= \left[-iG_{da}^0(y,x)\right]\left[-iG_{\mu b}^0(w,y)\right]\left[-iG_{c\alpha}^0(x,z)\right]\left[-iG_{\gamma\beta}^0(z,w)\right]\end{aligned}$$

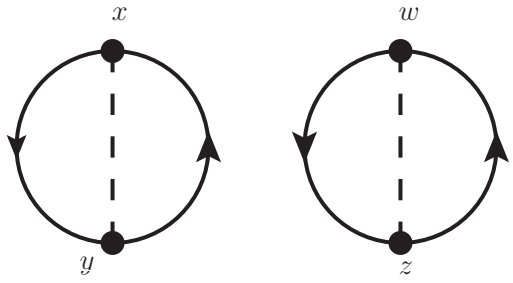

Figure B.1: Second-order energy correction $(1)^a$.

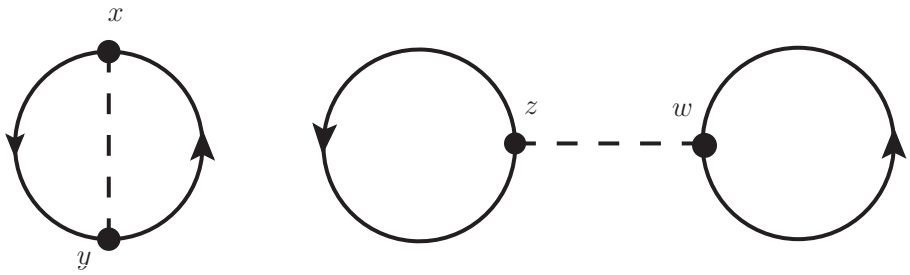

Figure B.2: Second-order energy correction $(1)^b$.

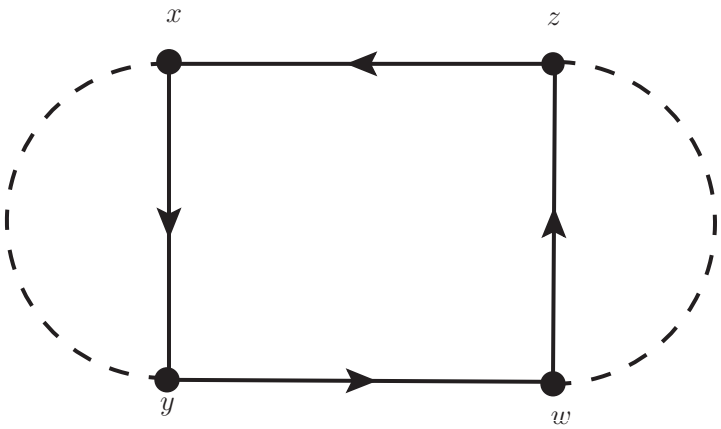

Figure B.3: Second-order energy correction $(1)^c$.

$$
\begin{aligned}
(1)^d &= -\psi_a^\dagger(x)\psi_d(y)\psi_b^\dagger(y)\psi_\mu(w)\psi_c(x)\psi_\beta^\dagger(w)\psi_\alpha^\dagger(z)\psi_\gamma(z) \\
&= \left[iG^0_{da}(y,x)\right]\left[-iG^0_{\mu b}(w,y)\right]\left[iG^0_{c\beta}(x,w)\right]\left[-iG^0_{\gamma\alpha}(z,z)\right]
\end{aligned}
$$

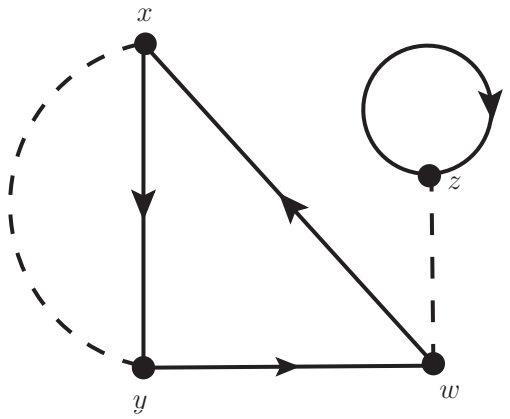

Figure B.4: Second-order energy correction $(1)^d$.

$$
\begin{aligned}
(1)^e &= \psi_a^\dagger(x)\psi_d(y)\psi_b^\dagger(y)\psi_\gamma(z)\psi_c(x)\psi_\alpha^\dagger(z)\psi_\mu(w)\psi_\beta^\dagger(w) \\
&= \left[-iG^0_{da}(y,x)\right]\left[-iG^0_{\gamma b}(z,y)\right]\left[iG^0_{c\alpha}(x,z)\right]\left[iG^0_{\mu\beta}(w,w)\right].
\end{aligned}
$$

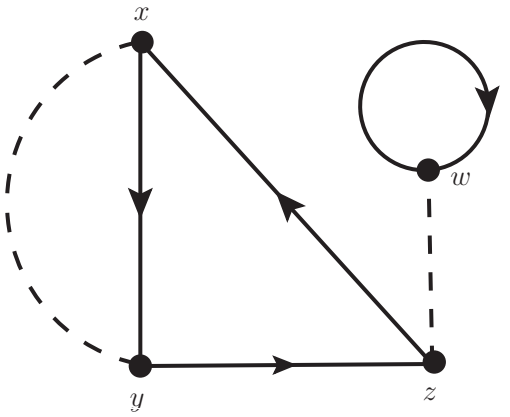

Figure B.5: Second-order energy correction $(1)^e$.

$$
\begin{aligned}
(1)^f &= \psi_a^\dagger(x)\psi_d(y)\psi_b^\dagger(y)\psi_\gamma(z)\psi_c(x)\psi_\beta^\dagger(w)\psi_\alpha^\dagger(z)\psi_\mu(w) \\
&= \left[-iG^0_{da}(y,x)\right]\left[-iG^0_{\gamma b}(z,y)\right]\left[iG^0_{c\beta}(x,w)\right]\left[-iG^0_{\mu\alpha}(w,z)\right].
\end{aligned}
$$

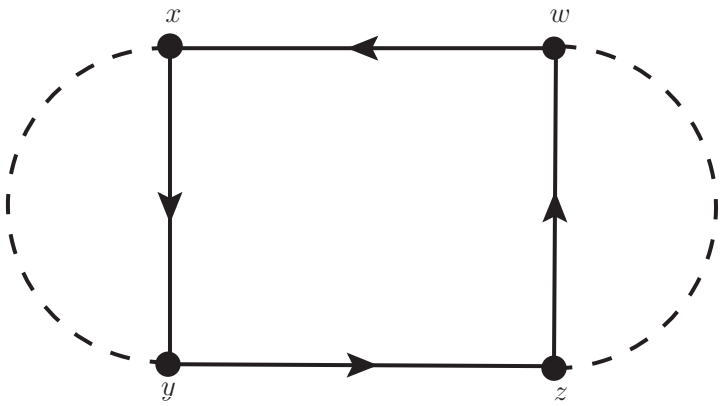

Figure B.6: Second-order energy correction $(1)^f$.

The expression of (2) is given by:

$$
\begin{aligned}
(2) = \psi_a^\dagger(x)\psi_c(x)\Big\{ & \quad \psi_d(y)\psi_b^\dagger(y)\left[\psi_\alpha^\dagger(z)\psi_\mu(w)\psi_\beta^\dagger(w)\psi_\gamma(z) + \psi_\alpha^\dagger(z)\psi_\gamma(z)\psi_\mu(w)\psi_\beta^\dagger(w)\right] \\
& - \psi_d(y)\psi_\alpha^\dagger(z)\left[\psi_b^\dagger(y)\psi_\mu(w)\psi_\beta^\dagger(w)\psi_\gamma(z) + \psi_b^\dagger(y)\psi_\gamma(z)\psi_\mu(w)\psi_\beta^\dagger(w)\right] \\
& + \psi_d(y)\psi_\beta^\dagger(w)\left[\psi_b^\dagger(y)\psi_\mu(w)\psi_\alpha^\dagger(z)\psi_\gamma(z) + \psi_b^\dagger(y)\psi_\gamma(z)\psi_\mu(w)\psi_\alpha^\dagger(z)\right]\Big\}.
\end{aligned}
$$

$$
\begin{aligned}
(2) &= (2)^a + (2)^b + (2)^c + (2)^d + (2)^e + (2)^f \\
&= \psi_a^\dagger(x)\psi_c(x)\psi_d(y)\psi_b^\dagger(y)\psi_\alpha^\dagger(z)\psi_\mu(w)\psi_\beta^\dagger(w)\psi_\gamma(z) \\
&\quad +\psi_a^\dagger(x)\psi_c(x)\psi_d(y)\psi_b^\dagger(y)\psi_\alpha^\dagger(z)\psi_\gamma(z)\psi_\mu(w)\psi_\beta^\dagger(w) \\
&\quad -\psi_a^\dagger(x)\psi_c(x)\psi_d(y)\psi_\alpha^\dagger(z)\psi_b^\dagger(y)\psi_\mu(w)\psi_\beta^\dagger(w)\psi_\gamma(z) \\
&\quad +\psi_a^\dagger(x)\psi_c(x)\psi_d(y)\psi_\alpha^\dagger(z)\psi_b^\dagger(y)\psi_\gamma(z)\psi_\mu(w)\psi_\beta^\dagger(w) \\
&\quad +\psi_a^\dagger(x)\psi_c(x)\psi_d(y)\psi_\beta^\dagger(w)\psi_b^\dagger(y)\psi_\mu(w)\psi_\alpha^\dagger(z)\psi_\gamma(z) \\
&\quad +\psi_a^\dagger(x)\psi_c(x)\psi_d(y)\psi_\beta^\dagger(w)\psi_b^\dagger(y)\psi_\gamma(z)\psi_\mu(w)\psi_\alpha^\dagger(z).
\end{aligned}
$$

$$
\begin{aligned}
(2)^a &= \psi_a^\dagger(x)\psi_c(x)\psi_d(y)\psi_b^\dagger(y)\psi_\alpha^\dagger(z)\psi_\mu(w)\psi_\beta^\dagger(w)\psi_\gamma(z) \\
&= \left[-iG^0_{ca}(x,x)\right]\left[iG^0_{db}(y,y)\right]\left[-iG^0_{\mu\alpha}(w,z)\right]\left[-iG^0_{\gamma\beta}(z,w)\right].
\end{aligned}
$$

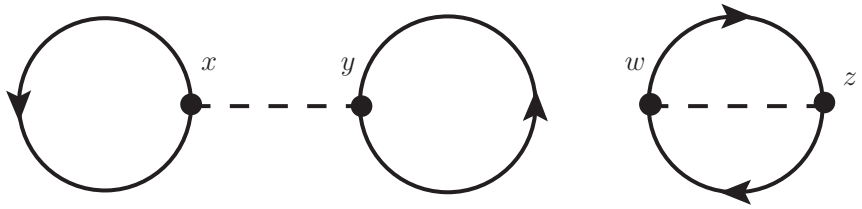

Figure B.7: Second-order energy correction $(2)^a$.

$$
\begin{aligned}
(2)^b &= \psi_a^\dagger(x)\psi_c(x)\psi_d(y)\psi_b^\dagger(y)\psi_\alpha^\dagger(z)\psi_\gamma(z)\psi_\mu(w)\psi_\beta^\dagger(w) \\
&= \left[-iG^0_{ca}(x,x)\right]\left[iG^0_{db}(y,y)\right]\left[-iG^0_{\gamma\alpha}(z,z)\right]\left[-iG^0_{\mu\beta}(w,w)\right].
\end{aligned}
$$

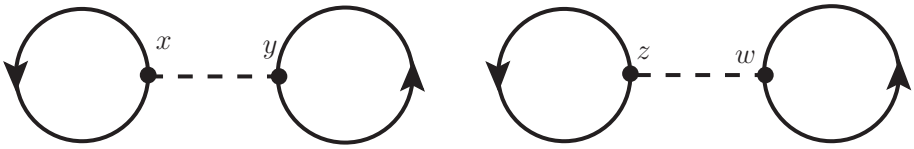

Figure B.8: Second-order energy correction $(2)^b$.

$$
\begin{aligned}
(2)^c &= -\psi_a^\dagger(x)\psi_c(x)\psi_d(y)\psi_\alpha^\dagger(z)\psi_b^\dagger(y)\psi_\mu(w)\psi_\beta^\dagger(w)\psi_\gamma(z) \\
&= \left[iG^0_{ca}(x,x)\right]\left[iG^0_{d\alpha}(y,z)\right]\left[-iG^0_{\mu b}(w,y)\right]\left[-iG^0_{\gamma\beta}(z,w)\right].
\end{aligned}
$$

$$
\begin{aligned}
(2)^d &= +\psi_a^\dagger(x)\psi_c(x)\psi_d(y)\psi_\alpha^\dagger(z)\psi_b^\dagger(y)\psi_\gamma(z)\psi_\mu(w)\psi_\beta^\dagger(w) \\
&= \left[-iG^0_{ca}(x,x)\right]\left[iG^0_{d\alpha}(y,z)\right]\left[-iG^0_{\gamma b}(z,y)\right]\left[iG^0_{\mu\beta}(w,w)\right].
\end{aligned}
$$

$$
\begin{aligned}
(2)^e &= \psi_a^\dagger(x)\psi_c(x)\psi_d(y)\psi_\beta^\dagger(w)\psi_b^\dagger(y)\psi_\mu(w)\psi_\alpha^\dagger(z)\psi_\gamma(z) \\
&= \left[-iG^0_{ca}(x,x)\right]\left[iG^0_{d\beta}(y,w)\right]\left[-iG^0_{\mu b}(w,y)\right]\left[-iG^0_{\gamma\alpha}(z,z)\right].
\end{aligned}
$$

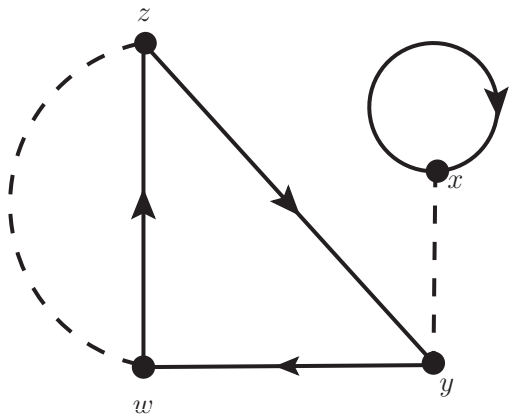

Figure B.9: Second-order energy correction $(2)^c$.

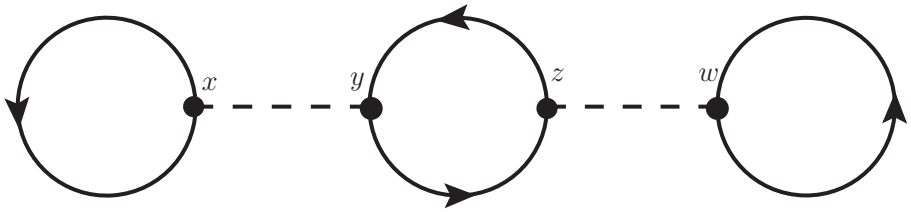

Figure B.10: Second-order energy correction $(2)^d$.

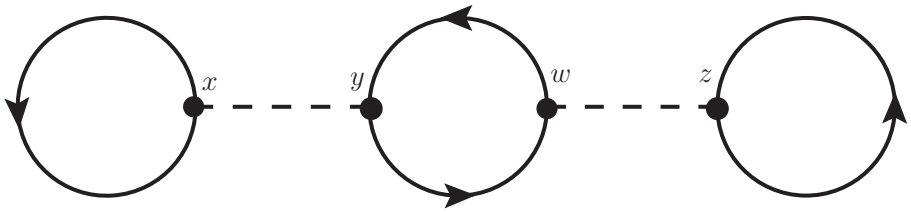

Figure B.11: Second-order energy correction $(2)^e$.

$$
\begin{aligned}
(2)^f &= \psi_a^\dagger(x)\psi_c(x)\psi_d(y)\psi_\beta^\dagger(w)\psi_b^\dagger(y)\psi_\gamma(z)\psi_\mu(w)\psi_\alpha^\dagger(z) \\
&= \left[-iG^0_{ca}(x,x)\right]\left[iG^0_{d\beta}(y,w)\right]\left[-iG^0_{\gamma b}(z,y)\right]\left[iG^0_{\mu\alpha}(w,z)\right].
\end{aligned}
$$

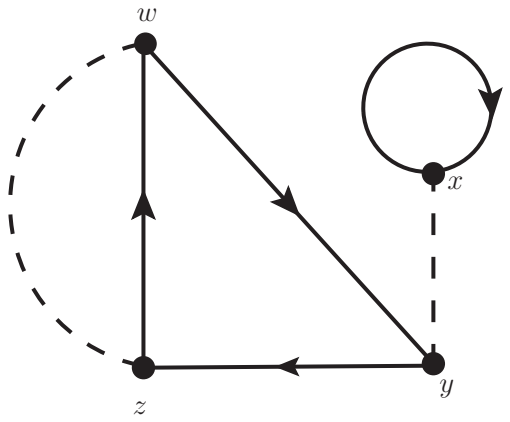

Figure B.12: Second-order energy correction $(2)^f$.

$$
\begin{aligned}
(3) = \psi_a^\dagger(x)\psi_\mu(w)\Big\{ & \quad \psi_d(y)\psi_b^\dagger(y)\left[\psi_c(x)\psi_\alpha^\dagger(z)\psi_\beta^\dagger(w)\psi_\gamma(z) - \psi_c(x)\psi_\beta^\dagger(w)\psi_\alpha^\dagger(z)\psi_\gamma(z)\right] \\
& + \psi_d(y)\psi_\alpha^\dagger(z)\left[\psi_b^\dagger(y)\psi_c(x)\psi_\beta^\dagger(w)\psi_\gamma(z) + \psi_b^\dagger(y)\psi_\gamma(z)\psi_c(x)\psi_\beta^\dagger(w)\right] \\
& - \psi_d(y)\psi_\beta^\dagger(w)\left[\psi_b^\dagger(y)\psi_c(x)\psi_\alpha^\dagger(z)\psi_\gamma(z) + \psi_b^\dagger(y)\psi_\gamma(z)\psi_c(x)\psi_\alpha^\dagger(z)\right]\Big\}.
\end{aligned}
$$

$$
\begin{aligned}
(3) &= \psi_a^\dagger(x)\psi_\mu(w)\psi_d(y)\psi_b^\dagger(y)\psi_c(x)\psi_\alpha^\dagger(z)\psi_\beta^\dagger(w)\psi_\gamma(z) \\
&\quad -\psi_a^\dagger(x)\psi_\mu(w)\psi_d(y)\psi_b^\dagger(y)\psi_c(x)\psi_\beta^\dagger(w)\psi_\alpha^\dagger(z)\psi_\gamma(z) \\
&\quad +\psi_a^\dagger(x)\psi_\mu(w)\psi_d(y)\psi_\alpha^\dagger(z)\psi_b^\dagger(y)\psi_c(x)\psi_\beta^\dagger(w)\psi_\gamma(z) \\
&\quad +\psi_a^\dagger(x)\psi_\mu(w)\psi_d(y)\psi_\alpha^\dagger(z)\psi_b^\dagger(y)\psi_\gamma(z)\psi_c(x)\psi_\beta^\dagger(w) \\
&\quad -\psi_a^\dagger(x)\psi_\mu(w)\psi_d(y)\psi_\beta^\dagger(w)\psi_b^\dagger(y)\psi_c(x)\psi_\alpha^\dagger(z)\psi_\gamma(z) \\
&\quad +\psi_a^\dagger(x)\psi_\mu(w)\psi_d(y)\psi_\beta^\dagger(w)\psi_b^\dagger(y)\psi_\gamma(z)\psi_c(x)\psi_\alpha^\dagger(z).
\end{aligned}
$$

$$
\begin{aligned}
(3)^a &= \psi_a^\dagger(x)\psi_\mu(w)\psi_d(y)\psi_b^\dagger(y)\psi_c(x)\psi_\alpha^\dagger(z)\psi_\beta^\dagger(w)\psi_\gamma(z) \\
&= \left[-iG^0_{\mu a}(w,x)\right]\left[iG^0_{db}(y,y)\right]\left[iG^0_{c\alpha}(x,z)\right]\left[-iG^0_{\gamma\beta}(z,w)\right].
\end{aligned}
$$

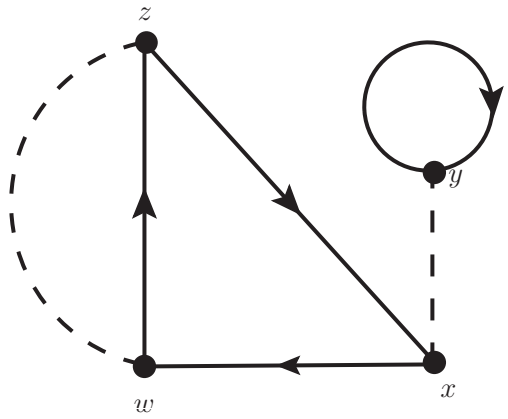

Figure B.13: Second-order energy correction $(3)^a$.

$$
\begin{aligned}
(3)^b &= -\psi_a^\dagger(x)\psi_\mu(w)\psi_d(y)\psi_b^\dagger(y)\psi_c(x)\psi_\beta^\dagger(w)\psi_\alpha^\dagger(z)\psi_\gamma(z) \\
&= \left[iG^0_{\mu a}(w,x)\right]\left[iG^0_{db}(y,y)\right]\left[iG^0_{c\beta}(x,w)\right]\left[-iG^0_{\gamma\alpha}(z,z)\right].
\end{aligned}
$$

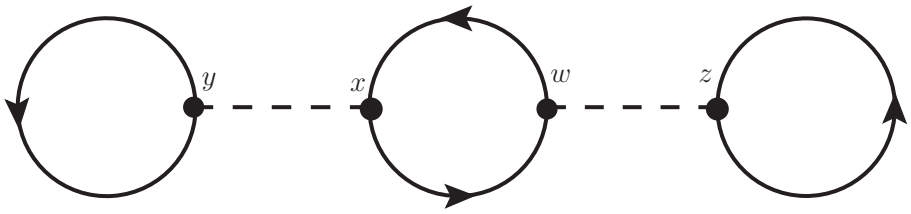

Figure B.14: Second-order energy correction $(3)^b$.

$$
\begin{aligned}
(3)^c &= \psi_a^\dagger(x)\psi_\mu(w)\psi_d(y)\psi_\alpha^\dagger(z)\psi_b^\dagger(y)\psi_c(x)\psi_\beta^\dagger(w)\psi_\gamma(z) \\
&= \left[-iG^0_{\mu a}(w,x)\right]\left[iG^0_{d\alpha}(y,z)\right]\left[-iG^0_{cb}(x,y)\right]\left[-iG^0_{\gamma\beta}(z,w)\right].
\end{aligned}
$$

$$
\begin{aligned}
(3)^d &= \psi_a^\dagger(x)\psi_\mu(w)\psi_d(y)\psi_\alpha^\dagger(z)\psi_b^\dagger(y)\psi_\gamma(z)\psi_c(x)\psi_\beta^\dagger(w) \\
&= \left[-iG^0_{\mu a}(w,x)\right]\left[iG^0_{d\alpha}(y,z)\right]\left[-iG^0_{\gamma b}(z,y)\right]\left[iG^0_{c\beta}(x,w)\right].
\end{aligned}
$$

$$
\begin{aligned}
(3)^e &= -\psi_a^\dagger(x)\psi_\mu(w)\psi_d(y)\psi_\beta^\dagger(w)\psi_b^\dagger(y)\psi_c(x)\psi_\alpha^\dagger(z)\psi_\gamma(z) \\
&= \left[iG^0_{\mu a}(w,x)\right]\left[iG^0_{d\beta}(y,w)\right]\left[-iG^0_{cb}(x,y)\right]\left[-iG^0_{\gamma\alpha}(z,z)\right].
\end{aligned}
$$

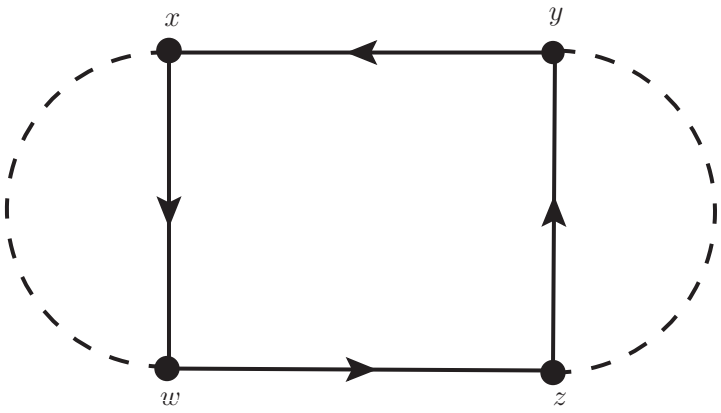

Figure B.15: Second-order energy correction $(3)^c$.

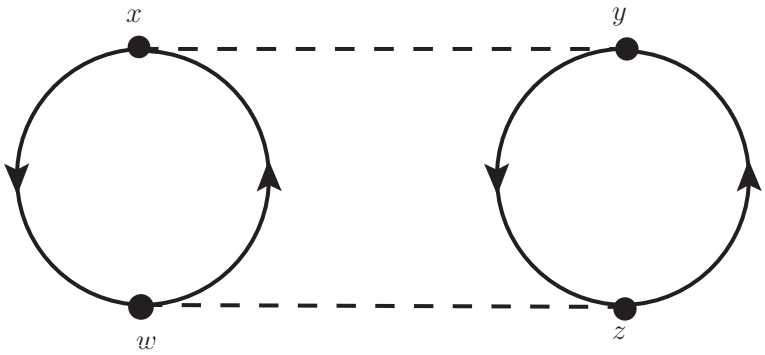

Figure B.16: Second-order energy correction $(3)^d$.

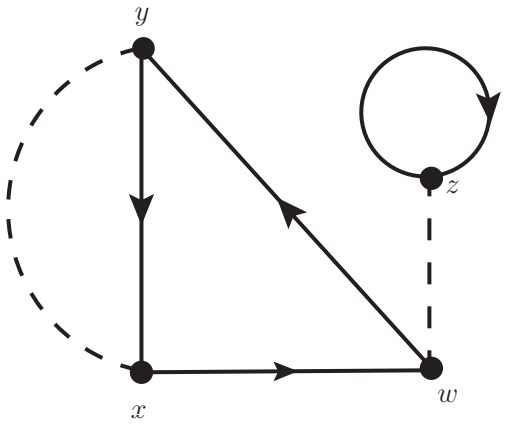

Figure B.17: Second-order energy correction $(3)^e$.

$$
\begin{aligned}
(3)^f &= +\psi_a^\dagger(x)\psi_\mu(w)\psi_d(y)\psi_\beta^\dagger(w)\psi_b^\dagger(y)\psi_\gamma(z)\psi_c(x)\psi_\alpha^\dagger(z) \\
&= \left[-iG^0_{\mu a}(w,x)\right]\left[iG^0_{d\beta}(y,w)\right]\left[-iG^0_{\gamma b}(z,y)\right]\left[iG^0_{c\alpha}(x,z)\right].
\end{aligned}
$$

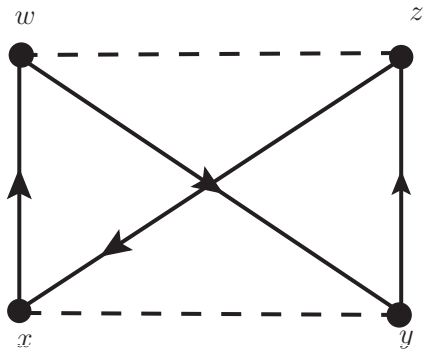

Figure B.18: Second-order energy correction $(3)^f$.

$$
\begin{aligned}
(4) = \psi_a^\dagger(x)\psi_\gamma(z)\Big\{ & \quad \psi_d(y)\psi_b^\dagger(y)\left[\psi_c(x)\psi_\alpha^\dagger(z)\psi_\mu(w)\psi_\beta^\dagger(w) + \psi_c(x)\psi_\beta^\dagger(w)\psi_\alpha^\dagger(z)\psi_\mu(w)\right] \\
& + \psi_d(y)\psi_\alpha^\dagger(z)\left[\psi_b^\dagger(y)\psi_c(x)\psi_\mu(w)\psi_\beta^\dagger(w) - \psi_b^\dagger(y)\psi_\mu(w)\psi_c(x)\psi_\beta^\dagger(w)\right] \\
& + \psi_d(y)\psi_\beta^\dagger(w)\left[\psi_b^\dagger(y)\psi_c(x)\psi_\alpha^\dagger(z)\psi_\mu(w) + \psi_b^\dagger(y)\psi_\mu(w)\psi_c(x)\psi_\alpha^\dagger(z)\right]\Big\}.
\end{aligned}
$$

$$
\begin{aligned}
(4) &= \psi_a^\dagger(x)\psi_\gamma(z)\psi_d(y)\psi_b^\dagger(y)\psi_c(x)\psi_\alpha^\dagger(z)\psi_\mu(w)\psi_\beta^\dagger(w) \\
&\quad +\psi_a^\dagger(x)\psi_\gamma(z)\psi_d(y)\psi_b^\dagger(y)\psi_c(x)\psi_\beta^\dagger(w)\psi_\alpha^\dagger(z)\psi_\mu(w) \\
&\quad +\psi_a^\dagger(x)\psi_\gamma(z)\psi_d(y)\psi_\alpha^\dagger(z)\psi_b^\dagger(y)\psi_c(x)\psi_\mu(w)\psi_\beta^\dagger(w) \\
&\quad -\psi_a^\dagger(x)\psi_\gamma(z)\psi_d(y)\psi_\alpha^\dagger(z)\psi_b^\dagger(y)\psi_\mu(w)\psi_c(x)\psi_\beta^\dagger(w) \\
&\quad +\psi_a^\dagger(x)\psi_\gamma(z)\psi_d(y)\psi_\beta^\dagger(w)\psi_b^\dagger(y)\psi_c(x)\psi_\alpha^\dagger(z)\psi_\mu(w) \\
&\quad +\psi_a^\dagger(x)\psi_\gamma(z)\psi_d(y)\psi_\beta^\dagger(w)\psi_b^\dagger(y)\psi_\mu(w)\psi_c(x)\psi_\alpha^\dagger(z).
\end{aligned}
$$

$$
\begin{aligned}
(4)^a &= \psi_a^\dagger(x)\psi_\gamma(z)\psi_d(y)\psi_b^\dagger(y)\psi_c(x)\psi_\alpha^\dagger(z)\psi_\mu(w)\psi_\beta^\dagger(w) \\
&= \left[-iG^0_{\gamma a}(z,x)\right]\left[iG^0_{db}(y,y)\right]\left[iG^0_{c\alpha}(x,z)\right]\left[-iG^0_{\mu\beta}(w,w)\right].
\end{aligned}
$$

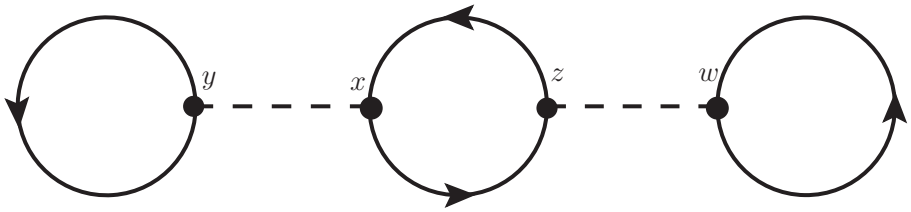

Figure B.19: Second-order energy correction $(4)^a$.

$$
\begin{aligned}
(4)^b &= +\psi_a^\dagger(x)\psi_\gamma(z)\psi_d(y)\psi_b^\dagger(y)\psi_c(x)\psi_\beta^\dagger(w)\psi_\alpha^\dagger(z)\psi_\mu(w) \\
&= \left[-iG^0_{\gamma a}(z,x)\right]\left[iG^0_{db}(y,y)\right]\left[-iG^0_{c\beta}(x,w)\right]\left[iG^0_{\mu\alpha}(w,z)\right].
\end{aligned}
$$

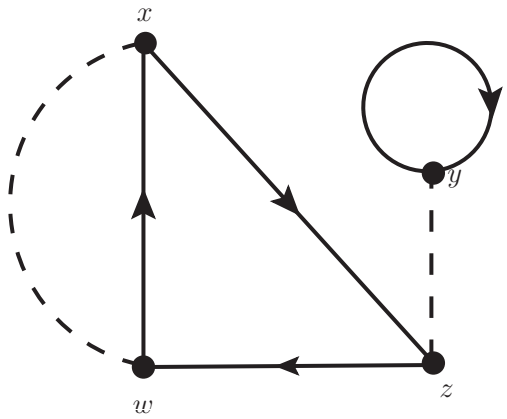

Figure B.20: Second-order energy correction $(4)^b$.

$$
\begin{aligned}
(4)^c &= +\psi_a^\dagger(x)\psi_\gamma(z)\psi_d(y)\psi_\alpha^\dagger(z)\psi_b^\dagger(y)\psi_c(x)\psi_\mu(w)\psi_\beta^\dagger(w) \\
&= \left[-iG^0_{\gamma a}(z,x)\right]\left[iG^0_{d\alpha}(y,z)\right]\left[-iG^0_{cb}(x,y)\right]\left[iG^0_{\mu\beta}(w,w)\right].
\end{aligned}
$$

$$
\begin{aligned}
(4)^d &= -\psi_a^\dagger(x)\psi_\gamma(z)\psi_d(y)\psi_\alpha^\dagger(z)\psi_b^\dagger(y)\psi_\mu(w)\psi_c(x)\psi_\beta^\dagger(w) \\
&= \left[iG^0_{\gamma a}(z,x)\right]\left[iG^0_{d\alpha}(y,z)\right]\left[-iG^0_{\mu b}(w,y)\right]\left[iG^0_{c\beta}(x,w)\right].
\end{aligned}
$$

$$
\begin{aligned}
(4)^e &= +\psi_a^\dagger(x)\psi_\gamma(z)\psi_d(y)\psi_\beta^\dagger(w)\psi_b^\dagger(y)\psi_c(x)\psi_\alpha^\dagger(z)\psi_\mu(w) \\
&= \left[-iG^0_{\gamma a}(z,x)\right]\left[iG^0_{d\beta}(y,w)\right]\left[-iG^0_{cb}(x,y)\right]\left[-iG^0_{\mu\alpha}(w,z)\right].
\end{aligned}
$$

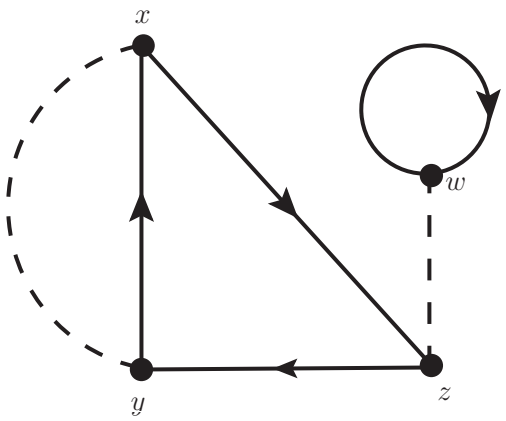

Figure B.21: Second-order energy correction $(4)^c$.

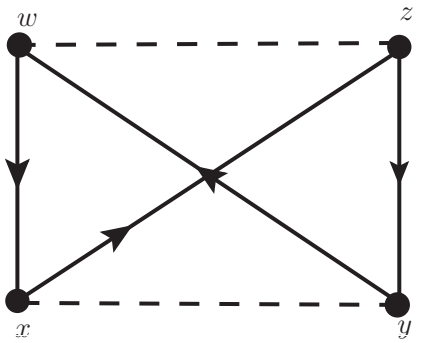

Figure B.22: Second-order energy correction $(4)^d$.

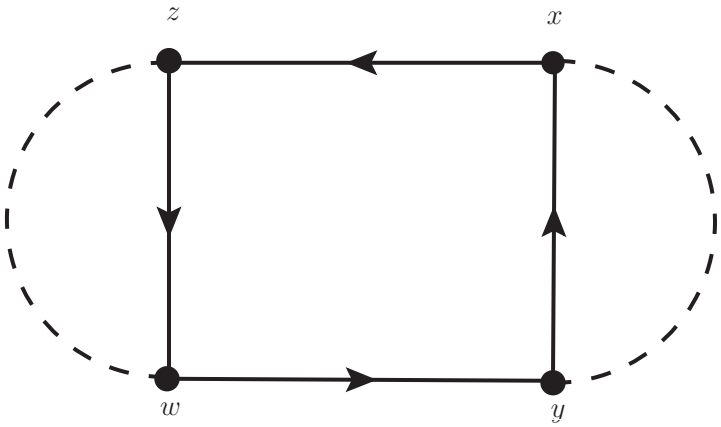

Figure B.23: Second-order energy correction $(4)^e$.

$$
\begin{aligned}
(4)^f &= +\psi_a^\dagger(x)\psi_\gamma(z)\psi_d(y)\psi_\beta^\dagger(w)\psi_b^\dagger(y)\psi_\mu(w)\psi_c(x)\psi_\alpha^\dagger(z) \\
&= \left[-iG^0_{\gamma a}(z,x)\right]\left[iG^0_{d\beta}(y,w)\right]\left[-iG^0_{\mu b}(w,y)\right]\left[-iG^0_{c\alpha}(x,z)\right].
\end{aligned}
$$

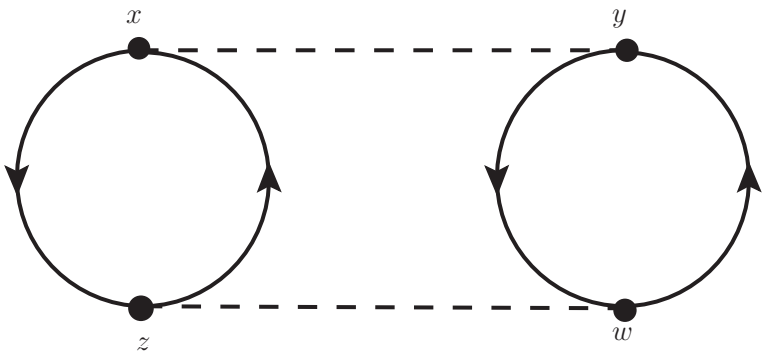

Figure B.24: Second-order energy correction $(4)^f$.

B.2 Application: direct diagram.

In this part, we are going to derive the expression for the second-order energy correction that corresponds to diagram $(3)^d$ shown in the figure below.

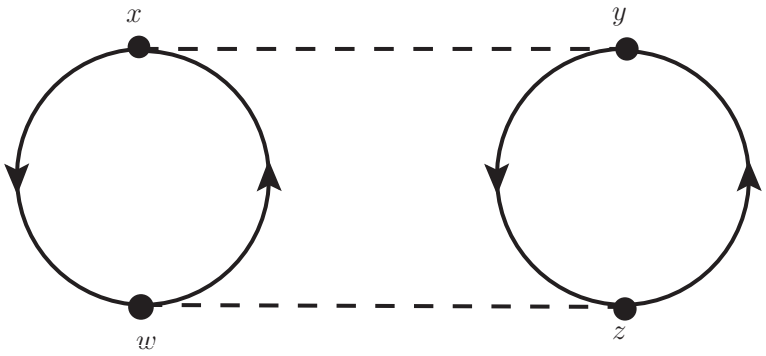

Figure B.25: Second-order energy correction (direct term).

From Eq. (B.2), we see that the second-order energy correction due to diagram $(3)^d$ can

be written as follows:

$$E_{3d}^{(2)} = \left(\frac{-i}{4}\right) \sum_{\substack{\alpha\beta\gamma\mu \\ abcd}} [\delta_{ac}\delta_{bd}\delta_{\alpha\gamma}\delta_{\beta\mu}] \int d^4x\, d^4y\, d^4z\, d^4w\, U(x,y)U(w,z) \times \left[\psi_a^\dagger(x)\psi_\mu(w)\psi_d(y)\psi_\alpha^\dagger(z)\psi_b^\dagger(y)\psi_\gamma(z)\psi_c(x)\psi_\beta^\dagger(w)\right].$$

Since $U(x,y) = U(x-y)$, then:

$$E_{3d}^{(2)} = \left(\frac{-i}{4}\right) \sum_{\substack{\alpha\beta\gamma\mu \\ abcd}} [\delta_{ac}\delta_{bd}\delta_{\alpha\gamma}\delta_{\beta\mu}] \int d^4x\, d^4y\, d^4z\, d^4w\, U(x-y)U(w-z) \times \left[-iG_{\mu a}^0(w,x)\right]\left[iG_{d\alpha}^0(y,z)\right]\left[-iG_{\gamma b}^0(z,y)\right]\left[iG_{c\beta}^0(x,w)\right].$$

After performing the Fourier transform, we get:

$$\begin{aligned} E_{3d}^{(2)} &= \left(\frac{-i}{4}\right) \sum_{\substack{\alpha\beta\gamma\mu \\ abcd}} [\delta_{ac}\delta_{bd}\delta_{\alpha\gamma}\delta_{\beta\mu}] \int d^4x\, d^4y\, d^4z\, d^4w \frac{1}{(2\pi)^8} \int d^4p_1\, d^4p_2\, e^{ip_1\cdot(x-y)}\, e^{ip_2\cdot(w-z)} \\ &\quad \times U(p_1)U(p_2)\frac{1}{(2\pi)^{16}} \int d^4p_3\, d^4p_4\, d^4p_5\, d^4p_6\, e^{ip_3\cdot(w-x)}G_{\mu a}^0(p_3)\, e^{ip_4\cdot(y-z)}G_{d\alpha}^0(p_4)\, e^{ip_5\cdot(z-y)} \\ &\quad \times G_{\gamma b}^0(p_5)\, e^{ip_6\cdot(x-w)}G_{c\beta}^0(p_6) \\ &= \left(\frac{-i}{4}\right) \sum_{\substack{\alpha\beta\gamma\mu \\ abcd}} [\delta_{ac}\delta_{bd}\delta_{\alpha\gamma}\delta_{\beta\mu}] \int d^4x\, d^4y\, d^4z\, d^4w \frac{1}{(2\pi)^8} \int d^3p_1\, d^3p_2\, e^{ix\cdot(p_1-p_3+p_6)}\, e^{iy\cdot(p_4-p_1-p_5)} \\ &\quad \times e^{iz\cdot(-p_2-p_4+p_5)}e^{iw\cdot(p_3+p_2-p_6)}U(p_1)U(p_2)\frac{1}{(2\pi)^{16}} \int d^4p_3\, d^4p_4\, d^4p_5\, d^4p_6 \\ &\quad \times G_{\mu a}^0(p_3)\, G_{d\alpha}^0(p_4)\, G_{\gamma b}^0(p_5)\, G_{c\beta}^0(p_6). \end{aligned}$$

Since there is energy and momentum conservation at each vertex,

$$\int d^4x\, e^{ix\cdot(p_1-p_3+p_6)} = (2\pi)^4\delta^4(p_1-p_3+p_6) \quad \text{and} \quad \int d^4z\, e^{iz\cdot(-p_2-p_4+p_5)} = (2\pi)^4\delta^4(p_2+p_4-p_5),$$

the second-order energy correction becomes:

$$\begin{aligned} E_{3d}^{(2)} &= \left(\frac{-i}{4}\right) \frac{1}{(2\pi)^{16}} \sum_{\substack{\alpha\beta\gamma\mu \\ abcd}} [\delta_{ac}\delta_{bd}\delta_{\alpha\gamma}\delta_{\beta\mu}] \int d^4y\, d^4w \int d^4p_1\, d^4p_2\, e^{iy\cdot(p_4-p_1-p_5)} \\ &\quad \times \delta^4(p_1-p_3+p_6)\delta^4(p_2+p_4-p_5)\, e^{iw\cdot(p_3+p_2-p_6)}U(p_1)U(p_2) \\ &\quad \times \int d^4p_3\, d^4p_4\, d^4p_5\, d^4p_6\, G_{\mu a}^0(p_3)\, G_{d\alpha}^0(p_4)\, G_{\gamma b}^0(p_5)\, G_{c\beta}^0(p_6). \end{aligned}$$

After performing the integration over p_1 and p_2, we get:

$$E_{3d}^{(2)} = \left(\frac{-i}{4}\right)\frac{1}{(2\pi)^{16}}\sum_{\substack{\alpha\beta\gamma\mu\\abcd}}[\delta_{ac}\delta_{bd}\delta_{\alpha\gamma}\delta_{\beta\mu}]\int d^4y\, d^4w\, e^{i(y-w)\cdot(p_4-p_3+p_6-p_5)}\, U(p_3-p_6)U(p_5-p_4)$$
$$\times\int d^4p_3\, d^4p_4\, d^4p_5\, d^4p_6\, G^0_{\mu a}(p_3)\, G^0_{d\alpha}(p_4)\, G^0_{\gamma b}(p_5)\, G^0_{c\beta}(p_6).$$

Noting that the integration over y and w yields

$$\int d^4y\, d^4w\, e^{i(y-w)\cdot(p_4-p_3+p_6-p_5)} = (2\pi)^4\delta^4(p_4-p_3+p_6-p_5)\Omega,$$

the expression for the second-order correction becomes:

$$E_{3d}^{(2)} = \left(\frac{-i}{4}\right)\frac{1}{(2\pi)^{12}}\sum_{\substack{\alpha\beta\gamma\mu\\abcd}}[\delta_{ac}\delta_{bd}\delta_{\alpha\gamma}\delta_{\beta\mu}]\int d^4p_3\, d^4p_4\, d^4p_5\, d^4p_6\, \delta^4(p_4-p_5-p_3+p_6)$$
$$\times U(p_3-p_6)U(p_5-p_4)G^0_{\mu a}(p_3)\, G^0_{d\alpha}(p_4)\, G^0_{\gamma b}(p_5)\, G^0_{c\beta}(p_6).$$

Using the fact that $G^0_{ab}(k) = \delta_{ab}G^0(k)$, we have:

$$\sum_{\substack{\alpha\beta\gamma\mu\\abcd}}[\delta_{ac}\delta_{bd}\delta_{\alpha\gamma}\delta_{\beta\mu}]\,[\delta_{\mu a}\delta_{d\alpha}\delta_{\gamma b}\delta_{c\beta}] = \sum_{\substack{\alpha\beta\gamma\mu\\abcd}}[\delta_{a\beta}\delta_{b\alpha}\delta_{\alpha b}\delta_{\beta a}] = \sum_{ab\alpha\beta}\delta_{a\beta}\delta_{b\alpha}.$$

By performing the integration over p_3, we get:

$$E_{3d}^{(2)} = \left(\frac{-i}{4}\right)\frac{g^2}{(2\pi)^{12}}\int d^4p_4\, d^4p_5\, d^4p_6\, U(p_4-p_5)U(p_5-p_4)$$
$$\times G^0(p_4-p_5+p_6)\, G^0(p_4)\, G^0(p_5)\, G^0(p_6).$$

In appendix B.4, we derive explicitly the compact expression of the second-order correction:

$$\boxed{E_{3d}^{(2)} = \left(\frac{g^2}{2}\right)\frac{1}{(2\pi)^9}\int_{C_I} d^3p_1\, d^3p_2\, d^3q\, \frac{V^2(q)}{\epsilon^{(0)}_{p_1}+\epsilon^{(0)}_{p_2}-\epsilon^{(0)}_{p_1+q}-\epsilon^{(0)}_{p_2-q}}.}$$

B.3 Application: exchange diagram.

From Eq. (B.2), we see that the second-order energy correction due to diagram $(3)^f$ can be written as follows:

$$E_{3f}^{(2)} = \left(\frac{-i}{4}\right)\sum_{\substack{\alpha\beta\gamma\mu\\abcd}}[\delta_{ac}\delta_{bd}\delta_{\alpha\gamma}\delta_{\beta\mu}]\int d^4x\, d^4y\, d^4z\, d^4w\, U(x,y)U(z,w)$$
$$\times\left[\psi^\dagger_a(x)\psi_\mu(w)\psi_d(y)\psi^\dagger_\beta(w)\psi^\dagger_b(y)\psi_\gamma(z)\psi_c(x)\psi^\dagger_\alpha(z)\right].$$

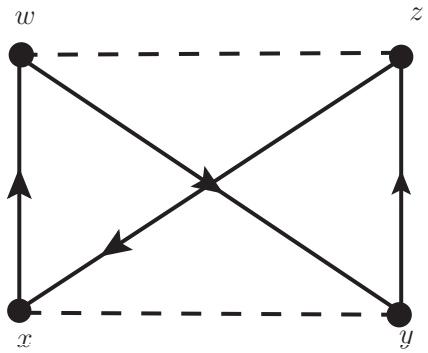

Figure B.26: Second-order energy correction (exchange term).

Since $U(x,y) = U(x-y)$, then:

$$\begin{aligned} E_{3f}^{(2)} &= \left(\frac{-i}{4}\right) \sum_{\substack{\alpha\beta\gamma\mu \\ abcd}} [\delta_{ac}\delta_{bd}\delta_{\alpha\gamma}\delta_{\beta\mu}] \int d^4x\ d^4y\ d^4z\ d^4w\ U(x-y)U(z-w) \\ &\quad \times \left[-iG^0_{\mu a}(w,x)\right] \left[iG^0_{d\beta}(y,w)\right] \left[-iG^0_{\gamma b}(z,y)\right] \left[iG^0_{c\alpha}(x,z)\right]. \end{aligned}$$

After performing the Fourier transform, we get:

$$\begin{aligned} E_{3f}^{(2)} &= \left(\frac{-i}{4}\right) \sum_{\substack{\alpha\beta\gamma\mu \\ abcd}} [\delta_{ac}\delta_{bd}\delta_{\alpha\gamma}\delta_{\beta\mu}] \int d^4x\ d^4y\ d^4z\ d^4w \frac{1}{(2\pi)^8} \int d^4p_1\ d^4p_2\ e^{ip_1\cdot(x-y)}\ e^{ip_2\cdot(z-w)} \\ &\quad \times U(p_1)U(p_2) \frac{1}{(2\pi)^{16}} \int d^4p_3\ d^4p_4\ d^4p_5\ d^4p_6\ e^{ip_3\cdot(w-x)} G^0_{\mu a}(p_3)\ e^{ip_4\cdot(y-w)} G^0_{d\beta}(p_4)\ e^{ip_5\cdot(z-y)} \\ &\quad \times G^0_{\gamma b}(p_5)\ e^{ip_6\cdot(x-z)} G^0_{c\alpha}(p_6) \\ &= \left(\frac{-i}{4}\right) \sum_{\substack{\alpha\beta\gamma\mu \\ abcd}} [\delta_{ac}\delta_{bd}\delta_{\alpha\gamma}\delta_{\beta\mu}] \int d^4x\ d^4y\ d^4z\ d^4w \frac{1}{(2\pi)^8} \int d^3p_1\ d^3p_2\ e^{ix\cdot(p_1-p_3+p_6)}\ e^{iy\cdot(p_4-p_1-p_5)} \\ &\quad \times e^{iz\cdot(p_2+p_5-p_6)} e^{iw\cdot(p_3-p_2-p_4)} U(p_1)U(p_2) \frac{1}{(2\pi)^{16}} \int d^4p_3\ d^4p_4\ d^4p_5\ d^4p_6 \\ &\quad \times G^0_{\mu a}(p_3)\ G^0_{d\beta}(p_4)\ G^0_{\gamma b}(p_5)\ G^0_{c\alpha}(p_6). \end{aligned}$$

Since there is energy and momentum conservation at each vertex,

$$\int d^4x\ e^{ix\cdot(p_1-p_3+p_6)} = (2\pi)^4\delta^4(p_1-p_3+p_6) \quad \text{and} \quad \int d^4z\ e^{iz\cdot(p_2+p_5-p_6)} = (2\pi)^4\delta^4(p_2+p_5-p_6),$$

the second-order energy correction becomes:

$$\begin{aligned} E_{3f}^{(2)} &= \left(\frac{-i}{4}\right)\frac{1}{(2\pi)^{16}}\sum_{\substack{\alpha\beta\gamma\mu\\ abcd}}[\delta_{ac}\delta_{bd}\delta_{\alpha\gamma}\delta_{\beta\mu}]\int d^4y\; d^4w\int d^4p_1\; d^4p_2\; e^{iy\cdot(p_4-p_1-p_5)} \\ &\quad\times\delta^4(p_1-p_3+p_6)\delta^4(p_2+p_5-p_6)\; e^{iw\cdot(p_3-p_2-p_4)}U(p_1)U(p_2) \\ &\quad\times\int d^4p_3\; d^4p_4\; d^4p_5\; d^4p_6\; G^0_{\mu a}(p_3)\; G^0_{d\beta}(p_4)\; G^0_{\gamma b}(p_5)\; G^0_{c\alpha}(p_6). \end{aligned}$$

After performing the integration over p_1 and p_2, we get:

$$\begin{aligned} E_{3d}^{(2)} &= \left(\frac{-i}{4}\right)\frac{1}{(2\pi)^{16}}\sum_{\substack{\alpha\beta\gamma\mu\\ abcd}}[\delta_{ac}\delta_{bd}\delta_{\alpha\gamma}\delta_{\beta\mu}]\int d^4y\; d^4w\; e^{i(y-w)\cdot(p_4-p_3+p_6-p_5)}\; U(p_3-p_6)U(p_6-p_5) \\ &\quad\times\int d^4p_3\; d^4p_4\; d^4p_5\; d^4p_6\; G^0_{\mu a}(p_3)\; G^0_{d\beta}(p_4)\; G^0_{\gamma b}(p_5)\; G^0_{c\alpha}(p_6). \end{aligned}$$

Noting that the integration over y and w yields

$$\int d^4y\; d^4w\; e^{i(y-w)\cdot(p_4-p_3+p_6-p_5)} = (2\pi)^4\delta^4(p_4-p_3+p_6-p_5)\Omega,$$

the expression for the second-order correction becomes:

$$\begin{aligned} E_{3f}^{(2)} &= \left(\frac{-i}{4}\right)\frac{1}{(2\pi)^{12}}\sum_{\substack{\alpha\beta\gamma\mu\\ abcd}}[\delta_{ac}\delta_{bd}\delta_{\alpha\gamma}\delta_{\beta\mu}]\int d^4p_3\; d^4p_4\; d^4p_5\; d^4p_6\; \delta^4(p_4-p_5-p_3+p_6) \\ &\quad\times U(p_3-p_6)U(p_6-p_5)G^0_{\mu a}(p_3)\; G^0_{d\beta}(p_4)\; G^0_{\gamma b}(p_5)\; G^0_{c\alpha}(p_6). \end{aligned}$$

By performing the integration over p_3 and using the fact that $G^0_{ab}(k) = \delta_{ab}G^0(k)$ and [1] $\delta_{ab}\delta_{bc} = \delta_{ac}$, we have:

$$\begin{aligned} E_{3f}^{(2)} &= \left(\frac{-i}{4}\right)\frac{g}{(2\pi)^{12}}\int d^4p_4\; d^4p_5\; d^4p_6\; U(p_4-p_5)U(p_6-p_5) \\ &\quad\times G^0(p_4-p_5+p_6)\; G^0(p_4)\; G^0(p_5)\; G^0(p_6), \end{aligned}$$

therefore, without loss of generality, the energy contribution due to the diagram $(3)^f$ is given by:

$$\boxed{E_{3f}^{(2)} = -\left(\frac{g}{2}\right)\frac{1}{(2\pi)^9}\int_{C_I} d^3p_1\; d^3p_2\; d^3q\; \frac{V(q)V(p_1-p_2-q)}{\epsilon^{(0)}_{p_1}+\epsilon^{(0)}_{p_2}-\epsilon^{(0)}_{p_1+q}-\epsilon^{(0)}_{p_2-q}}.}$$

[1] Remember: There will be an extra factor coming from the isospin labels which is $\delta_{\alpha'\gamma'}$.

B.4 Expression for the second-order corrections

In this appendix, we perform the integration over the fourth component $p_0 = \omega$ of momentum and derive the second-order energy correction in a compact form. The second-order correction for diagram $(3)^d$ reads:

$$E_{3d}^{(2)} = \left(\frac{-i}{4}\right)\frac{g^2}{(2\pi)^{12}}\int d^4p_4\, d^4p_5\, d^4p_6\, U(p_4-p_5)\, U(p_5-p_4) G^0(p_4-p_5+p_6)\, G^0(p_4)\, G^0(p_5)\, G^0(p_6).$$

By performing the change of variable $q = p_4 - p_5$ and $p_6 = p_5$, we get:

$$E_{3d}^{(2)} = \left(\frac{-i}{4}\right)\frac{g^2}{(2\pi)^{12}}\int d^4p_4\, d^4p_5\, d^4p_6\, U(q)U(-q) G^0(p_5+q)\, G^0(p_4-q)\, G^0(p_4)\, G^0(p_5).$$

In homogenous (uniform) systems, the non-interacting Green's function $G^0(|k|, k^0)$ consists of two disjoint pieces:

$$G^0(|k|,k^0) = \left[\frac{\theta(|k|-k_F)}{k^0-\omega_k+i\epsilon} + \frac{\theta(k_F-|k|)}{k^0-\omega_k-i\epsilon}\right], \quad \text{where} \quad \omega_k = \epsilon_k^{(0)}. \tag{B.3}$$

Using Eq. (B.3), the product of two Green's functions $G^0(p_5+q)\, G^0(p_4-q)$ is equal to:

$$\begin{aligned}
&= \left[\frac{\theta(|p_4-q|-k_F)}{p_4^0-q^0-\omega_{p_4-q}+i\eta} + \frac{\theta(k_F-|p_4-q|)}{p_4^0-q^0-\omega_{p_4-q}-i\eta}\right]\left[\frac{\theta(|p_5+q|-k_F)}{p_5^0+q^0-\omega_{p_5+q}+i\eta} + \frac{\theta(k_F-|p_5+q|)}{p_5^0+q^0-\omega_{p_5+q}-i\eta}\right] \\
&= \frac{\theta(|p_4-q|-k_F)}{(p_4^0-q^0-\omega_{p_4-q}+i\eta)}\frac{\theta(k_F-|p_5+q|)}{(p_5^0+q^0-\omega_{p_5+q}-i\eta)} + \frac{\theta(k_F-|p_4-q|)}{(p_4^0-q^0-\omega_{p_4-q}-i\eta)}\frac{\theta(|p_5+q|-k_F)}{(p_5^0+q^0-\omega_{p_5+q}+i\eta)} \\
&+ \frac{\theta(|p_4-q|-k_F)}{(p_4^0-q^0-\omega_{p_4-q}+i\eta)}\frac{\theta(|p_5+q|-k_F)}{(p_5^0+q^0-\omega_{p_5+q}+i\eta)} + \frac{\theta(k_F-|p_4-q|)}{(p_4^0-q^0-\omega_{p_4-q}-i\eta)}\frac{\theta(k_F-|p_5+q|)}{(p_5^0+q^0-\omega_{p_5+q}-i\eta)}.
\end{aligned}$$

The expression for $G^0(p_5+q)\, G^0(p_4-q)$ has four terms in all. The first two terms have both poles on the same side of the real q^0 axis; in this case, we close the contour in the opposite half plane, showing that these terms make no contribution. In contrast, each of the last remaining two terms has one pole above and one below the real axis. These contributions are evaluated with a contour integral, and we find:

$$\begin{aligned}
&\frac{1}{2\pi}\int dq^0\, G^0(p_5+q)\, G^0(p_4-q) = \\
&-i\left[\frac{\theta(|p_4-q|-k_F)\theta(|p_5+q|-k_F)}{p_5^0+p_4^0-\omega_{p_4-q}-\omega_{p_5+q}+i\eta} - \frac{\theta(k_F-|p_4-q|)\theta(k_F-|p_5+q|)}{p_5^0+p_4^0-\omega_{p_4-q}-\omega_{p_5+q}-i\eta}\right].
\end{aligned}$$

Next we calculate the following expression: $\frac{1}{2\pi}\int dq^0 G^0(p_5+q)\, G^0(p_4-q) G^0(p_4) =$

$$\begin{aligned}
&-i\left[\frac{\theta(|p_4-q|-k_F)\theta(|p_5+q|-k_F)}{p_5^0+p_4^0-\omega_{p_4-q}-\omega_{p_5+q}+i\eta} - \frac{\theta(k_F-|p_4-q|)\theta(k_F-|p_5+q|)}{p_5^0+p_4^0-\omega_{p_4-q}-\omega_{p_5+q}-i\eta}\right] \\
&\times\left[\frac{\theta(|p_4|-k_F)}{p_4^0-\omega_{p_4}+i\eta} + \frac{\theta(k_F-|p_4|)}{p_4^0-\omega_{p_4}-i\eta}\right].
\end{aligned}$$

After expanding the product of two factors, we get:

$$\begin{aligned}\frac{i}{2\pi}\int dq^0\; G^0(p_5+q)\; G^0(p_4-q)G^0(p_4) &= \frac{\theta(|p_4-q|-k_F)\theta(|p_5+q|-k_F)}{(p_5^0+p_4^0-\omega_{p_4-q}-\omega_{p_5+q}+i\eta)}\frac{\theta(|p_4|-k_F)}{(p_4^0-\omega_{p_4}+i\eta)}\\ &- \frac{\theta(k_F-|p_4-q|)\theta(k_F-|p_5+q|)}{(p_5^0+p_4^0-\omega_{p_4-q}-\omega_{p_5+q}-i\eta)}\frac{\theta(k_F-|p_4|)}{(p_4^0-\omega_{p_4}-i\eta)}\\ &+ \frac{\theta(|p_4-q|-k_F)\theta(|p_5+q|-k_F)}{(p_5^0+p_4^0-\omega_{p_4-q}-\omega_{p_5+q}+i\eta)}\frac{\theta(k_F-|p_4|)}{(p_4^0-\omega_{p_4}-i\eta)}\\ &- \frac{\theta(k_F-|p_4-q|)\theta(k_F-|p_5+q|)}{(p_5^0+p_4^0-\omega_{p_4-q}-\omega_{p_5+q}-i\eta)}\frac{\theta(|p_4|-k_F)}{(p_4^0-\omega_{p_4}+i\eta)}.\end{aligned}$$

The first two terms have both poles on the same side of the real p_4^0 axis; in this case, we close the contour in the opposite half plane, showing that these terms make no contribution. In contrast, each of the last remaining two terms has one pole above and one below the real axis. These contributions are evaluated with a contour integral, and we find:

$$\begin{aligned}&\frac{1}{(2\pi)^2}\int dp_4\; dq^0\; G^0(p_5+q)\; G^0(p_4-q)\; G^0(p_4) =\\ &\left[\frac{\theta(|p_4-q|-k_F)\theta(|p_5+q|-k_F)\theta(k_F-|p_4|)}{p_5^0-\omega_{p_4-q}-\omega_{p_5+q}+\omega_{p_4}+i\eta}+\frac{\theta(k_F-|p_4-q|)\theta(k_F-|p_5+q|)\theta(|p_4|-k_F)}{p_5^0-\omega_{p_4-q}-\omega_{p_5+q}+\omega_{p_4}-i\eta}\right].\end{aligned}$$

After that we calculate:

$$\begin{aligned}&\frac{1}{(2\pi)^2}\int dq^0\; dp_4^0\; G^0(p_5+q)\; G^0(p_4-q)\; G^0(p_4)\; G^0(p_5) =\\ &\left[\frac{\theta(|p_4-q|-k_F)\theta(|p_5+q|-k_F)\theta(k_F-|p_4|)}{p_5^0-\omega_{p_4-q}-\omega_{p_5+q}+\omega_{p_4}+i\eta}+\frac{\theta(k_F-|p_4-q|)\theta(k_F-|p_5+q|)\theta(|p_4|-k_F)}{p_5^0-\omega_{p_4-q}-\omega_{p_5+q}+\omega_{p_4}-i\eta}\right]\\ &\times\left[\frac{\theta(|p_5|-k_F)}{p_5^0-\omega_{p_5}+i\eta}+\frac{\theta(k_F-|p_5|)}{p_5^0-\omega_{p_5}-i\eta}\right].\end{aligned}$$

After expanding the above two factors, we get:

$$\begin{aligned}&\frac{1}{(2\pi)^2}\int dq^0\; dp_4^0\; G^0(p_5+q)\; G^0(p_4-q)\; G^0(p_4)\; G^0(p_5) =\\ &\frac{\theta(|p_4-q|-k_F)\theta(|p_5+q|-k_F)\theta(k_F-|p_4|)}{(p_5^0-\omega_{p_4-q}-\omega_{p_5+q}+\omega_{p_4}+i\eta)}\times\frac{\theta(|p_5|-k_F)}{(p_5^0-\omega_{p_5}+i\eta)}\\ &+\frac{\theta(k_F-|p_4-q|)\theta(k_F-|p_5+q|)\theta(|p_4|-k_F)}{(p_5^0-\omega_{p_4-q}-\omega_{p_5+q}+\omega_{p_4}-i\eta)}\times\frac{\theta(k_F-|p_5|)}{(p_5^0-\omega_{p_5}-i\eta)}\\ &+\frac{\theta(|p_4-q|-k_F)\theta(|p_5+q|-k_F)\theta(k_F-|p_4|)}{(p_5^0-\omega_{p_4-q}-\omega_{p_5+q}+\omega_{p_4}+i\eta)}\times\frac{\theta(k_F-|p_5|)}{(p_5^0-\omega_{p_5}-i\eta)}\\ &+\frac{\theta(k_F-|p_4-q|)\theta(k_F-|p_5+q|)\theta(|p_4|-k_F)}{(p_5^0-\omega_{p_4-q}-\omega_{p_5+q}+\omega_{p_4}-i\eta)}\times\frac{\theta(|p_5|-k_F)}{(p_5^0-\omega_{p_5}+i\eta)}.\end{aligned}$$

The first two terms have both poles on the same side of the real p_5^0 axis; in this case, we close the contour in the opposite half plane, showing that these terms make no contribution. In contrast, each of the last remaining two terms has one pole above and one below the real axis. These contributions are evaluated with a contour integral, and we find:

$$-\frac{i}{(2\pi)^3}\int dq^0\ dp_4^0\ dp_5^0\ G^0(p_5+q)\ G^0(p_4-q)\ G^0(p_4)\ G^0(p_5) =$$
$$\frac{\theta(|p_4-q|-k_F)\theta(|p_5+q|-k_F)\theta(k_F-|p_4|)\theta(k_F-|p_5|)}{\omega_{p_5}+\omega_{p_4}-\omega_{p_4-q}-\omega_{p_5+q}+i\eta}$$
$$-\frac{\theta(k_F-|p_4-q|)\theta(k_F-|p_5+q|)\theta(|p_4|-k_F)\theta(|p_5|-k_F)}{\omega_{p_5}+\omega_{p_4}-\omega_{p_4-q}-\omega_{p_5+q}-i\eta}.$$

Therefore, taking η to 0, we get:

$$\begin{aligned}
& -i\lim_{\eta\to 0}\int dq^0\ dp_4^0\ dp_5^0\ G^0(p_5+q)\ G^0(p_4-q)\ G^0(p_4)\ G^0(p_5) \\
= & \frac{\theta(|p_4-q|-k_F)\theta(|p_5+q|-k_F)\theta(k_F-|p_4|)\theta(k_F-|p_5|)}{\omega_{p_5}+\omega_{p_4}-\omega_{p_4-q}-\omega_{p_5+q}} \\
- & \frac{\theta(k_F-|p_4-q|)\theta(k_F-|p_5+q|)\theta(|p_4|-k_F)\theta(|p_5|-k_F)}{\omega_{p_5}+\omega_{p_4}-\omega_{p_4-q}-\omega_{p_5+q}}.
\end{aligned}$$

Consequently, the second-order energy correction for diagram $(3)^d$ becomes:

$$E_{3d}^{(2)} = \left(\frac{1}{4}\right)\frac{g^2}{(2\pi)^9}\int d^3p_4\ d^3p_5\ d^3p_6\ V^2(q)$$
$$\times\left\{\frac{\theta(|p_4-q|-k_F)\theta(|p_5+q|-k_F)\theta(k_F-|p_4|)\theta(k_F-|p_5|)}{\omega_{p_5}+\omega_{p_4}-\omega_{p_4-q}-\omega_{p_5+q}}\right.$$
$$\left.-\frac{\theta(k_F-|p_4-q|)\theta(k_F-|p_5+q|)\theta(|p_4|-k_F)\theta(|p_5|-k_F)}{\omega_{p_5}+\omega_{p_4}-\omega_{p_4-q}-\omega_{p_5+q}}\right\}.$$

After performing the change of variable in the second term of the integrand: $p_4^{'} = p_4 - q$ and $q_5^{'} = p_5 + q$, we get:

$$E_{3d}^{(2)} = \left(\frac{1}{2}\right)\frac{g^2}{(2\pi)^9}\int d^3p_4\ d^3p_5\ d^3p_6\ V^2(q)\frac{\theta(|p_4-q|-k_F)\theta(|p_5+q|-k_F)\theta(k_F-|p_4|)\theta(k_F-|p_5|)}{\omega_{p_5}+\omega_{p_4}-\omega_{p_4-q}-\omega_{p_5+q}}.$$

Consequently,

$$\boxed{E_{3d}^{(2)} = \left(\frac{1}{2}\right)\frac{g^2}{(2\pi)^9}\int_{C_I} d^3p_4\ d^3p_5\ d^3p_6\frac{V^2(q)}{\epsilon_{p_5}^{(0)}+\epsilon_{p_4}^{(0)}-\epsilon_{p_4-q}^{(0)}-\epsilon_{p_5+q}^{(0)}},}$$

where $C_I = \theta(|p_4-q|-k_F)\theta(|p_5+q|-k_F)\theta(k_F-|p_4|)\theta(k_F-|p_5|)$.

Appendix C

Calculation of $G(\mathbf{q})$

The second-order correction normalized within a box of volume Ω is given by (the corresponding direct and exchange diagrams are shown in the lower line of Fig. 5.6):

$$\Delta E = d\frac{\Omega^3}{(2\pi)^9}\int_{C_I} d^3\mathbf{q}\, d^3\mathbf{k}_1\, d^3\mathbf{k}_2\, \frac{V^2(\mathbf{q})}{\epsilon_{\mathbf{k}_1}+\epsilon_{\mathbf{k}_2}-\epsilon_{\mathbf{k}_1+\mathbf{q}}-\epsilon_{\mathbf{k}_2-\mathbf{q}}}. \tag{C.1}$$

The parameter d is expressed in terms of the level of degeneracy n as:

$$d = \frac{n^2-n}{2}, \quad n = 4 \text{ in the case of symmetric nuclear matter.}$$

The domain of integration C_I represents the intersection of the inner region of a sphere of radius k_F (that represents hole states), and the outer region of another sphere of radius k_F (that represents *p*article states):

$$C_I = \left\{ \begin{array}{ll} |\mathbf{k}_1| < k_F, & |\mathbf{k}_1+\mathbf{q}| > k_F \\ |\mathbf{k}_2| < k_F, & |\mathbf{k}_2-\mathbf{q}| > k_F. \end{array} \right. \tag{C.2}$$

The second-order energy correction in Eq.(C.1) becomes:

$$\Delta E \;=\; -d\frac{\Omega^3}{(2\pi)^9}\left(\frac{m^*}{\hbar^2}\right) k_F^7 \int_{|\mathbf{q}|>0} d^3\mathbf{q}\, V^2(q)\, G(q), \tag{C.3}$$

where the expression of $G(|\mathbf{q}|)$ is given by:

$$G(|\mathbf{q}|) = \int_0^\infty d\alpha\, e^{-\alpha\mathbf{q}^2} \int_{\substack{|\mathbf{k}_1|<1 \\ |\mathbf{k}_1+\mathbf{q}|>1}} d^3\mathbf{k}_1\, e^{-\alpha\mathbf{q}\cdot\mathbf{k}_1} \int_{\substack{|\mathbf{k}_2|<1 \\ |\mathbf{k}_2-\mathbf{q}|>1}} d^3\mathbf{k}_2\, e^{\alpha\mathbf{q}\cdot\mathbf{k}_2}.$$

Calculation of $G(|\mathbf{q}|)$

Let us start calculating $G(|\mathbf{q}|)$ in the region where $|q| > 2$. It can be easily checked that boundary condition in this case is reduced to:

$$(|p| < 1) \cap (|p \pm q| > 1) = \Theta(1-|p|)\Theta(|p-q|-1) = \Theta(1-|p|).$$

Then the expression of $G(|\mathbf{q}|)$ reduces to:

$$G(|\mathbf{q}|) = \int_0^\infty d\alpha\ e^{-\alpha q^2} \left(\int_{|k|<1} d^3\vec{k}\ e^{-\alpha \vec{q}\cdot\vec{k}} \right)^2 .$$

Now let us calculate the following integral:

$$\int_{|k|<1} d^3\vec{k}\ e^{-\alpha \vec{q}\cdot\vec{k}}.$$

Using the spherical coordinates, one can write:

$$\begin{aligned} \int_{|k|<1} d^3\vec{k}\ e^{-\alpha \vec{q}\cdot\vec{k}} &= 2\pi \int_0^1 \int_0^\pi k^2 \sin\theta\ e^{-\alpha|q||k|\cos\theta} d\theta\ dk \\ &= \frac{(2\pi)^2}{(\alpha|q|)^6} \left[(\alpha|q|-1)\ e^{\alpha|q|} + (\alpha|q|+1)\ e^{-\alpha|q|} \right]^2 , \end{aligned}$$

and therefore, $G(|\mathbf{q}|)$ reads:

$$G(|\mathbf{q}|) = \int_0^\infty d\alpha\ e^{-\alpha q^2} \frac{(2\pi)^2}{(\alpha|q|)^6} \left[(\alpha|q|-1)\ e^{\alpha|q|} + (\alpha|q|+1)\ e^{-\alpha|q|} \right]^2 .$$

Consequently, after taking $u = q/2$, we get:

$$\begin{aligned} G(u) &= \frac{(2\pi)^2}{30u}[(4 - 20u^2 - 20u^3 + 4u^5)\log(u+1) + (-4 + 20u^2 - 20u^3 + 4u^5)\log(u-1) \\ &\quad +22u + 4u^3 + (40u^3 - 8u^5)\log(u)]. \end{aligned}$$

For the region $0 < |q| < 2$, we use the techniques of Ref. [5, 9]:

$$\int_{\substack{|k|<1 \\ |k\pm q|>1}} d^3\vec{k}\ e^{-\alpha \vec{q}\cdot\vec{k}} = \int_0^1 d\beta \int_{|k|<1} d^3\vec{k}\ e^{-\alpha \vec{q}\cdot\vec{k}} \times \vec{q}\cdot\left(\vec{k} \pm \beta\vec{q}\right) \delta\left(|\vec{k} \pm \beta\vec{q}| - 1\right).$$

By making use of the spherical coordinates, we get:

$$\begin{aligned} \int_{\substack{|k|<1 \\ |k\pm q|>1}} d^3\vec{k}\ e^{-\alpha \vec{q}\cdot\vec{k}} &= 2\pi|q| \int_0^1 d\beta \int_{\frac{|q|\beta}{2}}^1 dx\ x\ e^{-\alpha|q|x} e^{\alpha\beta q^2} \\ &= \frac{(2\pi)}{(\alpha|q|)^3} \left[\alpha q^2\ e^{\frac{\alpha q^2}{2}} + (1+\alpha|q|)\ e^{-\alpha|q|} - (1+\alpha|q|)\ e^{\alpha|q|(|q|-1)} \right]. \end{aligned}$$

As a result, the expression of $G(|\mathbf{q}|)$ becomes:

$$G(|\mathbf{q}|) = \int_0^\infty d\alpha\ e^{-\alpha q^2} \frac{(2\pi)^2}{(\alpha|q|)^6} \left[\alpha q^2\ e^{\frac{\alpha q^2}{2}} + (1+\alpha|q|)\ e^{-\alpha|q|} - (1+\alpha|q|)\ e^{\alpha|q|(|q|-1)} \right]^2 .$$

By introducing the change of variable: $u = q/2$, we get:

$$\begin{aligned} G(u) &= \frac{(2\pi)^2}{30u}[(4 + \frac{15}{2}u - 5u^3 + \frac{3}{2}u^5)\log(1+u) \\ &\quad +(4 - \frac{15}{2} + 5u^3 - \frac{3}{2}u^5)\log(1-u) + 29u^2 - 3u^4 - 40u^2\log 2]. \end{aligned}$$

Appendix D

Functions

D.1 Functions $F_i^j(u)$

The expressions of the ten functions $F_1^j(u)$ and $F_2^j(u)$ (with j running from 1 to 5) are given by:

$$
\begin{aligned}
F_1^1(u) &= \left(4+\frac{15}{2}u-5u^3+\frac{3}{2}u^5\right)\log(1+u)+\left(4-\frac{15}{2}u+5u^3-\frac{3}{2}u^5\right)\log(1-u)\\
&\quad +29u^2-3u^4-40u^2\log 2.\\
F_2^1(u) &= \left(4-20u^2-20u^3+4u^5\right)\log(u+1)+\left(20u^2-20u^3+4u^5-4\right)\log(u-1)\\
&\quad +22u+4u^3+(40u^3-8u^5)\log u.\\
F_1^2(u) &= \left(\frac{15}{8}-\frac{6}{7u}+12u-\frac{195}{8}u^2+\frac{129}{8}u^4-\frac{267}{56}u^6\right)\log(1-u)-\frac{311u}{28}+\frac{1457u^3}{14}-\frac{267u^5}{28}\\
&\quad -\left(\frac{15}{8}+\frac{6}{7u}-12u-\frac{195}{8}u^2+\frac{129}{8}u^4-\frac{267}{56}u^6\right)\log(1+u)+\left(8u-140u^3\right)\log 2.\\
F_2^2(u) &= -\frac{58}{7}+\frac{550u^2}{7}+\frac{92u^4}{7}+\left(\frac{6}{7u}-16u+70u^3-68u^4+\frac{92}{7}u^6\right)\log(u-1)\\
&\quad +\left(136u^4-\frac{184}{7}u^6\right)\log u+\left(-\frac{6}{7u}+16u-70u^3-68u^4+\frac{92}{7}u^6\right)\log(u+1).\\
F_1^3(u) &= \left(\frac{15}{4}-\frac{12}{7u}+16u-\frac{135}{4}u^2+\frac{89}{4}u^4-\frac{183}{28}u^6\right)\log(1-u)-\frac{311u}{14}+\frac{1051u^3}{7}-\frac{183u^5}{14}\\
&\quad -\left(\frac{15}{4}+\frac{12}{7u}-16u-\frac{135}{4}u^2+\frac{89}{4}u^4-\frac{183}{28}u^6\right)\log(1+u)+\left(16u-200u^3\right)\log 2.\\
F_2^3(u) &= -\frac{116}{7}+\frac{792u^2}{7}+\frac{128u^4}{7}+\left(\frac{12}{7u}-24u+100u^3-96u^4+\frac{128}{7}u^6\right)\log(u-1)\\
&\quad +\left(192u^4-\frac{256}{7}u^6\right)\log u+\left(-\frac{12}{7u}+24u-100u^3-96u^4+\frac{128}{7}u^6\right)\log(u+1).\\
F_1^4(u) &= \left(\frac{15}{4}-\frac{12}{7u}+4u-\frac{45}{4}u^2+\frac{29}{4}u^4-\frac{57}{28}u^6\right)\log(1-u)-\frac{311u}{14}+\frac{442u^3}{7}-\frac{57u^5}{14}\\
&\quad +\left(16u-80u^3\right)\log 2+\left(-\frac{15}{4}-\frac{12}{7u}+4u+\frac{45}{4}u^2-\frac{29}{4}u^4+\frac{57}{28}u^6\right)\log(1+u).
\end{aligned}
$$

$$
\begin{aligned}
F_2^4(u) &= -\frac{116}{7} + \frac{330u^2}{7} + \frac{44u^4}{7} + \left(\frac{12}{7u} - 12u + 40u^3 - 36u^4 + \frac{44}{7}u^6\right)\log(u-1) \\
&\quad + \left(72u^4 - \frac{88}{7}u^6\right)\log u + \left(-\frac{12}{7u} + 12u - 40u^3 - 36u^4 + \frac{44}{7}u^6\right)\log(u+1). \\
F_1^5(u) &= \frac{311u}{420} - \frac{239u^3}{210} + \frac{u^5}{28} - \left[\frac{8}{15}u - \frac{4}{3}u^3\right]\log 2 - \left[\frac{1}{8} - \frac{2}{35u} - \frac{1}{8}u^2 + \frac{3}{40}u^4 - \frac{1}{56}u^6\right]\log[1-u] \\
&\quad + \left[\frac{1}{8} + \frac{2}{35u} - \frac{1}{8}u^2 + \frac{3}{40}u^4 - \frac{1}{56}u^6\right]\log[1+u]. \\
F_2^5(u) &= -\left[\frac{16}{15}u^4 - \frac{16}{105}u^6\right]\log u - \left[\frac{2}{35u} - \frac{4}{15}u + \frac{2}{3}u^3 - \frac{8}{15}u^4 + \frac{8}{105}u^6\right]\log[u-1]. \\
&\quad + \left[\frac{2}{35u} - \frac{4}{15}u + \frac{2}{3}u^3 + \frac{8}{15}u^4 - \frac{8}{105}u^6\right]\log[u+1] + \frac{58}{105} - \frac{88u^2}{105} - \frac{8u^4}{105}.
\end{aligned}
$$

D.2 Functions $F_i^{abc}(u)$

The expressions of the functions $F_1^{abc}(u)$, $F_2^{abc}(u)$ and $F_3^{abc}(u)$ are given by:

$$
\begin{aligned}
&F_1^{abc}(u) = \\
&\frac{u^2}{2}\left(11b^4c+18ab^3c^2+18a^2b^2c^3+11a^3bc^4\right)+u^3(18b^3c-9b^4c+6ab^2c^2-9b^3c^2-3ab^3c^2+18a^2bc^3 \\
&-3ab^2c^3-9a^2b^2c^3-9a^2bc^4)+u^4(6b^2c-6b^3c+2b^4c+6abc^2-6b^2c^2-6ab^2c^2+3b^3c^2-\frac{1}{2}ab^3c^2 \\
&-6abc^3-\frac{1}{2}b^2c^3+3ab^2c^3+2abc^4)+u^5(4bc-6b^2c-b^3c+\frac{3}{2}b^4c-6bc^2+6b^2c^2+\frac{1}{2}b^3c^2-bc^3 \\
&+\frac{1}{2}b^2c^3+\frac{3}{2}bc^4) \\
&+\log 2\Big\{-20u^2(b^4c+a^3bc^4)+u^3(30b^4c-60b^3c+30b^3c^2-60a^2bc^3+30a^2b^2c^3 \\
&+30a^2bc^4)+u^5(80bc-120b^2c+80b^3c-20b^4c-120bc^2+120b^2c^2-40b^3c^2+80bc^3-40b^2c^3 \\
&-20bc^4)\Big\}+10u^5bc(2-b-c)^3\log(2(2-b-c)u) \\
&+\Big\{\frac{1}{2}(b^5-5a^2b^3c^2-5a^3b^2c^3+a^5c^5)+\frac{15u}{4}(b^4-b^5-2a^2b^2c^2+2a^2b^3c^2+a^4c^4-a^4bc^4) \\
&+10u^2(b^3-2b^4+b^5+a^3c^3-2a^3bc^3+a^3b^2c^3)+10u^3(b^2-3b^3+3b^4-b^5+a^2c^2-3a^2bc^2+3a^2b^2c^2 \\
&-a^2b^3c^2)+u^5(-4+20b-40b^2+40b^3-20b^4+4b^5)\Big\}\log(b+ac+2u-2bu) \\
&+\Big\{(\frac{15}{4}a^4bc^4u+10a^3u^2(2bc^3-b^2c^3)+a^2u^3(30bc^2-30b^2c^2+\frac{15}{2}b^3c^2) \\
&+u^5(-20b+40b^2-30b^3+10b^4-\frac{5}{4}b^5)\Big\}\log(2ac+4u-2bu) \\
&+\Big\{\frac{1}{2}(b^5-5a^2b^3c^2-5a^3b^2c^3+a^5c^5)+\frac{15u}{4}(b^4-b^4c-2a^2b^2c^2+2a^2b^2c^3+a^4c^4-a^4c^5) \\
&+10u^2(b^3-2b^3c+b^3c^2+a^3c^3-2a^3c^4+a^3c^5)+10u^3(b^2-3b^2c+a^2c^2+3b^2c^2-3a^2c^3-b^2c^3 \\
&+3a^2c^4-a^2c^5)+u^5(-4+20c-40c^2+40c^3-20c^4+4c^5)\Big\}\log(b+ac+2u-2cu) \\
&+\Big\{\frac{15}{4}b^4cu+u^2(20b^3c-10b^3c^2)+u^3(30b^2c-30b^2c^2+\frac{15}{2}b^2c^3)+u^5(40c^2-20c-30c^3+10c^4 \\
&-\frac{5}{4}c^5)\Big\}\log(2b+4u-2cu)
\end{aligned}
$$

$$+\Bigg\{\frac{1}{2}(-b^5+5a^2b^3c^2+5a^3b^2c^3-a^5c^5)+\frac{15u}{4}(-b^4+b^5+b^4c+2a^2b^2c^2-2a^2b^3c^2-2a^2b^2c^3$$
$$-a^4c^4+a^4bc^4+a^4c^5)+u^2(-10b^3+20b^4-10b^5+20b^3c-20b^4c-10b^3c^2-10a^3c^3+20a^3bc^3$$
$$-10a^3b^2c^3+20a^3c^4-20a^3bc^4-10a^3c^5)$$
$$+u^3(-10b^2+30b^3-30b^4+10b^5+30b^2c-60b^3c+30b^4c-10a^2c^2+30a^2bc^2-30b^2c^2-30a^2b^2c^2$$
$$+30b^3c^2+10a^2b^3c^2+30a^2c^3-60a^2bc^3+10b^2c^3+30a^2b^2c^3-30a^2c^4+30a^2bc^4+10a^2c^5)$$
$$+u^5(4-20b+40b^2-40b^3+20b^4-4b^5-20c+80bc-120b^2c+80b^3c-20b^4c+40c^2-120bc^2$$
$$+120b^2c^2-40b^3c^2-40c^3+80bc^3-40b^2c^3+20c^4-20bc^4-4c^5)\Bigg\}\log(b+ac+2u-2bu-2cu)$$

$$+\Bigg\{-\frac{15}{4}a^4bc^4u+u^2(-20a^3bc^3+10a^3b^2c^3+20a^3bc^4)+u^3(-30a^2bc^2+30a^2b^2c^2-\frac{15}{2}a^2b^3c^2$$
$$+60a^2bc^3-30a^2b^2c^3-30a^2bc^4)+u^5(20b-40b^2+30b^3-10b^4+\frac{5}{4}b^5-80bc+120b^2c-60b^3c$$
$$+10b^4c+120bc^2-120b^2c^2+30b^3c^2-80bc^3+40b^2c^3+20bc^4)\Bigg\}\log(2ac+4u-2bu-4cu)$$

$$+\Bigg\{-\frac{15}{4}b^4cu+u^2(-20b^3c+20b^4c+10b^3c^2)+u^3(-30b^2c+60b^3c-30b^4c+30b^2c^2-30b^3c^2$$
$$-\frac{15}{2}b^2c^3)+u^5(20c-80bc+120b^2c-80b^3c+20b^4c-40c^2+120bc^2-120b^2c^2+40b^3c^2+30c^3$$
$$-60bc^3+30b^2c^3-10c^4+10bc^4+\frac{5}{4}c^5)\Bigg\}\log(4u-2cu+2b-4bu)$$

$$-\Bigg\{\frac{1}{2}(b^5-5a^2b^3c^2-5a^3b^2c^3+a^5c^5)+\frac{15u}{4}(b^4-2a^2b^2c^2+a^4c^4)+10u^2(b^3+a^3c^3)$$
$$+10u^3(b^2+a^2c^2)-4u^5\Bigg\}\log(b+ac+2u)$$

$$
\begin{aligned}
F_2^{abc}(u) \;=\;& \{\frac{1}{2}(b^5-5a^2b^3c^2-5a^3b^2c^3+a^5c^5)+\frac{15u}{4}(-b^4+2a^2b^2c^2-a^4c^4)\\
&+10u^2(b^3+a^3c^3)-10u^3(b^2+a^2c^2)+4u^5\}\log(2u-ac-b)\\
&+\{\frac{1}{2}(b^5-5a^2b^3c^2+5a^3b^2c^3-a^5c^5)+\frac{15u}{4}(b^4-2a^2b^2c^2+a^4c^4)\\
&+10u^2(b^3-a^3c^3)+10u^3(b^2+a^2c^2)-4u^5\}\log(2u-ac+b)\\
&+\{\frac{1}{2}(-b^5+5a^2b^3c^2-5a^3b^2c^3+a^5c^5)+\frac{15u}{4}(b^4-2a^2b^2c^2+a^4c^4)\\
&+10u^2(-b^3+a^3c^3)+10u^3(b^2+a^2c^2)-4u^5\}\log(2u+ac-b)\\
&-\{\frac{1}{2}(b^5-5a^2b^3c^2-5a^3b^2c^3+a^5c^5)+\frac{15u}{4}(b^4-2a^2b^2c^2+a^4c^4)\\
&+10u^2(b^3+a^3c^3)+10u^3(b^2+a^2c^2)-4u^5\}\log(2u+ac+b)\\
&+11abcu(b^2+a^2c^2)+4abcu^3
\end{aligned}
$$

$$
\begin{aligned}
&F_3^{abc}(u) = \\
&\frac{11u}{2}\left(ab^4c + a^3b^2c^3\right) + u^2\left(18ab^3c - 9ab^4c + 11a^3bc^3 - \frac{11}{2}a^3b^2c^3\right) + u^3\left(6ab^2c - 6ab^3c + 2ab^4c\right) \\
&+u^4\left(4abc - 6ab^2c - ab^3c + \frac{3}{2}ab^4c\right) + u^2\left(-40a^3bc^3 + 20a^3b^2c^3\right)\log 2 \\
&+\Bigg\{ -\frac{1}{2}b^5 + \frac{5}{2}a^2b^3c^2 - \frac{5}{2}a^3b^2c^3 + \frac{1}{2}a^5c^5 + u(-\frac{15}{4}b^4 + \frac{15}{4}b^5 + \frac{15}{2}a^2b^2c^2 - \frac{15}{2}a^2b^3c^2 - \frac{15}{4}a^4c^4 \\
&+\frac{15}{4}a^4bc^4) + u^2(-10b^3 + 20b^4 - 10b^5 + 10a^3c^3 - 20a^3bc^3 + 10a^3b^2c^3) \\
&+u^3(-10b^2 + 30b^3 - 30b^4 + 10b^5 - 10a^2c^2 + 30a^2bc^2 - 30a^2b^2c^2 + 10a^2b^3c^2) \\
&+u^5(4 - 20b + 40b^2 - 40b^3 + 20b^4 - 4b^5)\Bigg\}\log(b - ac + 2u - 2bu) \\
&+\Bigg\{\frac{1}{2}b^5 - \frac{5}{2}a^2b^3c^2 - \frac{5}{2}a^3b^2c^3 + \frac{1}{2}a^5c^5 + u(\frac{15}{4}b^4 - \frac{15}{4}b^5 - \frac{15}{2}a^2b^2c^2 + \frac{15}{2}a^2b^3c^2 + \frac{15}{4}a^4c^4 - \frac{15}{4}a^4bc^4) \\
&+u^2(10b^3 - 20b^4 + 10b^5 + 10a^3c^3 - 20a^3bc^3 + 10a^3b^2c^3) \\
&+u^3(10b^2 - 30b^3 + 30b^4 - 10b^5 + 10a^2c^2 - 30a^2bc^2 + 30a^2b^2c^2 - 10a^2b^3c^2) \\
&+u^5(-4 + 20b - 40b^2 + 40b^3 - 20b^4 + 4b^5\Bigg\}\log(b + ac + 2u - 2bu) \\
&+\Bigg\{\frac{15}{4}a^4bc^4u + u^2(20a^3bc^3 - 10a^3b^2c^3) + u^3(30a^2bc^2 - 30a^2b^2c^2 + \frac{15}{2}a^2b^3c^2) \\
&+u^5(-20b + 40b^2 - 30b^3 + 10b^4 - \frac{5}{4}b^5)\Bigg\}\log(2ac + 4u - 2bu) \\
&-\Bigg\{\frac{b^5}{2} - \frac{5}{2}a^2b^3c^2 - \frac{5}{2}a^3b^2c^3 + \frac{a^5c^5}{2} + u(\frac{15b^4}{4} - \frac{15}{2}a^2b^2c^2 + \frac{15}{4}a^4c^4) + u^2(10b^3 + 10a^3c^3) \\
&+u^3(10b^2 + 10a^2c^2) - 4u^5\Bigg\}\log(b + ac + 2u) \\
&+\frac{1}{8}(b - ac + 2u)^3(4b^2 + 4a^2c^2 - 6acu - 4u^2 + 3b(4ac + 2u))\log(b - ac + 2u) \\
&+\frac{5}{64}\left[-6ac - 4u + 2bu\right]\left[2ac - 4u + 2bu\right]^3\log(4u - 2bu - 2ac)
\end{aligned}
$$

D.3 Integrals in d dimensions

Let us define $I_d(\alpha, \mathbf{q})$ to be an integral in $d-$dimension as follows where $d \in \mathrm{C}$:

$$I_d(\alpha, q) = \int_{|\mathbf{k}|<1} d^d\mathbf{k}\; e^{-\alpha \mathbf{q}\cdot\mathbf{k}} \quad \text{where} \quad \Re[\alpha] > 0. \tag{D.1}$$

Working in the frame of polar coordinates in d-dimension, we can define a radial coordinate, $r = |\mathbf{k}|$, and $(d-1)$ angular coordinates $\phi,\ \theta_1, \theta_2, \ldots, \theta_{d-2}$, where $\phi \in [0, 2\pi]$ and $\theta_i \in\ [0, \pi]$, for $i = 1,\ 2, \cdots, d-2$. Then Eq. (D.1), becomes:

$$I_d(\alpha, q) \;\; = \;\; \int_0^{2\pi} d\phi \prod_{n=1}^{d-3} \int_0^{\pi} (\sin\theta_n)^n \; d\theta_n \int_0^1 \int_0^{\pi} k^{d-1} \;\sin^{d-2}\theta_{d-2}\; e^{-\alpha q k \cos\theta_{d-2}}\; d\theta_{d-2}\; dk$$

Let S_{d-1} be the solid angle in $(d-1)$-dimension:

$$S_{d-1} = \int_0^{2\pi} d\phi \prod_{n=1}^{d-3} \int_0^{\pi} (\sin\theta_n)^n \; d\theta_n = \frac{2\pi^{\frac{d-1}{2}}}{\Gamma\left(\frac{d-1}{2}\right)}.$$

Then $I_d(\alpha, q)$ becomes:

$$I_d(\alpha, q) = S_{d-1} \int_0^1 \int_0^{\pi} k^{d-1} \sin^{d-2}\theta\; e^{-\alpha q k\cos\theta}\; d\theta\;\; dk$$

Take the change of variable $u = \cos\theta$,

$$I_d(\alpha, q) = S_{d-1} \int_0^1 k^{d-1} dk \int_{-1}^1 (1-u^2)^{\frac{d-3}{2}} e^{-\alpha q k u} du = 2\; S_{d-1} \int_0^1 k^{d-1} dk \int_0^1 (1-u^2)^{\frac{d-3}{2}} \cosh(\alpha q k u) du.$$

The " $\cosh x$" function is analytic in an open disc centered at 0, so it can be represented by a convergent power series in this disc, i.e, $\cosh x = \sum_{n=0}^{\infty} \frac{x^{2n}}{(2n)!}$.
Consequently, $I_d(\alpha, q)$ becomes:

$$2\; S_{d-1} \int_0^1 k^{d-1} dk \int_0^1 (1-u^2)^{\frac{d-3}{2}} \sum_{n=0}^{\infty} \frac{(\alpha q k)^{2n}}{(2n!)} u^{2n} = 2\; S_{d-1} \sum_{n=0}^{\infty} \frac{(\alpha q)^{2n}}{(2n!)} \int_0^1 k^{2n+d-1} dk \int_0^1 u^{2n} (1-u^2)^{\frac{d-3}{2}} du$$

Now performing the change of variable $(u^2 \to u)$ and identifying the resulting integral as a beta-function:

$$I_d(\alpha, q) = S_{d-1} \sum_{n=0}^{\infty} \frac{(\alpha q)^{2n}}{(2n!)} \frac{1}{2n+d} \int_0^1 u^{n-\frac{1}{2}} (1-u)^{\frac{d-3}{2}} du = S_{d-1} \sum_{n=0}^{\infty} \frac{(\alpha q)^{2n}}{(2n!)} \frac{1}{2n+d}\; B\left(n+\frac{1}{2}, \frac{d-1}{2}\right)$$

Recalling some important identities involving the Gamma and Beta functions

$$B(x,y) = \frac{\Gamma(x)\Gamma(y)}{\Gamma(x+y)}, \quad \Gamma(1+x) = x\,\Gamma(x) \quad \text{and} \quad \Gamma\left(x+\frac{1}{2}\right) = 2^{1-2x}\sqrt{\pi}\frac{\Gamma(2x)}{\Gamma(x)}, \quad \forall\; x,\; y \in \mathbb{C} \tag{D.2}$$

$I_d(\alpha, q)$ becomes:

$$I_d(\alpha,q) = \frac{S_{d-1}}{2}\sum_{n=0}^{\infty}\frac{(\alpha q)^{2n}}{(2n!)}\frac{\Gamma(n+\frac{1}{2})\Gamma(\frac{d-1}{2})}{\Gamma(n+1+\frac{d}{2})} = S_{d-1}\frac{\Gamma\left(\frac{d-1}{2}\right)\sqrt{\pi}}{2\Gamma\left(1+\frac{d}{2}\right)}\sum_{n=0}^{\infty}\frac{1}{\left(1+\frac{d}{2}\right)_n}\frac{(\frac{\alpha^2q^2}{4})^n}{n!}$$

Identifying the above series as a member of the family of generalized hypergeometric functions, we finally get:

$$\boxed{I_d(\alpha,q) = \frac{\pi^{\frac{d}{2}}}{\Gamma\left(1+\frac{d}{2}\right)}\,{}_0\mathrm{F}_1\left(-;1+\frac{d}{2};\frac{\alpha^2q^2}{4}\right)}$$

Calculation of $G_d(\mathbf{q})$

Let $b,\ c \in\ \mathcal{R}$ and $z \in\ \mathcal{C}$, such that $b+c \neq 1$,then:

$${}_0\mathrm{F}_1\left(-;b;z\right)\ {}_0\mathrm{F}_1\left(-;c;z\right) = {}_2\mathrm{F}_3\left(\frac{b+c}{2},\frac{b+c-1}{2};b,c,b+c-1;4z\right)$$

Using the above Lemma for the case $b=c$, we get:

$$\left[I_d(\alpha,q)\right]^2 = \frac{\pi^d}{\left[\Gamma\left(1+\frac{d}{2}\right)\right]^2}\ \left[{}_0\mathrm{F}_1\left(-;1+\frac{d}{2};\frac{\alpha^2q^2}{4}\right)\right]^2 = \frac{\pi^d}{\left[\Gamma\left(1+\frac{d}{2}\right)\right]^2}\ {}_1\mathrm{F}_2\left(\frac{1+d}{2};1+\frac{d}{2},1+d;\alpha^2q^2\right)$$

In chapter 6, we have defined $G_d(\mathbf{q})$ in Eq. (6.3) as follows:

$$G_d(\mathbf{q}) = \int_0^{\infty} e^{-\alpha q^2}\ \left[I_d(\alpha,q)\right]^2\ d\alpha$$

For the sake of simplicity, we expand the hypergeometric function in terms of a Taylor series as follows:

$${}_1\mathrm{F}_2\left(\frac{1+d}{2};1+\frac{d}{2},1+d;\alpha^2q^2\right) =\ {}_1\mathrm{F}_2\left(a;b,c;\alpha^2q^2\right) = \sum_{n=0}^{\infty}\frac{(a)_n}{(b)_n\ (c)_n}\frac{(\alpha^2\ q^2)^n}{n!}$$

Then $G_d(\mathbf{q})$ becomes:

$$G_d(\mathbf{q}) = \frac{\pi^d}{\left[\Gamma\left(1+\frac{d}{2}\right)\right]^2}\sum_{n=0}^{\infty}\frac{(a)_n}{(b)_n\ (c)_n}\frac{q^{2n}}{n!}\int_0^{\infty}e^{-\alpha q^2}\ \alpha^{2n}\ d\alpha$$

Performing the change of variable $\alpha \rightarrow \alpha q^2$ and using the Legendre-duplication formula (D.2), we find:

$$\begin{aligned}
G_d(\mathbf{q}) &= \frac{\pi^d}{\left[\Gamma\left(1+\frac{d}{2}\right)\right]^2}\ \sum_{n=0}^{\infty}\frac{(a)_n}{(b)_n\ (c)_n}\frac{q^{-2n-2}}{n!}\ \Gamma(2n+1)\\
&= \frac{\pi^d}{\left[\Gamma\left(1+\frac{d}{2}\right)\right]^2}\frac{1}{q^2}\ {}_3\mathrm{F}_2\left(a,\frac{1}{2},1;b,c;\frac{4}{q^2}\right)\\
&= \frac{\pi^d}{\left[\Gamma\left(1+\frac{d}{2}\right)\right]^2}\frac{1}{q^2}\ {}_3\mathrm{F}_2\left(\frac{1+d}{2},\frac{1}{2},1;1+\frac{d}{2},1+d;\frac{4}{q^2}\right)
\end{aligned}$$

Calculation of $A(d)$

Define for $|q| > 2$ the d-dimensional integral $A(d)$:

$$A(d) = \left(\int_{|q|>2} d^d\vec{q}\, J_d(q) \right) - I_1 = \frac{\pi^d}{\left[\Gamma\left(1+\frac{d}{2}\right)\right]^2} \int_{|q|>2} \frac{d^d\vec{q}}{q^2} \left[\ {}_3\mathrm{F}_2\left(a, \frac{1}{2}, 1; b, c; \frac{4}{q^2}\right) - 1 \right]$$

First of all, a change of variable $q = 2u$ is applied. Then $A(d)$ becomes:

$$A(d) = \underbrace{2^{d-1} \frac{\pi^{3d/2}}{\Gamma\left(\frac{d}{2}\right)\left[\Gamma\left(1+\frac{d}{2}\right)\right]^2}}_{C(d)} \int_{|u|>1} \frac{d^d\vec{u}}{u^2} \left[\ {}_3\mathrm{F}_2\left(\frac{1+d}{2}, \frac{1}{2}, 1; 1+\frac{d}{2}, 1+d; \frac{1}{u^2}\right) - 1 \right]$$

We expand the above hypergeometric function in a power series for $|u| > 1$:

$$A(d) = C(d) \sum_{n=1}^{\infty} \frac{\left(\frac{1+d}{2}\right)_n \left(\frac{1}{2}\right)_n (1)_n}{\left(1+\frac{d}{2}\right)_n (1+d)_n \ n!} \int_1^{\infty} du\, u^{-2n+d-3} = 2^d \pi \sum_{n=1}^{\infty} \frac{\left(\frac{1+d}{2}\right)_n \left(\frac{1}{2}\right)_n (1)_n}{\left(1+\frac{d}{2}\right)_n (1+d)_n \ n!} \frac{1}{2n+2-d}$$

Therefore, after straight forward calculations, we get:

$$A(d) = \frac{C(d)}{2-d} \left[{}_4\mathrm{F}_3\left(\frac{1+d}{2}, \frac{1}{2}, 1, \frac{2-d}{2}; 1+\frac{d}{2}, 1+d, \frac{4-d}{2}; 1\right) - 1 \right]$$

Going back to 3−dimensions, we find that the value of $A(d \to 3)$ is finite and equals to:

$$A(3) = \lim_{d\to 3} A(d) = \left(\frac{256\pi^3}{9}\right)\left(-\frac{23}{35} + \frac{36}{35}\ln 2\right)$$

D.4 Functions $T_i^{abc}(u)$

Define the parameters a, b, and c:

$$\begin{aligned} a &= \frac{k_P}{k_N} = \left(\frac{1-\delta}{1+\delta}\right)^{1/3}, \\ b &= \frac{m_S^*}{m_N^*}, \\ c &= \frac{m_S^*}{m_P^*}, \end{aligned} \tag{D.3}$$

where k_P and m_P^* are the proton Fermi momentum and the proton effective mass, respectively.
For asymmetric matter, the beyond-mean-field EoS evaluated at the second-order is given by:

$$\frac{\Delta E^{AS}}{A}(\delta, \rho) = \sum_{i=1}^{6} \chi_i^{AS}(\rho, \delta)\ I_i(\rho, \delta),$$

where the six density-dependent coefficients $\chi^{AS}(\rho,\delta)$ and the factors $I_i(\rho,\delta)$ are given by:

$$
\begin{aligned}
\chi_1^{AS}(\rho,\delta) &= 8\,\pi^3\,\tilde{C}\,m_S^*\,k_N^4(\rho,\delta)\left(t_{03}^2+x_{03}^2\right), \\
\chi_2^{AS}(\rho,\delta) &= -16\,\pi^3\,\tilde{C}\,m_S^*\,k_N^4(\rho,\delta)\left(t_{03}\,x_{03}\right), \\
\chi_3^{AS}(\rho,\delta) &= 32\,\pi^3\,\tilde{C}\,m_S^*\,k_N^6(\rho,\delta)\left(t_{03}\,t_{12}+x_{03}\,x_{12}\right), \\
\chi_4^{AS}(\rho,\delta) &= 64\,\pi^3\,\tilde{C}\,m_S^*\,k_N^6(\rho,\delta)\left(t_{03}\,x_{12}+x_{03}\,t_{12}\right), \\
\chi_5^{AS}(\rho,\delta) &= 64\,\pi^3\,\tilde{C}\,m_S^*\,k_N^8(\rho,\delta)\left(t_{12}\,x_{12}\right), \\
\chi_6^{AS}(\rho,\delta) &= 64\,\pi^3\,\tilde{C}\,m_S^*\,k_N^8(\rho,\delta)\left(t_{12}^2+\,x_{12}^2\right),
\end{aligned}
$$

$$
\begin{aligned}
I_1 &= \frac{-11+2\ln 2}{105}\left(\frac{1}{b}+\frac{a^7}{c}\right)+4S_1, \\
I_2 &= \frac{-11+2\ln 2}{105}\left(\frac{1}{b}+\frac{a^7}{c}\right)-2S_1, \\
I_3 &= \frac{-167+24\ln 2}{2835}\left(\frac{1}{b}+\frac{a^9}{c}\right)+8S_2, \\
I_4 &= \frac{167-24\ln 2}{5670}\left(\frac{1}{b}+\frac{a^9}{c}\right)+2S_2, \\
I_5 &= \frac{461-24\ln 2}{31185}\left(\frac{1}{b}+\frac{a^{11}}{c}\right)+8S_3, \\
I_6 &= \frac{-4021+516\ln 2}{124740}\left(\frac{1}{b}+\frac{a^{11}}{c}\right)+8S_3.
\end{aligned}
$$

The dependence on δ of the quantities I_i is contained on the parameters a, b, and c. By using the DR technique with the MS scheme, $S_1,\ S_2$ and S_3 result:

$$
\begin{aligned}
S_1 &= \frac{1}{(bc)^3}\left[\frac{1}{15}\int_0^a u\,F_1^{abc}(u)\,du+\frac{1}{15}\int_a^1 u\,F_3^{abc}(u)\,du+T_1(a,b,c)\right], \\
S_2 &= \frac{1}{(bc)^3}\left[\frac{1}{15}\int_0^a u^3\,F_1^{abc}(u)\,du+\frac{1}{15}\int_a^1 u^3\,F_3^{abc}(u)\,du+T_2(a,b,c)\right], \\
S_3 &= \frac{1}{(bc)^3}\left[\frac{1}{15}\int_0^a u^5\,F_1^{abc}(u)\,du+\frac{1}{15}\int_a^1 u^5\,F_3^{abc}(u)\,du+T_3(a,b,c)\right].
\end{aligned}
$$

The integrals are calculated numerically. The expressions for the functions F_1^{abc} and F_3^{abc} are

provided in Appendix D.2 and the expressions for $T_1(a,b,c)$, $T_2(a,b,c)$ and $T_3(a,b,c)$ are,

$$\begin{aligned}
T_1(a,b,c) &= -\frac{abc}{420}\left(16+88b^2+b^4+88a^2c^2+22a^2b^2c^2+a^4c^4\right)+\frac{1}{3360}(2-b-ac)^4(-8-16b+8b^2\\
&+b^3-16ac-40abc-4ab^2c+8a^2c^2-4a^2bc^2+a^3c^3)\ln(2-b-ac)\\
&+\frac{1}{3360}(2+b-ac)^4(8-16b-8b^2+b^3+16ac-40abc+4ab^2c-8a^2c^2\\
&-4a^2bc^2-a^3c^3)\ln(2+b-ac)-\frac{1}{3360}(2-b+ac)^4(-8-16b+8b^2+b^3+16ac\\
&+40abc+4ab^2c+8a^2c^2-4a^2bc^2-a^3c^3)\ln(2-b+ac)\\
&-\frac{1}{3360}(2+b+ac)^4(8-16b-8b^2+b^3-16ac+40abc-4ab^2c-8a^2c^2-4a^2bc^2\\
&+a^3c^3)\ln(2+b+ac).
\end{aligned}$$

$$\begin{aligned}
T_2(a,b,c) &= -\frac{1}{45360}abc(1344+6096b^2+12b^4+3b^6+6096a^2c^2+136a^2b^2c^2+237a^2b^4c^2+12a^4c^4\\
&+237a^4b^2c^4+3a^6c^6)+\frac{1}{120960}(2-b-ac)^4(-224-448b+160b^2+40b^3+8b^4+b^5\\
&-448ac-1120abc-240ab^2c-40ab^3c-4ab^4c+160a^2c^2-240a^2bc^2-96a^2b^2c^2\\
&-17a^2b^3c^2+40a^3c^3-40a^3bc^3-17a^3b^2c^3+8a^4c^4-4a^4bc^4+a^5c^5)\ln(2-b-ac)\\
&+\frac{1}{120960}(2+b-ac)^4(224-448b-160b^2+40b^3-8b^4+b^5+448ac-1120abc\\
&+240ab^2c-40ab^3c+4ab^4c-160a^2c^2-240a^2bc^2+96a^2b^2c^2-17a^2b^3c^2-40a^3c^3\\
&-40a^3bc^3+17a^3b^2c^3-8a^4c^4-4a^4bc^4-a^5c^5)\ln(2+b-ac)\\
&-\frac{1}{120960}(2-b+ac)^4(-224-448b+160b^2+40b^3+8b^4+b^5+448ac+1120abc\\
&+240ab^2c+40ab^3c+4ab^4c+160a^2c^2-240a^2bc^2-96a^2b^2c^2-17a^2b^3c^2\\
&-40a^3c^3+40a^3bc^3+17a^3b^2c^3+8a^4c^4-4a^4bc^4-a^5c^5)\ln(2-b+ac)\\
&-\frac{1}{120960}(2+b+ac)^4(224-448b-160b^2+40b^3-8b^4+b^5-448ac+1120abc\\
&-240ab^2c+40ab^3c-4ab^4c-160a^2c^2-240a^2bc^2+96a^2b^2c^2-17a^2b^3c^2+40a^3c^3\\
&+40a^3bc^3-17a^3b^2c^3-8a^4c^4-4a^4bc^4+a^5c^5)\ln(2+b+ac)
\end{aligned}$$

$$
\begin{aligned}
T_3(a,b,c) \;=\; & -\frac{1}{3991680}abc(96768+393792b^2+240b^4+60b^6+15b^8+393792a^2c^2+2208a^2b^2c^2 \\
& +2180a^2b^4c^2+2820a^2b^6c^2+240a^4c^4+2180a^4b^2c^4+7770a^4b^4c^4+60a^6c^6+2820a^6b^2c^6 \\
& +15a^8c^8)+\frac{1}{10644480}(2-b-ac)^4(-16128-32256b+8960b^2+2800b^3+800b^4 \\
& +200b^5+40b^6+5b^7-32256ac-80640abc-22400ab^2c-5600ab^3c-1200ab^4c \\
& -200ab^5c-20ab^6c+8960a^2c^2-22400a^2bc^2-12800a^2b^2c^2-4600a^2b^3c^2 \\
& -1160a^2b^4c^2-170a^2b^5c^2+2800a^3c^3-5600a^3bc^3-4600a^3b^2c^3-1840a^3b^3c^3 \\
& -375a^3b^4c^3+800a^4c^4-1200a^4bc^4-1160a^4b^2c^4-375a^4b^3c^4+200a^5c^5-200a^5bc^5 \\
& -170a^5b^2c^5+40a^6c^6-20a^6bc^6+5a^7c^7)\ln(2-b-ac) \\
& +\frac{1}{10644480}(2+b-ac)^4(16128-32256b-8960b^2+2800b^3-800b^4+200b^5-40b^6 \\
& +5b^7+32256ac-80640abc+22400ab^2c-5600ab^3c+1200ab^4c-200ab^5c+20ab^6c \\
& -8960a^2c^2-22400a^2bc^2+12800a^2b^2c^2-4600a^2b^3c^2+1160a^2b^4c^2-170a^2b^5c^2 \\
& -2800a^3c^3-5600a^3bc^3+4600a^3b^2c^3-1840a^3b^3c^3+375a^3b^4c^3-800a^4c^4-1200a^4bc^4 \\
& +1160a^4b^2c^4-375a^4b^3c^4-200a^5c^5-200a^5bc^5+170a^5b^2c^5-40a^6c^6-20a^6bc^6 \\
& -5a^7c^7)\ln(2+b-ac)-\frac{1}{10644480}(2-b+ac)^4(-16128-32256b+8960b^2+2800b^3 \\
& +800b^4+200b^5+40b^6+5b^7+32256ac+80640abc+22400ab^2c+5600ab^3c+1200ab^4c \\
& +200ab^5c+20ab^6c+8960a^2c^2-22400a^2bc^2-12800a^2b^2c^2-4600a^2b^3c^2-1160a^2b^4c^2 \\
& -170a^2b^5c^2-2800a^3c^3+5600a^3bc^3+4600a^3b^2c^3+1840a^3b^3c^3+375a^3b^4c^3+800a^4c^4 \\
& -1200a^4bc^4-1160a^4b^2c^4-375a^4b^3c^4-200a^5c^5+200a^5bc^5+170a^5b^2c^5+40a^6c^6 \\
& -20a^6bc^6-5a^7c^7)\ln(2-b+ac) \\
& -\frac{1}{10644480}(2+b+ac)^4(16128-32256b-8960b^2+2800b^3-800b^4+200b^5-40b^6 \\
& +5b^7-32256ac+80640abc-22400ab^2c+5600ab^3c-1200ab^4c+200ab^5c \\
& -20ab^6c-8960a^2c^2-22400a^2bc^2+12800a^2b^2c^2-4600a^2b^3c^2+1160a^2b^4c^2 \\
& -170a^2b^5c^2+2800a^3c^3+5600a^3bc^3-4600a^3b^2c^3+1840a^3b^3c^3-375a^3b^4c^3 \\
& -800a^4c^4-1200a^4bc^4+1160a^4b^2c^4-375a^4b^3c^4+200a^5c^5+200a^5bc^5 \\
& -170a^5b^2c^5-40a^6c^6-20a^6bc^6+5a^7c^7)\ln(2+b+ac)
\end{aligned}
$$

Bibliography

[1] K. Brueckner, Phys. Rev. 100, 36 (1955).

[2] M. Gell-Mann and K. A. Brueckner, Phys. Rev. 106, 364 (1957).

[3] K. Sawada, K. A. Brueckner, N. Fukuda, and R. Brout, Phys. Rev. 108, 507 (1999).

[4] P. Nozières and D. Pines, Phys. Rev. 111, 442 (1958).

[5] H. Euler, Z. Physik 105, 553 (1937).

[6] R. Huby, Proc. Phys. Soc. (London) A62, 62 (1949).

[7] D.J. Thouless, Phys. Rev. 107, 559 (1957).

[8] J.S. Levinger *et al.*, Phys. Rev. 119, 230 (1960).

[9] K. Moghrabi, M. Grasso, G. Colò, and N. Van Giai, Phys. Rev. Lett. 105, 262501 (2010).

[10] K. Moghrabi, M. Grasso, X. Roca-Maza, and G. Coló , Phys. Rev. C85, 044323 (2012).

[11] Kassem Moghrabi and Marcella Grasso, Phys. Rev. C86, 044319 (2012).

[12] T.H.R. Skyrme, Phil. Mag. 1, 1043 (1956).

[13] T.H.R. Skyrme, Nucl. Phys. 9, 615 (1959).

[14] D. Vautherin, D. Brink, Phys. Rev. C5, 626 (1972).

[15] H. Yukawa, Proc. Math. Phys. Soc. Japan, 17, 48 (1935).

[16] M. Taketani et al., Prog. Theor. Phys. Suppl. 39, 1 (1967); 42, 1 (1968).

[17] R. Machleidt and I. Slaus, J. Phys. G27, R69 (2001).

[18] R. Jastrow, Phys. Rev. 81, 165 (1951).

[19] M. Oka, K. Shimizu and K. Yazaki, Prog. Theor. Phys. Suppl. 137, 1 (2000).

[20] R. Machleidt, Phys. Rev. C63, 024001 (2001).

[21] V. G. J. Stoks, R. A. M. Klomp, C. P. F. Terheggen and J. J. de Swart, Phys. Rev. C49, 2950 (1994).

[22] R. B. Wiringa, V. G. J. Stoks and R. Schiavilla, Phys. Rev. C51, 38 (1995).

[23] H. Heiselberg and V. Pandharipande, Ann. Rev. Nucl. Part. Sci. 50, 481 (2000).

[24] R. Machleidt, Q. MacPherson, E. Marji, R. Winzer, Ch. Zeoli, D. R. Entem, [nucl-th/1210.0992].

[25] J. Iwadare, S. Otsuki, R. Tamagaki, S. Machida, T. Toyoda and W. Watari, Prog. Theor. Phys. (Koyto), Supplement 3 (1956).

[26] M. Taketani, S. Machida, S. Onuma, Prog. Theor. Phys. (Kyoto) 7, 45 (1952).

[27] R. Machleidt, Adv. Nucl. Phys. 19, 189 (1989).

[28] M. Lacombe et al., Parametrization of the Paris N-N potential, Phys. Rev. C21, 861-873 (1980).

[29] Machleidt et al., Phys. Rep. 149, 1 (1987).

[30] M. M. Nagels, T. A. Rijken, and J. J. de Swart, Phys. Rev. D17, 768 (1978).

[31] V. G. J. Stoks, R. A. M. Klomp, C. P. F. Terheggen, and J. J. de Swart, Phys. Rev. C49, 2950 (1994).

[32] V. G. Neudatchin, Yu. F. Smirnov and R. Tamagaki, Prog. Theor. Phys. 58, 1072 (1977).

[33] K. A. Brueckner, Phys. Rev. 97, 1353 (1955).
K. A. Brueckner, C. A. Levinson, and H. M. Mahmoud, Phys. Rev., 95, 217 (1954).

[34] H. A. Bethe and J. Goldstone. Proc. Roy. Soc. (London) A238 551, 157 (1957).

[35] P. Ring and P. Schuck, The Nuclear Many-body Problem (Springer-Verlag, Berlin, 1980).

[36] G. P. Lepage, "What is Renormalization?", in *From Actions to Answers* (TASI-89), edited by T. DeGrand and D. Toussaint (World Scientific, Singapore, 1989); "How to Renormalize the Schrödinger Equation", [nucl-th/9706029].

[37] S.K. Bognera, b, R.J. Furnstahl, A. Schwenk, Prog. Part. Nucl. Phys. 65, 94 (2010).

[38] S. Bogner, T.T.S. Kuo, L. Coraggio, A. Covello, N. Itaco, Phys. Rev C65, 051301(R) (2002).

[39] D.B. Kaplan, M.J. Savage and M.B. Wise, Phys. Lett. B424, 390 (1998).

[40] R. J. Furnstahl, Nucl. Phys. B - Proceedings Supplements, 228 , 139 (2012).

[41] J. L. Gammel and R. M. Thaler, Phys. Rev. 107, 1337 (1957).

[42] P. S. Signell and R. E. Marshak, Phys. Rev. 109, 1229 (1958).

[43] David B. Kaplan, Effective Field Theory for Nuclear Physics, nucl-th/9901003.

[44] D. Gogny, Proceedings of the International Conference on Nuclear Self-Consistent Fields, Trieste, 1975. G. Ripka and M. Porneuf, Eds. North Hollande, Amsterdam, 1975.

[45] J. Dechargé, D. Gogny, Phys. Rev. C21, 1568 (1980).

[46] A. L. Fetter and J. D. Walecka, *Quantum Theory of Many-Particle Systems* (McGraw–Hill, New York, 1971).

[47] J. W. Negele and H. Orland, *Quantum Many-Particle Systems* (Addison-Wesley, New York, 1988).

[48] M. Bender, T. Duguet, and D. Lacroix, Phys. Rev. C79, 044319 (2009)

[49] D. Lacroix, T. Duguet, and M. Bender, Phys. Rev. C79, 044318 (2009)

[50] T. Duguet, M. Bender, K. Bennaceur, D. Lacroix, and T. Lesinski, Phys. Rev.C79, 044320 (2009).

[51] M. Anguiano, J.L. Egido, L.M. Robledo, Nucl. Phys. A 696, 467 (2001).

[52] H.-W. Hammer and R.J. Furnstahl, Nucl. Phys. A678, 277 (2000) [nucl-th/0208058].

[53] Tetsuo Sawada, nucl-th/0307023.

[54] D. M. Brink and E. Boeker, Nucl. Phys. A91, 1 (1967).

[55] J.F. Berger, M. Girod and D. Gogny, Nucl. Phys. A502, 85c (1989).

[56] L. M. Robledo, R. Rodríguez-Guzmmán, and P. Sarriguren, J. Phys. G36, 115104 (2009).

[57] F. Chappert, M. Girod, and S. Hilaire, Phys. Lett. B668, 420 (2008).

[58] S. Weinberg, Physica 96A, 327 (1979).

[59] U. van Kolck, Phys. Rev. C49, 2932 (1994).

[60] E. Epelbaum, H.-W. Hammer, and U.-G. Meiner, Rev. Mod. Phys. 81, 1773 (2009).

[61] R. Machleidt and D. Entem, Phys. Rep. 503, 1 (2011).

[62] A. Nogga, R. G. E. Timmermans and U. van Kolck, Phys. Rev. C72, 054006 (2005).

[63] M. Pavon Valderrama and E. Ruiz Arriola, Phys. Rev. C74, 054001 (2006).

[64] J. Rotureau, U. van kolck, Few-Body Syst. 54, 725 (2013).

[65] Norman D. Cook, Models of the Atomic Nucleus, Springer Berlin Heidelberg, 2010.

[66] M. G. Mayer, Phys. Rev. 75, 1969 (1949); 78, 16 (1950).

[67] O. Haxel, J. Hans D. Jensen, and Hans E. Suess, Phys. Rev. 75, 1766 (1949).

[68] I. Talmi, in: Contemporary Concepts in Physics: Simple Models of Complex Nuclei, vol. 7, Harwood Academic Publishers, 1993.

[69] C. J. Pethick and D. G. Ravenhall, Annu. Rev. Nucl. Part. Sci.45, 429 (1995).

[70] J.W. Negele, D. Vautherin, Phys. Rev. C5, 1472 (1972).

[71] M. Beiner, H. Flocard, Nguyen Van Giai, P. Quentin, Nucl. Phys. A238, 29 1975.

[72] B. D. Chang, Phys. Lett. B56, 205 (1975).

[73] J.R. Stone, P.-G. Reinhard, Prog. Part. Nucl. Phys. 58, 587 (2007).

[74] P. Hohenberg and W. Kohn, Phys. Rev. B136, 684 (1964).

[75] W. Kohn and L. J. Sham, Phys. Rev. A140, 1133 (1965).

[76] I.Zh. Petkov and M.V. Stoitsov. Nuclear Density Functional Theory. Clarendon Press, Oxford, 1991. Oxford Studies in Physics, volume 14.

[77] N. Schunck, J. Dobaczewski, J. McDonnell, J. Moré, W. Nazarewicz, J. Sarich, and M. V. Stoitsov, Phys. Rev. C81, 024316 (2010).

[78] J. Dobaczewski, K Bennaceur and F Raimondi, J. Phys. G: Nucl. Part. Phys. 39, 125103 (2012).

[79] J. Dobaczewski, et al. arXiv:1301.6151

[80] Jacek Dobaczewski J. Phys.: Conf. Ser. 312, 092002 (2011).

[81] J.C. Slater, Phys. Rev. 81, 85 (1951).

[82] M.J. Giannoni and Ph. Quentin, Phys. Rev. C21, 2076 (1980).

[83] C. Titin-Schnaider and Ph. Quentin, Phys. Lett. B49, 397 (1974).

[84] L. Satpathy et al. Phys. Rep. 319, 85 (1999).

[85] Y. Dewulf, et al., Phys. Rev. Lett. 90, 152501 (2003).

[86] C. S. Wang, K.C .Chung, A.J.Santiago, Phys. Rev. C60, 034310 (1999).

[87] J. Meyer, Ann. Phys. Fr. 28, n. 3 (2003).

[88] J. Treiner, H. Krivine, O. Bohigas, and J. Martorell; Nucl. Phys. A371 253 (1981).

[89] M.M. Sharma, W. Stocker, P. Gleissel, M. Brack, Nucl. Phys. A 04, 337 (1989).

[90] J. P. Blaizot, Phys. Rep. 64, 171 (1980).

[91] E. Khan, N. Paar, D. Vretenar, Li-Gang Cao, H. Sagawa, and G. Coló, Phys. Rev. C87, 064311 (2013).

[92] E. Khan, Phys. Rev. C80, 057302 (2009).

[93] C.J.Horowitz and J.Piekarewicz, Phys. Rev. Lett. 86, 5647 (2001).

[94] H. A. Bethe and R.F. Bacher, Rev. Mod. Phys. 8 (1936) 82.
P. Moller, W.D. Myers, H. Sagawa and S. Yoshida, Phys. Rev. Lett. 108, 052501 (2012).

[95] P. Möller, W.D. Myers, W.J. Swiatecki and J. Treiner, At. Data and Nucl. Data Tables 39, 225 (1988).
W.J. Swiatecki, Nucl. Phys. A 574 (1994) 237c.
P. Möller, J.R. Nix, W.D. Myers and W.J. Swiatecki, At. Data and Nucl. Data Tables 59, 185 (1995).

[96] M. Baldo and C. Maieron, J. Phys. G: Nucl. Part. Phys. 34, R243 (2007).

[97] A. Burrows, S. Reddy, and T. A. Thompson, Nucl. Phys. A777, 356 (2006).

[98] G.F. Bertsch and S. Das Gupta, Phys. Rep. 160, 189 (1988).

[99] S. Gandolfi, et al. Mon. Not. Roy. Astron. Soc. 404, L35 (2010).

[100] E. Chabanat, P. Bonche, P. Haensel, J. Meyer, and R. Schaeffer, Nucl. Phys. A627, 710 (1997); *ibid.* A 635, 231 (1998); *ibid.* A 643, 441 (1998).

[101] P. Danielewicz, R. Lacey, W.G. Lynch, Science 298, 1592 (2002).

[102] P.G. Hansen, A. S. Jensen, B. Jonson,Nuclear halos. Annu. Rev. Nucl. Part. Sci., 45: 591 (1995).
Gad Kh. Int. J. Mod. Phys. E14, 279 (2005).

[103] S. Goriely, S. Hilaire, M. Girod, and S. Péru, Phys. Rev. Lett. 102, 242501 (2009).

[104] S. Goriely, N. Chamel and J.M Pearson, Phys. Rev. Lett. 102, 152503 (2009).

[105] A. Bohr, and B. R. Mottelson, *Nuclear Structure. Vol. II* (W.A. Benjamin, New York, 1975).

[106] D. Pines, Elementary Exciiations in Solids. Benjamin, New York. N.Y. (1963).

[107] J. Bardeen, G. Baym, and D. Pines, Phys. Rev. 156, 207 (1967).

[108] V. Bernard, N. Van Giai, Nucl. Phys. A348, 75 (1980).

[109] Kazuhito Mizuyama, Gianluca Coló , and Enrico Vigezzi, Phys. Rev. C86, 034318 (2012).

[110] V. Bernard, Nguyen Van Giai, Nucl. Phys. A327. 397 (1979).

[111] G. Coló, H. Sagawa, and P.F. Bortignon, Phys. Rev. C82, 064307 (2010).

[112] E. Litvinova, P. Ring, Phys. Rev. C73, 044328 (2006).

[113] E.V. Litvinova and A.V. Afanasjev, Phys. Rev. C84, 014305 (2011).

[114] C. Mahaux, P.F. Bortignon, R.A Broglia, C. H. Dasso, Phys. Rep. 120, 1 (1985).

[115] M. Bender, P.H. Heenen, P.G. Reinhard, Rev. Mod. Phys. 75, 121 (2003).

[116] J. L. Egido, V. Martin, L. M. Robledo, and Y. Sun, Phys. Rev. C53, 2855 (1996).

[117] R. R. Rodrguez-Guzmán, J. L. Egido, and L. M. Robledo, Phys. Rev. C62, 054308 (2000).

[118] P.-G. Reinhard, and K. Goeke, Pep. Prog. Phys. 50, 1 (1987).

[119] J.J. Griffin, J.A. Wheeler, Phys. Rev. 108, 311 (1957).

[120] N. Sandulescu and G. F. Bertsch, Phys. Rev. C78, 064318 (2008).

[121] Guillaume Hupin and Denis Lacroix, Phys. Rev. C86, 024309 (2012).

[122] H. Liu and L. Zamick, Phys. Rev. C29, 1040 (1984); H. Liu, L. Zamick, and H. Jaqaman, ibid. 31, 2251 (1985); D. C. Zheng, D. Berdichevsky, and L. Zamick, ibid. 38, 437 (1988).

[123] N. Pillet, J.-F. Berger, and E. Caurier, Phys. Rev. C78, 024305 (2008).

[124] N. Pillet, P. Quentin, J. Libert, Nucl. Phys. A697, 141 (2002).

[125] D. Gambacurta, M. Grasso, and F. Catara, Phys. Rev. C81, 054312 (2010).

[126] D. Gambacurta, M. Grasso, V. De Donno, G. Co', and F. Catara, Phys. Rev. C86, 021304(R) (2012).

[127] D. Gambacurta, M. Grasso, and F. Catara, Phys. Rev. C84, 034301 (2011).

[128] Danilo Gambacurta, Francesco Catara, and Marcella Grasso, Phys. Rev. C80, 014303 (2009)

[129] P. Papakonstantinou and R. Roth, Phys. Rev. C81, 024317 (2010).

[130] P.J. Ellis, Nucl. Phys. A155, 625 (1970).

[131] N. Tajima, H. Flocard, P. Bonche, J. Dobaczewski, and P.-H. Heenen, Nucl. Phys. A542, 355 (1992).

[132] M. Anguiano, J.L. Egido, L.M. Robledo, Nucl. Phys. A683, 227 (2001).

[133] N. Tajima, H. Flocard, P. Bonche, J. Dobaczewski, and P.-H. Heenen, Nucl. Phys. A542, 355 (1992).

[134] Michael E. Peskin, Daniel V. Schroeder, *An Introduction to Quantum Field Theory*, Addison-Wesley Advanced Book Program (1995).

[135] G. Bruun, Y. Castin, R. Dum, and K. Burnett, Eur. Phys. J. D 7, 433 (1999).

[136] M. Grasso and M. Urban, Phys. Rev. A68, 033610 (2003).

[137] W. Pauli and F. Villars, Rev. Mod. Phys. 21, 434 (1949).

[138] E.R. Speer, *Generalized Feynman Amplitudes*, Princeton University, Princeton, 1969.

[139] G.'t Hooft and M. Veltman, Nucl. Phys. B44, 189 (1972).
C.G Bollini, J.J Giambiagi, Nuovo Cimento B12, 20 (1972).
G.'t Hooft, Nucl. Phys. B 61, 455 (1973).

[140] E.R Speer, J. Math. Phys. 15, 1 (1974).

[141] P. Breitenlohner and D. Maison, Comm. Math. Phys. 52, 11 (1977a) .
P. Breitenlohner and D. Maison, Comm. Math. Phys. 52, 39 (1977b).
P. Breitenlohner and D. Maison, Comm. Math. Phys. 52, 55 (1977c).

[142] David B. Kaplan, Martin J. Savage, Mark B. Wise, Nucl. Phys. B478, 629 (1996).

[143] William A. Bardeen, A. J. Buras, D. W. Duke, and T. Muta, Phys. Rev. D18, 3998 (1978).

[144] J. Collins, Renormalization: An Introduction to Renormalization, the Renormalization Group and the Operator-Product Expansion. Cambridge University Press, 1984.

[145] U. Van Kolck, Nucl. Phys. A645, 273 (1999).

[146] J. Gegelia, Phys. Lett. B429, 227 (1998).

[147] H. Lehmann, Nuovo Cimento, 11:342 (1954).

[148] G. C. Wick, Phys. Rev., 80, 268 (1950).

[149] F. J. Dyson, Phys. Rev. 75, 1736 (1949).

[150] J. Goldstone, Proc. Roy. Soc. A239, 267 (1957).

[151] G. F. Bertsch, P. F. Bortignon, R. A. Broglia and C. H. Dasso, Phys. Lett. 80B, 161 (1979).

[152] D.F. DuBois, Ann. Phys. (N.Y.) 8, 24 (1959).

[153] K. Moghrabi, M. Grasso, U. van kolck, in preparation.

[154] J. Dobaczewski, K. Bennaceur, F. Raimondi, J. Phys. G39, 125103 (2012).

[155] J. Dobaczewski, et al., Nucl. Phys. A422, 103 (1984).

[156] P. R. Bevington and D. K. Robinson, *Data reduction and error analysis for physical sciences*, Second Edition (McGraw-Hill, NeW York 1992).

[157] Georges Leibbrandt, Rev. Mod. Phys. 47, 849 (1975).

[158] I. Mitra, A. DasGupta, and B. Dutta-Roy, Am. J. Phys. 66, 1101 1109 (1998).

[159] K. Adhikari and A. Ghosh, J. Phys. A 30, 6553 6564 (1997).

[160] Larry C. Andrews, *Special Functions for Engineers and Applied Mathematics*, Macmillan Pub. Co. (1985).

[161] Jeremy W. Holt, Norbert Kaiser, Wolfram Weise, arXiv:1304.6350.

[162] P.-G. Reinhard, Nucl. Phys. A649, 305 (1999).

[163] G. F. Bertsch and R. A. Broglia, Oscillations in Finite Quantum Systems (University Press, Cambridge, 1994).

[164] D. Bohm and D. Pines, Phys. Rev. 92, 609 (1953).

[165] R. A. Ferrell and T. T. Quinn, Phys. Rev. 108, 570 (1957)
D.J. Thouless, Nucl. Phys. 22, 78 (1961).

[166] K. Sawada, Phys. Rev. 106, 372 (1957); M. Baranger, ibid. 120, 957 (1960); J. Sawicki, Nucl. Phys. 23, 285 (1961).

[167] D. J. Thouless, The Qnantnm Mechanics of Many Body Systems (Academic Press Inc. , New York, 1961).

[168] D.J. Thouless, Nucl. Phys. 21, 225 (1960).

[169] J. Martorell, O. Bohigas, S. Fallieros and A.M. Lane, Phys. Letters B60, 313 (1976).

[170] E. Lipparini, G. Orlandini and R. Leonardi, Phys. Rev. Lett. 36, 660 (1976).

[171] M. N. Harakeh and A. E. L. Dieperink, Phys. Rev. C23, 2329 (1981).

[172] G.Coló, L. Cao, N. Van Giai, L. Capelli, Comp. Phys. Comm. 184, 142 (2013).

[173] D.J.Rowe, Rev. Mod. Phys. 40, 153 (1968).

[174] Marco Brenna, PhD thesis (2010-2013).

[175] M. Gell-Mann and F. Low, Phys. Rev., 84:350 (1951)

[176] R.D. Mattuck: A Guide to Feynman Diagrams in the Many-Body Problem, McGraw-Hill (1967).